

**Instytut Chemii Bioorganicznej
Polskiej Akademii Nauk w Poznaniu**

Rozprawa doktorska

**Epigenetyczny mechanizm deregulacji szlaku sygnałowego
mTOR i procesu autofagii w nowych mysich modelach
choroby Alzheimerera**

Mgr Łukasz Witucki

Promotor: Prof. dr hab. Hieronim Jakubowski

Promotor pomocniczy: dr inż. Joanna Suszyńska-Zajczyk

Praca realizowana w Katedrze Biochemii i Biotechnologii Uniwersytetu Przyrodniczego w Poznaniu, Katedrze Genetyki i Podstaw Hodowli Zwierząt Uniwersytetu Przyrodniczego w Poznaniu oraz w Katedrze Mikrobiologii, Biochemii i Genetyki Molekularnej na Uniwersytecie Rutgers New Jersey Medical School w Newark, USA.

Poznań, 2023

„Nikt prawie nie wie, dokąd go zaprowadzi droga, póki nie stanie u celu”

J. R. R. Tolkien

Składam serdecznie podziękowania:

*Mojemu promotorowi Profesorowi Hieronimowi Jakubowskiemu
za przekazaną wiedzę, rady, poświęcony czas
oraz możliwość rozwoju zainteresowań naukowych*

*Mojemu promotorowi pomocniczemu Dr inż. Joannie Suszyńskiej-Zajczyk
za przekazaną wiedzę, wskazówki, poświęcony czas
oraz nieocenioną pomoc w realizacji badań*

*Koleżankom i Kolegom z Katedry Biochemii i Biotechnologii
i Katedry Genetyki i Podstaw Hodowli Zwierząt
Uniwersytetu Przyrodniczego w Poznaniu,
za wszelką pomoc oraz życzliwą atmosferę w pracy*

*Profesorowi Adamowi Kraszewskiemu oraz Pani Małgorzacie Dąbkiewicz
za wszelką udzieloną pomoc i wsparcie*

Najbliższej Rodzinie za udzielone wsparcie, pomoc oraz wiarę w moją osobę

*Pracę dedykuję Żonie Annie za okazane wsparcie,
cierpliwość, wyrozumiałość i motywację do pracy*

Spis treści

Lista publikacji wchodzących w skład rozprawy doktorskiej.....	6
Lista publikacji nie wchodzących w skład rozprawy doktorskiej.....	6
Streszczenie.....	8
Abstract.....	9
1. Wprowadzenie.....	10
1.1 Homocysteina.....	10
1.2 Hiperhomocysteinemia.....	11
1.3 Tioakton homocysteiny.....	11
1.4 Reakcja <i>N</i> -homocysteinyłacji.....	12
1.5 <i>N</i> -Hcy-białka.....	13
1.6 Paraoksonaza 1.....	13
1.7 Hydrolaza bleomycyny.....	14
1.8 Syntaza β -cystationiny.....	14
1.9 Kinaza serynowo-treoninowa mTOR.....	15
1.10 Autofagia.....	16
1.10 Demetylaza histonowa Phf8.....	17
1.11 Choroba Alzheimerera.....	17
1.12 Mechanizm rozwoju choroby Alzheimerera – APP i amyloid beta.....	18
1.13 Mysi model choroby Alzheimerera - 5xFAD.....	18
1.14 Komórkowy model choroby Alzheimerera- N2a-APP _{swe}	19
2. Cel pracy.....	20
3. Skrótowy opis prac naukowych wchodzących w skład rozprawy doktorskiej.....	21
3.1 Depletion of Paraoxonase 1 (Pon1) Dysregulates mTOR, Autophagy, and Accelerates Amyloid Beta Accumulation in Mice.....	21
3.2 Homocysteine Metabolites Inhibit Autophagy and Elevate Amyloid Beta by Impairing Phf8/H4K20me1-dependent Epigenetic Regulation of mTOR in Cystathionine β -Synthase-Deficient Mice.....	24

3.3 Deletion of the Homocysteine Thiolactone Detoxifying Enzyme Bleomycin Hydrolase, in Mice, Causes Memory- and Neurological Deficits and Worsens Alzheimer's Disease Related Behavioral and Biochemical Traits in the 5xFAD Model of Alzheimer's Disease .	28
4. Wnioski końcowe	34
5. Wykaz skrótów i rycin.....	35
6. Bibliografia.....	37
7. Publikacje wchodzące w skład rozprawy doktorskiej	45
8. Życiorys naukowy	125
9. Oświadczenia o wkładzie doktoranta w powstawanie prac naukowych wchodzących w skład rozprawy doktorskiej.....	129

Lista publikacji wchodzących w skład rozprawy doktorskiej

Witucki Ł, Jakubowski H,

Depletion of Paraoxonase 1 (Pon1) Dysregulates mTOR, Autophagy, and Accelerates Amyloid Beta Accumulation in Mice,

Cells 2023, 12(5), 746 DOI: 10.3390/cells12050746

Pięcioletni IF: 6,7, MEiN 140 punktów

Witucki Ł, Jakubowski H,

Homocysteine Metabolites Inhibit Autophagy and Elevate Amyloid Beta by Impairing Phf8/H4K20me1-dependent Epigenetic Regulation of mTOR in Cystathionine β -synthase-Deficient Mice,

J Inherit Metab Dis. 2023;1–17 DOI: 10.1002/jimd.12661

Pięcioletni IF: 4,429, MEiN 100 punktów

Witucki Ł, Borowczyk K, Suszyńska-Zajczyk J, Warzych E, Pawlak P, Jakubowski H,

Deletion of the Homocysteine Thiolactone Detoxifying Enzyme Bleomycin Hydrolase, in Mice, Causes Memory- and Neurological Deficits and Worsens Alzheimer's Disease Related Behavioral and Biochemical Traits in the 5xFAD Model of Alzheimer's Disease,

J Alzheimer's Dis 2023; accepted August 5

Pięcioletni IF: 4,372, MEiN 100 punktów

Lista publikacji nie wchodzących w skład rozprawy doktorskiej

Witucki Ł, Kurpik M, Jakubowski H, Szulc M, Mikołajczak Ł, Jodynis-Liebert J, Kujawska M,

Neuroprotective Effects of Cranberry Juice Treatment in a Rat Model of Parkinson's Disease, Nutrients 2022, 14, 2014

Pięcioletni IF: 7,185, MEiN 140 punktów

Kujawska M, Jourdes M, **Witucki Ł**, Karaźniewicz-Łada M, Szulc M, Górską A, Mikołajczak PŁ, Teissedre PL, Jodynis-Liebert J,

Pomegranate Juice Ameliorates Dopamine Release and Behavioral Deficits in a Rat Model of Parkinson's Disease,

Brain Sciences 2021, 11, 1127

Pięcioletni IF: 3,706, MEiN 100 punktów

Olejniczak M, Urbanek MO, Jaworska E, **Witucki Ł**, Szcześniak MW, Makałowska I, Krzyżosiak WJ,

Sequence-non-specific effects generated by various types of RNA interference triggers,

Biochimica et Biophysica Acta (BBA) - Gene Regulatory Mechanisms, 2016, 1859, 2, 306-314

Pięcioletni IF: 4,823, MEiN 140 punktów

Streszczenie

Hiperhomocysteinemia to patologiczny stan organizmu w którym dochodzi do akumulacji homocysteiny we krwi. Hiperhomocysteinemia wynika z niedoboru kwasu foliowego i witamin B₆, B₁₂, lub mutacji w genach kodujących enzymy metabolizujące homocysteinę. Homocysteina jest metabolizowana do cyklicznego tioestru - tiolaktonu homocysteiny szczególnie w organizmach z defektami genetycznymi występującymi w enzymach metabolizmu homocysteiny lub niedoborem witamin z grupy B. Tiolakton homocysteiny jest wysoce reaktywny i poprzez modyfikacje ε-aminowej grupy lizyny w reakcji zwanej *N*-homocysteinylacją wpływa na strukturę i zaburzenie funkcji modyfikowanego białka.

Wykazano, że hiperhomocysteinemia jest ryzykiem wielu chorób w tym chorób neurodegeneracyjnych. Choroba Alzheimera jest główną przyczyną otępienia umysłowego u osób starszych. Główne przyczyny rozwoju tej choroby to akumulacja amyloidu beta oraz fosforylowanego białka tau. Jednocześnie u chorych wykazano aktywację szlaku sygnałowego mTOR, który hamuje proces autofagii. W procesie autofagii usuwane są uszkodzone organelle komórkowe oraz białka w tym nagromadzony amyloid beta i fosforylowany tau. Molekularny mechanizm aktywacji mTOR oraz zahamowania autofagii nie został w pełni poznany.

Badania wskazują, że w mózgach osób cierpiących na chorobę Alzheimera poziom homocysteiny jest podwyższony oraz obniżona jest aktywność enzymów hydrolizujących tiolakton homocysteiny - paraoksonazy 1 oraz hydrolazy bleomycyny. Dodatkowo wykazano, że hiperhomocysteinemia prowadzi do aktywacji mTOR oraz zahamowania autofagii. Pomimo licznych badań mechanizm działania hiperhomocysteinemii na rozwój choroby Alzheimera nie został w pełni poznany.

Celem niniejszej rozprawy doktorskiej była analiza wpływu defektów genetycznych w metabolizmie tiolaktonu homocysteiny na chorobę Alzheimera poprzez epigenetyczny mechanizm regulacji ekspresji *mTOR* oraz procesu autofagii w nowych mysich modelach choroby Alzheimera.

Abstract

Accumulation of homocysteine in our body is known as hyperhomocysteinemia. It results from insufficient dietary intake of vitamin B₆, B₁₂, folic acid or mutations in homocysteine metabolism related genes. Accumulated homocysteine is metabolized to thioester homocysteine thiolactone. Homocysteine thiolactone is highly reactive and modifies ϵ -amino group of a protein Lys residue in a reaction known as *N*-homocysteinylation. Protein *N*-homocysteinylation can affect protein structure and impair protein function.

Hyperhomocysteinemia is a risk factor for many diseases, including neurodegenerative diseases such as Alzheimer's disease, the leading cause of dementia in the elderly. Alzheimer's disease is caused by accumulation of amyloid beta and phosphorylated tau proteins and is characterized by upregulation of the mTOR signaling pathway, which leads to autophagy inhibition. Autophagy is a multi-step process in which damaged organelles and proteins, including amyloid beta and phosphorylated tau, are removed. Molecular mechanisms of mTOR activation and autophagy inhibition remain to be fully elucidated.

Homocysteine level is elevated while the activity of homocysteine metabolism related enzymes such as paraoxonase 1 and bleomycin hydrolase are lowered in brains of Alzheimer's disease patients. In addition, hyperhomocysteinemia leads to mTOR activation and autophagy inhibition. The mechanism by which hyperhomocysteinemia leads to Alzheimer's disease is still not fully understood.

The overall goal of the present thesis was to examine mechanisms by which genetic deficiencies in homocysteine thiolactone metabolism can lead to Alzheimer's disease, focusing on an epigenetic mechanism of mTOR activation and autophagy inhibition in novel mouse models of Alzheimer's disease.

1. Wprowadzenie

1.1 Homocysteina

Homocysteina (Hcy) jest niebiałkowym aminokwasem, będącym uniwersalnym produktem pośrednim szlaków metabolicznych dwóch aminokwasów: metioniny oraz cysteiny. Różnica strukturalna budowy Hcy w porównaniu do metioniny to brak grupy metylowej. Natomiast w porównaniu do struktury cysteiny, Hcy wyróżnia się posiadaniem dodatkowej grupy metylenowej (1, 2). Metionina, dostarczana w pokarmie i uwolniona w procesie trawienia białek, jest wykorzystywana do biosyntezy nowych białek lub syntezy S-adenozylometioniny (SAM), uniwersalnego donora grup metylowych wykorzystywanych w reakcjach metylacji. W ramach tych reakcji, SAM jest przekształcany do S-adenozylhomocysteiny, która następnie ulega reakcji hydrolizy do Hcy oraz adenozy. Syntaza metioniny, której kofaktorem jest witamina B₁₂ wykorzystująca 5-10-metylenotetrahydrofolian jako donor grup metylowych przeprowadza proces remetylacji Hcy do metioniny. Remetylacja metioniny zachodzi również przy udziale metylotransferazy betainowo-homocysteinowej, w której donorem grup metylowych jest betaina.

W wątrobie, nerkach, trzustce oraz w jelicie cienkim Hcy ulega dwuetapowej reakcji transsulfurylacji do cysteiny. W pierwszym etapie homocysteina łączy się z seryną w reakcji katalizowanej przez syntazę β -cystationiny (ang. cystathionine β -synthase, Cbs), której kofaktorem jest witamina B₆. W drugim etapie, powstała cystationina jest przekształcana do cysteiny oraz α -ketomaślanu w reakcji katalizowanej przez γ -liazę cystationiny.

Ze względu na podobieństwo strukturalne do metioniny, Hcy jest substratem syntetazy metionyl-tRNA w reakcji syntezy aminoacylo adenylanu lecz nie w reakcji aminoacylacji tRNA. Mechanizm korekcyjny syntetazy metionyl-tRNA, w wyniku którego z Hcy~AMP powstaje cykliczny tioester - tiolakton homocysteiny (HTL), zapobiega wbudowaniu Hcy do syntetyzowanego białka. HTL jest usuwany poprzez enzymatyczną hydrolizę do Hcy w reakcjach katalizowanych przez trzy tiolaktonazy: hydrolazę bleomycyny (ang. Bleomycin hydrolase, Blmh), paraoskonazę 1 (ang. Paraoxonase 1, Pon1) i białko podobne do hydrolazy biphenylu (ang. Biphenyl hydrolase like, Bphl) oraz poprzez wydalanie z moczem (1).

1.2 Hiperhomocysteinemia

Akumulacja Hcy we krwi ($>15\mu\text{M}$) zwana hiperhomocysteinemią (HHcy) to patologiczny stan organizmu, który jest czynnikiem ryzyka wielu chorób. Podwyższony poziom Hcy wynika z mutacji występujących w genach kodujących enzymy związane z metabolizmem Hcy na drodze remetylacji i transsulfurylacji, niedoborem witamin B₆, B₁₂, niedoborem kwasu foliowego lub dietą bogatą w metioninę. Wykazano, że HHcy przyczynia się do rozwoju wielu chorób w tym: raka (3), układu krążenia (4), udaru (5), oczu (6), komplikacji ciąży (7) czy chorób neurodegeneracyjnych w tym choroby Alzheimera (AD) (8, 9).

Wykazano, że obniżenie poziomu HHcy u pacjentów w młodym wieku z opóźnieniem umysłowym oraz wysokim poziomem Hcy przyczynia się do poprawy stanu zdrowia tych pacjentów (10). Inne dane wskazują, że obniżenie poziomu Hcy poprzez suplementację witaminami z grupy B (program FACIT trail) spowalnia: zanik pamięci, upośledzenie sensomotorycznej szybkości, problemy z przetwarzaniem wiadomości oraz zaburzenia funkcji poznawczych (11). W innej próbie badawczej (VITACOG) wykazano, że 2-letnia terapia witaminami z grupy B przyczynia się do zahamowania atrofii mózgu w rejonie istoty szarej (region mózgu podatny na rozwój choroby Alzheimera) oraz utraty funkcji poznawczych poprzez obniżenie poziomu Hcy u pacjentów, u których na początku badania był podwyższony poziom Hcy (12, 13). Pomimo licznych badań dokładny mechanizm działania HHcy na rozwój chorób neurodegeneracyjnych nie został jednak poznany.

1.3 Tiolakton homocysteiny

HTL powstaje w reakcji korekcyjnej wynikającej poprzez błędne rozpoznanie Hcy przez syntetazę aminoacylo-tRNA. Syntetaza tRNA rozpoznaje aminokwas, który przekształcany jest do aminoacyloadenylationu, będącego produktem pośrednim reakcji aminoacylacji, który następnie jest przenoszony na tRNA. Istnieją dwa mechanizmy korekcyjnie zapobiegające błędnie rozpoznanemu aminokwasu wprowadzenie do sekwencji białka. Pierwsza reakcja korekcyjna (pre-transfer) polega na hydrolizie błędnie powstałego aminoacyloadenylationu. Druga reakcja korekcyjna (post-transfer) polega na hydrolizie błędnie załadowanego tRNA.

Syntetaza metionyno-tRNA, leucyno-tRNA oraz izoleucyno-tRNA błędnie rozpoznają Hcy ze względu na strukturę podobną do metioniny, leucyny i izoleucyny (14). W wyniku błędnie rozpoznanej Hcy powstaje adenylan homocysteiny (Hcy~AMP), który w ramach reakcji korekcyjnej jest usuwany. W procesie tym, boczny łańcuch tiolowy wypiera AMP

z aktywowanej grupy karboksylowej Hcy tworząc tiolakton homocysteiny – cykliczny tioester (15). Badania wykazały, że powstawanie HTL zachodzi we wszystkich żywych organizmach w tym u ludzi oraz, że jest to jedyny poznany mechanizm biosyntezy tiolaktonu (14,16–18). W osoczu zdrowych organizmów, HTL występuję w zakresie od poniżej nanomolarnego do nanomolarnego. W moczu poziom ten jest ok. 100 krotnie wyższy co wskazuje, że usuwanie HTL następuje w nerkach (19). Kilkudziesięciu krotne podwyższone poziomy HTL są skutkiem mutacji w genach kodujących enzymy metabolizujące homocysteinę lub hydrolizujące tiolakton homocysteiny.

Wykazano, że podwyższone poziomy HTL są toksyczne zarówno w badaniach *in-vitro* jak i *in-vivo*. Ludzkie komórki śródbłónka (ang. human umbilical vein endothelial cells, HUVECs) traktowane HTL w stężeniu 50-200 μM przez 24 h wkraczały na proces apoptozy (20). Inne badania wskazują, że HTL indukuje apoptozę, stres siateczki śródplazmatycznej czy szlak adaptacyjnej odpowiedzi na stres (ang. unfolded protein response, UPR) w trofoblastach, komórkach promieloidalnych oraz komórkach nabłonkowych siatkówki (21–23). Wykazano również, że HTL blokuje fosforylację kinazy syntazy glikogenu 3 (ang. Glycogen synthase kinase 3, GSK-3) oraz kinazy p70-S6k aktywowanych przez kinazę aktywowane mitogenami (ang. mitogen-activated protein kinases, MAPK) (24, 25). Dodatek HTL do diety powoduje rozwój miażdżycy u pawianów i szczurów (26, 27). Dootrzewnowe wstrzyknięcie toksycznych dawek HTL powoduje drgawki oraz śmierć myszy i szczurów (28–30). Wykazano, że myszy z deficytem Pon1 lub Blmh są bardziej wrażliwe na toksyczne dawki HTL (31, 32).

1.4 Reakcja *N*-homocysteinylacji

Po powstaniu HTL energia z bezwodnikowego wiązania Hcy~AMP zostaje zachowana w wewnątrzcząsteczkowym wiązaniu tioestrowym tiolaktonu. W warunkach fizjologicznych HTL jest wysoce reaktywny i modyfikuje ϵ -aminowe grupy lizyny w reakcji zwanej *N*-homocysteinylacją. Skutkuje to wprowadzeniem Hcy do białka i utworzeniem *N*-Hcy-białek (33, 34). Ilość zmodyfikowanych lizyn jest zależna od stężenia HTL.

W 1997 roku postawiono hipotezę toksyczności HHcy (33, 34) wskazującą, że konwersja Hcy do HTL a następnie *N*-homocysteinylacja białek inicjuje zmiany patologiczne poprzez zaburzenie szlaków metabolicznych. *N*-Hcy-białka z czasem mogą akumulować i aktywować procesy chorobotwórcze, odpowiedź autoimmunologiczną, toksyczność komórek,

stres oksydacyjny, stres siateczki śródplazmatycznej oraz błędne fałdowanie, agregacje i tworzenie form amyloidowych białek (33–36).

1.5 N-Hcy-białka

Ilość N-Hcy-białka powstałego w reakcji N-homocysteinyłacji jest zależna od stężenia HTL. Ilość zmodyfikowanych lizyn w cząsteczce białka jest zależna od ilości lizyn, struktury oraz wielkości modyfikowanego białka (35, 37, 38). Około pięć razy wyższe poziomy N-Hcy-białek zostały wykazane u pacjentów z mutacjami w genie *CBS* lub reduktazy metylenotetrahydrofolianu (ang. Methylenetetrahydrofolate reductase, *MTHFR*) (39). Podwyższone poziomy N-Hcy-białek wykazano również u myszy z deficytem *Cbs*, *Pon1* oraz *Blmh* (1, 2).

1.6 Paraoksonaza 1

Pon1 jest zewnątrzkomórkowym enzymem syntetyzowanym w wątrobie. Występuje głównie w krwiobiegu jako składnik frakcji lipoprotein o wysokiej gęstości (HDL) (40). W mniejszych ilościach występuje w wątrobie, nerkach, jelicie grubym oraz mózgu (41). Nazwa enzymu wzięła się od jednej z jego aktywności, detoksyfikacji paraoksonu – fosforanu organicznego. Późniejsze badania z użyciem kultur komórkowych wykazały aktywność HTazy (hydrolizy HTL do Hcy) (42).

Aktywność *PON1* jest determinowana przez naturalnie występującą zmienność genetyczną (43). Wykazano, że osoby posiadające genotyp związany z wyższą aktywnością *PON1* szybciej hydrolizują HTL w surowicy krwi co skutkuje akumulacją Hcy i mniejszą ilością N-Hcy-białek (42). U myszy, *Pon1* wykazuje właściwości chroniące przed rozwojem miażdżycy wywołane przez dietę wysokotłuszczową oraz związaną z polimorfizmem genu apolipoproteiny E (42, 43). Właściwości te mogą wynikać z funkcji antyoksydacyjnych enzymu lub zdolności hydrolizy HTL.

Zaobserwowano, że aktywność *PON1* jest niższa u ludzi cierpiących na chorobę Alzheimera w porównaniu do zdrowych pacjentów (44, 45). U pacjentów z łagodnymi zaburzeniami funkcji poznawczych, aktywność *PON1* jest skorelowana z zaburzeniami funkcji poznawczych, szybkością przetwarzania informacji oraz problemami z mową (48).

Immunobrawienie *Pon1* w mysim modelu AD (Tg2576) wykazało kolokalizację enzymu ze złoгами amyloidu beta ($A\beta$) (49). Badania mózgow myszy z deficytem genu *Pon1* wykazały podwyższony poziom białka klasteryny transportującego amyloid beta oraz zaburzenia procesów związanych z homeostazą mózgu co wskazuje, że *Pon1* odgrywa ważną rolę w prawidłowym funkcjonowanie mózgu poprzez zahamowanie akumulacji $A\beta$ (50).

1.7 Hydrolaza bleomycyny

Blmh jest wewnątrzkomórkową protezą cysteinową, która oprócz hydrolizy HTL, deaminuje lek przeciwnowotworowy – bleomycynę (51). Występuje głównie w jądrach, mięśniach szkieletowych, trzustce oraz mózgu. U myszy z deficytem *Blmh* na diecie wysokometioninowej wykazano większe poziomy HTL wydalanego w moczu w porównaniu do myszy typu dzikiego (31).

Badania mózgow myszy *Blmh*^{-/-} wykazały zaburzenia plastyczności synaps, podziałów komórkowych, metabolizmu energetycznego czy dynamiki cytoszkieletu w porównaniu do myszy typu dzikiego (52). Deficyt *Blmh* prowadzi do astroglejozy (53) i akumulacji HTL w mózgu myszy co wskazują na rolę *Blmh* w utrzymaniu homeostazy mózgu (32). *Blmh* uczestniczy w przetwarzaniu prekursorowego białka amyloidu (ang. amyloid precursore protein, APP) do $A\beta$ jak i w przetwarzaniu N-końca białka huntingtyny ulegającego zaburzeniom w chorobie Huntingtona (54). W mózgach ludzkich, BLMH występuje w neuronach kory nowej oraz w dystroficznych neurytach blaszek starczych (55). U ludzi z AD zaobserwowano obniżoną aktywność BLMH (56). Niektóre badania wskazują, że polimorfizm genu *BLMH* (substytucja I433V) jest powiązany ze zwiększonym ryzykiem zachorowania na AD (56, 57).

1.8 Syntaza β -cystationiny

Cbs jest pierwszym enzymem na drodze przekształcania Hcy w cysteinę na drodze transsulfurylacji. Syntetyzowany jest w mózgu, wątrobie i trzustce. Aktywność enzymu jest zależna od witaminy B₆ oraz od polimorfizmu genetycznego. Obniżona aktywność CBS u ludzi prowadzi do akumulacji Hcy co następnie skutkuje zmianami miażdżycowych oraz opóźnieniem umysłowym objawiającym się problemami z nauką czy niższym poziomem ilorazu inteligencji (58, 59).

Myszy z deficytem genu *Cbs* wykazują zaburzenia funkcji poznawczych, problemy z uczeniem się oraz zaburzenia pamięci (60, 61). W porównaniu do myszy typu dzikiego, myszy z deficytem *Cbs* wykazują podwyższony poziom 5-lipoksygenazy, która jest podwyższona u ludzi z AD (63). Dodatkowo w zakręcie zębatym hipokampu myszy *Cbs*^{-/-} wykazano podwyższony poziom A β oraz fosforylowanego białka tau jak i dwukrotnie większą neurodegenerację neuronów (64).

1.9 Kinaza serynowo-treoninowa mTOR

Ssaczy cel rapamycyny (ang. mammalian target of rapamycin, mTOR) pełni ważną rolę w prawidłowym funkcjonowaniu organizmu poprzez kontrolowanie: podziałów i różnicowania komórek, translacji, transkrypcji, metabolizmu energetycznego, odpowiedzi na stres, degradacji białek oraz procesu autofagii (64, 65). Aktywacja mTOR jest zależna od wielu czynników takich jak: dostępność czynników wzrostu i hormonów, głodu, stanu energetycznego komórki, wirusów oraz innych zewnątrzkomórkowych czynników stresu.

mTOR występuje w dwóch kompleksach białkowych mTORC1 i mTORC2, które różnią się pełnionymi funkcjami, oraz białkami tworzącymi kompleksy (64, 66). W skład mTORC1 wchodzi kinaza mTOR, mLST8/G β Lm Raprot, Pras40. Kompleks mTORC1 reguluje autofagię, podziały komórkowe, wzrost komórek poprzez aktywację kinazy rybosomalnej S6 oraz białka wiążącego eukariotyczny czynnik inicjacji translacji 4E (4E-BP1), które odpowiadają za translację mRNA i syntezę białek rybosomalnych. Miarą aktywności kompleksu mTORC1 jest fosforylacja seryny 2448 białka mTOR. W skład kompleksu mTORC2 wchodzi następujące białka: mTOR, Rictor, mSin1, mLST8, oraz Protor. Kompleks ten odpowiada za organizację cytoszkieletu komórki. Miarą aktywności kompleksu mTORC2 jest fosforylacja seryny 2481 białka mTOR (68).

Deregulacja szlaku sygnałowego mTOR jest przyczyną wielu chorób w tym stwardnienia guzowatego, zespołu łamliwego chromosomu X oraz choroby Alzheimerera (68, 69). U pacjentów z AD wykazano podwyższony poziom mTOR oraz podwyższony poziom fosforylowanej kinazy rybosomalnej S6 w porównaniu do osób zdrowych (70, 71). Badania pośmiertne mózgow wykazały również, że poziom fosforylacji kinazy rybosomalnej S6 jest pozytywnie skorelowany z ilością fosforylowanego białka tau (71).

Badania z mysimi modelami Alzheimerera wskazują, że wyższe poziomy mTOR są skorelowane z ilością amyloidu beta (71). Wykazano również, że w mysich modelach stwardnienia

guzowatego schorzenia powiązanego z opóźnieniem umysłowym, autyzmem i epilepsją podwyższone poziomy mTOR wpływają negatywnie na proces nauki (73).

1.10 Autofagia

Autofagia z greckiego oznacza samo zjadanie się. Wyróżnia się 3 typy autofagii: makroautofagia, mikroautofagia i autofagia zależna od chaperonów. Każdy typ autofagii prowadzi do proteolitycznej degradacji wybranych składników komórki wewnątrz lizosomów (74). Najlepiej poznanym typem autofagii jest makroautofagia (zwana dalej autofagią).

Proces autofagii rozpoczyna się od izolacji fragmentu membrany ze siateczki śródplazmatycznej, aparatu Golgiego lub endosomu. Proces wydzielania fragmentu membrany zwanego fagoforem jest regulowany przez białka ULK1, FIP200 oraz białka z rodziny genów związanych z autofagią (ang. autophagy related gene, Atg) - Atg13, Atg101 a jego dalsze formowanie przez Beklinę 1 (ang. Beclin-1 Becn-1), Atg14, VPS15 i VPS34 (74, 75). Zainicjowany fagofor rozszerza się i otacza agregaty białkowe, rybosomy czy zużyte organelle przeznaczone do degradacji. W procesie transportu do fagoforu selektywnie wybranych białek przeznaczonych do degradacji kluczową rolę odgrywa białko p62, oraz lekki łańcuch 3 białka związanego z mikrotubulami (ang. Microtubule-associated protein light chain 3, LC3). Cytozolowa forma białka LC3 (LC3-I), ulega przecięciu przez białko Atg4B a następnie połączeniu z fosfatydyloetanolaminą regulowanym przez białka Atg7, Atg3 oraz kompleks złożony z białek Atg12-Atg5-Atg16L. Zmodyfikowana forma LC3 (LC3-II) łączy się z zewnętrzną oraz wewnętrzną błoną fagoforu i oddziałuje z białkiem p62. Po złączeniu się obu końców fagoforu powstaje autofagosom, który następnie łączy się z lizosomem tworząc autolizosom. W autolizosomie dochodzi do proteolitycznej degradacji dostarczonej zawartości z autofagosom (77). Produkty degradacji zostają ponownie użyte do wytwarzania organelli lub do procesów metabolizmu komórkowego.

Inicjacja procesu autofagii jest odwrotnie skorelowana z aktywnością mTORC1 (78). Aktywacja mTORC1 prowadzi do zahamowania tworzenia się fagoforu poprzez oddziaływanie na kompleks białek ULK1, Atg13, Atg101 i FIP200 a w rezultacie do zahamowania kolejnych etapów autofagii (79). Wykazano, że zaburzenia procesu autofagii odgrywają rolę w wielu chorobach neurodegeneracyjnych w tym chorobie Parkinsona, Huntingtona czy Alzheimer. Zahamowanie autofagii przyczynia się do nagromadzenia amyloidu beta oraz tau, które stanowią przyczynę rozwoju AD (80).

1.10 Demetylaza histonowa Phf8

Demetylaza histonowa PHF8 (ang. plant homeodomain finger 8, PHF8) regulują ekspresję genów poprzez usuwanie grup metylowych z modyfikacji histonowych: H4K20me1, H3K9me1/me2 oraz H3K27me2 (81–84). PHF8 posiada dwie funkcjonalne domeny: JmjC, która katalizuje usuwanie grup metylowych z lizyn oraz domenę białkową o strukturze palca cynkowego (ang. PHD finger) odpowiadająca za rozpoznawanie tych trzech metylowanych lizyn w sekwencji histonów (85).

Mutacje genu *PHF8* powodują zaburzenia rozwoju twarzoczaszki charakteryzujące się rozszczepem wargi i/lub podniebienia, nadmiernym dystansem między parzystymi narządami (hipertolizm), małogłowiem, wydłużoną twarzą, opadaniem powiek oraz łagodną asymetrią twarzy (86–88). Mutacje genu *PHF8* powodują różny stopień upośledzenia umysłowego, który objawia się problemami z uczeniem i pamięcią (89). Wyciszenie ekspresji genu *Phf8* w kulturach komórkowych prowadzi do zaburzenia cyklu komórkowego oraz zaburzenia procesu różnicowania neuronów (81, 89). Deficyt genu *Phf8* u *Danio rerio* aktywuje apoptozę komórek nerwowych a u nicieni powoduje problemy z lokomocją (80, 82). Myszy z deficytem *Phf8* wykazują zaburzenia długotrwałego wzmocnienia synaptycznego (ang. long-term potentiation, LTP) problemy z uczeniem i pamięcią. Wykazano, że zmiany te spowodowane są nadmierną aktywacją szlaku sygnałowego mTOR, którego wzmożona ekspresja jest zależna od występowania na miejscu startu transkrypcji modyfikacji H4K20me1 (85). Badania wykazały, że H4K20me1 jest pozytywnym regulatorem transkrypcji. Występuje głównie w obszarze sekwencji genów, które ulegają transkrypcji i jest powiązany z rozluźnieniem chromatyny, która ułatwia proces transkrypcji (91).

1.11 Choroba Alzheimera

Choroba Alzheimera to neurodegeneracyjna postępująca z wiekiem choroba, która jest główną przyczyną otępienia umysłowego u osób starszych. Jest ona spowodowana akumulacją amyloidu beta oraz fosforylowanego tau (92). Charakterystyczne objawy tej choroby to zaburzenia pamięci i funkcji poznawczych, problemy z logicznym i przestrzennym myśleniem czy problemy z mową i poruszaniem oraz zmianami nastroju (93). Rozpoznano genetyczne jak i nie genetyczne czynniki ryzyka rozwoju AD. Głównym nie genetycznym czynnikiem ryzyka jest wiek. Ważną rolę pełni również styl życia, dieta, płeć, czynniki środowiskowe, wykształcenie oraz inne przebyte choroby (94). Mutacje w genach kodujących prekursorowe

białko amyloidu, presenilinę 1 i 2 (*PSEN1*, *PSEN2*) są przyczynami rozwoju rodzinnego/sporadycznego typu AD, którego oznaki kliniczne pojawiają się przed 65 rokiem życia (95). Wariant $\epsilon 4$ genu apolipoproteiny E stanowi natomiast główny genetyczny czynnik rozwoju AD u osób powyżej 65 roku życia. (95, 96).

1.12 Mechanizm rozwoju choroby Alzheimera – APP i amyloid beta

Główne przyczyny rozwoju AD to akumulacja amyloidu beta oraz fosforylowanego białka tau. Amyloid beta powstaje na skutek enzymatycznej obróbki transmembranowego białka APP. Istnieją dwa szlaki obróbki APP: prowadzący do powstania $A\beta$ (amyloidogenny), w którym kompleks β -sekreazy przecina APP prowadząc do powstania β CTF APP oraz uwalniając rozpuszczalny fragmentu APP ($sAPP\beta$). W szlaku nie prowadzącym do powstawania amyloidu beta, białko APP jest przecinane w innym miejscu przez kompleks α -sekreazy co prowadzi do uwolnienia dłuższego rozpuszczalnego fragmentu APP ($sAPP\alpha$) oraz powstania α CTF APP.

Kolejny etap przekształcania znajdującego się w błonie komórkowej α CTF APP oraz β CTF APP jest przeprowadzany przez kompleks γ -sekreazy. Cięcie α CTF APP uwalnia fragment o długości 83 nukleotydów, który jest następnie szybko hydrolizowany. Cięcie β CTF APP prowadzi natomiast do powstania amyloidu beta o długości ok. 39-43 aminokwasów. (98). Ze względu na hydrofobowe właściwości, $A\beta$ ulega szybko oligomeryzacji, które w późniejszych etapach formują się w bardziej toksyczne włókna i blaszki starcze, które są niepodatne na hydrolizę (98, 99). Nagromadzenie się oligomerów oraz włókien $A\beta$ skutkuje zaburzeniami działania synaps czy obumieraniem neuronów (100, 101).

1.13 Mysi model choroby Alzheimera - 5xFAD

Na przestrzeni kilkunastu ostatnich lat powstało wiele mysich modeli AD. W modelu 5xFAD (Tg6799) wprowadzono wszystkie mutacje powodujące rodzinny/sporadyczny typ choroby Alzheimera (103). W obrębie miejsca cięcia APP przez β - i γ -sekreazę wprowadzono mutacje szwedzką (K670N/M671L), florydzką (I716V), i londyńską (V717I). Mutacja szwedzka powoduje zwiększoną produkcją $A\beta$ o długości 40 i 42 aminokwasów (104). Natomiast 2 pozostałe mutacje w genie *APP* jak i mutacje M146L i L286V w genie *PSEN1* prowadzą do zwiększenia produkcji $A\beta$ o długości 42 aminokwasów (105–107).

W modelu 5xFAD akumulacja $A\beta$ rozpoczyna się w drugim miesiącu życia. Natomiast pierwsze blaszki starcze pojawiają się w szóstym miesiącu życia. Astroglejoza i mikroglejoza

pojawiają się w drugim miesiącu życia. Neurony zaczynają obumierać wraz z pojawieniem się złogów amyloidu beta. Degeneracja synaps występuje od dziewiątego miesiąca życia. Pierwsze objawy zmian behawioralnych – zaburzenia pamięci przestrzennej pojawiają się okresie czwartego i piątego miesiąca życia. Natomiast problemy z nauką zaburzenia socjalne oraz zaburzenia ruchowe pojawiają się w dziewiątym miesiącu życia (102, 107).

1.14 Komórkowy model choroby Alzheimera- N2a-APP_{swe}

W celu stworzenia *in-vitro* modelu AD do mysich komórek neuroblastomy wprowadzono zmutowany ludzki gen *APP* zawierający mutacje szwedzką (K670N/M671L) prowadzący do nadprodukcji amyloidu beta o długości 40 i 42 aminokwasów.

2. Cel pracy

Głównym celem rozprawy doktorskiej było poznanie mechanizmu działania hiperhomocysteinemii indukowanej genetycznie i dietetycznej oraz wpływu tiolaktonaz homocysteiny na markery choroby Alzheimera. Główny cel pracy został zrealizowany poprzez realizację poniższych celów szczegółowych:

1. Analiza wpływu deficytu Pon1 lub Blmh, wieku oraz diety wysokometioninowej na funkcje poznawcze u myszy 5xFAD.
2. Analiza wpływu deficytu Pon1 lub Blmh, wieku oraz diety wysokometioninowej na akumulację amyloidu beta w mózgach myszy 5xFAD.
3. Analiza wpływu metabolitów homocysteiny, deficytu Pon1, Blmh lub Cbs na akumulację amyloidu beta w transgenicznym komórkach neuroblastomy mysiej N2a-APP_{swe} ze zmutowanym ludzkim APP.
4. Analiza wpływu deficytu Pon1, Blmh, lub Cbs, wieku oraz diety wysokometioninowej na demetylazę histonową Phf8, H4K20me1, szlak sygnałowy mTOR oraz proces autofagii w mózgach myszy.
5. Analiza wpływu metabolitów homocysteiny, deficytu Pon1, Blmh lub Cbs na demetylazę histonową Phf8, H4K20me1, szlak sygnałowy mTOR oraz proces autofagii mysich komórkach neuroblastomy N2a oraz w mysich komórkach neuroblastomy ze zmutowanym ludzkim APP - N2a-APP_{swe}.

3. Skrótowy opis prac naukowych wchodzących w skład rozprawy doktorskiej

3.1 Depletion of Paraoxonase 1 (Pon1) Dysregulates mTOR, Autophagy, and Accelerates Amyloid Beta Accumulation in Mice

Cells 2023, 12(5), 746

PON1 pełni ważną funkcję ochronną w wielu chorobach, w tym chorobach układu krążenia, poprzez właściwości antyoksydacyjne oraz hydrolizę HTL. Obniżona aktywność PON1 jest obserwowana u osób chorujących na AD. Dane z mysich modeli wskazują, że Pon1 występuje w obrębie blaszek starczych A β oraz oddziałuje z klasteryną, która transportuje A β z krwi do mózgu. Dane wskazują, że PON1 pełni ważną rolę w utrzymaniu prawidłowego funkcjonowania mózgu. Jednak mechanizm ochronnego działania PON1 na homeostazę mózgu nie został w pełni poznany.

W niniejszej pracy w celu lepszego poznania mechanizmu działania ochronnego Pon1 w AD wykonano analizy behawioralne, akumulacji A β , zmian ilościowych kinazy mTOR, markerów procesu autofagii, demetylasy histonowej Phf8 oraz modyfikacji H4K20me1 w nowym mysim modelu AD - *Pon1*^{-/-}5xFAD skonstruowanym przez Prof. Hieronima Jakubowskiego. Uzyskane wyniki na mózgach myszy oraz zaproponowany mechanizm regulacji mTOR/procesu autofagii przez demetylazę histonową Phf8/H4K20me1 zostały potwierdzone *in vitro* przy użyciu mysiej linii komórkowej N2a-APP_{swe}.

Nowy mysim model AD - *Pon1*^{-/-}5xFAD został otrzymany poprzez krzyżowanie myszy *Pon1*^{-/-} z myszami 5xFAD. W celu określenia wpływu deficytu Pon1 na zmiany behawioralne w rocznych myszach *Pon1*^{-/-}5xFAD oraz *Pon1*^{+/+}5xFAD wykonano test zaciskania tylnych kończyn (ang. hindlimb clasping test), test chodzenia po krawędzi (ang. ledge test) oraz test aktywności w cylindrze (ang. cylinder test). We wszystkich przeprowadzonych testach myszy z deficytem Pon1 uzyskiwały podobne wyniki do myszy z grupy kontrolnej. Wskazuje to, że deficyt Pon1 nie powoduje neurodegeneracji oraz zaburzeń czuciowo-ruchowych.

Przeprowadzone eksperymenty z wykorzystaniem metody western blot wykazały, że statystycznie niższy poziom demetylasy histonowej Phf8 oraz istotnie statystycznie wyższy poziom H4K20me1 w 5 i 12 miesięcznych mózgach myszy *Pon1*^{-/-}5xFAD w porównaniu do grupy kontrolnej *Pon1*^{+/+}5xFAD na diecie standardowej jak i wysokometioninowej (dieta HHcy). Dodatkowo wykazaliśmy, że dieta HHcy prowadzi do istotnego statystycznie obniżenia ilości Phf8 oraz istotnego statystycznie podwyższenia ilości modyfikacji H4K20me1 u myszy *Pon1*^{+/+}5xFAD w porównaniu do myszy *Pon1*^{+/+}5xFAD na diecie standardowej. Nie

zaobserwowaliśmy istotnego statystycznie wpływu diety HHcy na zmiany Phf8 oraz H4K20me1 u myszy *Pon1*^{-/-}5xFAD.

Ponieważ Phf8 reguluje ekspresję *mTOR* poprzez H4K20me1 wykonaliśmy analizy western blot dla całkowitej ilości białka mTOR oraz jego formy fosforylowanej na serynie 2448 (pmTOR). Wykazaliśmy istotnie statystycznie wyższe poziomy mTOR i pmTOR u myszy *Pon1*^{-/-}5xFAD w porównaniu do grupy kontrolnej *Pon1*^{+/+}5xFAD na diecie standardowej jak i HHcy. Dieta HHcy prowadziła do istotnego statystycznie podniesienia poziomu mTOR i pmTOR u myszy *Pon1*^{+/+}5xFAD w porównaniu do myszy *Pon1*^{+/+}5xFAD na diecie standardowej. Natomiast dieta HHcy u myszy *Pon1*^{-/-}5xFAD podwyższała tylko istotnie statystycznie poziom mTOR.

Ponieważ fosforylacja mTOR na serynie 2448 wpływa na zahamowanie procesu autofagii w następnych eksperymentach przeanalizowano wpływ deficytu *Pon1* oraz diety HHcy na 3 markery autofagii: *Becn-1*, *Atg5* oraz *Atg7* będącymi regulatorami ładowania autofagosomu (ang. regulator autophagy assembly). Wykazaliśmy, że poziomy markerów autofagii są istotnie statystycznie niższe w mózgach myszy *Pon1*^{-/-}5xFAD w porównaniu do grupy kontrolnej *Pon1*^{+/+}5xFAD na diecie standardowej jak i HHcy. Jedynie poziom *Atg7* nie ulegał istotnie statystycznej zmianie u myszy *Pon1*^{-/-}5xFAD na diecie HHcy w porównaniu do myszy *Pon1*^{-/-}5xFAD na diecie standardowej.

Analizy western blot dla APP wykazały istotny wpływ genotypu oraz diety HHcy na zwiększenie ilości tego białka.

W celu weryfikacji czy omówione zmiany ilościowe na poziomie białka wynikają ze zmian transkrypcyjnych zastosowano metodę ilościowego PCR w czasie rzeczywistym (rt-qPCR). Przeprowadzone eksperymenty wykazały, że zmiany ilościowe na poziomie białka są skorelowane ze zmianami w ekspresji mRNA analizowanych genów.

W celu potwierdzenia obserwowanych zmian w mózgach myszy oraz przeprowadzenia kolejnych eksperymentów w badaniach wykorzystano myszą linię komórkową N2a-APP_{swe}, z wprowadzonym zmutowanym ludzkim genem *APP*.

Do wyciszenia ekspresji genu *Pon1* metodą interferencji RNA wykorzystano dwa siRNA celujące w mRNA *Pon1*. Następnie używając metody western blot wykazaliśmy, że wyciszenie ekspresji *Pon1* prowadzi do istotnie statystycznego obniżenia ilości Phf8 oraz markerów autofagii: *Becn-1*, *Atg5*, *Atg7* oraz jednoczesnego istotnie statystycznego podwyższenia

poziomów mTOR, pmTOR, H4K20me1 oraz APP. Uzyskane wyniki potwierdzają obserwacje przeprowadzone *in vivo*.

W celu weryfikacji czy wyciszenie ekspresji *Pon1* prowadzi do podwyższenia ilości mTOR poprzez zmiany wiązania H4K20me1 do genu *mTOR* wykonaliśmy eksperymenty immunoprecypitacji chromatyny związanej z H4K20me1 połączonej z analizą rt-qPCR. Wykazaliśmy, że wyciszenie ekspresji *Pon1* prowadzi do istotnego statystycznie większego występowania H4K20me1 na miejscu startu transkrypcji (ang. transcription start site, TSS) genu *mTOR*, powyżej TSS (-160 par zasad, pz) oraz poniżej TSS (+320 pz). Uzyskane wyniki wskazują, że wyciszenie ekspresji genu *Pon1* poprzez epigenetyczny mechanizm regulacji ekspresji genów prowadzi do zwiększonej ilości mTOR.

Zastosowanie immunofluorescencyjnego barwienia A β w komórkach N2a-APP_{swe} po wyciszeniu ekspresji genu *Pon1* pozwoliło określić efekt deficytu *Pon1* na akumulację A β . Analizy wykazały, że wyciszenie ekspresji genu *Pon1* prowadzi do istotnie statystycznej agregacji A β w porównaniu do prób kontrolnych (z ekspresją genu *Pon1*). Zmiany te charakteryzowały się istotnie statystycznie większą powierzchnią zajmowaną przez sygnały, istotnie statystycznie większym średnim rozmiarem pojedynczego sygnału oraz istotnie statystycznie większą intensywnością świecenia sygnałów.

Ponieważ wcześniej wykazano, że u myszy *Pon1*^{-/-} dochodzi do agregacji HTL oraz *N*-Hcy-białek przeprowadzono immunobarwienie A β po traktowaniu komórek N2a-APP_{swe} tymi metabolitami. Wykazaliśmy, że traktowanie komórek HTL w stężeniu 20 i 200 μ M skutkuje istotnie statystycznie większą powierzchnią sygnału oraz istotnie statystycznie większym średnim rozmiarem pojedynczego sygnału w porównaniu do próby kontrolnej. W przypadku traktowania 10 i 20 μ M *N*-Hcy-białkiem odnotowaliśmy jedynie istotnie statystycznie większą powierzchnię sygnału w porównaniu do próby kontrolnej. Uzyskane wyniki wskazują, że agregacja A β po wyciszeniu ekspresji genu *Pon1* może wynikać z akumulacji HTL lub *N*-Hcy-białek.

Analizy A β wykonane metodą dot blot na 5 i 12 miesięcznych mózgach myszy *Pon1*^{+/+}5xFAD oraz *Pon1*^{-/-}5xFAD wykazały, że deficyt *Pon1* oraz dieta HHcy prowadzą do istotnie statystycznej większej ilości A β w mózgach myszy.

Podsumowując wykazaliśmy, że *Pon1* odgrywa ważną rolę w prawidłowym funkcjonowaniu mózgu oraz chroni przed akumulacją A β . Wykazaliśmy, że w mózgach mysz *Pon1*^{-/-}5xFAD

dochodzi do obniżenia ekspresji mRNA oraz ilości białka demetylasy histonowej Phf8 oraz wybranych markerów autofagii. Jednocześnie wykazaliśmy, że dochodzi do akumulacji APP oraz mTOR, którego ekspresja jest zależna od H4K20me1. Wykazaliśmy również, że akumulacja A β jest zależna od diety HHcy oraz genotypu myszy. Zaobserwowane zmiany w mózgu myszy zostały potwierdzone *in vitro* poprzez wyciszenie ekspresji genu *Pon1* oraz traktowanie komórek metabolitami (HTL, N-Hcy-białka), których poziomy są podwyższone w myszach *Pon1*^{-/-}. Finalnie zaproponowaliśmy ochronny mechanizm działania *Pon1* hamujący agregację A β wynikającą z deregulacji mTOR/autofagii poprzez akumulację H4K20me1 na TSS genu *mTOR*.

3.2 Homocysteine Metabolites Inhibit Autophagy and Elevate Amyloid Beta by Impairing Phf8/H4K20me1-dependent Epigenetic Regulation of mTOR in Cystathionine β -Synthase-Deficient Mice

J Inherit Metab Dis. 2023;1–17 DOI: 10.1002/jimd.12661

Obniżona aktywność CBS wynikająca z mutacji genu *CBS* prowadzi do podwyższenia poziomu Hcy i jej metabolitów oraz wywołują zmiany patologicznego układu nerwowego. Pacjenci z mutacjami w genie *CBS* wykazują opóźnienie umysłowe, problemy z nauką, obniżony iloraz inteligencji oraz zmiany w zachowaniu. Dokładny mechanizm, który prowadzi do wyżej wymienionych zmian nie został w pełni poznany.

W niniejszej pracy wykazaliśmy wpływ deficytu genu *Cbs* na akumulację A β poprzez deregulację Phf8/H4K20me1, mTOR oraz procesu autofagii.

Przeprowadzone eksperyment z wykorzystaniem metody western blot wykazały istotnie statystycznie niższy poziom demetylasy histonowej Phf8 oraz istotnie statystycznie podwyższony poziom H4K20me1 w 9 tygodniowych oraz 1 rocznych mózgu myszy *Cbs*^{-/-} w porównaniu do myszy *Cbs*^{+/-}. Wykazaliśmy, że wiek myszy nie miał istotnego statystycznie wpływu na poziom Phf8, natomiast wpływał na obniżenie poziomu H4K20me1.

Ponieważ Phf8 poprzez demetylację H4K20me1 reguluje ekspresję *mTOR*, wykonaliśmy analizy western blot dla całkowitej ilości białka mTOR oraz jego formy ufosforylowanej na serynie 2448. Analizy mTOR wykazały istotnie statystycznie wyższy poziom mTOR u młodszych myszy *Cbs*^{-/-} w porównaniu do grupy kontrolnej. Natomiast w obu grupach wiekowych zaobserwowaliśmy istotnie statystycznie wyższy poziom pmTOR u myszy *Cbs*^{-/-} w porównaniu do grupy kontrolnej *Cbs*^{+/-}. Jednocześnie odnotowaliśmy istotny wpływ wieku na poziom mTOR w obu genotypach myszy.

Ponieważ fosforylacja mTOR na serynie 2448 jest związana z zahamowaniem procesu autofagii w następnych analizach przeanalizowaliśmy wpływ deficytu *Cbs* na markery autofagii: *Becn-1*, *Atg5*, *Atg7* oraz *p62* będącymi regulatorami ładowania autofagosomu. Wykazaliśmy istotnie statystycznie obniżenie poziomów *Becn-1*, *Atg5* i *Atg7* oraz istotnie statystycznie podwyższenie poziomu *p62* u myszy *Cbs*^{-/-} w porównaniu do grupy kontrolnej *Cbs*^{+/-}. Jednocześnie zaobserwowaliśmy obniżenie ilości markerów autofagii wraz z wiekiem myszy.

Analizy western blot wykazały istotny statystycznie wpływ genotypu *Cbs*^{-/-} oraz wieku na podwyższenie poziomu APP w mózgach myszy.

W celu weryfikacji czy deficyt *Cbs* prowadzi do neurodegeneracji wykonaliśmy analizy dwóch markerów neurodegeneracji, które są podwyższone w AD. Wykonane eksperymenty wykazały, że marker aktywacji astrocytów - *Gfap* (ang. Glial fibrillary acidic protein, *Gfap*) oraz marker uszkodzenia neuronów - *Nfl* (ang. Neurofilament light chain, *Nfl*) są istotnie statystycznie podwyższone u 1 rocznych myszy *Cbs*^{-/-} w porównaniu do myszy kontrolnych. U myszy 9 tygodniowych nie zaobserwowaliśmy istotnych statystycznie zmian obu markerów.

W celu weryfikacji czy omówione zmiany ilościowe na poziomie białka wynikają ze zmian transkrypcyjnych zastosowano metodę ilościowego PCR w czasie rzeczywistym. Przeprowadzone analizy wykazały, że zmiany ilościowe na poziomie białka są skorelowane ze zmianami w ekspresji mRNA testowanych genów.

W celu potwierdzenia obserwowanych zmian w mózgach myszy oraz przeprowadzenia kolejnych eksperymentów w badaniach wykorzystano mysią linię komórkową N2a oraz N2a-APP_{swe}, z wprowadzonym zmutowany ludzki transgenem *APP*.

Do wyciszenia ekspresji genu *Cbs* metodą interferencji RNA wykorzystano dwa siRNA regulujące mRNA *Cbs*. Używając metody western blot wykazaliśmy, że wyciszenie ekspresji *Cbs* w linii komórkowej N2a-APP_{swe} prowadzi do istotnego statystycznie obniżenia ilości *Phf8* oraz markerów autofagii: *Beclin-1*, *Atg5*, *Atg7* oraz jednoczesnego istotnie statystycznego podwyższenia mTOR, pmTOR, H4K20me1 oraz APP.

Analizy rt-qPCR wykazały, że wyciszenie ekspresji genu *Cbs* w komórkach N2a-APP_{swe}, zmienia ekspresję wybranych genów, która jest skorelowana z ilością danego białka. Jednocześnie uzyskane wyniki potwierdzają wyniki z eksperymentów przeprowadzonych na mózgach myszy.

Ponieważ wykazano, że u myszy *Cbs*^{-/-} poziomy Hcy, HTL oraz *N*-Hcy-białek są podwyższone, niemożliwe jest określenie czy tylko jeden z tych metabolitów powoduje wyżej wymienione zmiany w mózгах myszy. Podjęliśmy próbę rozwiązania tego problemu poprzez oddzielne traktowanie komórek N2a tymi metabolitami. Analizy western blot wykazały, że traktowanie komórek Hcy, HTL oraz *N*-Hcy-białkiem obniża poziom Phf8 oraz hamuje proces autofagii. Jednocześnie, zastosowane metabolity podwyższają ilości H4K20me1, mTOR, pmTOR oraz App. Zastosowane metabolity Hcy wykazały analogiczne efekty działania na omawiane białka.

W celu potwierdzenia, że wyciszenie ekspresji *Cbs* prowadzi do podwyższenia mTOR poprzez zmiany wiązania H4K20me1 do genu *mTOR* wykonaliśmy eksperymenty immunoprecypitacji chromatyny związanej z H4K20me1 połączonej z analizą rt-qPCR. Wykazaliśmy, że wyciszenie ekspresji *Cbs* prowadzi do istotnego statystycznie większego wiązania H4K20me1 na TSS, powyżej TSS (-160 pz) oraz poniżej TSS (+320 pz) genu *mTOR*. Jednocześnie wykazaliśmy, że wyciszenie genu *Cbs* prowadziło do istotnie statystycznie większej akumulacji H4K20me1 na miejscu TSS genu *mTOR* w porównaniu do fragmentu powyżej i poniżej TSS. Uzyskane wyniki wskazują, że wyciszenie ekspresji genu *Cbs* poprzez epigenetyczny mechanizm regulacji ekspresji genów prowadzi do zwiększonej ilości mTOR.

Analogiczne eksperymenty immunoprecypitacji chromatyny zostały wykonane dla komórek N2a po traktowaniu Hcy, HTL oraz *N*-Hcy-białkami. 20 i 200 μ M stężenie HTL oraz 200 μ M stężenie Hcy prowadziło do istotnie statystycznego większego występowania H4K20me1 na trzech testowanych miejscach genu *mTOR* w porównaniu do próby kontrolnej. 20 μ M stężenie Hcy prowadziło do istotnie statystycznego większego występowania H4K20me1 na TSS oraz poniżej TSS genu *mTOR*. W przypadku fragmentu powyżej TSS obserwowaliśmy jedynie większą tendencję występowania H4K20me1 w porównaniu do próby kontrolnej. 20 μ M stężenie *N*-Hcy-białek prowadziło do istotnie statystycznego większego występowania H4K20me1 na TSS oraz poniżej TSS genu *mTOR*. Dla 10 μ M stężenia *N*-Hcy-białka odnotowaliśmy jedynie tendencję wzrostową na TSS oraz powyżej TSS.

Zastosowanie immunofluorescencyjnego barwienia A β w komórkach N2a-APP_{swE} po wyciszeniu ekspresji genu *Cbs* pozwoliło określić efekt deficytu *Cbs* na akumulację A β . Analizy wykazały, że wyciszenie ekspresji genu *Cbs* prowadzi do agregacji A β w porównaniu do prób kontrolnych (z ekspresją genu *Cbs*). Zmiany te charakteryzowały się istotnie statystycznie większym średnim rozmiarem pojedynczego sygnału.

W celu weryfikacji czy Hcy, HTL, *N*-Hcy-białka, których poziomy są podwyższone u myszy *Cbs*^{-/-} wpływają na akumulację A β wykonano analogiczne testy immunofluorescencyjnego barwienia A β . Analizy wykazały, że wszystkie metabolity prowadzą do akumulacji A β . W przypadku traktowania HTL oraz Hcy w stężeniach 20 i 200 μ M obserwowano istotnie statystycznie większą powierzchnię sygnałów oraz istotnie statystycznie większy średni rozmiar pojedynczego sygnału w porównaniu do próby kontrolnej. Traktowanie komórek *N*-Hcy-białkiem skutkowało jedynie istotnie statystycznie większą powierzchnią sygnałów w porównaniu do próby kontrolnej.

W celu wykazania, że samo obniżenie poziomu Phf8 prowadzi do akumulacji A β poprzez deregulację mTOR oraz procesu autofagii, wykonano eksperymenty z wyciszoną ekspresją genu *Phf8* w komórkach N2a-APP_{swe}.

Metodą western blot wykazaliśmy, że obniżenie poziomu Phf8 prowadzi do istotnie statystycznego podwyższenia poziomów H4K20me1, mTOR oraz pmTOR. Jednocześnie obserwowaliśmy istotne statystycznie obniżenie poziomów Atg5 oraz Atg7. Natomiast poziomy Becn-1 oraz APP nie ulegały istotnym statystycznie zmianom po wyciszeniu ekspresji genu *Phf8* w porównaniu do prób kontrolnych.

Wykazaliśmy, że wyciszenie ekspresji genu *Phf8* prowadziło do istotnej akumulacji A β przeprowadzonej przy użyciu immunofluorescencyjnego barwienia A β . Wyciszenie ekspresji genu *Phf8* skutkowało istotnie statystycznie większą powierzchnią sygnałów oraz istotnie statystycznie większą intensywnością świecenia sygnału w porównaniu do prób kontrolnych.

Podsumowując wykazaliśmy, że *Cbs* oraz Phf8 odgrywają ważną rolę w prawidłowym funkcjonowaniu mózgu oraz chronią przed neuropatią zapobiegając akumulacji A β . Wykazaliśmy, że u myszy *Cbs*^{-/-} dochodzi do obniżenia ekspresji mRNA oraz ilości białka demetylazy histonowej Phf8 i wybranych markerów autofagii. Jednocześnie wykazaliśmy, że dochodzi do akumulacji App oraz mTOR, którego ekspresja jest zależna od H4K20me1. Wykazaliśmy również, że deficyt *Cbs* w myszach jednorocznych prowadził do neurodegeneracji, na co wskazuje akumulacja Gfap i Nfl. Wykazaliśmy, że wyciszenie ekspresji genu *Cbs* poprzez zahamowanie autofagii oraz zwiększoną syntezę APP prowadzi do akumulacji A β . Traktowanie Hcy, HTL oraz *N*-Hcy-białkami, które są podwyższone u myszy *Cbs*^{-/-} wpływały w ten sam sposób na A β , mTOR, autofagię, Phf8 oraz H4K20me1. Uzyskane

wyniki wskazują, że w przypadku wyciszenia genu *Phf8* akumulacja A β jest skutkiem deregulacji mTOR oraz procesu autofagii.

Finalnie zaproponowaliśmy mechanizm prowadzący do rozwoju AD poprzez agregację A β wynikającą z deregulacji mTOR/autofagii. Zmiany te są konsekwencją obniżenia ilości Phf8 co prowadzi do akumulacji H4K20me1 na TSS genu *mTOR*. Mechanizm ten jest indukowany przez akumulację Hcy, HTL oraz N-Hcy-białka, co jest skutkiem obniżenia czy braku ekspresji genu *Cbs*.

3.3 Deletion of the Homocysteine Thiolactone Detoxifying Enzyme Bleomycin Hydrolase, in Mice, Causes Memory- and Neurological Deficits and Worsens Alzheimer's Disease Related Behavioral and Biochemical Traits in the 5xFAD Model of Alzheimer's Disease

BLMH pełni ważną funkcję w utrzymaniu homeostazy mózgu poprzez hydrolizę HTL do Hcy. Aktywność BLMH jest obniżona u ludzi chorujących na AD. Dodatkowo *Blmh* bierze udział w procesowaniu APP oraz A β . Myszy z deficytem *Blmh* wykazują zmiany behawioralne oraz astrogliozę mózgu, która jest cechą charakterystyczną u osób z AD. Analizy proteomiczne mózgowi myszy *Blmh*^{-/-} wykazały zaburzenia wielu szlaków ważnych dla homeostazy mózgu. Dokładny mechanizm, który prowadzi do rozwoju AD w skutek deregulacji *Blmh* nie został jednak w pełni poznany.

W niniejszej pracy w celu zbadania mechanizmu działania ochronnego *Blmh* w AD wykonano analizy behawioralne, akumulacji A β , zmian ilościowych kinazy mTOR, markerów procesu autofagii, demetylasy histonowej Phf8 oraz H4K20me1 w nowym mysim modelu AD - *Blmh*^{-/-}5xFAD skonstruowanym przez Prof. Hieronima Jakubowskiego, *Blmh*^{+/+}5xFAD oraz w myszach *Blmh*^{-/-} i *Blmh*^{+/+}. Uzyskane wyniki na mózgowi myszy oraz zaproponowany przez nas mechanizm regulacji mTOR/procesu autofagii przez demetylazę Phf8/H4K20me1 zostały potwierdzone *in vitro* przy użyciu mysiej linii komórkowej N2a-APP_{swe}.

Nowy mysi model AD - *Blmh*^{-/-}5xFAD został otrzymany poprzez krzyżowanie myszy *Blmh*^{-/-} z myszami 5xFAD. W celu określenia wpływu deficytu *Blmh* na zmiany behawioralne w rocznych myszach *Blmh*^{-/-}5xFAD i *Blmh*^{+/+}5xFAD, oraz 2 i 4 miesięcznych myszach *Blmh*^{-/-} i myszach typu dzikiego wykonaliśmy test rozpoznawania nowego obiektu (ang. novel object recognition test, NOR), test zaciskania tylnych kończyn (ang. hindlimb clasp test), test chodzenia po krawędzi (ang. ledge test) oraz test aktywności w cylindrze (ang. cylinder test).

W teście NOR wykazaliśmy, że 4 miesięczne myszy *Blmh*^{-/-} na diecie standardowej i HHcy oraz 4 miesięczne myszy typu dzikiego na diecie HHcy nie rozpoznają nowego obiektu. W przypadku grup 2 miesięcznych, oba genotypy myszy na obu dietach spędzały istotnie statystycznie więcej czasu przy nowym obiekcie. Wyniki wskazują, że zaburzenia funkcji poznawczych oraz pamięci krótkotrwałej postępują wraz z wiekiem u myszy *Blmh*^{-/-}.

Test zaciskania tylnych kończyn oraz test chodzenia po krawędzi wykazały że genotyp jak i dieta wpływają na proces neurodegeneracji. Dieta HHcy wywoływała większy efekt neurodegeneracji u myszy *Blmh*^{+/+} niż u myszy *Blmh*^{-/-}, co sugeruje, że za ten efekt odpowiedzialna jest akumulacja metabolitów wspólnych dla deficytu *Blmh* i HHcy, t.j. HTL oraz *N*-Hcy białka.

Test NOR przeprowadzony na mysim modelu AD, *Blmh*^{-/-}5xFAD oraz *Blmh*^{+/+}5xFAD wykazał, że myszy z deficytem *Blmh* na obu typach diety wykazują zaburzenia funkcji poznawczych i pamięci krótkotrwałej objawiającej się niezdolnością do rozpoznania nowego obiektu. Jednocześnie zastosowanie diety HHcy u myszy *Blmh*^{+/+}5xFAD nie wpływało na zaburzenia funkcji poznawczych i pamięci krótkotrwałej.

W teście zaciskania tylnych kończyn wykazaliśmy, że deficyt *Blmh* wpływa w istotnym stopniu na proces neurodegeneracji. Dodatkowo zaobserwowaliśmy, że dieta HHcy wywoływała większy efekt neurodegeneracji u myszy *Blmh*^{+/+}5xFAD niż u myszy *Blmh*^{-/-}5xFAD. W teście aktywności w cylindrze wykazaliśmy, że deficyt *Blmh* i dieta HHcy wpływają w istotnym stopniu na proces neurodegeneracji.

Przeprowadzone eksperymenty z wykorzystaniem metody western blot wykazały istotnie statystycznie niższy poziom demetylazy histonowej Phf8 oraz istotnie statystycznie podwyższony poziom H4K20me1 w 2 i 4 miesięcznych mózgach myszy *Blmh*^{-/-} w porównaniu do grupy kontrolnej na diecie standardowej. Dodatkowo wykazaliśmy, że dieta HHcy prowadzi do istotnego statystycznie obniżenia ilości Phf8 w 2 miesięcznych myszach *Blmh*^{-/-} w porównaniu do myszy *Blmh*^{+/+}. Nie zaobserwowaliśmy istotnego wpływu diety HHcy na zmiany Phf8 oraz H4K20me1 u 4 miesięcznych myszy *Blmh*^{-/-} w porównaniu do myszy typu dzikiego. Analogiczne efekty deficytu *Blmh* oraz diety HHcy zostały wykazane na 5 i 12 miesięcznych mózgach myszach *Blmh*^{-/-}5xFAD oraz *Blmh*^{+/+}5xFAD.

Ponieważ Phf8 kontroluje ekspresję *mTOR* poprzez H4K20me1 wykonaliśmy analizy western blot dla całkowitej ilości białka *mTOR* oraz jego formy ufosforylowanej na serynie 2448. Wykazaliśmy istotnie statystycznie wyższe poziomy *mTOR* i *pmTOR* u 2 i 4 miesięcznych

myszy *Blmh*^{-/-} w porównaniu do grupy kontrolnej *Blmh*^{+/+} na diecie standardowej. Natomiast dieta HHcy prowadziła do istotnego statystycznie podniesienia poziomu pmTOR tylko u 4 miesięcznych myszy *Blmh*^{-/-} w porównaniu do grupy kontrolnej.

Ponieważ fosforylacja mTOR na serynie 2448 wpływa na zahamowanie procesu autofagii w następnych analizach sprawdziliśmy wpływ deficytu *Blmh* oraz zastosowania diety HHcy na trzy markery autofagii: *Becn-1*, *Atg5* oraz *Atg7*. Wykazaliśmy, że poziomy markerów autofagii są istotnie statystycznie obniżone w 2 i 4 miesięcznych mózgach myszy *Blmh*^{-/-} w porównaniu do grupy kontrolnej *Blmh*^{+/+} na diecie standardowej. Dodatkowo zaobserwowaliśmy istotny statystycznie efekt diety HHcy na obniżenie ilości *Becn-1* w 2 miesięcznych myszach *Blmh*^{-/-} w porównaniu do myszy *Blmh*^{+/+}.

Analogiczne eksperymenty przeprowadzone na 5 i 12 miesięcznych mózgach myszy *Blmh*^{-/-} 5xFAD oraz *Blmh*^{+/+} 5xFAD wykazały, że deficyt *Blmh* prowadzi do istotnego statystycznie zwiększenia ilości mTOR i pmTOR u myszy na diecie standardowej (z wyłączeniem mTOR dla 5 miesięcznych myszy). Dieta HHcy wywoływała jedynie istotne statystyczne podwyższenie poziomów mTOR i pmTOR u 5 miesięcznych myszy *Blmh*^{-/-} 5xFAD.

Jednocześnie wykazaliśmy istotne statystycznie obniżenie ilości *Atg5*, *Atg7* oraz *Becn-1* (z wyłączeniem *Becn-1* dla 5 miesięcznej grupy) w 5 i 12 miesięcznych myszach *Blmh*^{-/-} 5xFAD na diecie standardowej w porównaniu do grupy kontrolnej. Jednocześnie zaobserwowaliśmy istotny statystycznie wpływ diety HHcy na obniżenie *Becn-1* u 12 miesięcznych *Blmh*^{-/-} 5xFAD oraz obniżenie *Atg5* u 5 i 12 miesięcznych *Blmh*^{-/-} 5xFAD w porównaniu do grupy kontrolnej. Dodatkowo zaobserwowaliśmy istotnie statystycznie podwyższone poziom p62 w 5 i 12 miesięcznych myszach *Blmh*^{-/-} 5xFAD na diecie standardowej w porównaniu do myszy *Blmh*^{+/+} 5xFAD. Natomiast dieta HHcy prowadziła do istotnej statystycznej akumulacji p62 jedynie w 5 miesięcznych myszach *Blmh*^{-/-} 5xFAD.

W przypadku analiz App wykazaliśmy, że deficyt *Blmh* oraz dieta HHcy prowadzą do istotnie statystycznie podwyższenia poziomu tego białka w porównaniu do myszy *Blmh*^{+/+}. Analizy APP dla myszy *Blmh*^{-/-} 5xFAD oraz *Blmh*^{+/+} 5xFAD na diecie standardowej wykazały, że inaktywacja *Blmh* prowadzi do akumulacji APP. Dieta HHcy wywoływała jedynie efekt akumulacji APP w 5 miesięcznych myszach *Blmh*^{-/-} 5xFAD.

W celu potwierdzenia obserwowanych zmian w mózgach myszy oraz przeprowadzenia kolejnych eksperymentów w badaniach wykorzystano myszą linię komórkową N2a-APP_{swE} z wprowadzonym zmutowanym ludzkim transgenem *APP*.

Do wyciszenie ekspresji genu *Blmh* metodą interferencji RNA wykorzystano dwa siRNA celujące w mRNA *Blmh*. Używając metody western blot wykazaliśmy, że wyciszenie ekspresji *Blmh* prowadzi do istotnego statystycznie obniżenia ilości Phf8 oraz markerów autofagii: Becn-1, Atg5, Atg7 będącymi regulatorami ładowania autofagosomu, Lc3-I, Lc3-II oraz jednoczesnego istotnego statystycznie podwyższenia poziomów mTOR pmTOR, H4K20me1, p62 oraz APP.

W celu weryfikacji czy omówione zmiany ilościowe na poziomie białka wynikają ze zmian transkrypcyjnych zastosowano metodę ilościowego PCR w czasie rzeczywistym (rt-qPCR). Przeprowadzone analizy wykazały, że zmiany ilościowe na poziomie białka są skorelowane ze zmianami w ekspresji mRNA testowanych genów.

Ponieważ wykazano, że u myszy *Blmh*^{-/-} poziomy HTL oraz *N-Hcy*-białek są podwyższone niemożliwe jest określenie, który z tych metabolitów powoduje wyżej wymienione zmiany w mózgu myszy. Podjęliśmy próbę rozwiązania tego problemu poprzez oddzielne traktowanie komórek N2a-APP_{swe} tymi metabolitami. Analizy western blot wykazały, że traktowanie komórek HTL oraz *N-Hcy*-białkami istotnie statystycznie obniża ilości Phf8, Atg5, Atg7 i Becn-1. Stosunek Lc3-II/I określany jako miara strumienia autofagii (ang. autophagy flux) był istotnie statystycznie obniżony jedynie po traktowaniu HTL. Jednocześnie, zastosowane metabolity prowadzą do istotnego statystycznie podwyższenia mTOR oraz pmTOR (z wyłączeniem HTL 20 μM). Dodatkowo większe stężenie HTL i *N-Hcy*-białek istotnie statystycznie podwyższały poziomy H4K20me1 oraz p62. W przypadku APP nie odnotowaliśmy jedynie istotnego statystycznie podwyższenia poziomu APP po traktowaniu 10 μM *N-Hcy*-białkiem. Uzyskane wyniki wskazują, że deficyt *Blmh* poprzez akumulację HTL oraz *N-Hcy*-białek prowadzi do zmian ilościowych Phf8, H4K20me1, APP, mTOR oraz markerów autofagii.

W celu potwierdzenia, że wyciszenie ekspresji *Blmh* prowadzi do zwiększenia ilości mTOR poprzez zmiany wiązania H4K20me1 do genu *mTOR* wykonaliśmy eksperymenty immunoprecypitacji chromatyny związanej z H4K20me1 połączonej z analizą rt-qPCR. Wykazaliśmy, że wyciszenie ekspresji *Blmh* prowadzi do istotnej statystycznie akumulacji H4K20me1 na TSS, powyżej TSS (-160 pz) oraz poniżej TSS (+320 pz) genu *mTOR*. Jednocześnie istotnie statystyczną większą ilość związanego H4K20me1 zaobserwowaliśmy na miejscu TSS w porównaniu do pozycji powyżej i poniżej TSS. Uzyskane wyniki wskazują, że wyciszenie ekspresji genu *Blmh* poprzez epigenetyczny mechanizm regulacji ekspresji genów prowadzi do zwiększonej ilości mTOR.

Analogiczne eksperymenty immunoprecypitacji chromatyny zostały wykonane dla komórek N2a-APP_{swe} po traktowaniu HTL oraz *N*-Hcy-białkami. 200 μ M stężenie HTL prowadziło do istotnie statystycznie większego wiązania H4K20me1 do trzech testowanych miejsc genu *mTOR* w porównaniu do próby kontrolnej. 20 μ M stężenie *N*-Hcy-białek i 20 μ M stężenie HTL prowadziło do istotnie statystycznie większego wiązania H4K20me1 do miejsca poniżej TSS oraz na TSS. W przypadku 10 μ M stężenia *N*-Hcy-białek obserwowano jedynie tendencje wzrostową na TSS genu *mTOR*.

Zastosowanie immunofluorescencyjnego barwienia A β w komórkach N2a-APP_{swe} po wyciszeniu ekspresji genu *Blmh* pozwoliło określić efekt deficytu *Blmh* na akumulację A β . Analizy wykazały, że wyciszenie ekspresji genu *Blmh* prowadzi do agregacji A β w porównaniu do prób kontrolnych (z ekspresją genu *Blmh*). Zmiany te charakteryzowały się istotnie statystycznie większą powierzchnią zajmowaną przez sygnały oraz istotnie statystycznie większym średnim rozmiarem pojedynczego sygnału.

Analogiczne eksperymenty immunobarwienia zostały wykonane po traktowaniu komórek N2a-APP_{swe} dwoma stężeniami HTL oraz *N*-Hcy-białkami. Wykazaliśmy, że traktowanie komórek HTL w stężeniu 20 i 200 μ M skutkuje istotnie statystycznie większą powierzchnią sygnału A β oraz istotnie statystycznie większym średnim rozmiarem pojedynczego sygnału w porównaniu do próby kontrolnej. W przypadku traktowania *N*-Hcy-białkiem w stężeniu 10 i 20 μ M wykazaliśmy jedynie istotnie statystycznie większą powierzchnię sygnału w porównaniu do próby kontrolnej. Uzyskane wyniki wskazują, że agregacja A β po wyciszeniu ekspresji genu *Blmh* może być rezultatem akumulacji HTL lub *N*-Hcy-białek.

W celu analizy czy deficyt *Blmh* oraz dieta HHcy prowadzą do agregacji A β wykonano analizy western blot na mózgach myszy *Blmh*^{-/-}5xFAD oraz *Blmh*^{+/+}5xFAD. Eksperymenty wykonano w 3 frakcjach białkowych: rozpuszczalnej w lizującym buforze radioimmunoprecypitacyjnym (ang. Radio-Immunoprecipitation Assay Buffer, RIPA), frakcji rozpuszczalnej w 2% siarczanie dodecyłu sodu (ang. sodium dodecyl sulfate, SDS) oraz frakcji rozpuszczalnej w 70% kwasie mrówkowym. Analizy dla 5 miesięcznych myszy wykazały istotnie statystycznie większe ilości A β we frakcji RIPA i SDS w mózgach myszy *Blmh*^{-/-}5xFAD w porównaniu do grupy *Blmh*^{+/+}5xFAD na diecie standardowej. Dieta HHcy nie skutkowała istotnym statystycznie zwiększeniem akumulacji A β w obu genotypach myszy. 12 miesięczne myszy *Blmh*^{-/-}5xFAD na diecie HHcy wykazały istotnie statystycznie większą agregację A β we wszystkich frakcjach w porównaniu do myszy *Blmh*^{+/+}5xFAD na diecie HHcy. Dodatkowo dieta HHcy u myszy

Blmh^{+/+}5xFAD prowadziła do akumulacji A β we wszystkich 3 frakcjach w porównaniu do myszy *Blmh*^{+/+}5xFAD na diecie standardowej.

W celu wykazania, że samo obniżenie poziomu Phf8 (bez manipulacji ekspresji genu *Blmh*) prowadzi do akumulacji A β poprzez deregulację mTOR oraz procesu autofagii, wykonano eksperymenty z wyciszoną ekspresją genu *Phf8* w komórkach N2a-APP_{swe}.

Metodą western blot wykazaliśmy, że obniżenie poziomu Phf8 prowadzi do istotnego statystycznie podniesienia poziomów H4K20me1, mTOR oraz pmTOR. Jednocześnie obserwowaliśmy istotne statystycznie obniżenie ilości Atg5 oraz Atg7. Poziom Becn-1 oraz APP nie ulegały zmianom po wyciszeniu ekspresji genu *Phf8* w porównaniu do prób kontrolnych.

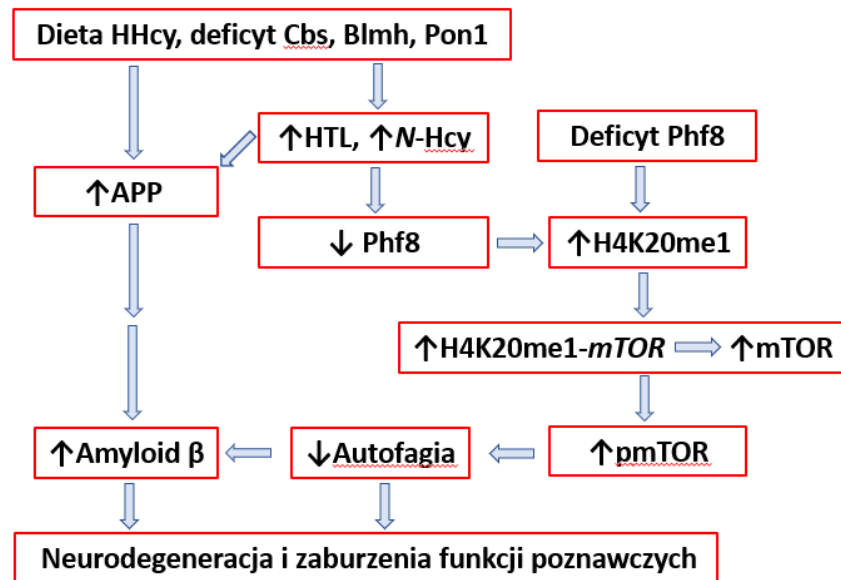
Wykazaliśmy, że wyciszenie ekspresji genu *Phf8* prowadziło do istotnej akumulacji A β poprzez zastosowanie techniki immunofluorescencyjnego barwienia A β . Wyciszenie ekspresji genu *Phf8* skutkowało istotnie statystycznie większą powierzchnią sygnałów oraz intensywnością sygnału.

Podsumowując wykazaliśmy, że *Blmh* odgrywa ważną rolę w prawidłowym funkcjonowaniu mózgu oraz chroni przed akumulacją A β . Odkryliśmy, że deficyt *Blmh* prowadzi do obniżenia ekspresji mRNA oraz ilości białka demetylazy histonowej Phf8 i wybranych markerów autofagii. Jednocześnie wykazaliśmy, że dochodzi do akumulacji APP oraz mTOR, którego ekspresja jest zależna od H4K20me1. Wykazaliśmy również, że akumulacja A β jest zależna od diety HHcy oraz genotypu myszy. Zaobserwowane zmiany w mózgach myszy zostały potwierdzone *in vitro* poprzez wyciszenie ekspresji genu *Blmh* oraz traktowanie komórek metabolitami (HTL, N-Hcy-białka), których poziomy są podwyższone w myszach *Blmh*^{-/-}. Wykazaliśmy, że wyciszenie ekspresji *Phf8* prowadzi do akumulacji A β , H4K20me1, mTOR pmTOR oraz obniżenia Atg5 i Atg7. Uzyskane wyniki nie wykazały wpływu wyciszenia ekspresji *Phf8* na APP co sugeruje, że w tym wypadku akumulacja A β wynika z zahamowania procesu autofagii.

Finalnie zaproponowaliśmy mechanizm prowadzący do rozwoju AD poprzez akumulację A β wynikającą z deregulacji mTOR/autofagii. Zmiany te są konsekwencją obniżenia ilości Phf8 co prowadzi do większego wiązania H4K20me1 na TSS genu *mTOR*. Zaproponowany mechanizm jest indukowany przez HTL, N-Hcy-białka oraz wyciszenie ekspresji genu *Blmh*.

4. Wnioski końcowe

Na podstawie uzyskanych wyników zaproponowano mechanizm wpływu deficytu *Cbs*, *Blmh* lub *Pon1* oraz diety wysokometioninowej (HHcy) na akumulację A β poprzez zaburzenia *Phf8*/H4K20me1 wpływające na szlak sygnałowy mTOR i proces autofagii oraz poprzez niezależną od *Phf8* stymulację ekspresji *APP* (Ryc. 1).



Ryc.1 Zaproponowany mechanizm wpływu deficytu *Blmh*, *Pon1* lub *Cbs* oraz diety HHcy na proces neurodegeneracji oraz zaburzenia funkcji poznawczych.

Wnioski szczegółowe:

1. Wykazaliśmy, że deficyt *Blmh* oraz dieta wysokometioninowa wywołują neurodegenerację oraz zaburzenia funkcji poznawczych u myszy. Inni badacze wykazali, że deficyt *Cbs* wywołuje neurodegenerację oraz zaburzenia funkcji poznawczych u myszy i ludzi.
2. Deficyt *Blmh*, *Pon1* lub *Cbs* oraz dieta wysokometioninowa podnoszą ilość APP i A β w mózgach myszy.
3. Deficyt *Blmh*, *Pon1* lub *Cbs* oraz dieta wysokometioninowa powodują podobne zmiany biochemiczne (wzrost poziomu HTL, *N*-Hcy-białek oraz Hcy), prowadzące do obniżenia ilości demetylasy histonowej *Phf8*, akumulacji H4K20me1, co prowadzi do aktywacji mTOR i zahamowania procesu autofagii w mózgach myszy. Obniżenie ekspresji *Phf8* również powoduje wzrost akumulacji A β poprzez aktywację szlaku H4K20me1->mTOR->autofagia.

5. Wykaz skrótów i rycin

A β – amyloid beta

AD – choroba Alzheimera

Atg – geny związane z autofagią

APP – prekursorowe białko amyloidu

Blmh – hydrolaza bleomycyny

Becn-1- Beklina 1

Bphl - białko podobne do hydrolazy biphenylu

Cbs – syntaza β -cystationiny

Dieta HHcy- dieta wysokometioninowa

Gfap – kwaśne białko włókienkowe

Hcy – homocysteina

HHcy – hiperhomocysteinemia

HTL – tiolakton homocysteiny

Lc3 - lekki łańcuch 3 białka związanego z mikrotubulami

mTOR- ssaczy cel rapamycyny

Nfl- łańcuch lekki neurofilamentu

NOR – test rozpoznawania nowego obiektu

pmTOR – fosforylowane białko mTOR na serynie 2441

Phf8 – demetylaza histonowa PHF8

Pon1 – paraoskonaza 1

PSEN1 – Presenilina 1

Pz – par zasad

RIPA- lizujący bufor radioimmunoprecypitacyjny

RT-qPCR - reakcja łańcuchowa polimerazy w czasie rzeczywistym

SAM - S-adenozylometionina

SDS – siarczan dodecyłu sodu

TSS – miejsce startu transkrypcji

Ryc. 1 strona 34

6. Bibliografia

1. Jakubowski H. Homocysteine Modification in Protein Structure/Function and Human Disease. *Physiol Rev.* styczeń 2019;99(1):555–604.
2. Jakubowski H. Homocysteine in protein structure/function and human disease. *Chem Biol Homocysteine Contain Proteins* Springer-Verl Wien Austria. 2013
3. Hasan T, Arora R, Bansal AK, Bhattacharya R, Sharma GS, Singh LR. Disturbed homocysteine metabolism is associated with cancer. *Exp Mol Med.* luty 2019;51(2):1–13.
4. Refsum H, Smith AD, Ueland PM, Nexø E, Clarke R, McPartlin J, i in. Facts and Recommendations about Total Homocysteine Determinations: An Expert Opinion. *Clin Chem.* 1 styczeń 2004;50(1):3–32.
5. Maron BA, Loscalzo J. The Treatment of Hyperhomocysteinemia. *Annu Rev Med.* 2009;60(1):39–54.
6. TA, Ranimenon. Homocysteine in ocular diseases. *Clin Chim Acta.* 23 październik 2015;450:316–21.
7. Refsum H, Nurk E, David Smith A, Ueland PM, Gjesdal CG, Bjelland I, i in. The Hordaland Homocysteine Study: A Community-Based Study of Homocysteine, Its Determinants, and Associations with Disease1. *J Nutr.* 1 czerwiec 2006;136(6):1731S-1740S.
8. Smith AD, Refsum H. Homocysteine, B Vitamins, and Cognitive Impairment. *Annu Rev Nutr.* 2016;36(1):211–39.
9. Smith AD, Refsum H. Homocysteine – from disease biomarker to disease prevention. *J Intern Med.* 2021;290(4):826–54.
10. Strauss KA, Morton DH, Puffenberger EG, Hendrickson C, Robinson DL, Wagner C, i in. Prevention of brain disease from severe 5,10-methylenetetrahydrofolate reductase deficiency. *Mol Genet Metab.* 1 czerwiec 2007;91(2):165–75.
11. Durga J, Boxtel MP van, Schouten EG, Kok FJ, Jolles J, Katan MB, i in. Effect of 3-year folic acid supplementation on cognitive function in older adults in the FACIT trial: a randomised, double blind, controlled trial. *The Lancet.* 20 styczeń 2007;369(9557):208–16.
12. Douaud G, Refsum H, de Jager CA, Jacoby R, E. Nichols T, Smith SM, i in. Preventing Alzheimer’s disease-related gray matter atrophy by B-vitamin treatment. *Proc Natl Acad Sci.* 4 czerwiec 2013;110(23):9523–8.
13. Smith AD, Smith SM, Jager CA de, Whitbread P, Johnston C, Agacinski G, i in. Homocysteine-Lowering by B Vitamins Slows the Rate of Accelerated Brain Atrophy in Mild Cognitive Impairment: A Randomized Controlled Trial. *PLOS ONE.* 8 wrzesień 2010;5(9):e12244.
14. Jakubowski H. Proofreading in Vivo: EDITING OF HOMOCYSTEINE BY AMINOACYL-tRNA SYNTHETASES IN ESCHERICHIA COLI(*). *J Biol Chem.* 28 lipiec 1995;270(30):17672–3.
15. Jakubowski H, R.Fersht A. Alternative pathways for editing non-cognate amino acids by aminoacyl-tRNA synthetases. *Nucleic Acids Res.* 10 lipiec 1981;9(13):3105–17.

16. Jakubowski H. Proofreading in vivo: editing of homocysteine by methionyl-tRNA synthetase in the yeast *Saccharomyces cerevisiae*. *EMBO J.* marzec 1991;10(3):593–8.
17. Jakubowski H. Proofreading in vivo: editing of homocysteine by methionyl-tRNA synthetase in *Escherichia coli*. *Proc Natl Acad Sci.* czerwiec 1990;87(12):4504–8.
18. Jakubowski H, Goldman E. Synthesis of homocysteine thiolactone by methionyl-tRNA synthetase in cultured mammalian cells. *FEBS Lett.* 1993;317(3):237–40.
19. Chwatko G, Jakubowski H. Urinary excretion of homocysteine-thiolactone in humans. *Clin Chem.* luty 2005;51(2):408–15.
20. Mercié P, Garnier O, Lascoste L, Renard M, Closse C, Durrieu F, i in. Homocysteine-thiolactone induces caspase-independent vascular endothelial cell death with apoptotic features. *Apoptosis.* 1 listopad 2000;5(5):403–11.
21. Huang RFS, Huang SM, Lin BS, Wei JS, Liu TZ. Homocysteine thiolactone induces apoptotic DNA damage mediated by increased intracellular hydrogen peroxide and caspase 3 activation in HL-60 cells. *Life Sci.* 11 maj 2001;68(25):2799–811.
22. Kamudhamas A, Pang L, Smith SD, Sadovsky Y, Nelson DM. Homocysteine thiolactone induces apoptosis in cultured human trophoblasts: a mechanism for homocysteine-mediated placental dysfunction? *Am J Obstet Gynecol.* 1 sierpień 2004;191(2):563–71.
23. Roybal CN, Yang S, Sun CW, Hurtado D, Jagt DLV, Townes TM, i in. Homocysteine Increases the Expression of Vascular Endothelial Growth Factor by a Mechanism Involving Endoplasmic Reticulum Stress and Transcription Factor ATF4 *. *J Biol Chem.* 9 kwiecień 2004;279(15):14844–52.
24. Najib S, Sanchez-Margalet V. Homocysteine thiolactone inhibits insulin signaling, and glutathione has a protective effect. *J Mol Endocrinol.* 1 sierpień 2001;27(1):85–91.
25. Najib S, Sánchez-Margalet V. Homocysteine thiolactone inhibits insulin-stimulated DNA and protein synthesis: possible role of mitogen-activated protein kinase (MAPK), glycogen synthase kinase-3 (GSK-3) and p70 S6K phosphorylation. *J Mol Endocrinol.* 1 luty 2005;34(1):119–26.
26. Endo N, Nishiyama K, Otsuka A, Kanouchi H, Taga M, Oka T. Antioxidant activity of vitamin B6 delays homocysteine-induced atherosclerosis in rats. *Br J Nutr.* czerwiec 2006;95(6):1088–93.
27. Harker LA, Ross R, Slichter SJ, Scott CR. Homocystine-induced arteriosclerosis. The role of endothelial cell injury and platelet response in its genesis. *J Clin Invest.* 1 wrzesień 1976;58(3):731–41.
28. Spence AM, Rasey JS, Dwyer-Hansen L, Grunbaum Z, Livesey J, Chin L, i in. Toxicity, biodistribution and radioprotective capacity of l-homocysteine thiolactone in CNS tissues and tumors in rodents: comparison with prior results with phosphorothioates. *Radiother Oncol.* 1 czerwiec 1995;35(3):216–26.
29. Langmeier M, Folbergrová J, Haugvicová R, Pokorný J, Mareš P. Neuronal Cell Death in Hippocampus Induced by Homocysteic Acid in Immature Rats. *Epilepsia.* 2003;44(3):299–304.
30. Folbergrová J. Anticonvulsant Action of both NMDA and Non-NMDA Receptor Antagonists against Seizures Induced by Homocysteine in Immature Rats. *Exp Neurol.* 1 czerwiec 1997;145(2):442–50.

31. Borowczyk K, Shih DM, Jakubowski H. Metabolism and Neurotoxicity of Homocysteine Thiolactone in Mice: Evidence for a Protective Role of Paraoxonase 1. *J Alzheimers Dis.* 1 styczeń 2012;30(2):225–31.
32. Borowczyk K, Tisończyk J, Jakubowski H. Metabolism and neurotoxicity of homocysteine thiolactone in mice: protective role of bleomycin hydrolase. *Amino Acids.* 1 wrzesień 2012;43(3):1339–48.
33. Jakubowski H. Protein homocysteinylation: possible mechanism underlying pathological consequences of elevated homocysteine levels. *FASEB J Off Publ Fed Am Soc Exp Biol.* grudzień 1999;13(15):2277–83.
34. Jakubowski H. Metabolism of homocysteine thiolactone in human cell cultures. Possible mechanism for pathological consequences of elevated homocysteine levels. *J Biol Chem.* 17 styczeń 1997;272(3):1935–42.
35. Jakubowski H. Pathophysiological consequences of homocysteine excess. *J Nutr.* czerwiec 2006;136(6 Suppl):1741S-1749S.
36. Paoli P, Sbrana F, Tiribilli B, Caselli A, Pantera B, Cirri P, i in. Protein N-homocysteinylation induces the formation of toxic amyloid-like protofibrils. *J Mol Biol.* 23 lipiec 2010;400(4):889–907.
37. Jakubowski H, Protein homocysteinylation: possible mechanism underlying pathological consequences of elevated homocysteine levels. *FASEB J Off Publ Fed Am Soc Exp Biol.* grudzień 1999;13(15):2277–83.
38. Jakubowski H. Homocysteine thiolactone: metabolic origin and protein homocysteinylation in humans. *J Nutr.* luty 2000;130(2S Suppl):377S-381S.
39. Jakubowski H, Boers GHJ, Strauss KA. Mutations in cystathionine β -synthase or methylenetetrahydrofolate reductase gene increase N-homocysteinylation protein levels in humans. *FASEB J.* 2008;22(12):4071–6.
40. Mackness B, Beltran-Debon R, Aragones G, Joven J, Camps J, Mackness M. Human tissue distribution of paraoxonases 1 and 2 mRNA. *IUBMB Life.* czerwiec 2010;62(6):480–2.
41. Leduc V, Legault V, Dea D, Poirier J. Normalization of gene expression using SYBR green qPCR: a case for paraoxonase 1 and 2 in Alzheimer's disease brains. *J Neurosci Methods.* 30 sierpień 2011;200(1):14–9.
42. Jakubowski H, Ambrosius WT, Pratt JH. Genetic determinants of homocysteine thiolactonase activity in humans: implications for atherosclerosis. *FEBS Lett.* 23 luty 2001;491(1–2):35–9.
43. Humbert R, Adler DA, Disteché CM, Hassett C, Omiecinski CJ, Furlong CE. The molecular basis of the human serum paraoxonase activity polymorphism. *Nat Genet.* styczeń 1993;3(1):73–6.
44. Shih DM, Gu L, Xia YR, Navab M, Li WF, Hama S, i in. Mice lacking serum paraoxonase are susceptible to organophosphate toxicity and atherosclerosis. *Nature.* 16 lipiec 1998;394(6690):284–7.
45. Shih DM, Xia YR, Wang XP, Miller E, Castellani LW, Subbanagounder G, i in. Combined serum paraoxonase knockout/apolipoprotein E knockout mice exhibit increased lipoprotein oxidation and atherosclerosis. *J Biol Chem.* 9 czerwiec 2000;275(23):17527–35.

46. Erlich PM, Lunetta KL, Cupples LA, Abraham CR, Green RC, Baldwin CT, i in. Serum paraoxonase activity is associated with variants in the PON gene cluster and risk of Alzheimer disease. *Neurobiol Aging*. maj 2012;33(5):1015.e7-23.
47. Dantoine TF, Debord J, Merle L, Lacroix-Ramiandrisoa H, Bourzeix L, Charmes JP. Paraoxonase 1 activity: a new vascular marker of dementia? *Ann N Y Acad Sci*. listopad 2002;977:96–101.
48. Perła-Kaján J, Włoczkowska O, Ziola-Frankowska A, Frankowski M, Smith AD, de Jager CA, i in. Paraoxonase 1, B Vitamins Supplementation, and Mild Cognitive Impairment. *J Alzheimers Dis JAD*. 2021;81(3):1211–29.
49. Salazar JG, Marsillach J, Reverte I, Mackness B, Mackness M, Joven J, i in. Paraoxonase-1 and -3 Protein Expression in the Brain of the Tg2576 Mouse Model of Alzheimer's Disease. *Antioxidants*. marzec 2021;10(3):339.
50. Moren X, Lhomme M, Bulla A, Sanchez JC, Kontush A, James RW. Proteomic and lipidomic analyses of paraoxonase defined high density lipoprotein particles: Association of paraoxonase with the anti-coagulant, protein S. *PROTEOMICS – Clin Appl*. 2016;10(3):230–8.
51. Zimny J, Sikora M, Guranowski A, Jakubowski H. Protective mechanisms against homocysteine toxicity: the role of bleomycin hydrolase. *J Biol Chem*. 11 sierpień 2006;281(32):22485–92.
52. Suszyńska-Zajczyk J, Łuczak M, Marczak Ł, Jakubowski H. Hyperhomocysteinemia and Bleomycin Hydrolase Modulate the Expression of Mouse Brain Proteins Involved in Neurodegeneration. *J Alzheimers Dis*. 1 styczeń 2014;40(3):713–26.
53. Montoya SE, Thiels E, Card JP, Lazo JS. Astroglial and behavioral changes in mice lacking the neutral cysteine protease bleomycin hydrolase. *Neuroscience*. 25 maj 2007;146(3):890–900.
54. Ratovitski T, Chighladze E, Waldron E, Hirschhorn RR, Ross CA. Cysteine proteases bleomycin hydrolase and cathepsin Z mediate N-terminal proteolysis and toxicity of mutant huntingtin. *J Biol Chem*. 8 kwiecień 2011;286(14):12578–89.
55. Namba Y, Ouchi Y, Takeda A, Ueki A, Ikeda K. Bleomycin hydrolase immunoreactivity in senile plaque in the brains of patients with Alzheimer's disease. *Brain Res*. 29 maj 1999;830(1):200–2.
56. Suszynska J, Tisonczyk J, Lee H gon, Smith MA, Jakubowski H. Reduced homocysteine-thiolactonase activity in Alzheimer's disease. *J Alzheimers Dis JAD*. 2010;19(4):1177–83.
57. Montoya SE, Aston CE, DeKosky ST, Kamboh MI, Lazo JS, Ferrell RE. Bleomycin hydrolase is associated with risk of sporadic Alzheimer's disease. *Nat Genet*. marzec 1998;18(3):211–2.
58. Papassotiropoulos A, Bagli M, Jessen F, Frahnert C, Rao ML, Maier W, i in. Confirmation of the association between bleomycin hydrolase genotype and Alzheimer's disease. *Mol Psychiatry*. marzec 2000;5(2):213–5.
59. Abbott MH, Folstein SE, Abbey H, Pyeritz RE, Opitz JM. Psychiatric manifestations of homocystinuria due to cystathionine β -synthase deficiency: Prevalence, natural history, and relationship to neurologic impairment and vitamin B6-responsiveness. *Am J Med Genet*. 1987;26(4):959–69.
60. El Bashir H, Dekair L, Mahmoud Y, Ben-Omran T. Neurodevelopmental and Cognitive Outcomes of Classical Homocystinuria: Experience from Qatar. *JIMD Rep*. 25 luty 2015;21:89–95.

61. Majtan T, Park I, Cox A, Branchford BR, di Paola J, Bublil EM, i in. Behavior, body composition, and vascular phenotype of homocystinuric mice on methionine-restricted diet or enzyme replacement therapy. *FASEB J Off Publ Fed Am Soc Exp Biol.* listopad 2019;33(11):12477–86.
62. Akahoshi N, Kobayashi C, Ishizaki Y, Izumi T, Himi T, Suematsu M, i in. Genetic background conversion ameliorates semi-lethality and permits behavioral analyses in cystathionine beta-synthase-deficient mice, an animal model for hyperhomocysteinemia. *Hum Mol Genet.* 1 lipiec 2008;17(13):1994–20051
63. Di Meco A, Li JG, Praticò D. Dissecting the Role of 5-Lipoxygenase in the Homocysteine-Induced Alzheimer’s Disease Pathology. Perry G, Avila J, Tabaton M, Zhu X, redaktorzy. *J Alzheimers Dis.* 13 marzec 2018;62(3):1337–44.
64. Khayati K, Antikainen H, Bonder EM, Weber GF, Kruger WD, Jakubowski H, i in. The amino acid metabolite homocysteine activates mTORC1 to inhibit autophagy and form abnormal proteins in human neurons and mice. *FASEB J Off Publ Fed Am Soc Exp Biol.* luty 2017;31(2):598–609.
65. Loewith R, Jacinto E, Wullschleger S, Lorberg A, Crespo JL, Bonenfant D, i in. Two TOR complexes, only one of which is rapamycin sensitive, have distinct roles in cell growth control. *Mol Cell.* wrzesień 2002;10(3):457–68.
66. Oddo S. The role of mTOR signaling in Alzheimer disease. *Front Biosci-Sch.* 1 styczeń 2012;4(3):941–52.
67. Wullschleger S, Loewith R, Hall MN. TOR Signaling in Growth and Metabolism. *Cell.* 10 luty 2006;124(3):471–84.
68. Chiang GG, Abraham RT. Phosphorylation of Mammalian Target of Rapamycin (mTOR) at Ser-2448 Is Mediated by p70S6 Kinase *. *J Biol Chem.* 8 lipiec 2005;280(27):25485–90.
69. Ryskalin L, Limanaqi F, Frati A, Busceti CL, Fornai F. mTOR-Related Brain Dysfunctions in Neuropsychiatric Disorders. *Int J Mol Sci.* sierpień 2018;19(8):2226.
70. Chrienova Z, Nepovimova E, Kuca K. The role of mTOR in age-related diseases. *J Enzyme Inhib Med Chem.* 1 styczeń 2021;36(1):1678–92.
71. An WL, Cowburn RF, Li L, Braak H, Alafuzoff I, Iqbal K, i in. Up-Regulation of Phosphorylated/Activated p70 S6 Kinase and Its Relationship to Neurofibrillary Pathology in Alzheimer’s Disease. *Am J Pathol.* 1 sierpień 2003;163(2):591–607.
72. Pei JJ, Hugon J. mTOR-dependent signalling in Alzheimer’s disease. *J Cell Mol Med.* 2008;12(6b):2525–32.
73. Ehninger D, Han S, Shilyansky C, Zhou Y, Li W, Kwiatkowski DJ, i in. Reversal of learning deficits in a Tsc2+/- mouse model of tuberous sclerosis. *Nat Med.* sierpień 2008;14(8):843–8.
74. Glick D, Barth S, Macleod KF. Autophagy: cellular and molecular mechanisms. *J Pathol.* 2010;221(1):3–12.
75. Axe EL, Walker SA, Manifava M, Chandra P, Roderick HL, Habermann A, i in. Autophagosome formation from membrane compartments enriched in phosphatidylinositol 3-phosphate and dynamically connected to the endoplasmic reticulum. *J Cell Biol.* 25 sierpień 2008;182(4):685–701.

76. Simonsen A, Tooze SA. Coordination of membrane events during autophagy by multiple class III PI3-kinase complexes. *J Cell Biol.* 21 wrzesień 2009;186(6):773–82.
77. Mizushima N. Autophagy: process and function. *Genes Dev.* 15 listopad 2007;21(22):2861–73.
78. Díaz-Troya S, Pérez-Pérez ME, Florencio FJ, Crespo JL. The role of TOR in autophagy regulation from yeast to plants and mammals. *Autophagy.* 1 październik 2008;4(7):851–65.
79. Kundu M, Lindsten T, Yang CY, Wu J, Zhao F, Zhang J, i in. Ulk1 plays a critical role in the autophagic clearance of mitochondria and ribosomes during reticulocyte maturation. *Blood.* 15 sierpień 2008;112(4):1493–502.
80. Funderburk SF, Marcellino BK, Yue Z. Cell “Self-Eating” (Autophagy) Mechanism in Alzheimer’s Disease. *Mt Sinai J Med J Transl Pers Med.* 2010;77(1):59–68.
81. Qi HH, Sarkissian M, Hu GQ, Wang Z, Bhattacharjee A, Gordon DB, i in. Histone H4K20/H3K9 demethylase PHF8 regulates zebrafish brain and craniofacial development. *Nature.* lipiec 2010;466(7305):503–7.
82. Liu W, Tanasa B, Tyurina OV, Zhou TY, Gassmann R, Liu WT, i in. PHF8 mediates histone H4 lysine 20 demethylation events involved in cell cycle progression. *Nature.* lipiec 2010;466(7305):508–12.
83. Kleine-Kohlbrecher D, Christensen J, Vandamme J, Abarategui I, Bak M, Tommerup N, i in. A Functional Link between the Histone Demethylase PHF8 and the Transcription Factor ZNF711 in X-Linked Mental Retardation. *Mol Cell.* 23 kwiecień 2010;38(2):165–78.
84. Zhu Z, Wang Y, Li X, Wang Y, Xu L, Wang X, i in. PHF8 is a histone H3K9me2 demethylase regulating rRNA synthesis. *Cell Res.* lipiec 2010;20(7):794–801.
85. Chen X, Wang S, Zhou Y, Han Y, Li S, Xu Q, i in. Phf8 histone demethylase deficiency causes cognitive impairments through the mTOR pathway. *Nat Commun.* 9 styczeń 2018;9(1):114.
86. Abidi F, Miano M, Murray J, Schwartz C. A novel mutation in the PHF8 gene is associated with X-linked mental retardation with cleft lip/cleft palate. *Clin Genet.* 2007;72(1):19–22.
87. Koivisto A, Ala-Mello S, Lemmelä S, Komu H, Rautio J, Järvelä I. Screening of mutations in the PHF8 gene and identification of a novel mutation in a Finnish family with XLMR and cleft lip/cleft palate. *Clin Genet.* 2007;72(2):145–9.
88. Laumonier F, Holbert S, Ronce N, Faravelli F, Lenzner S, Schwartz CE, i in. Mutations in PHF8 are associated with X linked mental retardation and cleft lip/cleft palate. *J Med Genet.* 1 październik 2005;42(10):780–6.
89. Sobering AK, Bryant LM, Li D, McGaughran J, Maystadt I, Moortgat S, i in. Variants in PHF8 cause a spectrum of X-linked neurodevelopmental disorders and facial dysmorphology. *HGG Adv.* 14 lipiec 2022;3(3):100102.
90. Qiu J, Shi G, Jia Y, Li J, Wu M, Li J, i in. The X-linked mental retardation gene PHF8 is a histone demethylase involved in neuronal differentiation. *Cell Res.* sierpień 2010;20(8):908–18.

91. Shoaib M, Chen Q, Shi X, Nair N, Prasanna C, Yang R, i in. Histone H4 lysine 20 mono-methylation directly facilitates chromatin openness and promotes transcription of housekeeping genes. *Nat Commun.* 20 sierpień 2021;12(1):4800.
92. Ferrari C, Sorbi S. The complexity of Alzheimer's disease: an evolving puzzle. *Physiol Rev.* lipiec 2021;101(3):1047–81.
93. Förstl H, Kurz A. Clinical features of Alzheimer's disease. *Eur Arch Psychiatry Clin Neurosci.* 1 grudzień 1999;249(6):288–90.
94. Cations M, Draper B, Low LF, Radford K, Trollor J, Brodaty H, i in. Non-Genetic Risk Factors for Degenerative and Vascular Young Onset Dementia: Results from the INSPIRED and KGOW Studies. *J Alzheimers Dis.* 1 styczeń 2018;62(4):1747–58.
95. Shea YF, Chu LW, Chan AOK, Ha J, Li Y, Song YQ. A systematic review of familial Alzheimer's disease: Differences in presentation of clinical features among three mutated genes and potential ethnic differences. *J Formos Med Assoc.* 1 luty 2016;115(2):67–75.
96. Haass C, Kaether C, Thinakaran G, Sisodia S. Trafficking and Proteolytic Processing of APP. *Cold Spring Harb Perspect Med.* 5 styczeń 2012;2(5):a006270.
97. Liu CC, Kanekiyo T, Xu H, Bu G. Apolipoprotein E and Alzheimer disease: risk, mechanisms and therapy. *Nat Rev Neurol.* luty 2013;9(2):106–18.
98. Zhang Y wu, Thompson R, Zhang H, Xu H. APP processing in Alzheimer's disease. *Mol Brain.* 7 styczeń 2011;4(1):3.
99. Seuma M, Lehner B, Bolognesi B. An atlas of amyloid aggregation: the impact of substitutions, insertions, deletions and truncations on amyloid beta fibril nucleation. *Nat Commun.* 18 listopad 2022;13(1):7084.
100. Sengupta U, Nilson AN, Kaye R. The Role of Amyloid- β Oligomers in Toxicity, Propagation, and Immunotherapy. *eBioMedicine.* 1 kwiecień 2016;6:42–9.
101. Carrillo-Mora P, Luna R, Colín-Barenque L. Amyloid Beta: Multiple Mechanisms of Toxicity and Only Some Protective Effects? *Oxid Med Cell Longev.* 5 luty 2014;2014:e795375.
102. Shankar GM, Walsh DM. Alzheimer's disease: synaptic dysfunction and A β . *Mol Neurodegener.* 23 listopad 2009;4(1):48.
103. Oakley H, Cole SL, Logan S, Maus E, Shao P, Craft J, i in. Intraneuronal β -Amyloid Aggregates, Neurodegeneration, and Neuron Loss in Transgenic Mice with Five Familial Alzheimer's Disease Mutations: Potential Factors in Amyloid Plaque Formation. *J Neurosci.* 4 październik 2006;26(40):10129–40.
104. Mullan M, Crawford F, Axelman K, Houlden H, Lilius L, Winblad B, i in. A pathogenic mutation for probable Alzheimer's disease in the APP gene at the N-terminus of β -amyloid. *Nat Genet.* sierpień 1992;1(5):345–7.
105. Eckman CB, Mehta ND, Crook R, Perez-tur J, Prihar G, Pfeiffer E, i in. A New Pathogenic Mutation in the APP Gene (I716V) Increases the Relative Proportion of A β 42(43). *Hum Mol Genet.* 1 listopad 1997;6(12):2087–9.

106. Goate A, Chartier-Harlin MC, Mullan M, Brown J, Crawford F, Fidani L, et al. Segregation of a missense mutation in the amyloid precursor protein gene with familial Alzheimer's disease. *Nature*. luty 1991;349(6311):704–6.
107. Esler WP, Wolfe MS. A Portrait of Alzheimer Secretases--New Features and Familiar Faces. *Science*. 24 sierpień 2001;293(5534):1449–54.
108. Flanigan TJ, Xue Y, Kishan Rao S, Dhanushkodi A, McDonald MP. Abnormal vibrissa-related behavior and loss of barrel field inhibitory neurons in 5xFAD transgenics. *Genes Brain Behav*. 2014;13(5):488–500.

7. Publikacje wchodzące w skład rozprawy doktorskiej

1. **Witucki Ł**, Jakubowski H,

Depletion of Paraoxonase 1 (Pon1) Dysregulates mTOR, Autophagy, and
Accelerates Amyloid Beta Accumulation in Mice,

Cells 2023, 12(5), 746 DOI: 10.3390/cells12050746

Pięcioletni IF: 7.677, MEiN 140 punktów

Article

Depletion of Paraoxonase 1 (Pon1) Dysregulates mTOR, Autophagy, and Accelerates Amyloid Beta Accumulation in Mice

Łukasz Witucki^{1,2}  and Hieronim Jakubowski^{1,2,*} 



Citation: Witucki, Ł.; Jakubowski, H. Depletion of Paraoxonase 1 (Pon1) Dysregulates mTOR, Autophagy, and Accelerates Amyloid Beta Accumulation in Mice. *Cells* **2023**, *12*, 746. <https://doi.org/10.3390/cells12050746>

Academic Editor: Hermona Soreq

Received: 20 January 2023

Revised: 16 February 2023

Accepted: 22 February 2023

Published: 26 February 2023



Copyright: © 2023 by the authors. Licensee MDPI, Basel, Switzerland. This article is an open access article distributed under the terms and conditions of the Creative Commons Attribution (CC BY) license (<https://creativecommons.org/licenses/by/4.0/>).

¹ Department of Biochemistry and Biotechnology, Poznań

University of Life Sciences, 60-637 Poznań, Poland

² Department of Microbiology, Biochemistry and Molecular Genetics, International Center for Public Health, New Jersey Medical School, Rutgers University, Newark, NJ 07103, USA

* Correspondence: jakubows@rutgers.edu; Tel.: +48-973-972-8733; Fax: +48-973-972-8981

Abstract: Paraoxonase 1 (PON1), a homocysteine (Hcy)-thiolactone detoxifying enzyme, has been associated with Alzheimer's disease (AD), suggesting that PON1 plays an important protective role in the brain. To study the involvement of PON1 in the development of AD and to elucidate the mechanism involved, we generated a new mouse model of AD, the *Pon1*^{-/-}xFAD mouse, and examined how Pon1 depletion affects mTOR signaling, autophagy, and amyloid beta (Aβ) accumulation. To elucidate the mechanism involved, we examined these processes in N2a-APP_{swe} cells. We found that Pon1 depletion significantly downregulated Phf8 and upregulated H4K20me1; mTOR, phospho-mTOR, and App were upregulated while autophagy markers Bcln1, Atg5, and Atg7 were downregulated at the protein and mRNA levels in the brains of *Pon1*^{-/-}5xFAD vs. *Pon1*^{+/+}5xFAD mice. Pon1 depletion in N2a-APP_{swe} cells by RNA interference led to downregulation of Phf8 and upregulation of mTOR due to increased H4K20me1-*mTOR* promoter binding. This led to autophagy downregulation and significantly increased APP and Aβ levels. Phf8 depletion by RNA interference or treatments with Hcy-thiolactone or *N*-Hcy-protein metabolites similarly increased Aβ levels in N2a-APP_{swe} cells. Taken together, our findings define a neuroprotective mechanism by which Pon1 prevents Aβ generation.

Keywords: APP; amyloid beta; *Pon1*^{-/-}5xFAD mouse model; N2a-APP_{swe} cells; Pon1; homocysteine thiolactone; Phf8; H4K20me1; mTOR; autophagy

Introduction

Paraoxonase 1 (PON1), named for its ability to hydrolyze and inactivate the organophosphate paraoxon, is synthesized exclusively in the liver, circulates in the blood as a component of high-density lipoproteins (HDL) [1], and is present in many organs, including the brain [2]. In addition to protecting from organophosphate toxicity [3], PON1 protects against atherosclerosis induced by a high-fat diet [4] or ApoE depletion [5] in mice. Large-scale human studies showed that high arylesterase activity of PON1 protects from cardiovascular disease (CVD) in patients with coronary artery disease undergoing elective diagnostic coronary angiography [6,7] and in patients with chronic kidney disease [8], while low homocysteine thiolactonase activity of PON1 was associated with worse long-term mortality [9]. In the PREVENT prospective study involving 6902 participants, PON1 activity predicted CVD events [10]. The cardioprotective function of PON1 can be due both to its antioxidative function [4,6,11] and the ability to detoxify homocysteine (Hcy)thiolactone [12–15], thereby attenuating lipid peroxidation, oxidative protein modification, and protein *N*-homocysteinylation.

PON1 has also been implicated in Alzheimer's disease (AD) [16,17], which can be expected given that AD has a significant vascular component [18]. For example, PON1 activity is lower in AD and dementia patients compared with healthy controls [19–22]

and correlates with the severity of AD-related cognitive decline [23]. In patients with mild cognitive impairment, PON1 activity predicted global cognition, verbal episodic memory, and attention/processing speed [24]. In mice, *ApoE^{-/-}Pon1^{-/-}* animals, which have severe carotid atherosclerosis [5], showed AD markers and impaired vasculature in their brains at 14 months, although it was not clear whether brain pathology was caused by *ApoE^{-/-}*, *Pon1^{-/-}*, or both knockouts [25]. In a mouse model of AD (Tg2576), immunohistochemical fluorescence signals for Pon1 protein in various regions of the brain were found to surround A β plaques but could not be colocalized to any brain cell type [26].

Deletion of the *Pon1* gene in mice impairs the metabolic conversion of Hcy-thiolactone to Hcy, increases brain Hcy-thiolactone levels, and makes the animals overly sensitive to the neurotoxicity of Hcy-thiolactone injections [12]. Studies of *Pon1^{-/-}* mouse brain proteome demonstrated that Pon1 interacts with diverse cellular processes, such as energy metabolism, anti-oxidative defenses, cell cycle, cytoskeleton dynamics, and synaptic plasticity, that are essential for brain homeostasis [27]. Clusterin (CLU or APOJ), involved in the transport of amyloid beta (A β) from plasma to brain in humans (reviewed in [28]), is carried on a distinct HDL subspecies that contains three major proteins: PON1, CLU, and APOA1 [29]. Notably, levels of Clu (ApoJ) are significantly elevated in the plasma of *Pon1^{-/-}* vs. *Pon1^{+/+}* mice [30]. These findings suggest that Pon1 plays a key role in brain homeostasis, possibly protecting from A β accumulation.

The present work was undertaken to examine the effects of Pon1 depletion on A β levels in a novel model of AD, the *Pon1^{-/-}5xFAD* mouse, generated in the present study and to elucidate the mechanism involved. Because dysregulated mTOR signaling and autophagy have been implicated in A β accumulation in Alzheimer's disease [31,32], and H4K20me1 demethylation by PHF8 is important for maintaining homeostasis of mTOR signaling [33], we studied how these processes are affected by Pon1 depletion in the mouse neuroblastoma N2a-APP_{swE} cells and *Pon1^{-/-}5xFAD* mice. We also examined how changes in these processes affect the behavioral performance of *Pon1^{-/-}5xFAD* mice.

2. Materials and Methods

2.1. Mice

Pon1^{-/-} [4] mice (kindly provided by Diane M. Shih) and 5xFAD mice [34] (The Jackson Laboratory, Bar Harbor, Maine, USA) on the C57BL/6J background were housed and bred at the New Jersey Medical School Animal Facility. 5xFAD mice overexpress the K670N/M671L (Swedish), I716V (Florida), and V717I (London) mutations in human APP (695), and M146L and L286V mutations in human PS1 and accumulate high levels of A β 42 beginning around 2 months of age [35] (<https://www.alzforum.org/researchmodels/5xfad-b6sji>) (accessed 27 December 2022). The *Pon1^{-/-}* mice were crossed with 5xFAD animals to generate *Pon1^{-/-}5xFAD* mice and their *Pon1^{+/+}5xFAD* sibling controls. Mouse *Pon1* genotype was established by PCR of tail clips DNA using the Pon1 forward primer p1 (5'-TGGGCTGCAGGTCTCAGGACTGA-3'), Pon1 exon 1 reverse primer p2 (5'-ATAGGAAGACCGATGGTTCT-3'), and neomycin cassette reverse primer p3 (5'-TCCTCGTGCTTTACGGTATCG-3') [4]. The Pon1 genotype was also confirmed by RTqPCR assays, which did not detect any Pon1 mRNA in the brains of *Pon1^{-/-}5xFAD* mice but showed robust expression of Pon1 mRNA in the brains of their *Pon1^{+/+}5xFAD* siblings.

The 5xFAD genotype was established using human APP and PS1 primers (hAPP forward 5'-AGAGTACCAACTTGCATGACTACG-3' and reverse 5'-ATGCTGGATAACTGCC TTCTTATC-3'; hPS1 forward 5'-GCTTTTCCAGCTCTCATTACTC-3' and reverse 5'-

AAAATTGATGGAATGCTAATTGGT-3'). The mice were fed a standard rodent chow diet (LabDiet 5010, Purina Mills International, St. Louis, MO, USA).

Water supplemented with 1% methionine was used to induce hyperhomocysteinemia [12,27]. The high Met diet increases plasma total Hcy levels 5.6- and 10.4-fold in *Pon1^{-/-}* (from 8.5 to 48 μ M) and *Pon1^{+/+}* mice (from

7.4 to 77 μ M) [27]. Animal procedures were approved by the Institutional Animal Care and Use Committee at the New Jersey Medical School.

2.2. Brain Protein Extraction

Mice were euthanized by CO₂ inhalation; the brains were collected and frozen on dry ice. Frozen brains were pulverized with dry ice using a mortar and pestle and stored at -80° C. Proteins were extracted from the pulverized brains (50 ± 5 mg; 30 ± 3 mg brain was used for A β analyses) using RIPA buffer (4 v/w, containing protease and phosphatase inhibitors) with sonication (Bandelin SONOPLUS HD 2070) on wet ice (three sets of five 1-s strokes with 1 min cooling interval between strokes). Brain extracts were clarified by centrifugation ($15,000\times g$, 30 min, 4° C) and clear supernatants containing 8–12 mg protein/mL were collected (RIPA-soluble fraction). Protein concentrations were measured with BCA kit (Thermo Fisher Scientific, Waltham, MA, USA).

For A β analyses, pellets remaining after protein extraction with RIPA buffer were reextracted by brief sonication in 2% SDS, centrifuged ($15,000\times g$, 15 min, room temperature), and the supernatants collected again (SDS-soluble fraction). The SDS-extracted pellets were then extracted by sonication in 70% formic acid (FA), centrifuged, and the supernatants were collected (the FA-soluble fraction) [35].

2.3. A β Quantification

A β was quantified using a dot blot assay [36]. Briefly, brain protein extracts (1 μ L) were spotted onto the nitrocellulose membranes and dried (37° C, 1 h). The membranes were washed with TBST buffer (RT, 15 min) and blocked with 5% BSA in TBST buffer (RT, 1 h). Blocked membranes were washed three times with TBST buffer (10 min each) and incubated with monoclonal anti-A β antibody (CS #8243; 4° C, 16 h). Membranes were then washed three times with TBST buffer (10 min each) and incubated with goat horseradish peroxidase-conjugated anti-rabbit IgG secondary antibody. Positive signals were detected using Western Bright Quantum-Advansta K12042-D20 and GeneGnome XRQ NPC chemiluminescence detection system. Signal intensity was assessed using the Gene Tools program from Syngene.

2.4. Cell Culture and Treatments

Mouse neuroblastoma N2a-APP^{swE} cells, harboring a human APP transgene with the K670N and M671L Swedish mutations [37] were grown (37° C, 5% CO₂) in DMEM/F12 medium (Thermo Fisher Scientific, Waltham, MA, USA) supplemented with 5% FBS, nonessential amino acids, and antibiotics (MilliporeSigma, Saint Louis, MO, USA).

After cells reached 70–80% confluency, the monolayers were washed twice with PBS and overlaid with DMEM medium without methionine (Thermo Scientific), supplemented with 5% dialyzed fetal bovine serum (FBS) (MilliporeSigma) and non-essential amino acids. L-Hcy-thiolactone (20 and 200 μ M) (MilliporeSigma) or N-Hcy-protein (10 and 20 μ M), prepared as described in ref. [38], were added, and the cultures were incubated at 37° C in a 5% CO₂ atmosphere for 24 h.

For gene silencing, siRNAs targeting the *Pon1* (Cat. # s71950 and s71951) or *Phf8* gene (Cat. # s115808, and s115809) (Thermo Scientific) were transfected into cells maintained in Opti-MEM medium by 48-h Lipofectamine RNAiMax (Thermo Scientific) treatments. Cellular RNA for RT-qPCR analysis was isolated as described in Section 2.5. For protein extraction, RIPA buffer (MilliporeSigma) was used according to the manufacturer's protocol.

2.5. Western Blots

Proteins were separated by SDS-PAGE on 10% gels (20 μ g protein/lane) and transferred to a PVDF membrane (Bio-Rad) for 20 min at 0.1 A, 25 V using the Trans Blot Turbo Transfer System (Bio-Rad). After blocking with 5% bovine serum albumin in TBST buffer (1 h, room temperature), the membranes were incubated with monoclonal anti-Pon1 (ab126597, Abcam, Cambridge, MA, USA), anti-Phf8 (Abcam, ab36068), anti-H4K20me1 (Abcam ab177188), anti-mTOR (Cell Signaling Technology, Danvers, MA, USA, CS #2983), anti-pmTOR Ser2448 (CS, #5536), anti-Atg5 (CS, #12994), anti-Atg7 (CS, #8558), anti-Becn1 (CS, #3495), anti-Gapdh (CS, #5174), or

anti-App (Abcam, ab126732) overnight at 4 °C. Membranes were washed three times with TBST buffer, for 10 min each, and incubated with goat anti-rabbit IgG secondary antibody conjugated with horseradish peroxidase. Positive signals were detected using Western Bright Quantum-Advansta K12042-D20 and GeneGnome XRQ NPC chemiluminescence detection system. Band intensity was calculated using the Gene Tools program from Syngene.

2.6. RNA Isolation, cDNA Synthesis, RT-qPCR Analysis

Total RNA was isolated using Trizol reagent (MilliporeSigma). cDNA synthesis was conducted using Revert Aid First cDNA Synthesis Kit (Thermo Fisher Scientific) according to the manufacturer's protocol. Nucleic acid concentration was measured using NanoDrop (Thermo Fisher Scientific). RT-qPCR was performed with SYBR Green Mix and CFX96 thermocycler (Bio-Rad, Hercules, CA, USA). The $2^{-\Delta\Delta Ct}$ method was used to calculate the relative expression levels [39]. Data analysis was performed with the CFX Manager™ Software, Microsoft Excel, and Statistica. RT-qPCR primer sequences are listed in Table S1.

2.7. Chromatin Immunoprecipitation Assay

For CHIP assays we used CUT&RUN Assay Kit #86652 (Cell Signaling Technology, Danvers, MA, USA) following the manufacturer's protocol. Each CHIP assay was repeated three times. Briefly, for each reaction, we used 100,000 cells. Cells were trypsinized and harvested, washed 3× in ice-cold PBS, and bound to concanavalin A-coated magnetic beads for 5 min, at RT. Cells were then incubated (4 h, 4 °C) with 2.5 µg of anti-PHF8 antibody (Abcam, ab36068) or anti-H4K20me1 antibody (Abcam, ab177188) in the antibody-binding buffer plus digitonin that permeabilizes cells. Next, cells were treated with pAG-MNase (1 h, 4 °C), washed, and treated with CaCl₂ to activate DNA digestion (0.5 h, 4 °C). Cells were then treated with the stop buffer and spike-in DNA was added for each reaction for signal normalization, and incubated (10–30 min, 37 °C). Released DNA fragments were purified using DNA Purification Buffers and Spin Columns (CS #14209) and quantified by RT-qPCR using primers targeting the promoter, upstream, and downstream regions of the *mTOR* gene (Table S1). Rabbit (DA1E) mAb IgG XP® Isotype Control included in the CUT&RUN kit did not afford any signals in the RT-qPCR assays targeting *mTOR*.

2.8. Confocal Microscopy, A β Quantification in N2a-APPswe Cells

Mouse neuroblastoma N2a-APPswe cells were cultured in Millicell EZ SLIDE 8-well glass slides (Merck, Darmstadt, Germany). After treatments, cells were washed 3 times with PBS for 10 min. Cells were fixed with 4% PFA (MilliporeSigma) (37 °C, 15 min), washed 3 times with PBS buffer, permeabilized with 0.1% Triton X-100 solution (RT, 20 min), blocked with 0.1% BSA (RT, 1h), and incubated with anti-A β antibody (CS #8243; 4 °C, 16 h). Cells were then washed 3 times with PBS and stained with secondary antibody Goat Anti-Rabbit IgG H&L (Alexa Fluor® 488) (Abcam, ab150077; RT, 1 h) to visualize and quantify A β . DAPI (Vector Laboratories, Newark, CA, USA) was used to visualize nuclei. Fluorescence signals were monitored by using a Zeiss LSM 880 confocal microscope with a 488 nm filter for the Alexa Fluor® 488 (A β) and 420–480 nm filter for DAPI, taking a z stack of 20–30 sections with an interval of 0.66 µm and a range of 15 µm. Zeiss Plan-Apochromat X40/1.2 Oil differential interference contrast objective were used for imaging. Images were quantified with the ImageJ Fiji 2.9.0 software (NIH, Bethesda, MD, USA).

2.9. Behavioral Testing

2.9.1. Hindlimb Test

The hindlimb clasping test is used to assess neurodegeneration in mouse models [40]. For this test, mice were suspended by the base of the tail and videotaped for 10 s. Three separate trials were taken over three consecutive days. Hindlimb clasping was scored from 0 to 3: 0 = hindlimbs splayed outward and away from the abdomen; 1 = one hindlimb retracted inwards towards the abdomen for at least 50% of the observation period; 2 = both hindlimbs partially retracted inwards towards the abdomen for at least 50% of the observation period; and 3 = both hindlimbs completely retracted inwards towards the abdomen for at least 50% of the observation period. Hindlimb clasping scores were added together for the three separate trials.

2.9.2. Ledge Test

The ledge test is used to assess motor deficits in rodent models of CNS disorders [41]. Typically, mice walk along the ledge of a cage and try to descend back into the cage. Three separate trials were taken for each mouse. The ledge test was scored from 0 to 3 points: 0 = a mouse walked along the ledge without slipping and lowered itself back into the cage using paws; 1 = the mouse lost its footing during walking along the ledge but otherwise appeared coordinated; 2 = the mouse did not effectively use its hind legs and landed on its head rather than paws when descending into the cage; and 3 = the mouse fell off the ledge or was shaking and/or barely moving.

2.9.3. Cylinder Test

The cylinder test is used to assess sensorimotor function in rodent models of CNS disorders. A mouse is placed in a transparent 500 mL plastic cylinder. The number of times the mouse rears up and touches the cylinder wall during a period of 3 min is counted. A rear is defined as a vertical movement with both forelimbs off the floor so that the mouse is standing only on its hindlimbs. At the end of 3 min, the mouse was removed and placed back into its home cage. Because spontaneous activity in the cylinder is affected by repeated testing, resulting in reduced activity over time, mice were tested only once in their lifetime.

2.10. Statistical Analysis

The results were calculated as mean \pm standard deviation. A two-sided unpaired t test was used for comparisons between two groups of variables; $p < 0.05$ was considered significant. Statistical analysis was performed using Statistica, Version 13 (TIBCO Software Inc., Palo Alto, CA, USA, <http://statistica.io>) (accessed 2 November 2022).

3. Results

3.1. Pon1 Depletion Downregulates the Expression of Histone Demethylase Phf8 and Increases the H4K20me1 Epigenetic Mark in Mouse Brain

To determine if Pon1 interacts with Phf8, we quantified Phf8 protein in the brains of *Pon1*^{-/-}5xFAD mice and their *Pon1*^{+/+}5xFAD sibling controls by Western blotting. We also examined the effects of hyperhomocysteinemia (HHcy), induced by providing 1% methionine in drinking water, on the Pon1–Phf8 interaction. Pictures of Western blots are shown in Figures 1A and 2B, while quantification of individual proteins is illustrated by corresponding bar graphs in Figures 1 and 2 for 5-month-old and 12-month-old mice, respectively. We found that Phf8 protein was significantly downregulated in the brains of *Pon1*^{-/-}5xFAD mice vs. *Pon1*^{+/+}5xFAD sibling controls in animals fed with a standard chow diet (5-month-old: from 1.0 ± 0.1 to 0.68 ± 0.15 , $P_{\text{genotype}} = 2 \times 10^{-5}$, Figure 1A; 12-month-old: from 1.0 ± 0.2 to 0.65 ± 0.12 , $P_{\text{genotype}} = 1 \times 10^{-4}$, Figure 2A). Reduced expression of Phf8 in *Pon1*^{-/-}5xFAD vs. *Pon1*^{+/+}5xFAD brains was also observed in mice fed with the HHcy diet (from 0.76 ± 0.11 to 0.60 ± 0.10 , $P_{\text{genotype}} = 0.001$; Figure 1A).

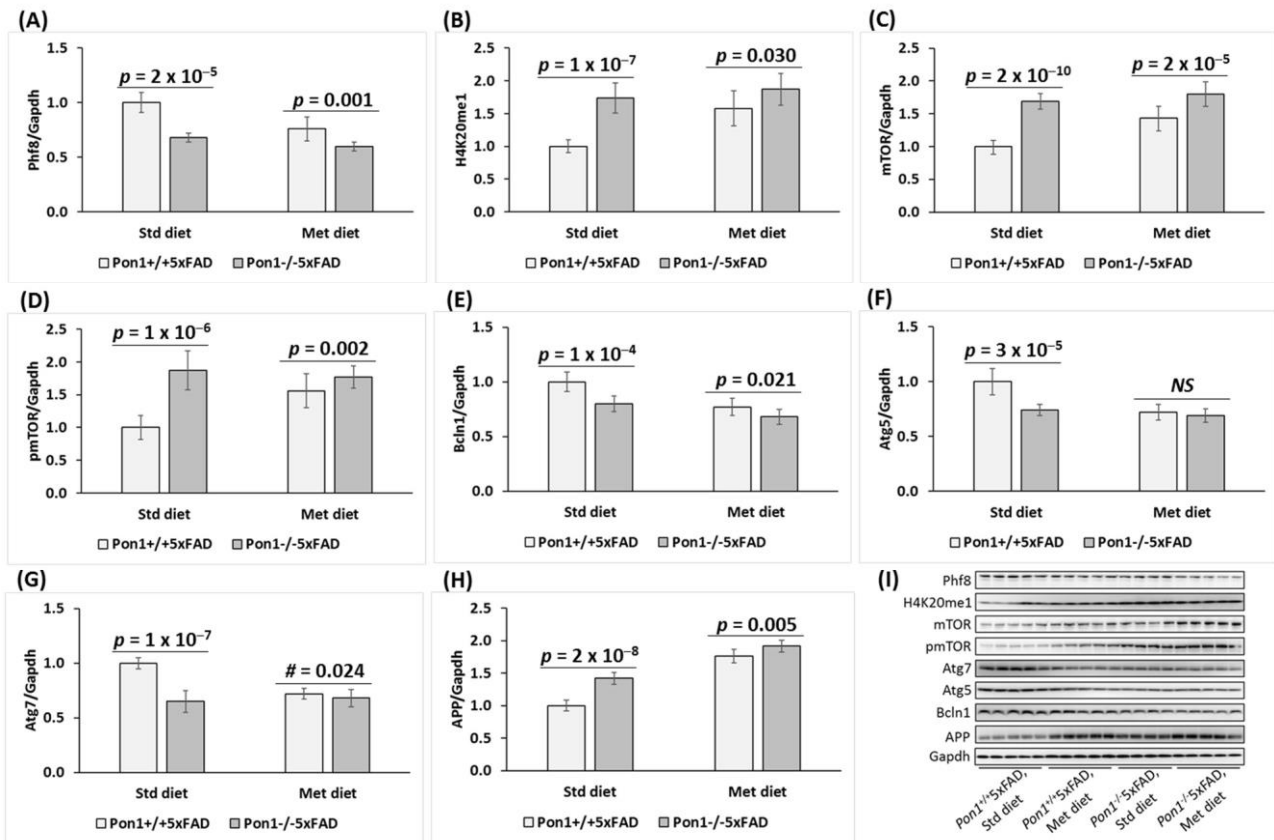


Figure 1. Pon1 depletion affects the expression of histone demethylase Phf8, histone H4K20me1 epigenetic mark, mTOR, pmTOR, autophagy-related proteins, and App in the *Pon1*^{-/-}5xFAD mouse brain. (A–H) 5-month-old mice: One-month-old *Pon1*^{-/-}5xFAD mice and *Pon1*^{+/+}5xFAD sibling controls fed with HHcy high Met diet (1% Met in drinking water) or control diet for 4 months were used in experiments. Each genotype/diet group included 8–10 mice of both sexes. Bar graphs illustrating Western blot quantification of the following brain proteins are shown: Phf8 (A), H4K20me1 (B), mTOR (C), pmTOR (D), Bcln1 (E), Atg5 (F), Atg7 (G), and App (H). Representative pictures of Western blots are shown in panel (I). Gapdh protein was used for normalization. Data are averages of three independent experiments.

HHcy diet significantly downregulated Phf8 expression in the brains of *Pon1*^{+/+}5xFAD mice (to 0.76 ± 0.11 , $P_{\text{diet}} = 6 \times 10^{-5}$). In contrast, Phf8 expression in the brains of *Pon1*^{-/-}5xFAD mice was essentially not affected by the HHcy diet (0.60 ± 0.19 vs. 0.68 ± 0.15 , $P_{\text{diet}} = 0.099$) (Figure 1A). The histone H4K20me1 epigenetic mark was significantly upregulated in *Pon1*^{-/-}5xFAD vs. *Pon1*^{+/+}5xFAD brains (5-month-old: 1.74-fold, $P_{\text{genotype}} = 1 \times 10^{-7}$, Figure 1B; 12-month-old: 1.41-fold, $P_{\text{genotype}} = 1 \times 10^{-4}$, Figure 2). Upregulated expression of H4K20me1 in 5-month-old *Pon1*^{-/-}5xFAD vs. *Pon1*^{+/+}5xFAD brains was also observed in mice fed with the HHcy diet (from 1.58 ± 0.27 to 1.87 ± 0.24 , $P_{\text{genotype}} = 0.030$; Figure 1B). HHcy diet significantly upregulated H4K20me1 levels in 5-month-old *Pon1*^{+/+} mice (1.6-fold, $P_{\text{diet}} = 6 \times 10^{-6}$) but not in *Pon1*^{-/-} animals (1.74 - vs. 1.87 -fold, $P_{\text{diet}} = 0.275$; Figure 1B).

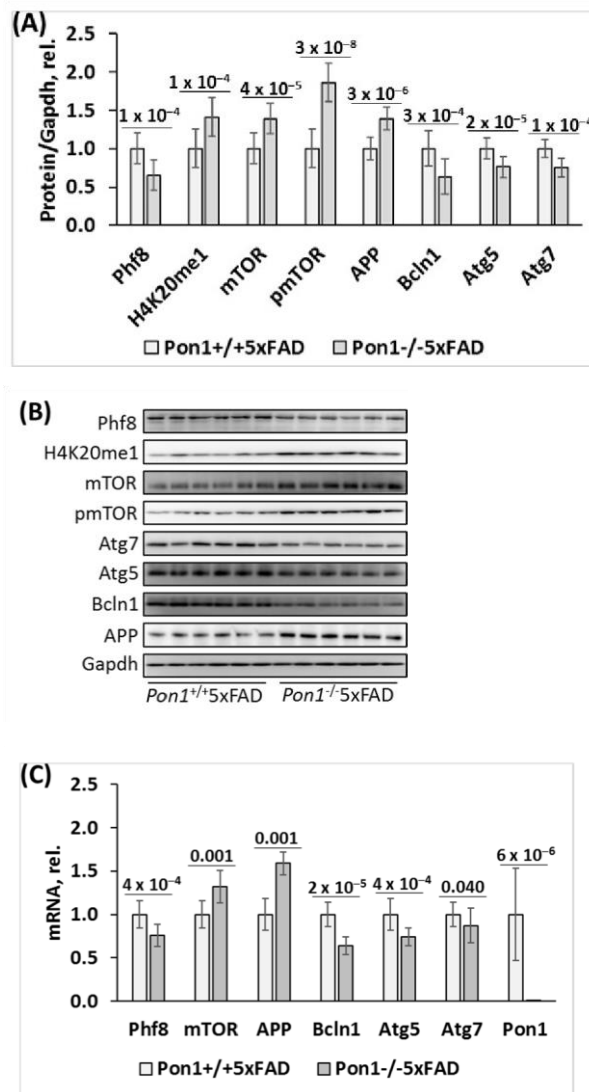


Figure 2. *Pon1* depletion affects the expression of histone demethylase Phf8, histone H4K20me1 epigenetic mark, mTOR, autophagy, and App in the brains of 12-month-old *Pon1*^{-/-}5xFAD mice. After weaning at 1 month, *Pon1*^{-/-}5xFAD mice and *Pon1*^{+/+}5xFAD sibling controls were fed with a standard diet for 11 month. Each genotype group included 10–12 mice of both sexes. (A) Bar graphs illustrate Western blot quantification of the indicated brain proteins. (B) Pictures of Western blots. (C) Bar graphs showing RT-qPCR quantification of mRNA for *Pon1*, Phf8, mTOR, autophagy-related proteins, and App. Gapdh mRNA levels was used as a reference for quantification. As expected, *Pon1* was absent in the *Pon1*^{-/-}5xFAD mice.

3.2. *Pon1* Depletion Upregulates mTOR and Inhibits Autophagy in Mouse Brain

Because Phf8/H4K20me1 regulate mTOR signaling, we next examined the effects of *Pon1* depletion on levels of mTOR and its active form, phosphorylated at Ser2448 (pmTOR). We found that mTOR protein was significantly upregulated in the brains of *Pon1*^{-/-}5xFAD vs. *Pon1*^{+/+}5xFAD mice (5-month-old: 1.69-fold, $P_{\text{genotype}} = 2 \times 10^{-10}$, Figure 1C; 12-month-old: 1.39-fold, $P_{\text{genotype}} = 4 \times 10^{-5}$, Figure 2A). Upregulated expression of mTOR in *Pon1*^{-/-}5xFAD vs. *Pon1*^{+/+}5xFAD brains was also observed in mice fed with the HHcy diet (from 1.43 ± 0.18 to 1.97 ± 0.19 , $P_{\text{genotype}} = 2 \times 10^{-5}$; Figure 1C).

HHcy diet significantly upregulated mTOR protein expression in *Pon1*^{-/-}5xFAD mice (1.97 ± 0.19 vs. 1.69 ± 0.12 , $P_{\text{diet}} = 0.003$) and *Pon1*^{+/+}5xFAD animals (1.43 ± 0.18 vs. 1.00 ± 0.09 , $P_{\text{diet}} = 5 \times 10^{-6}$) (Figure 1C).

Because mTOR is activated by phosphorylation, we quantified mTOR phosphorylated at Ser2448 (pmTOR). We found that pmTOR was also significantly upregulated in the brains of *Pon1*^{-/-}5xFAD vs. *Pon1*^{+/+}5xFAD mice (5-month-old: 1.69-fold, $P_{\text{genotype}} = 2 \times 10^{-10}$, Figure 1C; 12-month-old: 1.86-fold, $P_{\text{genotype}} = 3 \times 10^{-8}$, Figure 2A).

Upregulated expression of pmTOR in *Pon1*^{-/-}5xFAD vs. *Pon1*^{+/+}5xFAD brains was also observed in mice fed with the HHcy diet (1.95 ± 0.17 vs. 1.56 ± 0.26, $P_{\text{genotype}} = 0.002$) (Figure 1D). HHcy diet significantly elevated pmTOR levels in *Pon1*^{+/+}5xFAD mice (1.56 ± 0.26 vs. 1.00 ± 0.18, $P_{\text{diet}} = 4 \times 10^{-5}$) but not in *Pon1*^{-/-}5xFAD mice (1.95 ± 0.17 vs. 1.87 ± 0.30, $P_{\text{diet}} = 0.528$) (Figure 1D). Overall, the effects of the *Pon1*^{-/-} genotype on mTOR and pmTOR levels were attenuated by the HHcy diet (Figure 1C,D). These findings indicate that *Pon1* depletion upregulated pmTOR to a similar extent as mTOR, suggesting that the *Pon1*^{-/-} genotype affects mTOR signaling mostly at the level of mTOR protein expression.

Because mTOR is a major regulator of autophagy, we quantified autophagy-related proteins in *Pon1*^{-/-}5xFAD mice. We found that the regulators of autophagosome assembly, Bcln1, Atg5, and Atg7, were significantly downregulated in the brains of *Pon1*^{-/-}5xFAD vs. *Pon1*^{+/+}5xFAD sibling controls (by 22–35%, $P_{\text{genotype}} = 1 \times 10^{-7}$ to 1×10^{-4} , Figure 1E–G; 12-month-old: by 24–37%, $P_{\text{genotype}} = 2 \times 10^{-5}$ to 3×10^{-4} , Figure 2A). The HHcy diet significantly decreased Bcln1, Atg5, and Atg7 expression in 5-month-old *Pon1*^{+/+}5xFAD mice (by 23–28%, $P_{\text{diet}} = 2 \times 10^{-5}$ to 2×10^{-9}). In 5-month-old *Pon1*^{-/-}5xFAD mice, the HHcy diet also significantly decreased Bcln1 (0.68 vs. 0.80, $P_{\text{diet}} = 0.003$) and Atg5 levels (0.66 vs. 0.74, $P_{\text{diet}} = 0.008$); however, Atg7 levels were essentially not affected by the HHcy diet in *Pon1*^{-/-}5xFAD mice (0.63 ± 0.05 vs. 0.65 ± 0.05, $P_{\text{diet}} = 0.714$). Overall, the effects of the *Pon1*^{-/-} genotype on the brain Bcln1, Atg5, and Atg7 levels were attenuated by the HHcy diet (Figure 1E–G). These findings indicate that autophagy was impaired by the *Pon1*^{-/-} genotype.

3.3. *Pon1* Depletion Upregulates APP Protein Expression in Mouse Brain

We found that APP protein was significantly elevated in the brains of *Pon1*^{-/-}5xFAD mice vs. *Pon1*^{+/+}5xFAD sibling controls in mice fed with a standard diet (5-month-old: 1.42-fold, $P_{\text{genotype}} = 2 \times 10^{-8}$; Figure 1H; 12-month-old: 1.39-fold, $P_{\text{genotype}} = 3 \times 10^{-6}$, Figure 2A). Upregulated expression of APP protein in 5-month-old *Pon1*^{-/-}5xFAD vs. *Pon1*^{+/+}5xFAD brains was also observed in mice fed with the HHcy diet (from 1.76 ± 0.08 to 1.92 ± 0.10, $P_{\text{genotype}} = 0.005$; Figure 1H).

Met diet increased APP protein levels in the brains of 5-month-old *Pon1*^{+/+}5xFAD mice (1.76-fold, $P_{\text{diet}} = 1 \times 10^{-13}$) and, to a lesser extent, in *Pon1*^{-/-}5xFAD animals (1.35-fold, from 1.42 to 1.92, $P_{\text{diet}} = 4 \times 10^{-7}$) (Figure 1H).

3.4. *Pon1* Gene Exerts Transcriptional Control on the Expression of *Phf8*, mTOR, Autophagy-Related Proteins, and APP in *Pon1*^{-/-}5xFAD Mice

To determine if the observed changes in the protein levels of *Phf8*, mTOR, autophagy related proteins, and APP are caused by the transcriptional effects of the *Pon1*^{-/-} genotype, we quantified the corresponding mRNAs by RT-qPCR. We found that *Phf8* mRNA was significantly downregulated in the brains of *Pon1*^{-/-}5xFAD mice vs. *Pon1*^{+/+}5xFAD sibling controls in animals fed with a standard chow diet (5-month-old: from 1.00 ± 0.15 to 0.66 ± 0.09, $P_{\text{genotype}} = 1 \times 10^{-4}$, Figure S1A; 12-month-old: from 1.00 ± 0.16 to 0.76 ± 0.13, $P_{\text{genotype}} = 4 \times 10^{-4}$, Figure 2C). HHcy did not affect the effects of the *Pon1* genotype on *Phf8* mRNA: reduced expression of *Phf8* in the brains of 5-month-old *Pon1*^{-/-}5xFAD vs. *Pon1*^{+/+}5xFAD mice was observed in mice fed with the Met diet (from 0.63 ± 0.27 to 0.37 ± 0.23, $P_{\text{genotype}} = 0.048$; Figure S1A).

HHcy significantly downregulated *Phf8* mRNA expression in the brains of 5-month-old 5xFAD mice, regardless of *Pon1* genotype: from 1.00 ± 0.15 in mice fed with a standard diet to 0.63 ± 0.27 in animals fed with the Met diet, $P_{\text{diet}} = 0.002$ in *Pon1*^{+/+}5xFAD mice, and from 0.66 ± 0.09 (std diet) to 0.37 ± 0.23 (Met diet), $P_{\text{diet}} = 0.002$ in *Pon1*^{-/-}5xFAD animals (Figure S1A).

We found that mTOR mRNA was significantly upregulated in the brains of *Pon1*^{-/-}5xFAD vs. *Pon1*^{+/+}5xFAD mice (5-month-old: 1.55-fold, $P_{\text{genotype}} = 0.006$, Figure S1B; 12-month-old: 1.32-fold, $P_{\text{genotype}} = 4 \times 10^{-5}$, Figure 2C). However, HHcy abrogated the effects of the *Pon1* genotype on mTOR mRNA expression: similar levels of mTOR mRNA were found in *Pon1*^{-/-}5xFAD and *Pon1*^{+/+}5xFAD mice fed with the high Met diet (1.79 ± 0.55 and 1.46 ± 0.61, respectively, $P_{\text{genotype}} = 0.258$; Figure S1B).

HHcy diet significantly upregulated mTOR mRNA in *Pon1*^{+/+}5xFAD mice (1.46 ± 0.61 vs. 1.00 ± 0.15 , $P_{\text{diet}} = 0.044$) but not in *Pon1*^{-/-}5xFAD animals (1.79 ± 0.55 vs. 1.55 ± 0.46 , $P_{\text{diet}} = 0.352$) (Figure S1B).

We also found that mRNA for the regulators of autophagosome assembly, Bcln1, Atg5, and Atg7, were downregulated in the brains of *Pon1*^{-/-}5xFAD vs. *Pon1*^{+/+}5xFAD sibling controls (Bcln1 and Atg7 mRNA by 31% and 22%, $P_{\text{genotype}} = 0.005$ and 0.008 , respectively, Figure S1C,E; 12-month-old: by 13–36%, $P_{\text{genotype}} = 2 \times 10^{-5}$ to 0.040 , Figure 2C). Met diet significantly decreased Bcln1 and Atg7 mRNA expression in 5-month-old *Pon1*^{+/+}5xFAD mice (by 18–20%, $P_{\text{diet}} = 0.044$ and 0.008 , respectively) but not in *Pon1*^{-/-}5xFAD animals. The Atg5 mRNA level was not affected by the Met diet regardless of *Pon1* genotype. However, Atg5 mRNA was significantly reduced by the *Pon1*^{-/-} genotype in mice fed with the Met diet but in *Pon1*^{-/-}5xFAD mice. Overall, the effects of the *Pon1*^{-/-} genotype on the brain Bcln1 and Atg7 levels were attenuated by the HHcy diet (Figure S1C,E).

We found that APP mRNA was significantly elevated in the brains of *Pon1*^{-/-}5xFAD mice vs. *Pon1*^{+/+}5xFAD sibling controls in mice fed with a standard diet (5-month-old: 1.52-fold, $P_{\text{genotype}} = 0.002$; Figure S1F; 12-month-old: 1.59-fold, $P_{\text{genotype}} = 0.003$, Figure 2C). Upregulated expression of APP mRNA in 5-month-old *Pon1*^{-/-}5xFAD vs. *Pon1*^{+/+}5xFAD brains was also observed in mice fed with the HHcy diet (from 1.76 ± 0.08 to 1.92 ± 0.10 , $P_{\text{genotype}} = 0.005$; Figure S1F).

Met diet increased APP mRNA levels in the brains of 5-month-old *Pon1*^{+/+}5xFAD mice (1.75-fold, $P_{\text{diet}} = 0.010$) but not in *Pon1*^{-/-}5xFAD animals ($P_{\text{diet}} = 0.482$) and abrogated the effects of the *Pon1*^{-/-} genotype on APP mRNA (Figure S1F). As expected, Pon1 mRNA was absent in *Pon1*^{-/-}5xFAD brains (Figure S1G). Met diet did not affect Pon1 mRNA in *Pon1*^{+/+}5xFAD mice brains (Figure S1G).

These findings indicate that the *Pon1* gene exerts transcriptional control over the expression of Phf8, mTOR, autophagy-related proteins, and APP in the mouse brain.

3.5. *Pon1* Gene Silencing Downregulates the Histone Demethylase Phf8, Upregulates H4K20me1 Epigenetic Mark, mTOR and pmTOR, APP, and Inhibits Autophagy in Mouse Neuroblastoma N2a-APPswe Cells

To elucidate the mechanism by which Pon1 depletion impacts Phf8 and its downstream effects on mTOR, autophagy, and APP, we first examined whether the findings in *Pon1*^{-/-} mice can be recapitulated in cultured mouse neuroblastoma N2a-APPswe cells that overproduce A β from a mutated human APP transgene [38]. We silenced the *Pon1* gene in these cells by RNA interference using *Pon1*-targeting siRNA and studied how the silencing impacts Phf8 and its downstream effects. Changes in specific protein levels in *Pon1*-silenced and control cells were analyzed by Western blotting using Gapdh protein as a reference.

We found that the Pon1 protein level was reduced by 71% in *Pon1*-silenced cells ($p = 1 \times 10^{-5}$; Figure 3A). We also found that the histone demethylase Phf8 protein level was significantly downregulated (by 33%, $p = 4 \times 10^{-4}$; Figure 3B), while the histone H4K20me1 level was significantly upregulated (1.70–1.76-fold, $p = 0.001$; Figure 3C) in *Pon1*-silenced N2a-APPswe cells.

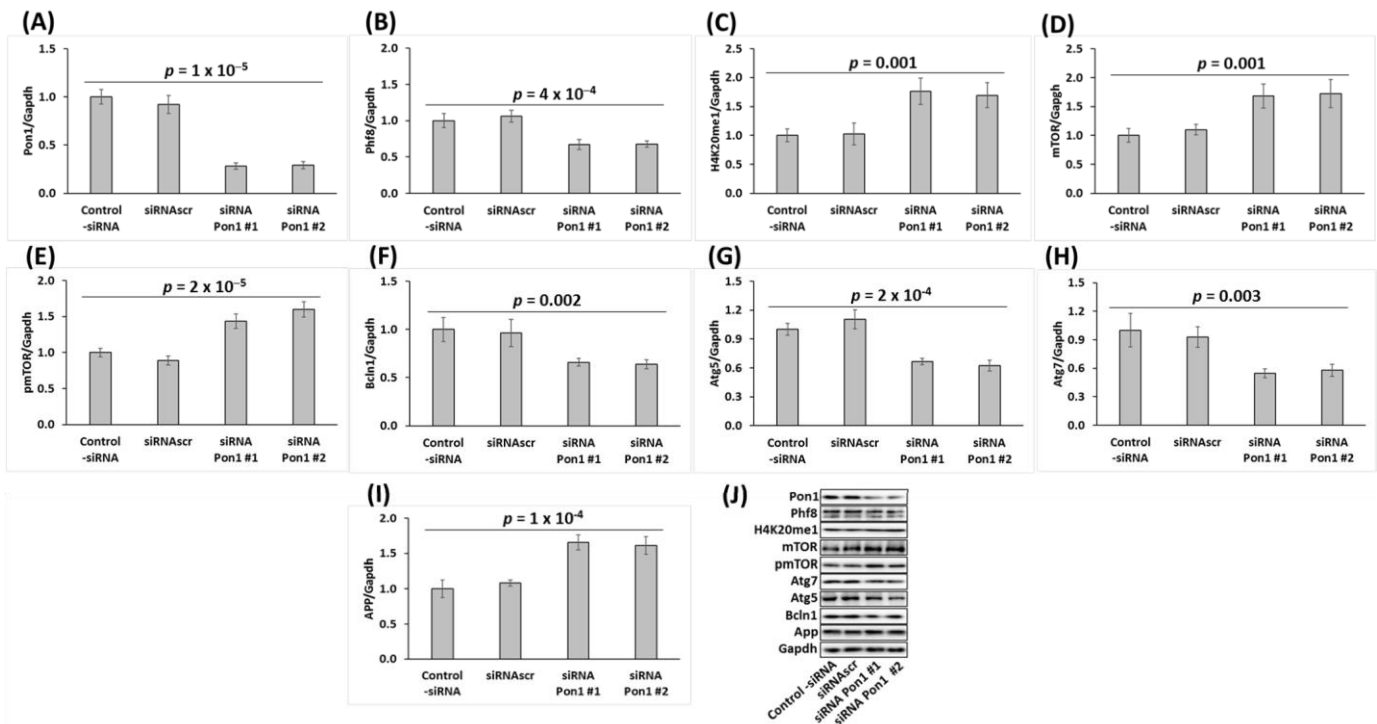


Figure 3. *Pon1* gene silencing in mouse neuroblastoma N2a-APPswe cells recapitulates changes in histone demethylase Phf8, H4K20me1, mTOR signaling, APP, and autophagy-related protein levels observed in *Pon1*^{-/-} mouse brain. Bar graphs illustrating the quantification of Pon1 (A), Phf8 (B), H4K20me1 (C), mTOR (D), pmTOR (E), Bcln1 (F), Atg5 (G), Atg7 (H), and App (I) in N2a-APPswe cells transfected with two different siRNAs targeting the *Pon1* gene (siRNA *Pon1* #1 and #2) are shown. Representative pictures of Western blots are shown in panel (J). Transfections without siRNA (Control -siRNA) or with scrambled siRNA (siRNAsc) were used as controls. Gapdh was used as a reference protein. Data are averages of three independent experiments.

At the same time, the mTOR protein was significantly upregulated in *Pon1*-silenced N2a-APPswe cells (1.7-fold, $p = 0.001$; Figure 3D), as were pmTOR (1.6-fold, $p = 2 \times 10^{-5}$; Figure 3E) and APP (1.6-fold, $p = 1 \times 10^{-4}$; Figure 3I), while autophagy-related proteins Bcln1, Atg5, and Atg7 (Figure 3F–H, respectively) were significantly downregulated (by 33–45%, $p = 2 \times 10^{-4}$ to 0.003).

The Western blot results show that the changes in Phf8, H4K20m31, mTOR signaling, autophagy, and APP induced by *Pon1* gene silencing in N2a-APPswe cells (Figure 3) recapitulate the in vivo findings in the *Pon1*^{-/-}5xFAD mouse brain (Figures 1 and 2).

3.6. Pon1 Gene Silencing Increases H4K20me1 Biding to mTOR Promoter in N2a-APPswe Cells

To determine whether increased levels of the histone H4K20me1 mark can promote mTOR gene expression by binding to its promoter in Pon1-depleted cells, we carried out ChIP experiments using anti-H4K20me1 antibody (Figure 4). The *Pon1* gene was silenced by transfecting N2a-APPswe cells using two different *Pon1*-targeting siRNAs. The cells were permeabilized and treated with anti-H4K20me1 antibody and a recombinant micrococcal nuclease-protein A/G. DNA fragments released from N2a-APPswe cells were quantified by RT-qPCR using primers targeting the transcription start site (TSS) of the mTOR gene as well as upstream (UP) and downstream (DOWN) regions.

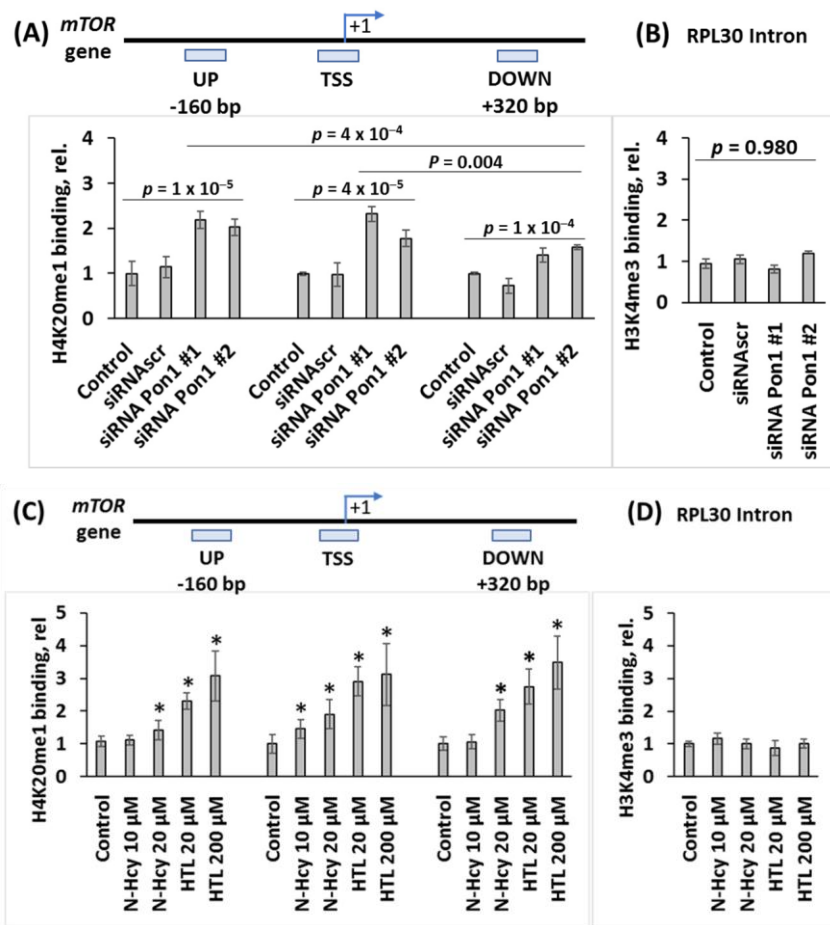


Figure 4. Pon1 depletion or treatments with Hcy-thiolactone or *N*-Hcy-protein increase H4K20me1 binding at the *mTOR* promoter in mouse neuroblastoma N2a-APPswe cells. CHIP assays with anti-H4K20me1 antibody show the specific binding of H4K20me1 at the transcription start site (TSS) of the *mTOR* gene as well as downstream and upstream sites. Bar graphs show the relative H4K20me1 binding at indicated regions of the *mTOR* gene. **(A)** N2a-APPswe cells were transfected with two different siRNAs targeting the *Pon1* gene (siRNA *Pon1* #1 and #2) (48 h, 37 °C). Transfections without siRNA (Control -siRNA) or with scrambled siRNA (siRNAscr) were used as controls. **(B)** Control CHIP experiment with anti-H3K4me3 antibody shows that *Pon1* gene-silencing did not affect the binding of H3K4me3 at the Rpl30 intron. **(C)** N2a-APPswe cells were treated with indicated concentrations of *N*-Hcy-protein or Hcy-thiolactone (HTL) (24 h, 37 °C). Untreated cells were used as controls. **(D)** Control CHIP experiment with anti-H3K4me3 antibody shows that Hcy-thiolactone or *N*-Hcy-protein did not affect binding of H3K4me3 at the Rpl30 intron. RT-qPCR was conducted on the input and precipitated DNA fragments. Data are averages of three independent experiments. * Significant differences vs. controls, $p < 0.05$.

We found that in *Pon1*-silenced N2a-APPswe cells, the binding of H4K20me1 was significantly increased at the *mTOR* TSS (1.8 to 2.3-fold, $p = 4 \times 10^{-5}$), *mTOR* UP (2.0 to 2.2-fold, $p = 2 \times 10^{-5}$), and *mTOR* DOWN sites (1.4 to 1.6-fold, $p = 1 \times 10^{-4}$) (Figure 4A). Importantly, in *Pon1*-silenced cells there were significantly more DNA fragments from the *mTOR* TSS (2.3 ± 0.2 and 1.8 ± 0.2 for siRNA *Pon1* #1 and #2, respectively) than from the DOWN site (1.4 ± 0.2 and 1.6 ± 0.1 for siRNA *Pon1* #1 and #2, respectively; $p = 0.004$). There were also more DNA fragments from the UP site than from the DOWN site (2.2 ± 0.2 and 2.1 ± 0.2 for siRNA *Pon1* #1 and #2 vs. 1.4 ± 0.2 and 1.6 ± 0.1 for siRNA *Pon1* #1 and #2; $p = 0.0004$). Numbers of DNA fragments from the TSS and UP sites were similar ($p = 0.713$) (Figure 4A). Control experiments showed that the binding of H3K4me3 to RPL30 intron was not affected by *Pon1* gene silencing (Figure 4B). These findings indicate that *Pon1* gene silencing induces H4K20me1 binding at the *mTOR* gene, significantly higher at the *mTOR* TSS and UP site than at the DOWN site in *Pon1*-silenced cells.

CHIP experiments using anti-Phf8 antibody showed that *Pon1* gene silencing or treatments with Hcy-thiolactone or *N*-Hcy-protein did not affect binding of Phf8 to the *mTOR* gene.

3.7. Pon1 Depletion Increases A β Accumulation in N2a-APPswe Cells

To determine whether Pon1 depletion affects A β accumulation, we silenced the *Pon1* gene by RNA interference and quantified A β in N2a-APP_{sw} cells by fluorescence confocal microscopy using anti-A β antibody. The *Pon1* gene was silenced by transfection with two different siRNAs targeting *Pon1*; the cells were permeabilized, treated with anti-A β antibody, and A β was visualized with fluorescent secondary antibody and quantified. Representative confocal microscopy images are shown in Figure 5A. We found that *Pon1* gene silencing led to increased A β generation manifested by significantly increased area (from 173 ± 27 and $162 \pm 22 \mu\text{m}^2$ for -siRNA and siRNAscrl controls, respectively, to $225 \pm 28 \mu\text{m}^2$ for siRNA Pon1 #1, $p = 0.013$) and average size (from 0.63 ± 0.02 and 0.61 ± 0.06 for -siRNA and siRNAscrl controls, respectively, to $1.29 \pm 0.17 \mu\text{m}^2$ and $0.99 \pm 0.09 \mu\text{m}^2$ for siRNA Pon1 #1 and #2, respectively; $p = 1 \times 10^{-4}$) of fluorescent A β puncta in Pon1 siRNA-treated N2a-APP_{sw} cells compared with siRNAscrl or -siRNA controls (Figure 5B). Signal intensity increased from 1.00 ± 0.16 and 0.86 ± 0.28 for -siRNA and siRNAscrl controls, respectively, to 2.08 ± 0.27 and 2.01 ± 0.23 for siRNA Pon1 #1 and #2, respectively; $p = 3 \times 10^{-4}$) (Figure 5B).

Because Pon1 depletion elevates Hcy-thiolactone and N-Hcy-protein in mice [12], we examined whether any of these metabolites can induce A β accumulation in N2a-APP_{sw} cells. In cells treated with Hcy-thiolactone (20–200 μM) or N-Hcy-protein (10–20 μM), there was significantly more A β , manifested by significantly increased area of fluorescent A β puncta in confocal immunofluorescence images compared with control-siRNA and siRNAscrl (Figure 5C,D). However, while treatments with Hcy-thiolactone led to increased size and signal intensity of the fluorescent A β puncta, treatments with N-Hcy-protein did not (Figure 5D), suggesting different effects of Hcy-thiolactone and N-Hcy-protein on the structure of A β deposits. These findings suggest that Hcy-thiolactone and N-Hcy-protein contribute to elevated A β levels induced by *Pon1* gene silencing.

3.8. Pon1 Depletion Increases A β Accumulation in *Pon1*^{-/-}5xFAD Mice

A β was extracted from brains of 5- and 12-month-old mice fed with a standard chow diet, and from 5-month-old mice with the HHcy diet (1% Met in drinking water) since weaning at the age of 1 month. SDS-soluble and formic acid (FA)-soluble A β fractions, which contain the bulk of A β [36], as well as a minor RIPA-soluble A β fraction were obtained. A β was quantified in these fractions by a dot blot assay with a monoclonal anti-A β antibody [37].

We found that RIPA- and SDS-soluble A β was significantly elevated ($P_{\text{genotype}} = 2 \times 10^{-5}$ and 1×10^{-8} , respectively), and FA-soluble A β tended to be elevated ($P_{\text{genotype}} = 0.058$) in the brains of 12-month-old *Pon1*^{-/-}5xFAD mice vs. *Pon1*^{+/+}5xFAD sibling controls fed with a standard diet (Figure 6A). Similarly, elevated A β was found in 5-month-old *Pon1*^{-/-}5xFAD vs. *Pon1*^{+/+}5xFAD mice fed with a standard diet (Figure 6B) or the HHcy diet (Figure 6C). This indicates that neither age nor HHcy influenced the effects of the *Pon1*^{-/-} genotype on A β levels.

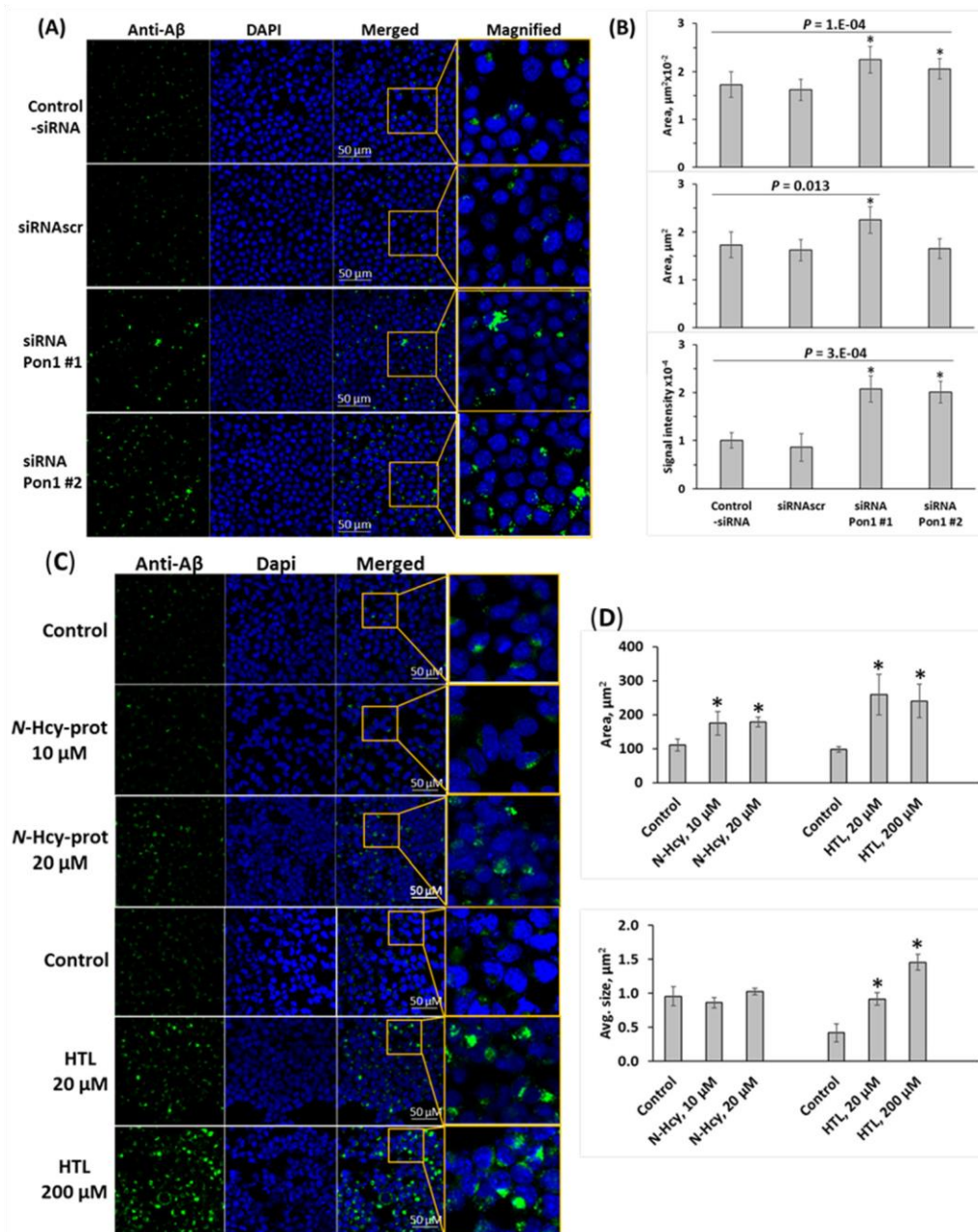


Figure 5. Pon1 depletion promotes A β accumulation in N2a-APPsw cells. **(A–D)** Analysis of A β in mouse neuroblastoma N2a-APPsw cells by confocal immunofluorescence microscopy using anti-A β antibody. **(A,B)** The cells were transfected with siRNAs targeting the *Pon1* gene (siRNA Pon1 #1 and #2). Transfections without siRNA (Control -siRNA) or with scrambled siRNA (siRNAscr) were used as controls. Confocal microscopy images **(A)** and quantification of A β signals **(B)** from *Pon1*-silenced and control cells are shown. **(C,D)** N2a-APPsw cells were treated with indicated concentrations of N-Hcy-protein or Hcy-thiolactone (HTL) for 24 h at 37 °C. Untreated cells were used as controls. Each data point is an average of three independent experiments with triplicate measurements in each. * Significant difference from control, $p < 0.05$.

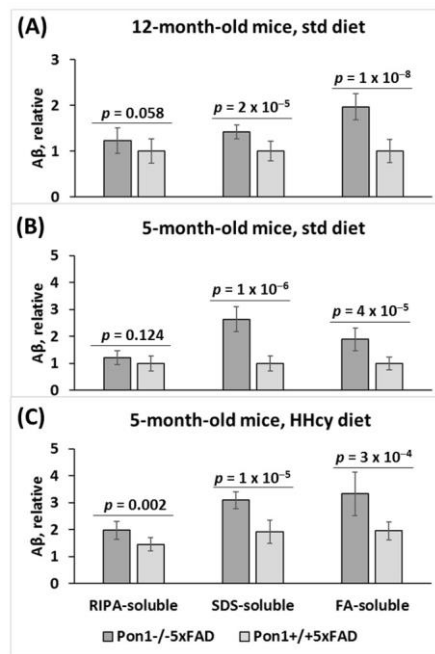


Figure 6. Pon1 depletion promotes A β accumulation in *Pon1*^{-/-}5xFAD vs. *Pon1*^{+/+}5xFAD mice. A β was quantified in RIPA-soluble, SDS-soluble, and FA-soluble fractions extracted from mouse brain. Twelve-month-old (A) and 5-month-old mice (B) fed with a standard diet as well as 5-month-old mice fed with a HHcy diet (C) were used in the experiments. Each measurement for an individual mouse was repeated three times. A β values shown are averages of measurements for 8–10 mice/group.

However, the HHcy diet significantly elevated RIPA-, SDS-, and FA-soluble A β in 5-month-old *Pon1*^{-/-}5xFAD mice (from 1.21 to 1.97, $P_{\text{diet}} = 1 \times 10^{-4}$; 2.62 to 3.09, $P_{\text{diet}} = 0.034$; 1.88 to 3.33, $P_{\text{diet}} = 1 \times 10^{-6}$, respectively) and in 5-month-old *Pon1*^{+/+}5xFAD mice, (from 1.00 to 1.95, $P_{\text{diet}} = 0.002$; 1.00 to 1.91, $P_{\text{diet}} = 4 \times 10^{-4}$; 1.00 to 1.45, $P_{\text{diet}} = 5 \times 10^{-4}$, respectively) (Figure 6C). This indicates that HHcy and *Pon1*^{-/-} genotype exert similar effects on A β levels.

3.9. Pon1 Depletion Does Not Induce Sensorimotor Deficits

To examine the effects of Pon1 depletion on neurodegeneration and sensorimotor activity, 12-month-old *Pon1*^{-/-}5xFAD mice and their *Pon1*^{+/+}5xFAD sibling controls were assessed in the hindlimb clasping, ledge, and cylinder tests.

The hindlimb test showed a similar degree of clasping (scores) in *Pon1*^{-/-}5xFAD mice vs. their *Pon1*^{+/+}5xFAD littermates (2.24 ± 0.44 vs. 2.08 ± 0.43 , $p = 0.335$; Figure S2A). These findings indicate that the *Pon1*^{-/-} genotype did not induce neurodegeneration in *Pon1*^{-/-}5xFAD mice relative to *Pon1*^{+/+}5xFAD animals.

The ledge test showed similar performances (scores) in *Pon1*^{-/-}5xFAD mice vs. their *Pon1*^{+/+}5xFAD littermates (2.07 ± 0.43 vs. 1.97 ± 0.38 , $p = 0.589$; Figure S2B). The cylinder test also showed similar performances (number of rears) in *Pon1*^{-/-}5xFAD mice vs. their *Pon1*^{+/+}5xFAD littermates (8.5 ± 6.0 vs. 10.4 ± 5.1 , $p = 0.307$; Figure S2C). These findings indicate that the *Pon1*^{-/-} genotype did not induce sensorimotor deficits in *Pon1*^{-/-}5xFAD mice relative to *Pon1*^{+/+}5xFAD animals.

4. Discussion

In previous studies, we found that Pon1 is a Hcy-thiolactone-hydrolyzing enzyme [13] and that Pon1 depletion in mice elevated brain Hcy-thiolactone and *N*-Hcy-protein [12], increased the animals' susceptibility to Hcy-thiolactone-induced seizures [12], and resulted in pro-neurodegenerative changes in brain proteome [27], suggesting that Pon1 plays an important protective role in brain homeostasis.

Our present findings show that Pon1 protects from amyloidogenic APP processing to A β in mice brains (Figure 6) and unravel the mechanistic basis of the protective role of Pon1 in the CNS. Specifically, we found that Pon1 depletion downregulated histone demethylase Phf8 both at the protein and mRNA level, increased H4K20me1 binding at the mTOR promotor (Figure 4A), and upregulated mTOR expression and phosphorylation in the mouse brain (Figure 1C,D) and neuroblastoma N2a-APPswe cells (Figure 3D,E). Treatments with Hcy-thiolactone and *N*-Hcy-protein, metabolites that are elevated in *Pon1*^{-/-} mice, also increased H4K20me1 binding at the mTOR promotor in N2a-APPswe cells (Figure 4C). This suggests that Pon1 is a negative regulator of mTOR signaling by controlling levels of Hcy metabolites that affect binding of H4K20me1 at the mTOR promotor. The effects of Hcythiolactone and *N*-Hcy-protein on mTOR are explained by findings that Phf8, the regulator of mTOR expression, was downregulated by Pon1 depletion (Figures 1A and 2A), whereas H4K20me1 was upregulated (Figures 1B and 2A). These findings provide direct mechanistic evidence linking Hcy-thiolactone and *N*-Hcy-protein with dysregulated mTOR signaling and its downstream consequences such as downregulation of autophagy and upregulation of A β . This mechanism is further supported by our findings that Phf8 depletion by RNA interference affected mTOR, autophagy, APP, and A β , similar to treatments with Hcythiolactone or *N*-Hcy-protein [42]

In the present study, we found that depletion of Pon1 upregulated APP in the *Pon1*^{-/-}5xFAD mouse brain (Figures 1H, 2 and S1F) and in mouse neuroblastoma N2aAPPswe cells (Figure 3I). In contrast, depletion of Phf8 did not affect APP expression [42]. These findings suggest that Pon1 interacts with APP in the *Pon1*^{-/-}5xFAD mouse brain while Phf8 does not. However, whether the Pon1–APP interaction is direct or indirect remains to be determined.

Although Pon1 depletion in mouse neuroblastoma N2a-APPswe cells downregulated Phf8 (Figures 1A and 2A) and upregulated APP (Figures 1H and 2A) and A β (Figure 5), depletion of Phf8 upregulated A β but not APP [42]. These findings suggest that two pathways can lead to increased A β generation in Pon1-depleted brains and neural cells. One pathway involves Hcy metabolites, which upregulate APP, while another pathway involves impaired A β clearance due to downregulated autophagy.

Notably, Pon1 depletion caused changes in the Phf8- > H4K20me1- > mTOR- > autophagy pathway akin to the changes induced by HHcy in the mouse brain (Figure 1) and neuroblastoma cells (Figure 3). Pon1 depletion or HHcy similarly increased accumulation of A β in the brain (Figure 6). Our previous work showed that a common primary biochemical outcome of Pon1 depletion or of HHcy was essentially the same: HHcy caused elevation of Hcy-thiolactone and *N*-Hcy-protein [43] as did Pon1 depletion [12,14]. In the present work, Pon1 depletion by RNA interference or treatments with Hcy-thiolactone or *N*-Hcy-protein similarly increased the accumulation of A β in mouse neuroblastoma cells (Figure 5). Taken together, these findings suggest that increased accumulation of A β in Pon1-depleted brains is mediated by the effects of Hcy metabolites on mTOR signaling and autophagy.

5xFAD mice develop sensorimotor deficits beginning at about 9 months of age (<https://www.alzforum.org/research-models/5xfad-b6sjl>) (accessed 27 December 2022). For example, 5xFAD mice perform worse than the wild-type animals in the hindlimb and balance beam tests [44,45]. We found that depletion of Pon1 did not aggravate these deficits: there was no difference in sensorimotor performance between *Pon1*^{-/-}5xFAD mice vs. *Pon1*^{+/+}5xFAD animals in the hindlimb, ledge, and cylinder tests (Figure S2). These findings suggest that upregulated A β accumulation may not be causing sensorimotor impairment. However, other aspects of sensorimotor abilities may be affected by Pon1, which remains to be assessed in future studies, as are the effects of Pon1 on various domains of cognition [24].

In conclusion, our findings define a mechanism by which Pon1 prevents A β generation in a mouse model of AD and neural cells.

Supplementary Materials: The following supporting information can be downloaded at: <https://www.mdpi.com/article/10.3390/cells12050746/s1>, Figure S1: Pon1 depletion affects the expression of mRNAs for Phf8, mTOR, autophagy-related proteins, and App in the *Pon1*^{-/-}5xFAD mouse brain; Figure S2: Pon1 depletion did not affect sensorimotor activity in mice; Table S1: Primers used for PCR or RT-qPCR.

Author Contributions: L.W. performed and analyzed the experiments, carried out behavioral assessments; H.J. conceived the idea for the project, designed the study, generated *Pon1*^{-/-}5xFAD mouse model, bred the mice, collected tissue samples, analyzed the data, and wrote the paper. All authors have read and agreed to the published version of the manuscript.

Funding: This research was funded by the National Science Center, Poland grant numbers 2018/29/ B/NZ4/00771, 2019/33/B/NZ4/01760, 2021/43/B/NZ4/00339, the American Heart Association grant number 17GRNT32910002.

Institutional Review Board Statement: The animal study protocol was approved by the Institutional Animal Care and Use Committee (IACUC) of the New Jersey Medical School (Animal Care and Use Protocol #: 16114D0320, date of approval 29 March 2017).

Informed Consent Statement: Not applicable.

Data Availability Statement: The data that support the findings of this study are available in the methods and/or supplementary material of this article.

Acknowledgments: We thank D. M. Shih for kindly providing *Pon1*^{-/-} mice and S. S. Sisodia for kindly providing mouse neuroblastoma cells expressing human APP-695 harboring the K670N/M671L Swedish double mutation associated with familial early-onset Alzheimer's disease, N2a-APP_{swe}.

Conflicts of Interest: The authors declare no conflict of interest.

References

1. Perla-Kajan, J.; Jakubowski, H. Paraoxonase 1 and homocysteine metabolism. *Amino Acids* **2012**, *43*, 1405–1417. [[CrossRef](#)] [[PubMed](#)]
2. Marsillach, J.; Mackness, B.; Mackness, M.; Riu, F.; Beltran, R.; Joven, J.; Camps, J. Immunohistochemical analysis of paraoxonases 1, 2, and 3 expression in normal mouse tissues. *Free Radic. Biol. Med.* **2008**, *45*, 146–157. [[CrossRef](#)]
3. Costa, L.G.; Giordano, G.; Cole, T.B.; Marsillach, J.; Furlong, C.E. Paraoxonase 1 (PON1) as a genetic determinant of susceptibility to organophosphate toxicity. *Toxicology* **2013**, *307*, 115–122. [[CrossRef](#)]
4. Shih, D.M.; Gu, L.; Xia, Y.R.; Navab, M.; Li, W.F.; Hama, S.; Castellani, L.W.; Furlong, C.E.; Costa, L.G.; Fogelman, A.M.; et al. Mice lacking serum paraoxonase are susceptible to organophosphate toxicity and atherosclerosis. *Nature* **1998**, *394*, 284–287. [[CrossRef](#)]
5. Shih, D.M.; Xia, Y.R.; Wang, X.P.; Miller, E.; Castellani, L.W.; Subbanagounder, G.; Cheroutre, H.; Faull, K.F.; Berliner, J.A.; Witztum, J.L.; et al. Combined serum paraoxonase knockout/apolipoprotein E knockout mice exhibit increased lipoprotein oxidation and atherosclerosis. *J. Biol. Chem.* **2000**, *275*, 17527–17535. [[CrossRef](#)] [[PubMed](#)]
6. Bhattacharyya, T.; Nicholls, S.J.; Topol, E.J.; Zhang, R.L.; Yang, X.; Schmitt, D.; Fu, X.M.; Shao, M.Y.; Brennan, D.M.; Ellis, S.G.; et al. Relationship of paraoxonase 1 (PON1) gene polymorphisms and functional activity with systemic oxidative stress and cardiovascular risk. *JAMA-J. Am. Med. Assoc.* **2008**, *299*, 1265–1276. [[CrossRef](#)] [[PubMed](#)]
7. Tang, W.H.; Hartiala, J.; Fan, Y.; Wu, Y.; Stewart, A.F.; Erdmann, J.; Kathiresan, S.; Consortium, C.A.; Roberts, R.; McPherson, R.; et al. Clinical and genetic association of serum paraoxonase and arylesterase activities with cardiovascular risk. *Arterioscler. Thromb. Vasc. Biol.* **2012**, *32*, 2803–2812. [[CrossRef](#)] [[PubMed](#)]
8. Kennedy, D.J.; Tang, W.H.; Fan, Y.; Wu, Y.; Mann, S.; Pepoy, M.; Hazen, S.L. Diminished antioxidant activity of high-density lipoprotein-associated proteins in chronic kidney disease. *J. Am. Heart Assoc.* **2013**, *2*, e000104. [[CrossRef](#)]
9. Hassan, A.; Dohi, T.; Miyauchi, K.; Ogita, M.; Kurano, M.; Ohkawa, R.; Nakamura, K.; Tamura, H.; Isoda, K.; Okazaki, S.; et al. Prognostic impact of homocysteine levels and homocysteine thiolactonase activity on long-term clinical outcomes in patients undergoing percutaneous coronary intervention. *J. Cardiol.* **2017**, *69*, 830–835. [[CrossRef](#)]
10. Kunutsor, S.K.; Bakker, S.J.; James, R.W.; Dullaart, R.P. Serum paraoxonase-1 activity and risk of incident cardiovascular disease: The PREVENT study and meta-analysis of prospective population studies. *Atherosclerosis* **2016**, *245*, 143–154. [[CrossRef](#)] [[PubMed](#)]
11. Tward, A.; Xia, Y.R.; Wang, X.P.; Shi, Y.S.; Park, C.; Castellani, L.W.; Lusis, A.J.; Shih, D.M. Decreased atherosclerotic lesion formation in human serum paraoxonase transgenic mice. *Circulation* **2002**, *106*, 484–490. [[CrossRef](#)] [[PubMed](#)]
12. Borowczyk, K.; Shih, D.M.; Jakubowski, H. Metabolism and neurotoxicity of homocysteine thiolactone in mice: Evidence for a protective role of paraoxonase 1. *J. Alzheimer's Dis. JAD* **2012**, *30*, 225–231. [[CrossRef](#)] [[PubMed](#)]
13. Jakubowski, H. Calcium-dependent human serum homocysteine thiolactone hydrolase. A protective mechanism against protein N-homocysteinylation. *J. Biol. Chem.* **2000**, *275*, 3957–3962. [[CrossRef](#)]
14. Perla-Kajan, J.; Jakubowski, H. Paraoxonase 1 protects against protein N-homocysteinylation in humans. *FASEB J.* **2010**, *24*, 931–936. [[CrossRef](#)]
15. Perla-Kajan, J.; Borowczyk, K.; Glowacki, R.; Nygard, O.; Jakubowski, H. Paraoxonase 1 Q192R genotype and activity affect homocysteine thiolactone levels in humans. *FASEB J.* **2018**, *32*, 6019–6024. [[CrossRef](#)] [[PubMed](#)]
16. Menini, T.; Gugliucci, A. Paraoxonase 1 in neurological disorders. *Redox. Rep.* **2014**, *19*, 49–58. [[CrossRef](#)]
17. Marsillach, J.; Adorni, M.P.; Zimetti, F.; Papotti, B.; Zuliani, G.; Cervellati, C. HDL Proteome and Alzheimer's Disease: Evidence of a Link. *Antioxidants* **2020**, *9*, 1224. [[CrossRef](#)]
18. de la Torre, J.C. Alzheimer disease as a vascular disorder: Nosological evidence. *Stroke* **2002**, *33*, 1152–1162. [[CrossRef](#)] [[PubMed](#)]

19. Erlich, P.M.; Lunetta, K.L.; Cupples, L.A.; Abraham, C.R.; Green, R.C.; Baldwin, C.T.; Farrer, L.A. Serum paraoxonase activity is associated with variants in the PON gene cluster and risk of Alzheimer disease. *Neurobiol. Aging* **2012**, *33*, 1015.e7–1015.e23. [[CrossRef](#)] [[PubMed](#)]
20. Bednarska-Makaruk, M.E.; Krzykowski, T.; Graban, A.; Lipczynska-Lojkowska, W.; Bochynska, A.; Rodo, M.; Wehr, H.; Ryglewicz, D.K. Paraoxonase 1 (PON1) gene-108C>T and p.Q192R polymorphisms and arylesterase activity of the enzyme in patients with dementia. *Folia Neuropathol.* **2013**, *51*, 111–119. [[CrossRef](#)]
21. Dantoine, T.F.; Debord, J.; Merle, L.; Lacroix-Ramiandrisoa, H.; Bourzeix, L.; Charmes, J.P. Paraoxonase 1 activity: A new vascular marker of dementia? *Ann. N. Y. Acad. Sci.* **2002**, *977*, 96–101. [[CrossRef](#)]
22. Paragh, G.; Balla, P.; Katona, E.; Seres, I.; Egerhazi, A.; Degrell, I. Serum paraoxonase activity changes in patients with Alzheimer's disease and vascular dementia. *Eur. Arch. Psychiatry Clin. Neurosci.* **2002**, *252*, 63–67. [[CrossRef](#)]
23. Bednarz-Misa, I.; Berdowska, I.; Zboch, M.; Misiak, B.; Zielinski, B.; Placzkowska, S.; Fleszar, M.; Wisniewski, J.; Gamian, A.; Krzystek-Korpaczka, M. Paraoxonase 1 decline and lipid peroxidation rise reflect a degree of brain atrophy and vascular impairment in dementia. *Adv. Clin. Exp. Med.* **2020**, *29*, 71–78. [[CrossRef](#)]
24. Perla-Kajan, J.; Wloczkowska, O.; Ziola-Frankowska, A.; Frankowski, M.; Smith, A.D.; de Jager, C.A.; Refsum, H.; Jakubowski, H. Paraoxonase 1, B Vitamins Supplementation, and Mild Cognitive Impairment. *J. Alzheimers Dis.* **2021**, *81*, 1211–1229. [[CrossRef](#)] [[PubMed](#)]
25. Aluganti Narasimhulu, C.; Mitra, C.; Bhardwaj, D.; Burge, K.Y.; Parthasarathy, S. Alzheimer's Disease Markers in Aged ApoE-PON1 Deficient Mice. *J. Alzheimers Dis.* **2019**, *67*, 1353–1365. [[CrossRef](#)] [[PubMed](#)]
26. Salazar, J.G.; Marsillach, J.; Reverte, I.; Mackness, B.; Mackness, M.; Joven, J.; Camps, J.; Colomina, M.T. Paraoxonase-1 and -3 Protein Expression in the Brain of the Tg2576 Mouse Model of Alzheimer's Disease. *Antioxidants* **2021**, *10*(3), 339. [[CrossRef](#)]
27. Suszynska-Zajczyk, J.; Luczak, M.; Marczak, L.; Jakubowski, H. Inactivation of the paraoxonase 1 gene affects the expression of mouse brain proteins involved in neurodegeneration. *J. Alzheimers Dis.* **2014**, *42*, 247–260. [[CrossRef](#)] [[PubMed](#)]
28. Tanzi, R.E. The genetics of Alzheimer disease. *Cold Spring Harb. Perspect. Med.* **2012**, *2*, a006296. [[CrossRef](#)]
29. Blatter, M.C.; James, R.W.; Messmer, S.; Barja, F.; Pometta, D. Identification of a distinct human high-density lipoprotein subspecies defined by a lipoprotein-associated protein, K-45. Identity of K-45 with paraoxonase. *Eur. J. Biochem.* **1993**, *211*, 871–879. [[CrossRef](#)]
30. Sikora, M.; Bretes, E.; Perla-Kajan, J.; Lewandowska, I.; Marczak, L.; Jakubowski, H. Genetic Attenuation of Paraoxonase 1 Activity Induces Proatherogenic Changes in Plasma Proteomes of Mice and Humans. *Antioxidants* **2020**, *9*, 1198. [[CrossRef](#)]
31. Khayati, K.; Antikainen, H.; Bonder, E.M.; Weber, G.F.; Kruger, W.D.; Jakubowski, H.; Dobrowolski, R. The amino acid metabolite homocysteine activates mTORC1 to inhibit autophagy and form abnormal proteins in human neurons and mice. *FASEB J.* **2017**, *31*, 598–609. [[CrossRef](#)]
32. Yates, S.C.; Zafar, A.; Hubbard, P.; Nagy, S.; Durant, S.; Bicknell, R.; Wilcock, G.; Christie, S.; Esiri, M.M.; Smith, A.D.; et al. Dysfunction of the mTOR pathway is a risk factor for Alzheimer's disease. *Acta Neuropathol. Commun.* **2013**, *1*, 3. [[CrossRef](#)]
33. Chen, X.; Wang, S.; Zhou, Y.; Han, Y.; Li, S.; Xu, Q.; Xu, L.; Zhu, Z.; Deng, Y.; Yu, L.; et al. Phf8 histone demethylase deficiency causes cognitive impairments through the mTOR pathway. *Nat. Commun.* **2018**, *9*, 114. [[CrossRef](#)] [[PubMed](#)]
34. Oakley, H.; Cole, S.L.; Logan, S.; Maus, E.; Shao, P.; Craft, J.; Guillozet-Bongaarts, A.; Ohno, M.; Disterhoft, J.; Van Eldik, L.; et al. Intraneuronal beta-amyloid aggregates, neurodegeneration, and neuron loss in transgenic mice with five familial Alzheimer's disease mutations: Potential factors in amyloid plaque formation. *J. Neurosci.* **2006**, *26*, 10129–10140. [[CrossRef](#)] [[PubMed](#)]
35. Murphy, M.P.; Beckett, T.L.; Ding, Q.; Patel, E.; Markesbery, W.R.; St Clair, D.K.; LeVine, H., 3rd; Keller, J.N. Aβ solubility and deposition during AD progression and in APPxPS-1 knock-in mice. *Neurobiol. Dis.* **2007**, *27*, 301–311. [[CrossRef](#)] [[PubMed](#)]
36. Sadleir, K.R.; Eimer, W.A.; Cole, S.L.; Vassar, R. Aβ reduction in BACE1 heterozygous null 5XFAD mice is associated with transgenic APP level. *Mol. Neurodegener.* **2015**, *10*, 1–16. [[CrossRef](#)]
37. Thinakaran, G.; Teplow, D.B.; Siman, R.; Greenberg, B.; Sisodia, S.S. Metabolism of the "Swedish" amyloid precursor protein variant in neuro2a (N2a) cells. Evidence that cleavage at the "beta-secretase" site occurs in the golgi apparatus. *J. Biol. Chem.* **1996**, *271*, 9390–9397. [[CrossRef](#)]
38. Gurda, D.; Handschuh, L.; Kotkowiak, W.; Jakubowski, H. Homocysteine thiolactone and N-homocysteinylated protein induce pro-atherogenic changes in gene expression in human vascular endothelial cells. *Amino. Acids* **2015**, *47*, 1319–1339. [[CrossRef](#)]
39. Livak, K.J.; Schmittgen, T.D. Analysis of relative gene expression data using real-time quantitative PCR and the 2⁻(Delta Delta C(T)) Method. *Methods* **2001**, *25*, 402–408. [[CrossRef](#)]
40. Lieu, C.A.; Chinta, S.J.; Rane, A.; Andersen, J.K. Age-related behavioral phenotype of an astrocytic monoamine oxidase-B transgenic mouse model of Parkinson's disease. *PLoS ONE* **2013**, *8*, e54200. [[CrossRef](#)]
41. Guyenet, S.J.; Furrer, S.A.; Damian, V.M.; Baughan, T.D.; La Spada, A.R.; Garden, G.A. A simple composite phenotype scoring system for evaluating mouse models of cerebellar ataxia. *J. Vis. Exp.* **2010**, *39*, e1787.
42. Witucki, Ł.; Jakubowski, H. Deletion of bleomycin hydrolase gene in mice induces biochemical and behavioral hallmarks of Alzheimer's disease. *J. Alzheimer's Dis.* **2023**. *submitted*.
43. Jakubowski, H.; Perla-Kajan, J.; Finnell, R.H.; Cabrera, R.M.; Wang, H.; Gupta, S.; Kruger, W.D.; Kraus, J.P.; Shih, D.M. Genetic or nutritional disorders in homocysteine or folate metabolism increase protein N-homocysteinylation in mice. *Faseb. J.* **2009**, *23*, 1721–1727. [[CrossRef](#)] [[PubMed](#)]
44. O'Leary, T.P.; Robertson, A.; Chipman, P.H.; Rafuse, V.F.; Brown, R.E. Motor function deficits in the 12 month-old female 5x3FAD mouse model of Alzheimer's disease. *Behav. Brain Res.* **2018**, *337*, 256–263. [[CrossRef](#)]

45. O'Leary, T.P.; Mantolino, H.M.; Stover, K.R.; Brown, R.E. Age-related deterioration of motor function in male and female 5xFAD mice from 3 to 16 months of age. *Genes Brain Behav.* **2020**, *19*, e12538. [CrossRef]

Disclaimer/Publisher's Note: The statements, opinions and data contained in all publications are solely those of the individual author(s) and contributor(s) and not of MDPI and/or the editor(s). MDPI and/or the editor(s) disclaim responsibility for any injury to people or property resulting from any ideas, methods, instructions or products referred to in the content.

Supplementary Material

Supplementary Figure S1

Supplementary Figure S2

Supplementary Table S1

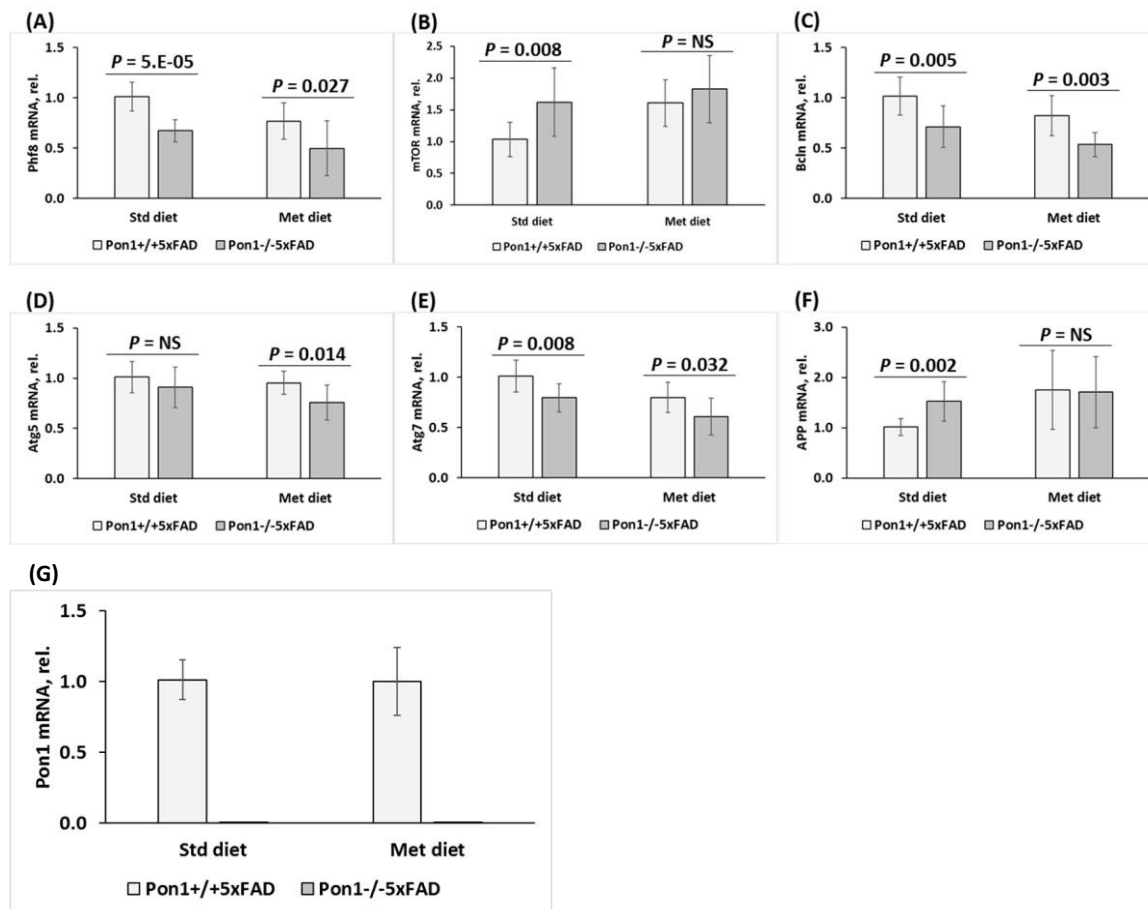


Figure S1. Pon1 depletion affects the expression of mRNAs for Phf8, mTOR, autophagy-related proteins, and App in the *Pon1*^{-/-}5xFAD mouse brain. Bar graphs illustrating the quantification by RT-qPCR of mRNAs for Phf8 (A), mTOR (B), Bcln1 (C), Atg5 (D), Atg7 (E), and App (F) are shown. Pon1 mRNA was absent in *Pon1*^{-/-}5xFAD brains (G). Met diet did not affect Pon1 mRNA in *Pon1*^{+/+}5xFAD mouse brain. Gapdh mRNA was used as a reference.

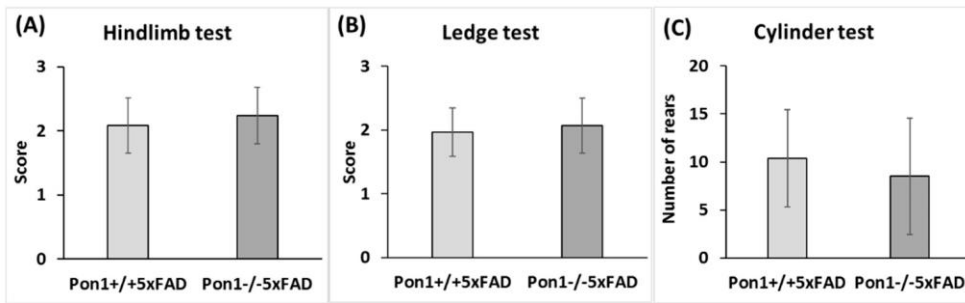


Figure S2. Pon1 depletion did not affect sensorimotor activity in mice. Behavioral performance of 12-month-old *Pon1*^{-/-}5xFAD (n = 21) and *Pon1*^{+/+}5xFAD (n = 18) mice was assessed in the hindlimb clasp test (A), ledge test (B), and cylinder test (C).

Table S1 Primers used for PCR or RT-qPCR	
Gene	Primer sequence
<i>APP</i>	Forward: 5'-CTTCCCAAGATCCTGATAAACT-3'
	Reverse: 5'-CCGGGTGTCTCCAGGACT-3'
<i>Atg5</i>	Forward: 5'-AAGGCACACCCCTGAAATGG-3'
	Reverse: 5'-TGATGTTCCAAGGAAGAGCTGAA-3'
<i>Atg7</i>	Forward: 5'-GCCAACTCCACACTGCTTTC-3'
	Reverse: 5'-TCTTCTGGGTCAGTTCGTGC-3'
<i>Beclin-1</i>	Forward: 5'GAG GAA GCT CAG TAC CAG CG 3'
	Reverse: 5'CCA GAT GTG GAA GGT GGC AT 3'
<i>Pon1</i>	Forward p1: 5'-CACTGTAGCTGTACTCACAC-3'
	Reverse p2: 5'-ATAGGAAGACCGATGGTTCT-3';
	Reverse p3 (5'-TCCTCGTGCTTTACGGTATCG-3') (neomycin cassette)
<i>Gapdh</i>	Forward: 5'-GGACTGGATAAGCAGGGCG-3'
	Reverse: 5'-TTTTGTCTACGGGACGAGGC-3'
<i>mTOR</i>	Forward: 5'-GCCACTCTGACCCAGTTC-3'
	Reverse: 5'-ATGCCAAGACACAGTAGCGG-3'
<i>Phf8</i>	Forward: 5'-TGGGAGCATGCTTCAAGG-3'
	Reverse: 5'-GATTTCAAAGCAGGGTCATCA-3'
<i>hAPP transgene in 5xFAD mice</i>	Forward: 5'-AGAGTACCAACTTGCATGACTACG-3';
	Reverse: 5'-ATGCTGGATAACTGCCTTCTTATC-3'
<i>hPS1 transgene in 5xFAD mice</i>	Forward: 5'-GCTTTTCCAGCTCTCATTACTC-3'
	Reverse: 5'-AAAATTGATGGAATGCTAATTGGT-3'
<i>mTOR upstream TSS*</i>	Forward: 5'-TTGCCAACTGGTGCTCGTTT-3'
	Reverse: 5'-AAGAATTGGAGCTCGGGACC-3'
<i>mTOR TSS*</i>	Forward: 5'-GGATGTTCTCCCAATCTTCG-3'
	Reverse: 5'-CAGACCCACCTAACTGACCGT-3'
<i>mTOR downstream TSS*</i>	Forward: 5'-TAGGGGGCAGATCCCGAAAC-3'
	Reverse: 5'-CACTGTAGCTGTAACCTCACAC-3'

* TSS, transcription start site

Witucki Ł, Jakubowski H,

Homocysteine Metabolites Inhibit Autophagy and Elevate Amyloid Beta by Impairing Phf8/H4K20me1-
dependent Epigenetic Regulation of mTOR in cystathionine β -synthase-deficient mice,

J Inherit Metab Dis. 2023;1–17 DOI: 10.1002/jimd.12661

Pięcioletni IF: 4,429, MEiN 100 punktów

Homocysteine metabolites inhibit autophagy, elevate amyloid beta, and induce neuropathy by impairing Phf8/ H4K20me1-dependent epigenetic regulation of mTOR in cystathionine β -synthase-deficient mice

Łukasz Witucki^{1,2}  | Hieronim Jakubowski^{1,2} 

¹Department of Microbiology, Biochemistry and Molecular Genetics, Rutgers University, New Jersey Medical School, Newark, New Jersey, USA

²Department of Biochemistry and Biotechnology, Poznan University of Life Sciences, Poznan, Poland

Correspondence

Hieronim Jakubowski, Department of Microbiology, Biochemistry and Molecular Genetics, Rutgers-New Jersey Medical School, International Center for Public Health, 225 Warren Street, Newark, New Jersey 07103, USA. Email: jakubows@rutgers.edu

Funding information American Heart Association, Grant/Award Number: 17GRNT32910002; Narodowe Centrum Nauki, Grant/Award Numbers: 2018/29/B/NZ4/00771, 2019/33/B/NZ4/01760, 2021/43/B/NZ4/00339

Communicating Editor: Clara van Karnebeek

Abstract

The loss of cystathionine β -synthase (CBS), an important homocysteine (Hcy)-metabolizing enzyme or the loss of PHF8, an important histone demethylase participating in epigenetic regulation, causes severe intellectual disability in humans. Similar neuropathies were also observed in *Cbs*^{-/-} and *Phf8*^{-/-} mice.

How CBS or PHF8 depletion can cause neuropathy was unknown. To answer this question, we examined a possible interaction between PHF8 and CBS using *Cbs*^{-/-} mouse and neuroblastoma cell models. We quantified gene expression by RT-qPCR and western blotting, mTOR-bound H4K20me1 by chromatin immunoprecipitation (CHIP) assay, and amyloid β (A β) by confocal fluorescence microscopy using anti-A β antibody. We found significantly reduced expression of Phf8, increased H4K20me1, increased mTOR expression and phosphorylation, and increased App, both on protein and mRNA levels in brains of *Cbs*^{-/-} mice versus *Cbs*^{+/-} sibling controls. Autophagy-related *Becn1*, *Atg5*, and *Atg7* were downregulated while *p62*, *Nfl*, and *Gfap* were upregulated on protein and mRNA levels, suggesting reduced autophagy and increased neurodegeneration in *Cbs*^{-/-} brains. In mouse neuroblastoma N2a or N2a-APPswe cells, treatments with Hcy-thiolactone, N-Hcy-protein or Hcy, or *Cbs* gene silencing by RNA interference significantly reduced Phf8 expression and increased total H4K20me1 as well as mTOR promoter-bound H4K20me1. This led to transcriptional mTOR upregulation, autophagy downregulation, and significantly increased APP and A β levels. The Phf8 gene silencing increased A β , but not APP, levels. Taken together, our findings identify Phf8 as a regulator of A β synthesis and suggest that neuropathy of *Cbs* deficiency is mediated by Hcy metabolites, which transcriptionally dysregulate the Phf8 ! H4K20me1 ! mTOR ! autophagy pathway thereby increasing A β accumulation.

This is an open access article under the terms of the [Creative Commons Attribution](https://creativecommons.org/licenses/by/4.0/) License, which permits use, distribution and reproduction in any medium, provided the original work is properly cited.

© 2023 The Authors. Journal of Inherited Metabolic Disease published by John Wiley & Sons Ltd on behalf of SSIEM.

KEYWORDS

amyloid beta, APP, autophagy, *Cbs*^{-/-} mouse, H4K20me1, homocysteine thiolactone, mTOR signaling, N-homocysteinylation protein, Phf8

1 | INTRODUCTION

The sulfur-containing amino acids methionine (Met), homocysteine (Hcy), and cysteine (Cys) are metabolically related and play important roles in cellular physiology.¹ Met is an essential amino acid that participates in the biosynthesis of proteins (>20 000) and S-adenosylmethionine (AdoMet). AdoMet provides methyl groups for the biological methylation reactions (>300) and propyl groups for the polyamine spermidine and spermine biosynthesis. The methylation reactions generate S-adenosylhomocysteine (AdoHcy). Enzymatic hydrolysis of AdoHcy is the only known metabolic source of Hcy. Remethylation of Hcy, which regenerates Met, is essential for the folate and one-carbon metabolism, which provides one-carbon units for nucleotides required for DNA and RNA biosynthesis. Transsulfuration of Hcy generates Cys, a semi-essential amino acid, participating in the biosynthesis of proteins, glutathione, hydrogen sulfide, and taurine. Hcy is also metabolized by methionyl-tRNA synthetase to Hcy-thiolactone,^{2–5} which modifies proteins in a nonenzymatic N-homocysteinylation reaction that generates N-Hcy-protein.^{5,6}

Elevated levels of Hcy due to nutritional or genetic deficiencies are associated with neuropathology affecting the central nervous system (CNS). Cystathionine β -synthase (CBS) deficiency due to mutations in the CBS gene is the most prevalent inborn error in the sulfur amino acid metabolism that results in severe hyperhomocysteinemia (HHcy) characterized by elevated levels of Hcy and its metabolites such as Hcy-thiolactone and N-Hcy-protein.¹ CBS deficiency affects the CNS and causes severe learning and intellectual disability, reduced IQ,⁷ psychosis, obsessive-compulsive and behavior/personality disorders.⁸ Accelerated brain atrophy related to elevated plasma Hcy has been reported in patients with Alzheimer's disease,⁹ in patients with alcoholism,¹⁰ and in healthy elderly individuals.¹¹ These phenotypes were replicated in *Cbs*^{-/-} mice on the C57BL/6J background, which show cognitive impairment manifested as reduced problem-solving abilities, learning disability, and short-term and long-term memory in the puzzle box test.¹² *Cbs*^{-/-} mice on the C3H/HeJ background show cerebellar, although not cerebral, malformation and a transient learning deficit on day 2 in the passive avoidance step-through test.¹³

The molecular bases of neurological impairments in CBS deficiency are not fully understood. Although Hcy, Hcy-thiolactone, and N-Hcy-proteins accumulate in CBS-

deficient patients and mice,^{14–17} it is unclear whether each of these metabolites can contribute to neuropathy associated with CBS deficiency. Individuals with elevated plasma total Hcy show accelerated brain atrophy, impaired cognition, and are at higher risk and developing Alzheimer's disease¹⁸ which is also associated with up-regulated brain mTOR signaling.¹⁹

Plant homeodomain finger protein 8 (PHF8) has been identified as one of the X chromosome genes linked to the intellectual disability syndrome, autism spectrum disorder, attention deficit hyperactivity disorder,²⁰ and severe intellectual disability.²¹ PHF8 is a histone demethylase that can demethylate H4K20me1, H3K9me2/me1, and H3K27me2. Demethylation of H4K20me1 by PHF8 is important for maintaining homeostasis of mTOR signaling. The human PHF8 deficiency phenotype has been replicated in *Phf8*^{-/-} mice, which show impaired hippocampal long-term potentiation and behavioral deficits in learning and memory.²²

How CBS or PHF8 depletion can cause neuropathy is not fully understood. The present work was undertaken to test a hypothesis that CBS depletion reduces the expression of PHF8, increases H4K20me1, mTOR expression and phosphorylation, inhibits autophagy, and increases amyloid β (A β) accumulation. Towards this end, we studied how *Cbs* gene deletion affects *Phf8* expression and H4K20me1 levels, mTOR signaling/autophagy, and neurodegeneration markers (Nfl, Gfap) expression in the mouse brain. We also used mouse neuroblastoma N2a and A β -overproducing N2a-APP^{swe} cells to study how individual Hcy metabolites or depletion of *Cbs* or *Phf8* by RNA interference affect *Phf8* expression and its downstream effects on the expression of mTOR and autophagy-related proteins, as well as App expression and A β accumulation.

2 | MATERIALS AND METHODS 2.1 |

Mice

Transgenic Tg-I278T *Cbs*^{-/-} mice^{23,24} on the C57BL/6J background were housed and bred at the Rutgers-New Jersey Medical School Animal Facility. Transgenic harboring human CBS I278T (Tg-I278T) variant was used to rescue the neonatal lethality associated with homozygosity for *Cbs*^{-/-}. In these animals, the human mutant CBS,

which has less than 3% of the activity of wild-type enzyme, is under control of the zinc-inducible metallothionein promoter, which allows to rescue the neonatal lethality phenotype of *Cbs*^{-/-} in mice by supplementing the drinking water of pregnant dams with 25 mM zinc chloride. Zinc-water was replaced by plain water after weaning at 30 days. Only *Cbs*^{-/-} mice exhibit changed phenotype characterized by facial alopecia, thin, smooth, shiny tail, reduced body weight and shortened life span compared to *Cbs*^{+/-} animals.^{23,24} *Cbs*^{-/-} mice had severely elevated plasma tHcy (plasma 272 ± 50 μM, urine 4.1 ± 1.4 mM), N-Hcy-protein (plasma 16.6 ± 4.1 μM; urine 10.8 ± 4.1 μM), and Hcy-thiolactone (urine 11.8 ± 0.9 μM) compared to *Cbs*^{+/-} (plasma tHcy 5.0 ± 2.6 μM and N-Hcy-protein, 2.6 ± 1.7 μM; urine Hcy-thiolactone, <0.2 nM) and *Cbs*^{+/+} animals (plasma tHcy 3.4 ± 0.3 μM and N-Hcy-protein 1.9 ± 0.7 μM; Hcy-thiolactone, urine <0.2 nM).^{16,17} Mouse *Cbs* genotypes were established by PCR using the following primers: forward 5⁰-GGTCTGGAATTCATATGT AGC-3⁰, wild type reverse 5⁰-CGGATGACCTGCATTCATCT -3⁰, mutant reverse: 5⁰-GAGGTGACGGTATCGATA-3⁰. The mice were fed with a standard rodent chow (LabDiet5010; Purina Mills International, St. Louis, MO, USA). Two- to 12-month-old *Cbs*^{-/-} mice were used in experiments. Control animals were *Cbs*^{+/-} siblings. Animal procedures were approved by the Institutional Animal Care and Use Committee at Rutgers-New Jersey Medical School.

2.2 | Brain protein extraction

Mice were euthanized by CO₂ inhalation, the brains collected and frozen on dry ice. Frozen brains were pulverized with dry ice using a mortar and pestle and stored at 80 C. Proteins were extracted from the pulverized brains (50 ± 5 mg) using RIPA buffer (4 v/w, containing protease and phosphatase inhibitors) with sonication (Bandelin SONOPLUS HD 2070) on wet ice (three sets of five 1-s strokes with 1 min cooling interval between strokes). Brain extracts were clarified by centrifugation (15 000 g, 15 min, 4 C) and clear supernatants containing 8–12 mg protein/mL were collected. Protein concentrations were measured with BCA kit (Thermo Scientific).

2.3 | Cell culture and treatments

Mouse neuroblastoma N2a or N2a-APP^{swe} cells, harboring a human APP transgene with the K670N and M671L Swedish mutations²⁵ were grown in DMEM/F12 medium (Thermo Scientific) supplemented with 5% FBS, non-essential amino acids, and antibiotics (MilliporeSigma) (37 C, 5% CO₂).

After reaching 70%–80% confluency, cell monolayers were washed 2-times with PBS and overlaid with DMEM medium without Met (Thermo Scientific), supplemented with 5% dialyzed FBS (MilliporeSigma) and non-essential amino acids. D,L-Hcy, L-Hcy-thiolactone (MilliporeSigma), or N-Hcy-protein (prepared by modification of FBS proteins with Hcy-thiolactone as described in ref. (26)) were added (at concentrations indicated in figure legends) and the cultures were incubated at 37 C in 5% CO₂ atmosphere for 24 h. For gene silencing, siRNAs specific for the *Cbs* (Cat. # 100821 and s63474) or *Phf8* gene (Cat. # S115808, and S115809) (Thermo Scientific) were transfected into cells maintained in Opti-MEM medium by 24-h Lipofectamine RNAiMax (Thermo Scientific) treatments. Cellular RNA for RT-q PCR analysis was isolated as described in section 2.5 below. For protein extraction, RIPA buffer (MilliporeSigma) was used according to manufacturer's protocol.

2.4 | Western blots

Proteins were separated by SDS-PAGE on 10% gels (20 μg protein/lane) and transferred to PVDF membrane (Bio-Rad) for 20 min at 0.1 A, 25 V using Trans Blot Turbo Transfer System (Bio-Rad). After blocking with 5% bovine serum albumin in TBST buffer (1 h, room temperature), the membranes were and incubated overnight with anti-*Phf8* (Abcam, ab36068), anti-H4K20me1 (Abcam ab177188), anti-mTOR (CS #2983), anti-pmTOR Ser2448 (CS, #5536), anti-Atg5 (CS, #12994), anti-Atg7 (CS, #8558), anti-Beclin-1 (CS, #3495), anti-p62 (CS, #23214), anti-neurofilament-L (Nfl; CS, #2837), anti-glial fibrillary acidic protein (Gfap; CS, #80788), anti-Gapdh (CS, #5174), anti-*Cbs* (Abcam, ab135626), or anti-App (Abcam, ab126732). Membranes were washed three times with TBST buffer, 10 min each, and incubated with goat anti-rabbit IgG secondary antibody conjugated with horseradish peroxidase. Positive signals were detected using Western Bright Quantum-Advanta K12042-D20 and GeneGnome XRQ NPC chemiluminescence detection system. Bands intensity was calculated using Gene Tools program from Syngene.

2.5 | RNA isolation, cDNA synthesis, RT-qPCR analysis

Total RNA was isolated using Trizol reagent (MilliporeSigma). cDNA synthesis was conducted using Revert Aid First cDNA Synthesis Kit (Thermo Fisher Scientific) according to manufacturer's protocol. Nucleic

acid concentration was measured using NanoDrop (Thermo Fisher Scientific). RT-qPCR was performed with SYBR Green Mix and CFX96 thermocycler (Bio-Rad). The $2^{-\Delta\Delta Ct}$ method was used to calculate the relative expression levels.²⁷ Data analysis was performed with the CFX Manager™ Software, Microsoft Excel, and Statistica. RT-qPCR primer sequences are listed in Table S1.

2.6 | Chromatin immunoprecipitation assay

For CHIP assays we used CUT&RUN Assay Kit #86652 (Cell Signaling Technology, Danvers, MA, USA) following the manufacturer's protocol. Each ChIP assay was repeated three times. Briefly, for each reaction we used 100 000 cells. Cells were trypsinized and harvested, washed 3 in ice-cold PBS, bound to concanavalin A-coated magnetic beads for 5 min, RT. Cells were then incubated (4 h, 4 C) with 2.5 μ g of anti-PHF8 antibody (Abcam, ab36068) or anti-H4K20me1 antibody (Abcam, ab177188) in the antibody-binding buffer plus digitonin that permeabilizes cells. Next, cells are treated with pAG-MNase (1 h, 4 C), washed, and treated with CaCl₂ to activate DNA digestion (0.5 h, 4 C). Cells were then treated with the stop buffer and spike-in DNA was added for each reaction for signal normalization, and incubated (10–30 min, 37 C). Released DNA fragments were purified using DNA Purification Buffers and Spin Columns (CS #14209) and quantified by RT-qPCR using primers targeting the promoter, upstream, and downstream regions of the mTOR gene (Table S1). Rabbit (DA1E) mAb IgG XP® Isotype control included in the CUT&RUN kit did not afford any signals in RT-qPCR assays targeting mTOR.

2.7 | Confocal microscopy, A β staining in N2a-APPsw cells

Mouse neuroblastoma N2a-APPsw cells were cultured in Millicell EZ SLIDE 8-well glass (Merck). After treatments cells were washed 3 with PBS for 10 min. Cells were fixed with 4% PFA (MilliporeSigma) (37 C, 15 min). After fixation, cells were again washed three times with PBS buffer and permeabilized in 0.1% Triton X-100 solution (RT, 20 min), blocked with 0.1% BSA (RT, 1 h), and incubated with anti-A β antibody (CS #8243; 4 C, 16 h). Cells were then washed three times with PBS and stained with secondary antibody Goat Anti-Rabbit IgG H&L (Alexa Fluor® 488) (Abcam, ab150077; RT, 1 h) to detect A β . DAPI (Vector Laboratories) was used to visualize nuclei. Fluorescence signals were detected by using a

Zeiss LSM 880 confocal microscope with a 488 nm filter for the Alexa Fluor® 488 (A β) and 420–480 nm filter for DAPI, taking a z stack of 20–30 sections with an interval of 0.66 μ m and a range of 15 μ m. Zeiss Plan-Apochromat X40/1.2 Oil differential interference contrast objective were used for imaging. Images were quantified with the ImageJ Fiji software (NIH).

2.8 | Statistical analysis

The results were calculated as mean \pm standard deviation. Values for each experimental/treatment group were normalized to controls. Data were analyzed using one-way analysis of variance (ANOVA) with Tukey's multiple comparisons post-test using GraphPad Prism7 software (GraphPad Holdings LLC, San Diego, CA, USA, <https://www.graphpad.com>).

3 | RESULTS

3.1 | Cbs deficiency downregulates the histone demethylase Phf8 expression and upregulates H4K20me1 epigenetic mark in the mouse brain

To determine if neuropathy in Cbs^{-/-} mice can be caused by the interaction between Cbs and Phf8 genes, we quantified Phf8 protein and mRNA in brains of 9-week-old and 1-year-old Tg-I278T Cbs^{-/-} mice and Tg-I278T Cbs^{+/-} sibling controls by using western blotting and RT-qPCR assays, respectively. We found that the Phf8 protein levels were significantly reduced in brains of Tg-I278T Cbs^{-/-} mice vs. Tg-I278T Cbs^{+/-} sibling controls, regardless of age (9-week-old mice: 0.38 \pm 0.27 vs. 0.89

\pm 0.21, $P = 0.0001$; 1-year-old mice: 0.47 \pm 0.14 vs. 0.93 \pm 0.23, $P < 0.0001$; Figure 1A).

Phf8 mRNA levels were also significantly reduced in brains of Tg-I278T Cbs^{-/-} vs. Tg-I278T Cbs^{+/-} mice (9-week-old mice: 0.73 \pm 0.15 vs. 1.00 \pm 0.15, $P = 0.046$; 1-year-old mice: 0.67 \pm 0.26 vs. 1.21 \pm 0.27, $P < 0.0001$; Figure 1B). These findings indicate that Cbs^{-/-} genotype transcriptionally attenuated Phf8 expression while age did not affect Phf8 levels in Cbs^{-/-} nor Cbs^{+/-} mice.

The histone H4K20me1 epigenetic mark was significantly elevated in Tg-I278T Cbs^{-/-} brains compared with Tg-I278T Cbs^{+/-} brains (9-week-old mice 2.42 \pm 0.52 vs. 1.34 \pm 0.31, $P = 0.002$; 1-year-old mice: 1.33 \pm 0.56 vs. 0.81 \pm 0.37, $P = 0.048$; Figure 1C). Although Cbs^{-/-} genotype upregulated H4K20me1 in 1-year-old mice, age significantly reduced H4K20me1 levels in 1-year-old vs. 9-week-old Cbs^{-/-} animals (1.33 \pm 0.56 vs. 2.42

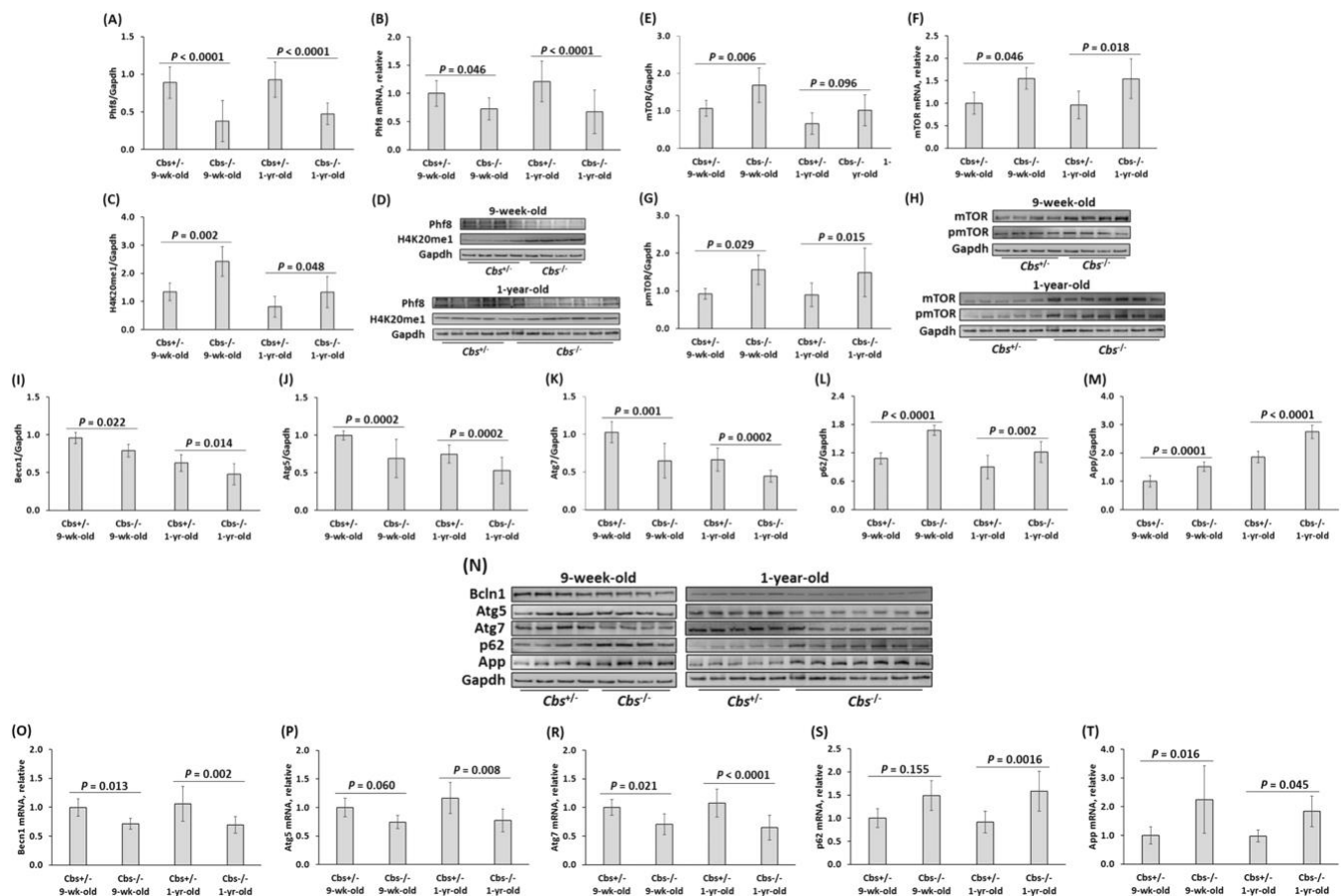


FIGURE 1 Deletion of the *Cbs* gene affects the expression of histone demethylase Phf8, histone H4K20me1 epigenetic mark, mTOR signaling, autophagy, and App in the mouse brain. Nine-week-old and 1-year-old Tg-I278T *Cbs*^{-/-} mice ($n = 7$ and 14) and their Tg-I278T *Cbs*^{+/+} sibling controls ($n = 10$ and 10) were used in experiments. Bar graphs illustrating quantification of the following brain proteins by western blotting are shown: Phf8 (A), H4K20me1 (C), mTOR (E), pmTOR (G), Becn1 (I), Atg5 (J), Atg7 (K), and p62 (L), and App (M). Pictures of western blots used for protein quantification are shown in panels (D), (H), and (N). Bar graphs illustrating quantification of the following brain mRNAs by RT-qPCR are also shown: Phf8 (B), mTOR (F), Becn1 (O), Atg5 (P), Atg7 (R), and p62 (S), and App (T). Gapdh protein and mRNA were used as references for normalization. P values were calculated by one-way ANOVA with Tukey's multiple comparisons test.

± 0.52 , $P < 0.0001$). In contrast, although H4K20me1 tended to be reduced in older vs. younger *Cbs*^{+/+} mice, the reduction was not significant (0.81 ± 0.37 vs. 1.34 ± 0.31 , $P = 0.064$). These findings show that although age attenuated H4K20me1 levels in *Cbs*^{-/-} and *Cbs*^{+/+} mice, the *Cbs*^{-/-} genotype effect on H4K20me1 was independent of age.

3.2 | Transcriptional upregulation of mTOR and inhibition of autophagy in *Cbs*^{-/-} mouse brain

We found that mTOR protein was upregulated in brains of Tg-I278T *Cbs*^{-/-} versus Tg-I278T *Cbs*^{+/+} mice (9-week-old mice: 1.68 ± 0.46 vs. 1.07 ± 0.21 , $P = 0.006$; 1-year-old mice: 1.02 ± 0.41 vs. 0.66 ± 0.29 , $P = 0.096$;

Figure 1E). mTOR mRNA was also similarly upregulated in Tg-I278T *Cbs*^{-/-} vs. Tg-I278T *Cbs*^{+/+} mice (9-week-old mice: 1.55 ± 0.24 vs. 1.00 ± 0.25 , $P = 0.046$; 1-year-old mice: 1.55 ± 0.44 vs. 0.96 ± 0.30 , $P = 0.018$; Figure 1F). While *Cbs*^{-/-} genotype upregulated mTOR in 1-year-old mice, age attenuated mTOR in 1-year-old vs. 9-week-old *Cbs*^{-/-} (1.02 ± 0.41 vs. 1.68 ± 0.46 , $P = 0.002$) and *Cbs*^{+/+} mice (0.66 ± 0.29 vs. 1.07 ± 0.21 , $P = 0.068$). These findings show that *Cbs*^{-/-} genotype transcriptionally upregulated mTOR in young and old mice while age attenuated mTOR expression both in *Cbs*^{-/-} and *Cbs*^{+/+} mice.

As mTOR is activated by phosphorylation, we quantified mTOR phosphorylated at Ser2448 (pmTOR). We found that pmTOR was significantly elevated in brains of Tg-I278T *Cbs*^{-/-} compared to Tg-I278T *Cbs*^{+/+} mice (9-week-old mice: 1.56 ± 0.39 vs. 0.92 ± 0.14 , $P = 0.029$;

1-year-old mice: 1.49 ± 0.65 vs. 0.90 ± 0.31 , $P = 0.015$; Figure 1G). These findings indicate that Cbs deficiency upregulated pmTOR to the same extent as mTOR and that Cbs^{+/+} age did not affect pmTOR levels in Cbs^{-/-} nor mice ($P = 0.999$ and 0.987 , respectively).

Because mTOR is a major regulator of autophagy, we quantified autophagy-related proteins in Tg-I278T Cbs^{-/-} mice. We found that the regulators of autophagosome assembly Becn1, Atg5, and Atg7 were significantly downregulated in brains of 9-week-old Tg-I278T Cbs^{-/-} mice vs. Tg-I278T Cbs^{+/+} sibling controls (Becn1: 0.79 ± 0.09 vs. 0.96 ± 0.07 , $P = 0.022$, Figure 1I; Atg5: 0.69 ± 0.25 vs. 0.99 ± 0.06 , $P = 0.0002$, Figure 1J; Atg7: 0.65 ± 0.23 vs. 1.03 ± 0.14 , $P = 0.001$, Figure 1K). Cbs^{-/-} genotype significantly downregulated Becn1 ($P = 0.014$), Atg5 ($P = 0.0002$), and Atg7 ($P = 0.0002$) also in 1-year-old mice (Figure 1I–K, respectively). However, Becn1, Atg5, and Atg7 levels were significantly reduced in 1-year-old versus 9-week-old mice, both in Cbs^{-/-} (Becn1: 0.63 ± 0.11 vs. 0.96 ± 0.07 , $P < 0.0001$; Atg5: 0.53 ± 0.17 vs. 0.69 ± 0.25 , $P = 0.084$; Atg7: 0.45 ± 0.08 vs. 0.65 ± 0.23 , $P = 0.007$) and Cbs^{+/+} animals (Becn1: 0.48 ± 0.14 vs. 0.79 ± 0.09 , $P < 0.0001$; Atg5: 0.75 ± 0.12 vs. 0.99 ± 0.06 , $P < 0.0001$; Atg7: 0.67 ± 0.15 vs. 1.03 ± 0.14 , $P = 0.0001$). The p62 protein, a receptor for degradation of ubiquitinated substrates, was upregulated in 9-week-old Tg-I278T Cbs^{-/-} mice vs. Tg-I278T Cbs^{+/+} sibling controls (1.68 ± 0.11 vs. 1.08 ± 0.12 , $P < 0.0001$; Figure 1L). Cbs^{-/-} genotype upregulated p62 also in 1-year-old mice (1.22 ± 0.22 vs. 0.90 ± 0.25 , $P = 0.002$). However, p62 levels were reduced in 1-year-old versus 9-week-old mice (Cbs^{-/-}: 1.22 ± 0.22 vs. 1.68 ± 0.11 , $P < 0.0001$; Cbs^{+/+}: 0.90 ± 0.25 vs. 1.08 ± 0.12 , $P = 0.181$). These findings suggest that autophagy was impaired in Cbs^{-/-} mouse brain. We found similar Cbs genotype-dependent changes in autophagy-related mRNAs. Specifically, Becn1, Atg5, and Atg7 mRNAs (Figure 1O,P,R, respectively) were significantly downregulated, while p62 mRNA (Figure 1S), were significantly upregulated in Tg-I278T Cbs^{-/-} compared with Tg-I278T Cbs^{+/+} mice, reflecting changes in the corresponding protein levels. These findings indicate that Cbs gene exerts transcriptional control over the expression of mTOR, Becn1, Atg5, Atg7, and p62 in the mouse brain.

3.3 | Cbs deficiency upregulates App expression in the mouse brain

We have previously found that A β was elevated in brains of 1-year-old mice Cbs^{-/-} mice compared to Cbs^{+/+} controls.²⁸ To determine whether upregulated App expression might be responsible for elevated A β , we quantified

App protein and mRNA in Tg-I278T Cbs^{-/-} and Tg-I278T Cbs^{+/+} mice by western blotting (Figure 1M) and RT-qPCR (Figure 1T), respectively.

We found that App protein was significantly elevated in 9-week-old Tg-I278T Cbs^{-/-} vs. Tg-I278T Cbs^{+/+} mice (1.52-fold: 1.52 ± 0.16 vs. 1.01 ± 0.20 , $P = 0.0001$). We found a similar elevation in App protein in 1-year-old Tg-I278T Cbs^{-/-} vs. Tg-I278T Cbs^{+/+} mice (1.49-fold, 2.75 ± 0.23 vs. 1.85 ± 0.20 , $P < 0.0001$) (Figure 1M). App mRNA was also upregulated in Tg-I278T Cbs^{-/-} vs. Tg-I278T Cbs^{+/+} mice (9-week-old mice: 2.25 ± 1.17 vs. 1.00 ± 0.30 , $P = 0.016$; 1-year-old mice: 1.84 ± 0.54 vs. 0.98 ± 0.21 , $P = 0.045$; Figure 1T). These findings indicate that Cbs exerts transcriptional control over App expression.

We also found that App protein significantly increased with age (Figure 1M), irrespective of Cbs genotype: old/young Tg-I278T Cbs^{-/-} mice 1.80-fold, $P < 0.0001$; old/young Tg-I278T Cbs^{+/+} mice 1.85-fold, $P < 0.0001$. However, age did not affect App mRNA levels (Figure 1T). These findings suggest that age exerts translational control over App expression independent of Cbs genotype or that age exerts posttranslational control by reducing the turnover of App protein.

3.4 | Cbs gene silencing downregulates the histone demethylase Phf8, upregulates H4K20me1, mTOR, pmTOR, APP, and inhibits autophagy in mouse neuroblastoma N2A-APPsw cells

To elucidate the mechanism by which Cbs deficiency impacts Phf8 and its downstream effects on mTOR, autophagy, and App we first examined whether the findings in Cbs^{-/-} mice can be recapitulated in cultured mouse neuroblastoma N2A-APPsw cells. We silenced the Cbs gene by transfecting corresponding siRNAs into N2A-APPsw cells and studied how the silencing impacts the level of Phf8 and its downstream effects. Changes in individual mRNA and protein levels in Cbs-silenced cells were analyzed by RT-qPCR and western blotting, respectively, using Gapdh mRNA and protein as references.

We found that the Cbs protein level was reduced by 80% in Cbs-silenced cells ($P < 0.0001$; Figure S1A). We also found that the histone demethylase Phf8 protein level was also significantly reduced (by 39%, $P < 0.001$; Figure S1B), while the histone H4K20me1 level was significantly elevated (2-fold, $P < 0.01$; Figure S1C) in Cbs-silenced N2a-APPsw cells.

At the same time, mTOR protein was significantly upregulated in Cbs-silenced N2a-APPsw cells (1.7-fold, $P < 0.001$; Figure S1D), as was pmTOR (2-fold, $P < 0.0001$; Figure S1E) and APP (1.5-fold, $P < 0.0001$;

Figure S1F), while autophagy-related proteins Becn1, Atg5, and Atg7 (Figure S1G–I, respectively) were significantly downregulated (by 30%–40%, $P < 0.0001$ to < 0.01).

We found similar changes in levels of mRNAs in Cbs-silenced N2a-APP_{swe} cells (Figure S2). Specifically, Cbs mRNA level was reduced (by 85%, $P < 0.0001$; Figure S2A), as were Phf8 mRNA (by 50%, $P < 0.001$; Figure S2B) and mRNAs for autophagy-related proteins Becn1, Atg5, and Atg7 (by 30%–40%, $P < 0.01$; Figure S2D–F, respectively). mTOR mRNA was significantly upregulated (1.5–1.7-fold, $P = 0.019$; Figure S2C) as was APP mRNA (1.7–1.9-fold, $P < 0.01$ to < 0.05 ; Figure S2G) in Cbs-silenced N2a-APP_{swe} cells, reflecting changes in the corresponding protein levels (Figure 1A–N). These findings indicate that Cbs gene exerts transcriptional control over the expression of Phf8, mTOR, APP, Becn1, Atg5, and Atg7 in these cells.

The western blot and RT-qPCR results show that the changes in Phf8, H4K20me1, mTOR signaling, autophagy, and APP induced by Cbs gene silencing in the mouse neuroblastoma cells (Figures S1 and S2) recapitulate the in vivo findings in the Cbs^{-/-} mouse brain (Figure 1).

3.5 | Hcy-thiolactone, N-Hcy-protein, and Hcy downregulate the histone demethylase Phf8, upregulate the H4K20me1 epigenetic mark and mTOR, and impair autophagy in N2a cells

Because Hcy-thiolactone and N-Hcy-protein,^{14–17} in addition to Hcy,²⁹ are elevated in Cbs^{-/-} mice, it is difficult to assign observed phenotypes to a specific metabolite in these mice. However, this limitation can be overcome in cultured cells

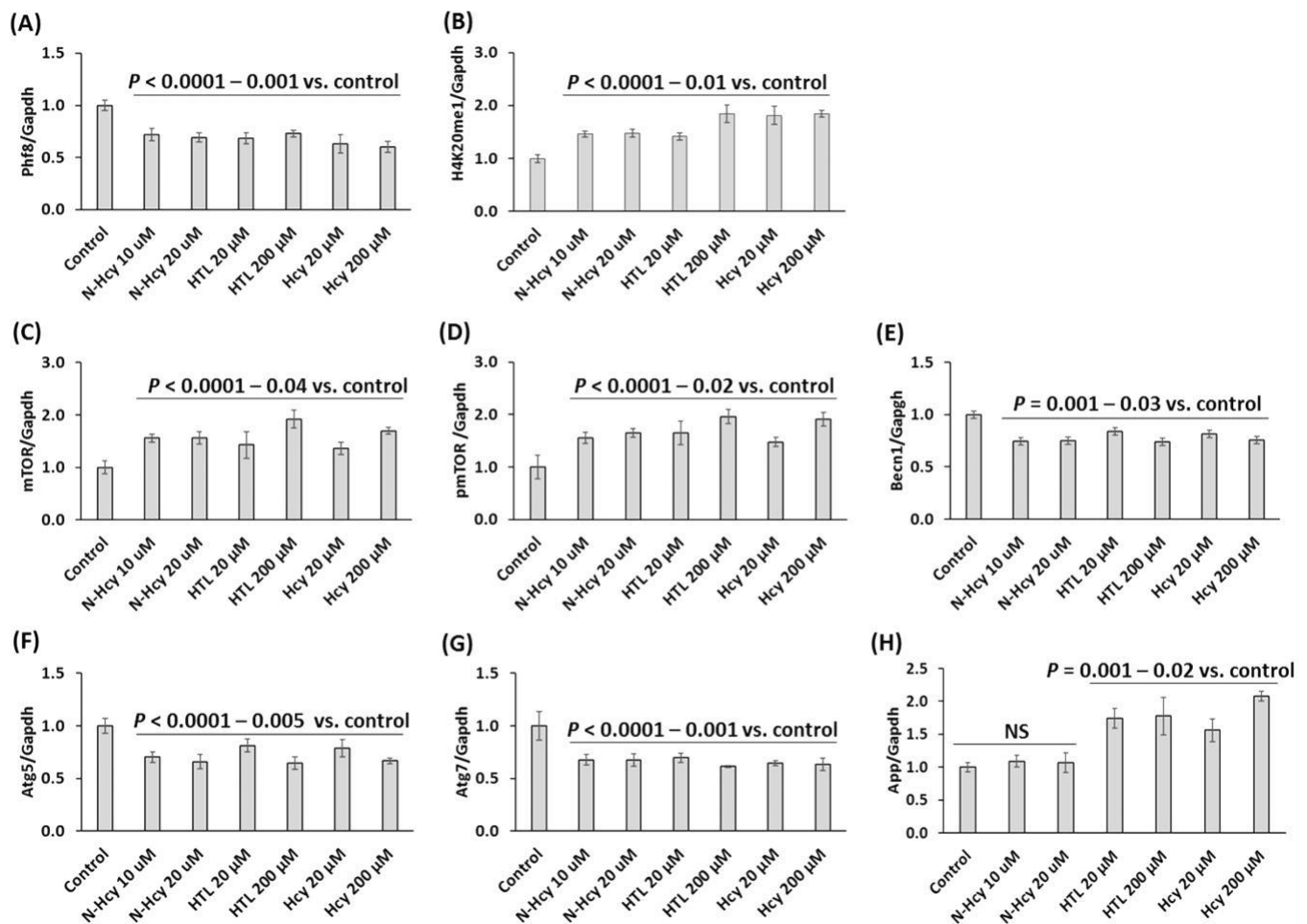


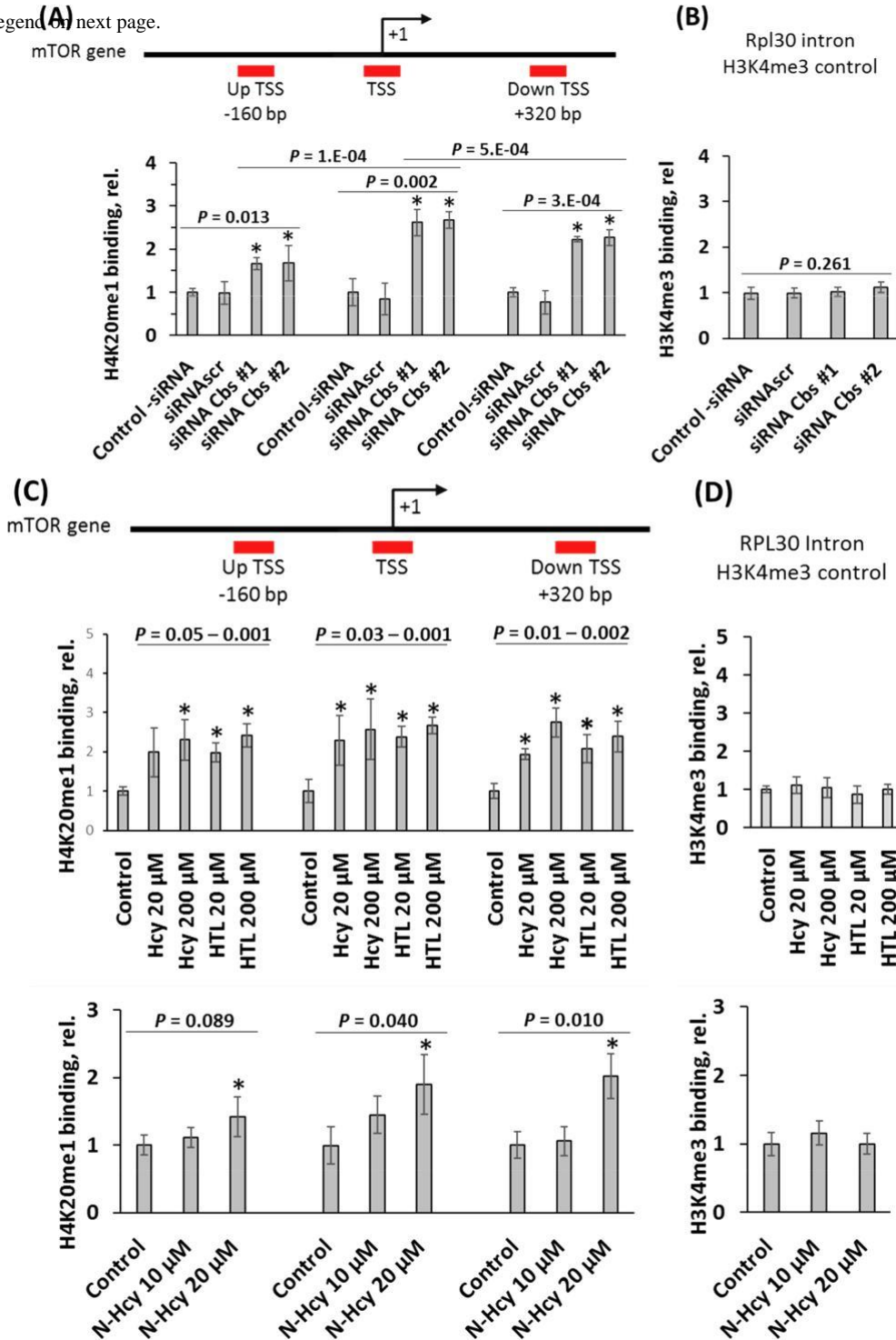
FIGURE 2 Hcy-thiolactone, N-Hcy-protein, and Hcy downregulate Phf8, upregulate H4K20me1 epigenetic mark, mTOR signaling, App, and impair autophagy in mouse neuroblastoma N2a cells. N2a cells were treated with indicated concentrations of N-Hcy-protein, Hcy-thiolactone (HTL), or Hcy for 24 h at 37 C as described in Materials and Methods. Bar graphs illustrating the quantification of Phf8 (A), H4K20me1 (B), mTOR (C), pmTOR (D), Becn1 (E), Atg5 (F), Atg7 (G), and App (H) based on western blot analyses with corresponding antibodies are shown. Gapdh was used as a reference protein. Data are averages of three independent experiments. P values were calculated by one-way ANOVA with Tukey's multiple comparisons test.

by treatments with an excess of a specific metabolite. To determine how each metabolite affects the expression of Phf8 and its effects on downstream targets, we treated N2a cells with Hcy-thiolactone, N-Hcy-protein, and Hcy.

We found significantly reduced Phf8 levels in N2a cells treated with 20 μ M Hcy-thiolactone (0.69 ± 0.05), Hcy (0.63 ± 0.09), or 10 μ M N-Hcy-protein (0.72 ± 0.06) compared to control (1.00 ± 0.05 , $P < 0.001$; Figure 2A).

In contrast, levels of H4K20me1 mark were significantly elevated in N2a cells treated with 20 μ M Hcy-thiolactone (1.42 ± 0.07), Hcy (1.81 ± 0.17), or 10 μ M N-Hcy-protein (1.46 ± 0.05) compared to untreated control cells (1.00 ± 0.07 , $P < 0.01$; Figure 2B). mTOR levels were significantly upregulated in N2a cells by treatments with these metabolites: 20 μ M Hcy-thiolactone (1.46 ± 0.25), Hcy (1.36 ± 0.12), or 10 μ M N-

FIGURE 3 Legend (A) next page.



Hcy-protein (1.56 ± 0.08) compared to untreated control cells (1.00 ± 0.12 , $P < 0.0001$ to <0.04 ; Figure 2C). Levels of pmTOR were also significantly upregulated by these treatments: 20 μM Hcy-thiolactone (1.65 ± 0.22), Hcy (1.48 ± 0.08), 10 μM N-Hcy-protein (1.56 ± 0.11) compared to control (1.00 ± 0.12 , $P < 0.0001$ to <0.02 ; Figure 2D).

Autophagy-related proteins Becn1, Atg5, and Atg7 were significantly downregulated (by 16%–25%, $P < 0.001$) in N2a cells treated with Hcy-thiolactone, N-Hcy-protein, or Hcy (Figure 2E,F,G, respectively). Similar effects were seen in N2a cells treated with 10-fold higher concentrations of Hcy-thiolactone and Hcy (200 μM), or 2-fold higher N-Hcy-protein (20 μM) (Figure 2).

App levels were significantly upregulated in N2a cells treated with 20 μM Hcy-thiolactone (1.74-fold, $P = 0.001$) or Hcy (1.56-fold, $P = 0.002$) (Figure 2H). Increasing Hcy to 200 μM significantly increased upregulation of App from 1.56- to 2.08-fold ($P = 0.002$) while higher concentration of Hcy-thiolactone did not further elevate App levels (Figure 2H).

These findings show that Hcy and its downstream metabolites Hcy-thiolactone and N-Hcy-protein, which are elevated in Cbs^{-/-} mice,^{14–17} each can affect the expression of Phf8 and its downstream targets.

3.6 | Cbs gene silencing increased H4K20me1 binding to mTOR promoter in N2a cells

To determine whether increased levels of the histone H4K20me1 mark can promote mTOR gene expression by binding to its promoter, we carried out ChIP experiments using anti-H4K20me1 antibody (Figure 3). The Cbs gene was silenced by transfecting N2a using two different siRNAs. The cells were permeabilized, treated with anti-H4K20me1 antibody and a recombinant micrococcal

nuclease-protein A/G. DNA fragments released from N2a-APPswe cells were quantified by RT-qPCR using primers targeting the transcription start site (TSS) of the mTOR gene as well as upstream (UP) and downstream (DOWN) regions from the TSS. We found that in siRNA Cbs-silenced N2a-APPswe cells the binding of H4K20me1 was significantly increased at the mTOR TSS (2.7-fold, $P = 0.002$), UP (1.7-fold, $P = 0.013$), and DOWN (2.2-fold, $P = 3 \times 10^{-4}$) sites (Figure 3A). Importantly, there were significantly more DNA fragments from the TSS site (2.62 ± 0.31 and 2.68 ± 0.19 for siRNA Cbs #1 and #2, respectively) than from the UP (1.67 ± 0.14 to 1.68 ± 0.41 for siRNA Cbs #1 and #2, respectively; $P = 1 \times 10^{-4}$) and DOWN (2.22 ± 0.06 to 2.27 ± 0.19 for siRNA Cbs #1 and #2, respectively; $P = 5 \times 10^{-4}$) sites (Figure 3A). Control experiments show that the binding of H3K4me3 to RPL30 intron was not affected by Cbs gene silencing (Figure 3B). These findings indicate that the binding of H4K20me1 was significantly higher at TSS than at UP and DOWN sites in siRNA Cbs-silenced cells. Similar results were obtained with N2a-APPswe cells (not shown).

CHIP experiments with anti-Phf8 antibody showed that Cbs silencing did not affect binding of Phf8 to the mTOR gene (not shown).

3.7 | Hcy-thiolactone, N-Hcy-protein, and Hcy increase H4K20me1 binding to mTOR promoter in N2a cells

Hcy-thiolactone and N-Hcy-protein^{14–17} are elevated in Cbs^{-/-} mice, as is Hcy.²⁹ Each of these metabolites can affect mTOR expression by promoting H4K20me1 binding at the mTOR promoter. To examine this possibility, we treated N2a-APPswe cells with Hcy-thiolactone, N-Hcy-protein, or Hcy for 24 h and analyzed how these treatments affect levels of H4K20me1 bound to the

FIGURE 3 Cbs gene silencing or treatments with Hcy-thiolactone, N-Hcy-protein, and Hcy increase H4K20me1 binding at the mTOR promoter in mouse neuroblastoma N2a cells. (A) CHIP assays with anti-H4K20me1 antibody show the specific binding of H4K20me1 at the transcription start site (TSS) of the mTOR gene as well as downstream and upstream sites in Cbs siRNA silenced N2a cells. Bar graphs show the relative H4K20me1 binding at indicated regions of the mTOR gene in N2a cells transfected with two different siRNAs targeting the Cbs gene (siRNA Cbs #1 and #2). Transfections without siRNA (control-siRNA) or with scrambled siRNA (siRNAsc) were used as controls. (B) Control CHIP experiment with anti-H3K4me3 antibody shows that Cbs gene-silencing did not affect the binding of H3K4me3 at the Rpl30 intron. RT-qPCR was carried out on the input and precipitated DNA fragments. P values vs. 'control-siRNA' plus 'siRNAsc' were calculated by one-way ANOVA with Tukey's multiple comparisons test. (C) N2a cells were treated with shown concentrations of N-Hcy-protein, Hcy-thiolactone (HTL), or Hcy for 24 h at 37 C. Untreated cells were used as controls. CHIP assays with anti-H4K20me1 antibody show the binding of H4K20me1 at the transcription start site (TSS) of the mTOR gene as well as downstream and upstream sites. Bar graphs show the relative H4K20me1 binding at the indicated regions of the mTOR gene. (D) Control CHIP assay with anti-H3K4me3 antibody shows that Hcy-thiolactone, N-Hcy-protein, and Hcy did not affect the binding of H3K4me3 at the Rpl30 intron. RT-qPCR was carried out on the input and precipitated DNA fragments. P values were calculated by one-way ANOVA with Tukey's multiple comparisons test. *Significant difference vs. control, $P < 0.05$.

mTOR gene using ChIP experiments with anti-H4K20me1 antibody. We found that Hcy-thiolactone at 20 μ M increased binding of H4K20me1 at the mTOR TSS (2.4-fold, $P = 0.004$), UP (2.0-fold, $P = 0.003$), and DOWN (2.1-fold, $P = 0.011$) sites (Figure 3C). Similar results were obtained with 200 μ M Hcy-thiolactone.

Hcy at 20 μ M increased binding of H4K20me1 at the mTOR TSS (2.3-fold, $P = 0.032$), UP sites (2.3-fold, $P = 0.052$), and DOWN sites (1.9-fold, $P = 0.002$). Hcy at 200 μ M significantly increased binding of H4K20me1 at the mTOR TSS (2.6-fold, $P = 0.030$), UP (2.4-fold, $P = 0.013$), and DOWN sites (2.8-fold, $P = 0.002$) TSS (Figure 3C). Similar results were obtained with N2a-APPsw cells (not shown).

N-Hcy-protein at 20 μ M significantly increased binding of H4K20me1 at the mTOR TSS (1.9-fold, $P = 0.040$) and DOWN (2.0-fold, $P = 0.010$) sites, but not UP site (1.4-fold, $P = 0.089$) (Figure 3C). Smaller, nonsignificant increases were observed with 10 μ M N-Hcy-protein.

Neither Hcy, Hcy-thiolactone, nor N-Hcy-protein affected binding of Phf8 at the mTOR TSS, UP and down sites of the mTOR gene (not shown).

Control experiments show that H3K4me3 binding to RPL30 intron was not affected by Hcy, Hcy-thiolactone nor N-Hcy-protein (Figure 3D). These findings indicate that Hcy-thiolactone significantly increased binding of H4K20me1 at the mTOR gene TSS, UP, and DOWN sites while Hcy significantly increased binding of H4K20me1 at the mTOR TSS.

3.8 | Cbs gene silencing upregulates A β in N2a-APPsw cells

To determine whether Cbs depletion in neural cells could affect A β accumulation, we silenced the Cbs gene in N2a-APPsw cells and quantified A β by fluorescence confocal microscopy using anti-A β antibody. The cells were transfected with two different Cbs-targeting siRNAs, permeabilized, treated with anti-A β antibody, and A β was visualized with fluorescent secondary antibody (Figure 4A) and quantified (Figure 4B). We found that Cbs-silencing led to increased A β accumulation, manifested by significant increases in an average size of fluorescent A β puncta (from 0.32 ± 0.02 to 0.80 ± 0.02 and to $0.90 \pm 0.06 \mu\text{m}^2$ for siRNA Cbs #1 and #2, respectively; $P = 1E-6$) in Cbs siRNA-treated N2a-APPsw cells compared to siRNAscr-treated cells or control without siRNA (Figure 4B). Less significant increases were also observed in the area of fluorescent A β puncta (from 130 ± 7 to 189 ± 47 and $183 \pm 13 \mu\text{m}^2$ for siRNA Cbs #1 and #2, respectively; $P = 0.055-0.079$).

3.9 | Hcy-thiolactone, N-Hcy-protein, and Hcy upregulate A β accumulation in N2a-APPsw cells

To ascertain how each Hcy metabolite can affect A β accumulation, we treated N2a-APPsw cells with Hcy-thiolactone, N-Hcy-protein,³⁰ or Hcy and quantified A β by fluorescence confocal microscopy using anti-A β antibody (Figure 4C,D). The metabolite-treated and untreated control cells were permeabilized, treated with anti-A β antibody, followed by fluorescent secondary antibody to visualize A β signals. We found that A β was significantly upregulated in N2a-APPsw cells treated with 20 μ M Hcy, Hcy-thiolactone, or 10 μ M N-Hcy-protein, manifested by significantly increased average size and signal intensity of the fluorescent A β puncta, compared to untreated cells (Figure 4D). Similar results were obtained with N2a-APPsw cells treated with 10-fold higher concentrations of Hcy, Hcy-thiolactone (200 μ M), or 2-fold higher N-Hcy-protein (20 μ M).³⁰ However, while treatments with Hcy or Hcy-thiolactone increased the size of the fluorescent A β puncta, treatments with N-Hcy-protein did not affect the size of A β signal (Figure 4D), suggesting different effects of these metabolites on the structure of A β aggregates. These findings indicate that Hcy and its downstream metabolites Hcy-thiolactone and N-Hcy-protein contribute to the accumulation of A β induced by the metabolic stress of HHcy.

3.10 | Phf8 gene silencing upregulates A β but not APP in N2a-APPsw cells

The findings that Phf8 expression was attenuated in brains of Cbs^{-/-} mice and in Cbs-silenced or Hcy metabolite-treated mouse neuroblastoma N2a-APPsw cells raises a possibility that Phf8 loss by itself can affect biochemical pathways leading to A β accumulation. To examine this possibility, we silenced the Phf8 gene by transfection of N2a-APPsw cells with Phf8-targeting siRNAs³¹ and quantified by western blotting proteins that were affected by Cbs depletion in the mouse brain (Figure 1). We found significantly reduced Phf8 levels (by 80%, $P < 0.0001$; Figure 5A), significantly increased

H4K20me1 (3-fold, $P < 0.001$; Figure 5B), mTOR (1.4-fold, $P < 0.001$; Figure 5C), and pmTOR (1.6-fold, $P < 0.01$; Figure 5D) levels in Phf8-silenced cells. Autophagy-related proteins Atg5 and Atg7 were significantly downregulated (by 20%–35%, $P < 0.0001$ and < 0.01 ; Figure 5E,F) while Beclin1 was not affected in Phf8-silenced cells (Figure 5G).

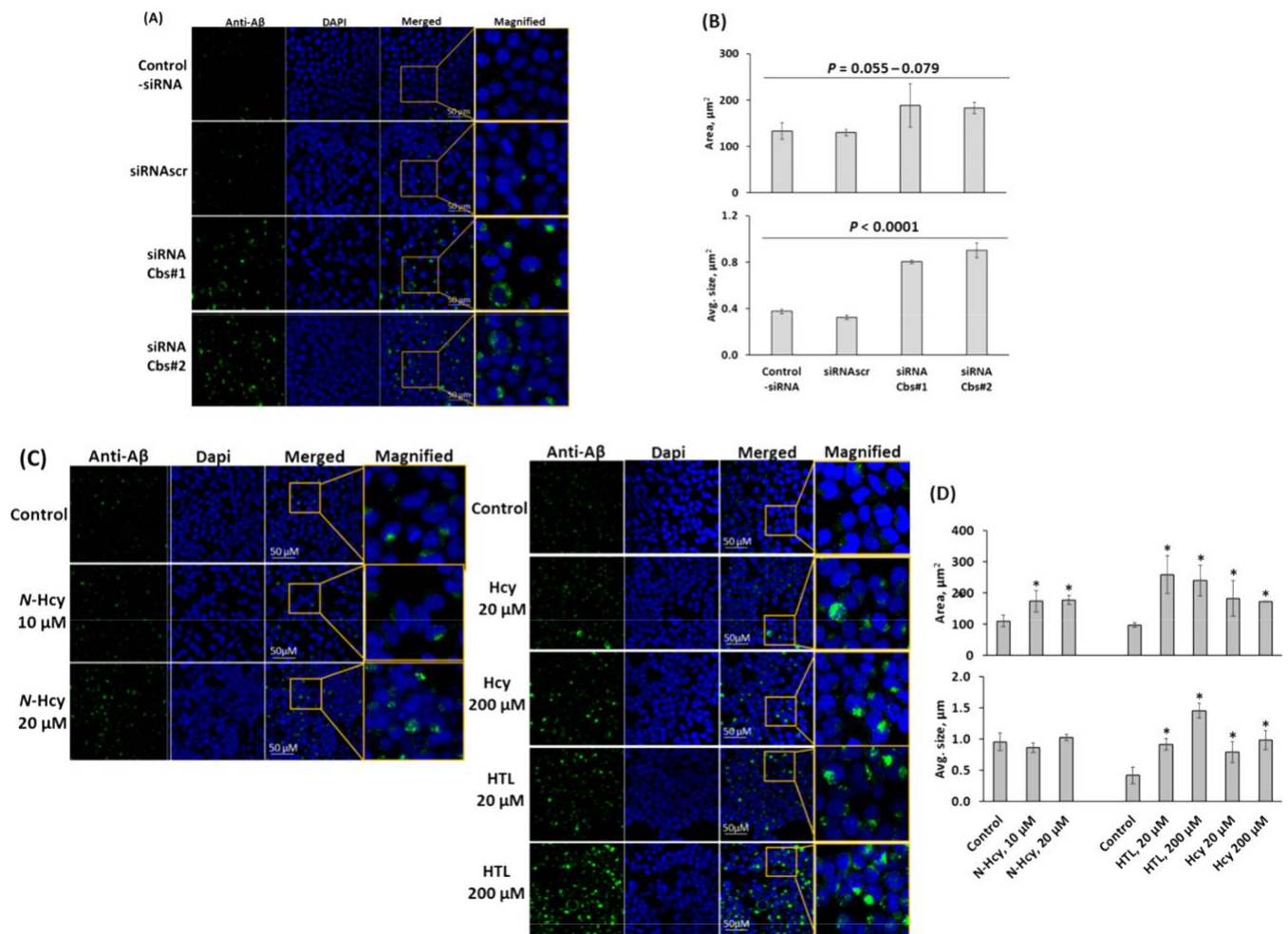


FIGURE 4 Cbs depletion or treatments with Hcy-thiolactone, N-Hcy-protein, and Hcy promote A β accumulation in the mouse neuroblastoma N2a-APPsw cells. (A, B) The cells were transfected with siRNAs targeting the Cbs gene. Transfections without siRNA (control-siRNA) or with scrambled siRNA (siRNAsc) were used as controls. A β was detected and quantified by confocal immunofluorescence microscopy using anti-A β antibody. (A) Confocal microscopy images of A β signals from Cbs-silenced N2a-APPsw cells. (B) Bar graphs show quantification of A β signals in Cbs-silenced and control cells. (C, D) N-Hcy-protein, Hcy-thiolactone (HTL), or Hcy promote A β accumulation in mouse neuroblastoma N2a-APPsw cells. N2a-APPsw cells were treated with indicated concentrations of N-Hcy-protein, Hcy-thiolactone (HTL), or Hcy for 24 h at 37 C. Untreated cells were used as controls. Confocal microscopy images (C) and quantification of A β signals (D) from treated and untreated N2a-APPsw cells. P values vs. 'control-siRNA' plus 'siRNAsc' were calculated by one-way ANOVA with Tukey's multiple comparisons test. Data for cells treated with Hcy-thiolactone and N-Hcy-protein in panels (C, D) were reproduced with permission from Ref. (30).

Importantly, western blot analyses showed that the Phf8 gene silencing did not affect APP levels in N2a-APPsw cells (Figure 5H). In contrast, fluorescence con-focal microscopy analyses showed that A β was significantly upregulated in Phf8-silenced cells, manifested by significantly increased average size ($P < 0.001$) and signal intensity ($P < 0.001$) of the fluorescent A β puncta compared to controls without siRNA or with siRNAsc (Figure 5J,K).³¹ Taken together, these findings clearly show that A β accumulation in the Phf8-silenced cells occurred independently of APP and suggest that most likely it was caused by impaired autophagy.

3.11 | Cbs deficiency accelerates age-dependent neurodegeneration in the mouse brain

Glial fibrillary acidic protein (GFAP)³¹ and neurofilament light chain (NfL)³² increase with age and have been associated with Alzheimer's disease. GFAP, an astrocytic cytoskeletal protein, is a marker of astrogliosis, abnormal activation and proliferation of astrocytes due to neuronal damage.³¹ NfL is a marker of neuro-axonal damage, resulting because of neurologic diseases.³³ To find whether Cbs deficiency accelerates neuronal damage we

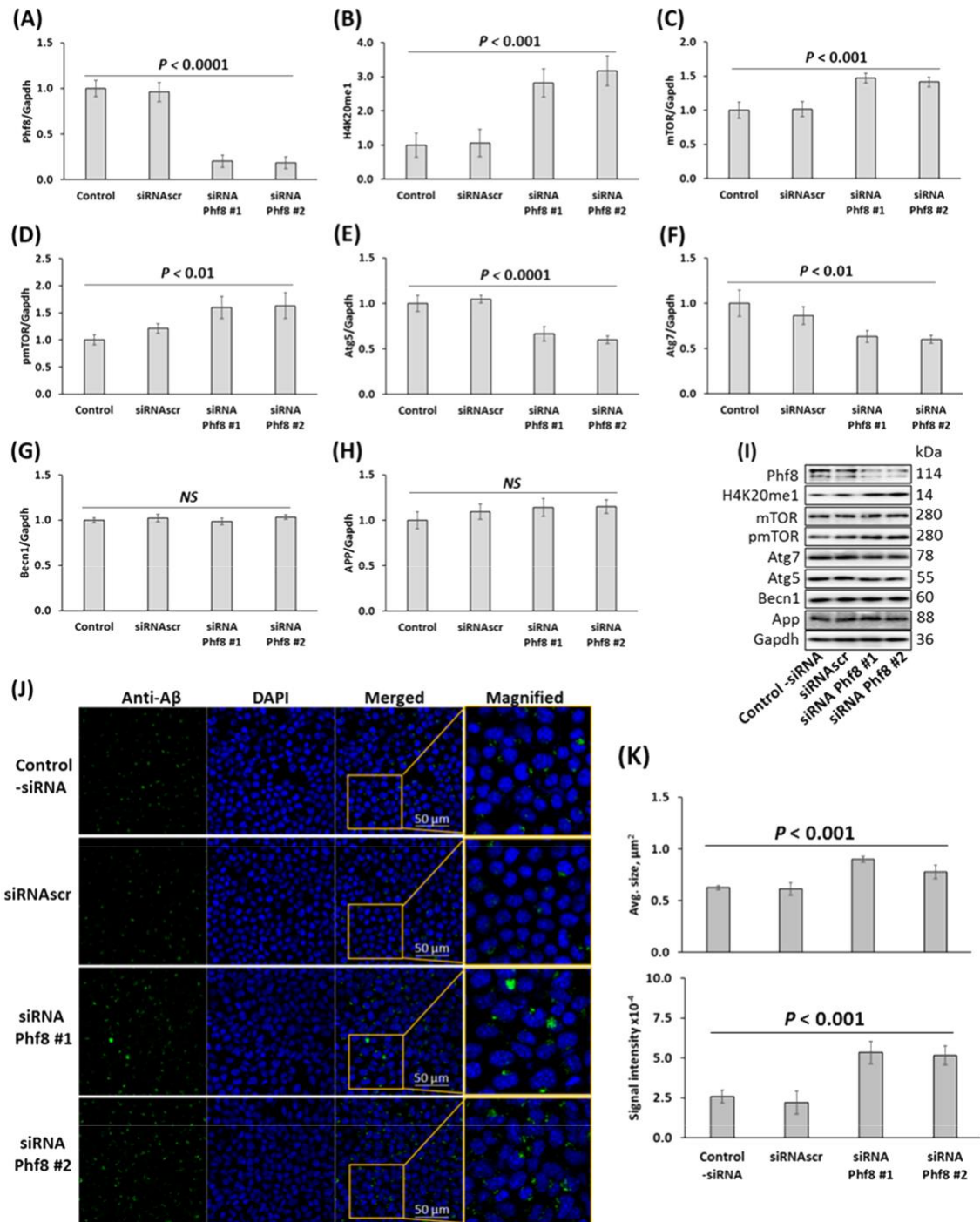


FIGURE 5 Silencing Phf8 gene promotes A β accumulation mediated by upregulation of mTOR signaling and inhibition of autophagy in the mouse neuroblastoma N2a-APPswe cells. The cells were transfected with siRNAs targeting the Phf8 gene (Phf8 siRNA #1 and #2). Transfections without siRNA (control-siRNA) or with scrambled siRNA (siRNA-scr) were used as controls. Proteins were quantified by western blotting. Bar graphs illustrate levels of (A) Phf8, (B) H4K20me1, (C) mTOR, (D) pmTOR, (E) Atg5, (F) Atg7, (G) Becn1, and (H) APP. A β was detected and quantified by confocal immunofluorescence microscopy using anti-A β antibody. Representative western blot is shown in panel (I). Confocal microscopy images of A β signals from Phf8-silenced and control N2a-APPswe cells. (J) Bar graphs show quantification of A β signals. P values vs. 'control-siRNA' plus 'siRNA-scr' were calculated by one-way ANOVA with Tukey's multiple comparisons test. NS, not significant.

examined the expression of Nfl and Gfap in brains of Tg-I278T Cbs^{-/-} mice and Tg-I278T Cbs^{+/-} sibling controls by using western blotting and RT-qPCR. We found that

the Nfl and Gfap protein levels were significantly increased in brains of older (1-year-old) Tg-I278T Cbs^{-/-} mice vs. Tg-I278T Cbs^{+/-} sibling controls (Nfl: 2.48

± 0.39 vs. 1.74 ± 0.38 , $P < 0.0001$, Figure 6A; Gfap: 2.14 ± 0.24 vs. 1.63 ± 0.21 , $P < 0.0001$, Figure 6B). In contrast, in younger (9-week-old) mice levels of Nfl and Gfap proteins were not affected by Cbs deficiency (Figure 6A,B). Nfl and Gfap mRNAs were also significantly upregulated in brains of older (1-year-old) Tg-I278T Cbs^{-/-} vs. Tg-I278T Cbs^{+/-} mice (Nfl mRNA: 1.55 ± 0.42 vs. 0.92 ± 0.20 , $P = 0.0004$, Figure 6C; Gfap mRNA: 1.34 ± 0.43 vs. 0.88 ± 0.28 , $P = 0.027$, Figure 6D). In contrast, levels of Nfl and Gfap mRNAs were not affected by Cbs deficiency in younger (9-week-old) mice (Figure 6C,D). Although Nfl and Gfap proteins and mRNAs increased significantly with age in Cbs^{-/-} mice and Cbs^{+/-}, the increases were faster in Cbs^{-/-} animals (Figure 6A–D). These findings show that Cbs^{-/-} genotype transcriptionally upregulates Nfl and Gfap genes in old but not in young mice and that Cbs protects mice from age-dependent neurodegeneration.

4 | DISCUSSION

The loss of CBS, an important Hcy-metabolizing enzyme,^{12,13} or the loss of PHF8,^{21,22} an important histone demethylase participating in epigenetic regulation, causes severe intellectual disability in humans. Similar neuropathies are also observed in Cbs^{-/-} and Phf8^{-/-} mice. Because PHF8 participates in epigenetic regulation, we surmised that dysregulation of epigenetic mechanisms involving PHF8 could underlie neuropathy associated with CBS deficiency. The present study substantiated this supposition by showing that the expression of Phf8 mRNA and protein was downregulated while H4K20me1 epigenetic mark was upregulated in brains of Cbs^{-/-} mice (Figure 1) and in Cbs-depleted mouse neuroblas-toma cells (Figures S1,S2).

We also found that metabolites that are elevated in CBS-deficient humans and mice—Hcy-thiolactone, N-

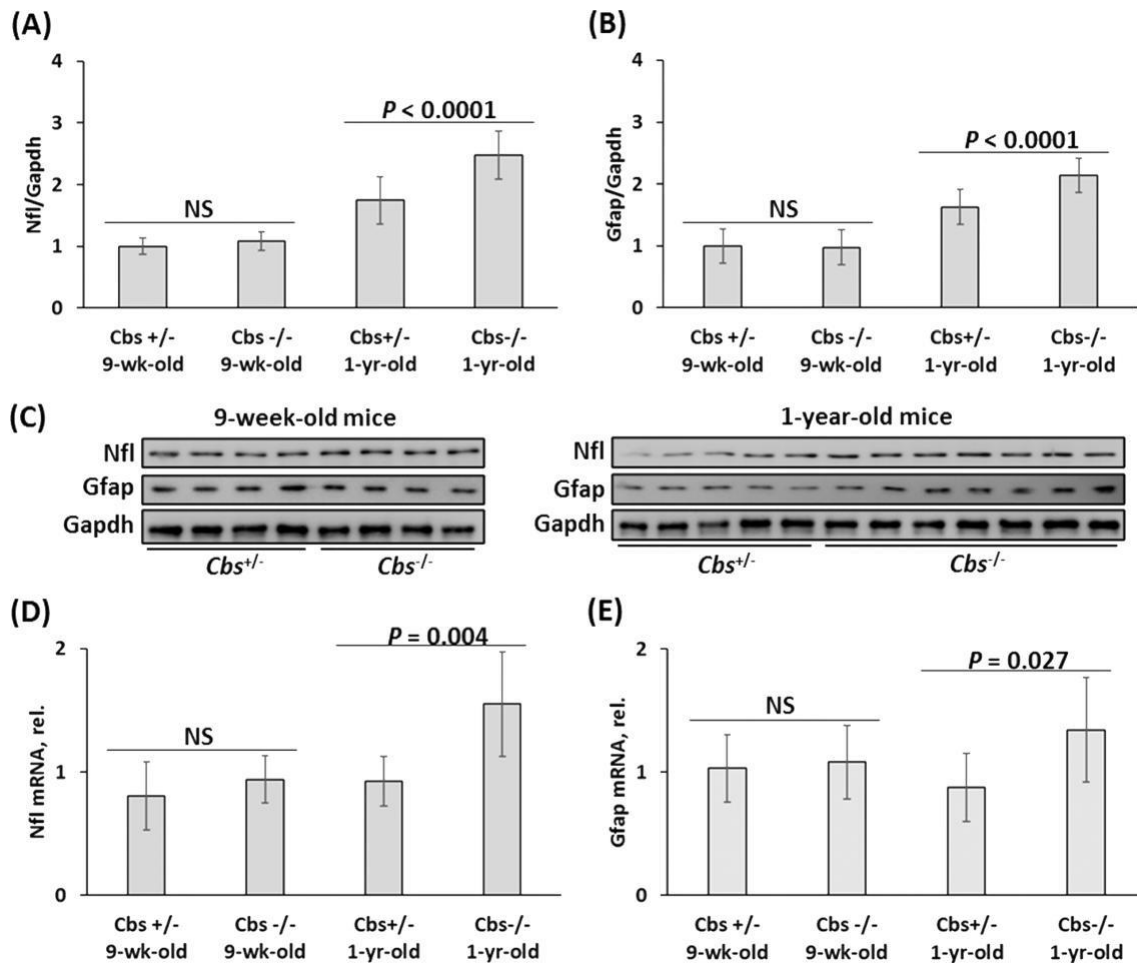


FIGURE 6 Deletion of the Cbs gene upregulates Nfl and Gfap expression of neurodegeneration markers in the mouse brain. Nine-week-old and 1-year-old Tg-I278T Cbs^{-/-} mice ($n = 7$ and 14) and their Tg-I278T Cbs^{+/-} sibling controls ($n = 10$ and 10) were used in experiments. Bar plots show the quantification of brain Nfl (A) and Gfap (B) proteins by western blotting—representative images shown in panel (C)—and of brain Nfl (D) and Gfap mRNAs (E). Gapdh protein and mRNA were used as references for normalization. P values shown on the graphs were calculated by one-way ANOVA with Tukey's multiple comparisons test.

Hcy-protein, and Hcy—downregulated Phf8 (Figure 2A) and upregulated histone H4K20me1 (Figure 2B) in cultured mouse neuroblastoma cells. This suggests that Hcy-thiolactone, N-Hcy-protein, and Hcy are responsible for Phf8 downregulation (Figure 1A) and H4K20me1 upregulation (Figure 1B) found in vivo in brains of *Cbs*^{-/-} mice. We also showed that treatments with siRNA targeting *Cbs* gene or with Hcy-thiolactone or Hcy, which metabolically downregulated Phf8 expression (Figure S1B, Figure 2A), promoted the accumulation of both APP (Figure 2H) and A β (Figure 4) in mouse neuroblastoma cells. In contrast, attenuation of Phf8 expression by treatments with siRNAs targeting Phf8 gene promoted A β accumulation (Figure 5J,K), but did not affect APP levels (Figure 5H). These disparate effects of metabolic and genetic Phf8 depletion on APP expression suggest that A β accumulation can occur by two different mechanisms in *Cbs*-depleted brain and neural cells: upregulated APP expression caused by Hcy-thiolactone, N-Hcy-protein, and Hcy, and impaired A β clearance caused by downregulation of autophagy (Figure 7A). In Phf8-depleted cells, only one mechanism, downregulated autophagy, leads to accumulation of A β .

The findings that upregulation of APP (Figure 1M,T; Figures S1F and S2G) was associated with downregulation of *Becn1* in *Cbs*^{-/-} mice (Figure 1I,O) and *Cbs*-depleted mouse neural cells (Figures S1G and S2D) suggest a third pathway that can contribute to A β accumulation. In this pathway *Becn1* is a negative regulator of APP expression and processing (Figure 7B). This pathway is consistent with the findings showing that *Becn1*, a protein with a key role in the initiation of autophagy, is decreased in human AD brains and that genetic depletion of *Becn1* in mice that overexpress APP (*APP*⁺*Becn1*^{-/-} mice) increased

A β accumulation in neurons.³⁴ *Becn1* can also regulate APP processing and turnover. For example, depletion of *Becn1* by RNA interference in rat neuroblastoma cells expressing human APP transgene (B103/hAPPwt cells) increased APP, Lc3, and A β , while *Becn1* overexpression downregulated APP.³⁵ The involvement of autophagy in *Cbs* depletion-induced APP and A β accumulation needs to be confirmed in future experiments by boosting autophagy (e.g., by treatment with TAT-Beclin1), which should rescue APP and A β accumulation in *Cbs*-depleted cells.

Our findings suggest that Phf8 regulates A β accumulation through its effects on mTOR and autophagy. Specifically, we found that treatments with Hcy-thiolactone, N-Hcy-protein, or Hcy, which downregulated Phf8 expression (Figure 2A) and upregulated the histone mark H4K20me1 (Figure 2B), also increased H4K20me1 binding to the mTOR promoter in mouse neuroblastoma cells (Figure 3C). These findings provide direct mechanistic evidence linking each of the Hcy metabolites with dysregulated mTOR signaling and its downstream consequences. Concomitant inhibition of autophagy (Figure 2E–G) and upregulation of A β (Figure 4C,D) by Hcy-thiolactone, N-Hcy-protein, and Hcy identify a likely mechanism (Figure 7) that accelerates neuronal damage in CBS deficiency, manifested by elevated *Nfl* and *Gfap* levels (Figure 6). This mechanism can also account for the association of HHcy with Alzheimer's disease.¹⁸

Previous studies showed that Phf8 bound at the TSS of *Kras*, *Camk2d*, and *Rps6ka1* genes involved in mTOR signaling and that depletion of Phf8 increased binding of H4K20me1 at the TSS in *Kras*, *Camk2d*, and *Rps6ka1* genes in mice²²; H4K20me1 binding at the mTOR gene was not examined in that study. In the present study we found that Phf8 depletion in mouse neuroblastoma N2a

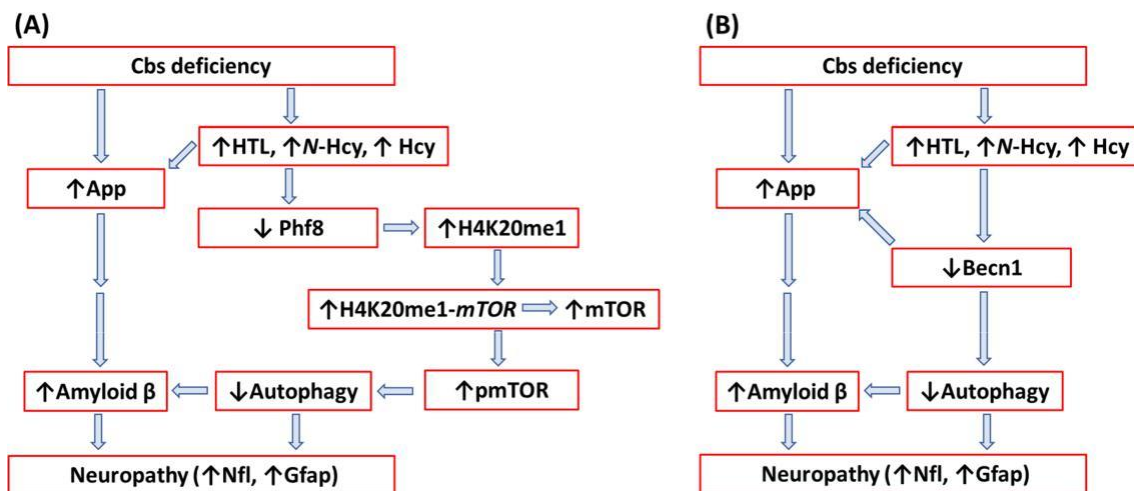


FIGURE 7 Mechanisms underlying neuropathy in the *Cbs*-deficient brain. Up and down arrows show the direction of changes in the indicated metabolites, proteins, and molecular processes. App, amyloid beta precursor protein; CBS, cystathionine β -synthase; Hcy, homocysteine; HTL, Hcy-thiolactone; mTOR, mammalian target of rapamycin; Phf8, plant homeodomain finger protein 8.

cells by treatments with Hcy-thiolactone, N-Hcy-protein, or Hcy (Figure 2A), or by silencing Cbs gene with siRNAs (Figure S2B), increased H4K20me1 binding at the TSS as well as down and up sites of the mTOR gene (Figure 3A,C). Our findings add mTOR to the list of genes regulated by H4K20me1. However, in contrast to TSS of the Kras, Camk2d, and Rps6ka1 genes, which bound Phf8,²² we could not detect any binding of Phf8 to TSS of the mTOR gene.

We found that the effects of Cbs deficiency were mimicked by Hcy, Hcy-thiolactone, and N-Hcy proteins. This may not be surprising given that Hcy is metabolized to Hcy-thiolactone which then modifies proteins generating N-Hcy-protein, as originally demonstrated in 1997⁵ and confirmed in a variety of cell types and in animal and human studies.¹ Similarities in pathophysiological effects of each of the three metabolites also include their cytotoxicity (reviewed in¹), demonstrated for N-Hcy-protein (e.g.,^{36,37}), Hcy-thiolactone (e.g.,³⁸), and Hcy (e.g.,³⁹). However, how each of these metabolites exerts its effects needs to be examined in future studies.

Previous studies have found that Cbs^{-/-} mice have elevated Hcy-thiolactone and N-Hcy-protein,^{14–17} in addition to Hcy,²⁹ which was accompanied by increased brain A β accumulation²⁸ and cognitive impairments.^{12,13} In the present study we have found significantly depleted Phf8 in brains of Cbs^{-/-} mice (Figure 1A). Although depletion of Phf8 is linked to intellectual disability, autism spectrum disorder, attention deficit hyperactivity disorder,²⁰ and mental retardation,²¹ it was not known to be associated with Alzheimer's disease. Our present findings that Phf8 depletion in the mouse neuroblastoma cells, induced by Phf8 siRNA interference (Figure 5A), or by supplementation with Hcy-thiolactone, N-Hcy-protein, or Hcy (Figure 2A), significantly increased A β accumulation (Figure 5J,K), suggest that Phf8 depletion can contribute to the association of Alzheimer's disease with HHcy.¹⁸

In conclusion, our findings find the histone demethylase Phf8 as a regulator of A β accumulation and suggest that neuropathy of Cbs deficiency is mediated by Hcy metabolites-dependent depletion of Phf8, which upregulates mTOR through increased H4K20me1 binding at the mTOR promoter, which in turn inhibits autophagy, leads to A β accumulation, and neuronal damage, manifested by elevation of brain Nfl and Gfap levels. We have also shown that Cbs-depletion and Hcy metabolites, independently of their inhibitory effect on Phf8 expression, upregulated APP expression, which can also contribute to A β accumulation.

AUTHOR CONTRIBUTIONS

Łukasz Witucki performed and analyzed the experiments; Hieronim Jakubowski conceived the idea for the

project, designed the study, bred the mice, collected mouse tissue samples, analyzed data, and drafted the paper.

ACKNOWLEDGMENTS

We thank S. S. Sisodia for kindly providing mouse neuroblastoma cells expressing human APP-695 harboring the K670N/M671L Swedish double mutation associated with familial early-onset Alzheimer's disease, N2a-APPswe. Supported in part by grants 2018/29/B/NZ4/00771, 2019/33/B/NZ4/01760, and 2021/43/B/NZ4/00339 from the National Science Center, Poland.

CONFLICT OF INTEREST STATEMENT

No conflicts of interest, financial or otherwise, are declared by the authors.

DATA AVAILABILITY STATEMENT

The data that support the findings of this study are available in the methods and/or supplementary material of this article.

ETHICS STATEMENT

The animal study protocol was approved by the Institutional Animal Care and Use Committee (IACUC) of the New Jersey Medical School (Animal Care and Use Protocol #: 16114D0320, date of approval 29 March 2017).

ORCID

Łukasz Witucki  <https://orcid.org/0000-0002-3908-7735>

Hieronim Jakubowski  <https://orcid.org/0000-0001-5845-4409>

REFERENCES

- Jakubowski H. Homocysteine modification in protein structure/function and human disease. *Physiol Rev.* 2019;99: 555-604.
- Jakubowski H, Zhang L, Bardeguet A, Aviv A. Homocysteine thiolactone and protein homocysteinylation in human endothelial cells: implications for atherosclerosis. *Circ Res.* 2000;87: 45-51.
- Jakubowski H. Proofreading in vivo: editing of homocysteine by methionyl-tRNA synthetase in the yeast *Saccharomyces cerevisiae*. *EMBO J.* 1991;10:593-598.
- Jakubowski H, Goldman E. Synthesis of homocysteine thiolactone by methionyl-tRNA synthetase in cultured mammalian cells. *FEBS Lett.* 1993;317:237-240.
- Jakubowski H. Metabolism of homocysteine thiolactone in human cell cultures. Possible mechanism for pathological consequences of elevated homocysteine levels. *J Biol Chem.* 1997; 272:1935-1942.
- Jakubowski H. Protein homocysteinylation: possible mechanism underlying pathological consequences of elevated homocysteine levels. *FASEB J.* 1999;13:2277-2283.

7. El Bashir H, Dekair L, Mahmoud Y, Ben-Omran T. Neurodevelopmental and cognitive outcomes of classical homocystinuria: experience from Qatar. *JIMD Rep.* 2015;21:89-95.
8. Abbott MH, Folstein SE, Abbey H, Pyeritz RE. Psychiatric manifestations of homocystinuria due to cystathionine beta-synthase deficiency: prevalence, natural history, and relationship to neurologic impairment and vitamin B6-responsiveness. *Am J Med Genet.* 1987;26:959-969.
9. Clarke R, Smith AD, Jobst KA, Refsum H, Sutton L, Ueland PM. Folate, vitamin B12, and serum total homocysteine levels in confirmed Alzheimer disease. *Arch Neurol.* 1998;55: 1449-1455.
10. Bleich S, Bandelow B, Javaheripour K, et al. Hyperhomocysteinemia as a new risk factor for brain shrinkage in patients with alcoholism. *Neurosci Lett.* 2003;335:179-182.
11. Sachdev PS, Valenzuela M, Wang XL, Looi JC, Brodaty H. Relationship between plasma homocysteine levels and brain atrophy in healthy elderly individuals. *Neurology.* 2002;58: 1539-1541.
12. Majtan T, Park I, Cox A, et al. Behavior, body composition, and vascular phenotype of homocystinuric mice on methionine-restricted diet or enzyme replacement therapy. *FASEB J.* 2019; 33:12477-12486.
13. Akahoshi N, Kobayashi C, Ishizaki Y, et al. Genetic background conversion ameliorates semi-lethality and permits behavioral analyses in cystathionine beta-synthase-deficient mice, an animal model for hyperhomocysteinemia. *Hum Mol Genet.* 2008;17:1994-2005.
14. Chwatko G, Boers GH, Strauss KA, Shih DM, Jakubowski H. Mutations in methylenetetrahydrofolate reductase or cystathionine beta-synthase gene, or a high-methionine diet, increase homocysteine thiolactone levels in humans and mice. *FASEB J.* 2007;21:1707-1713.
15. Jakubowski H, Boers GH, Strauss KA. Mutations in cystathionine beta-synthase or methylenetetrahydrofolate reductase gene increase N-homocysteinylation protein levels in humans. *FASEB J.* 2008;22:4071-4076.
16. Jakubowski H, Perla-Kajan J, Finnell RH, et al. Genetic or nutritional disorders in homocysteine or folate metabolism increase protein N-homocysteinylation in mice. *FASEB J.* 2009; 23:1721-1727.
17. Jakubowski H. Quantification of urinary S- and N-homocysteinylation protein and homocysteine-thiolactone in mice. *Anal Biochem.* 2016;508:118-123.
18. Smith AD, Refsum H. Homocysteine – from disease biomarker to disease prevention. *J Intern Med.* 2021;290:826-854.
19. Yates SC, Zafar A, Hubbard P, et al. Dysfunction of the mTOR pathway is a risk factor for Alzheimer's disease. *Acta Neuropathol Commun.* 2013;1:3.
20. Sobering AK, Bryant LM, Li D, et al. Variants in PPHF8 cause a spectrum of X-linked neurodevelopmental disorders and facial dysmorphism. *HGG Adv.* 2022;3:100102.
21. Laumonnier F, Holbert S, Ronce N, et al. Mutations in PPHF8 are associated with X linked mental retardation and cleft lip/cleft palate. *J Med Genet.* 2005;42:780-786.
22. Chen X, Wang S, Zhou Y, et al. Pph8 histone demethylase deficiency causes cognitive impairments through the mTOR pathway. *Nat Commun.* 2018;9:114.
23. Gupta S, Kuhnisch J, Mustafa A, et al. Mouse models of cystathionine beta-synthase deficiency reveal significant threshold effects of hyperhomocysteinemia. *FASEB J.* 2009;23:883-893.
24. Perla-Kajan J, Utyro O, Rusek M, Malinowska A, Sitkiewicz E, Jakubowski H. N-Homocysteinylation impairs collagen cross-linking in cystathionine beta-synthase-deficient mice: a novel mechanism of connective tissue abnormalities. *FASEB J.* 2016; 30:3810-3821.
25. Thinakaran G, Teplow DB, Siman R, Greenberg B, Sisodia SS. Metabolism of the "Swedish" amyloid precursor protein variant in neuro2a (N2a) cells. Evidence that cleavage at the "beta-secretase" site occurs in the golgi apparatus. *J Biol Chem.* 1996; 271:9390-9397.
26. Gurda D, Handschuh L, Kotkowiak W, Jakubowski H. Homocysteine thiolactone and N-homocysteinylation protein induce proatherogenic changes in gene expression in human vascular endothelial cells. *Amino Acids.* 2015;47:1319-1339.
27. Livak KJ, Schmittgen TD. Analysis of relative gene expression data using real-time quantitative PCR and the 2^{-Delta Delta C(T)} method. *Methods.* 2001;25:402-408.
28. Khayati K, Antikainen H, Bonder EM, et al. The amino acid metabolite homocysteine activates mTORC1 to inhibit autophagy and form abnormal proteins in human neurons and mice. *FASEB J.* 2017;31:598-609.
29. Watanabe M, Osada J, Aratani Y, et al. Mice deficient in cystathionine beta-synthase: animal models for mild and severe homocyst(e)inemia. *Proc Natl Acad Sci U S A.* 1995;92:1585-1589.
30. Witucki L, Jakubowski H. Depletion of Paraoxonase 1 (Pon1) dysregulates mTOR, autophagy, and accelerates amyloid beta accumulation in mice. *Cell.* 2023;12:746.
31. Chatterjee P, Pedrini S, Stoops E, et al. Plasma glial fibrillary acidic protein is elevated in cognitively normal older adults at risk of Alzheimer's disease. *Transl Psychiatry.* 2021;11:27.
32. Quiroz YT, Zetterberg H, Reiman EM, et al. Plasma neurofilament light chain in the presenilin 1 E280A autosomal dominant Alzheimer's disease kindred: a cross-sectional and longitudinal cohort study. *Lancet Neurol.* 2020;19:513-521.
33. Khalil M, Pirpamer L, Hofer E, et al. Serum neurofilament light levels in normal aging and their association with morphologic brain changes. *Nat Commun.* 2020;11:812.
34. Pickford F, Masliah E, Britschgi M, et al. The autophagy-related protein beclin 1 shows reduced expression in early Alzheimer disease and regulates amyloid beta accumulation in mice. *J Clin Invest.* 2008;118:2190-2199.
35. Jaeger PA, Pickford F, Sun CH, Lucin KM, Masliah E, Wyss-Coray T. Regulation of amyloid precursor protein processing by the Beclin 1 complex. *PLoS One.* 2010;5:e11102.
36. Ferretti G, Bacchetti T, Moroni C, Vignini A, Nanetti L, Curatola G. Effect of homocysteinylation of low density lipoproteins on lipid peroxidation of human endothelial cells. *J Cell Biochem.* 2004;92:351-360.
37. Paoli P, Sbrana F, Tiribilli B, et al. Protein N-homocysteinylation induces the formation of toxic amyloid-like protofibrils. *J Mol Biol.* 2010;400:889-907.
38. Mercie P, Garnier O, Lascoste L, et al. Homocysteine-thiolactone induces caspase-independent vascular endothelial cell death with apoptotic features. *Apoptosis.* 2000;5:403-411.

39. Kerkeni M, Tnani M, Chuniaud L, Miled A, Maaroufi K, Trivin F. Comparative study on in vitro effects of homocysteine thiolactone and homocysteine on HUVEC cells: evidence for a stronger proapoptotic and proinflammatory homocysteine thiolactone. *Mol Cell Biochem.* 2006;291:119-126.

Supplementary Material

Supplementary Figure S1

Supplementary Figure S2

Supplementary Table S1

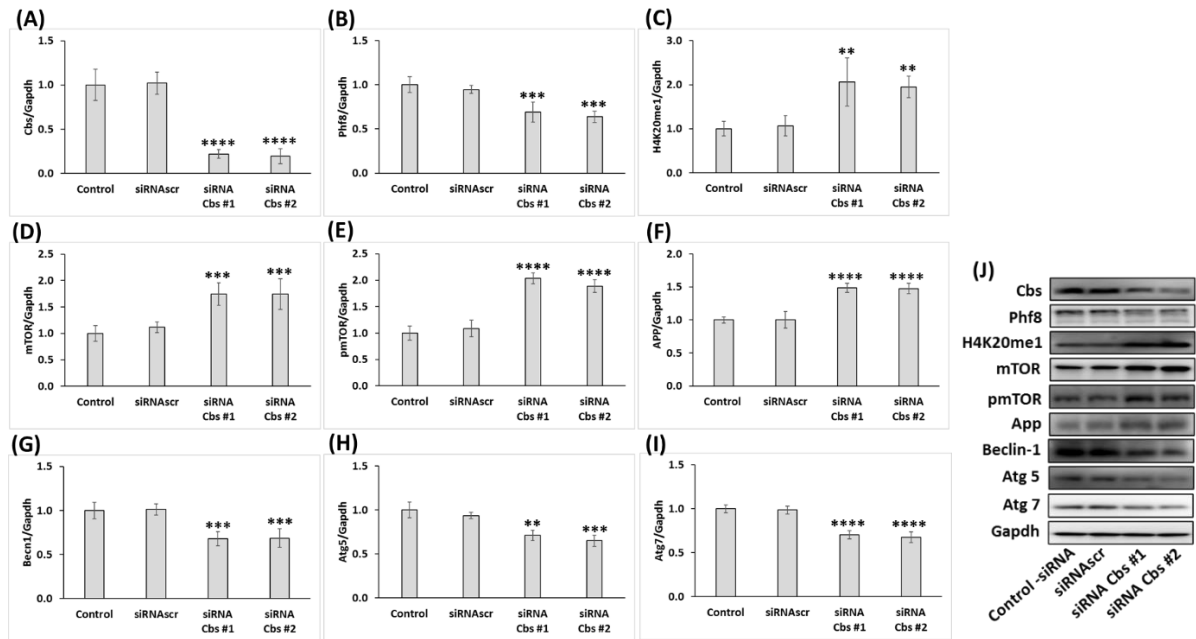


Figure S1. *Cbs* gene silencing in mouse neuroblastoma N2a-APPsw cells recapitulates changes in histone demethylase Phf8, H4K20me1, mTOR signaling, App, and autophagy-related protein levels observed in *Cbs*^{-/-} mouse brain. Bar graphs illustrating the quantification of Cbs (A), Phf8 (B), H4K20me1 (C), mTOR (D), pmTOR (E), Bcln1 (F), Atg5 (G), Atg7 (H), and App (I) in N2a-APPsw cells transfected with two different siRNAs targeting the *Cbs* gene (siRNA Cbs #1 and #2) are shown. Transfections without siRNA (Control -siRNA) or with scrambled siRNA (siRNAscr) were used as controls. Representative Western blots are shown in panel (J). Gapdh was used as a reference protein. Data are averages of three independent experiments. *P*-values vs. 'control -siRNA' plus 'siRNAscr' were calculated by one-way ANOVA with Tukey's multiple comparisons test. ** *P* < 0.01, *** *P* < 0.001, or **** *P* < 0.0001.

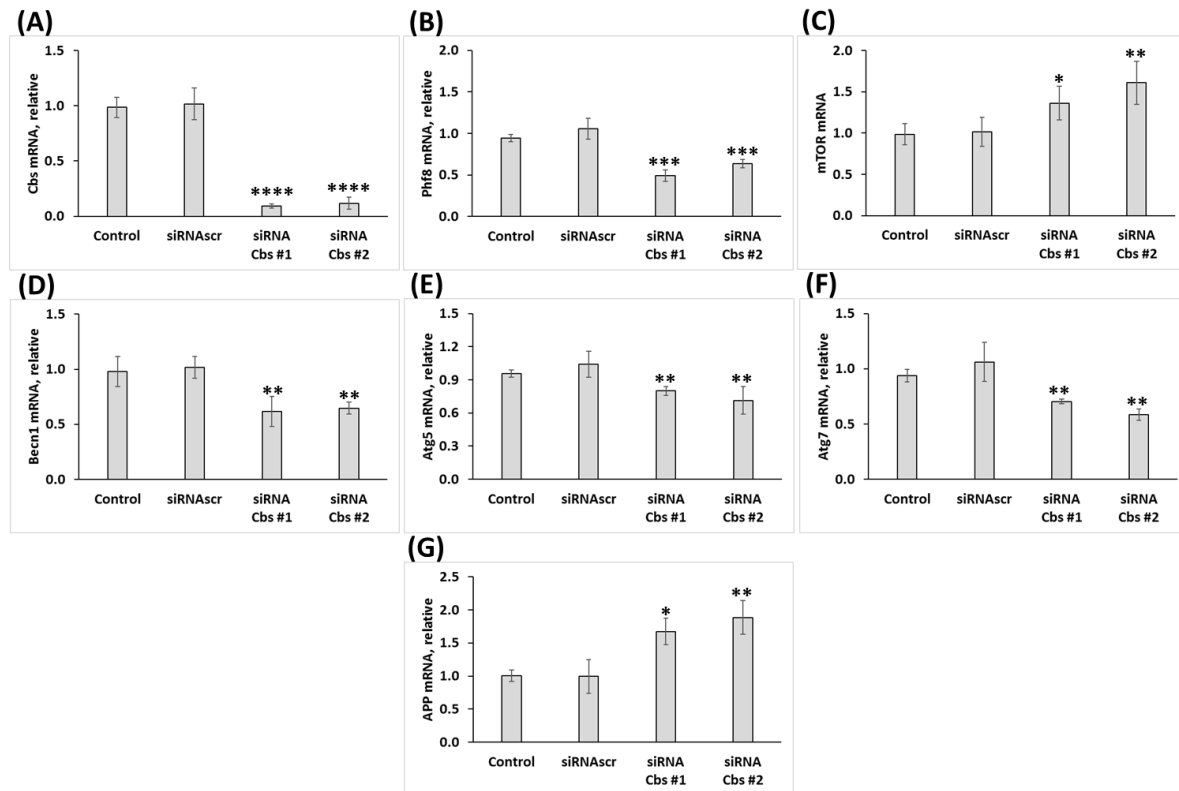


Figure S2. *Cbs* gene silencing affects mRNA for Phf8, mTOR, App, and autophagy-related proteins in mouse neuroblastoma N2a-APPsw cells. Bar graphs illustrating the quantification by RT-qPCR of mRNAs for *Cbs* (A), Phf8 (B), mTOR (C), Bcln1 (D), Atg5 (E), Atg7 (F), and App (G), in N2a-APPsw cells transfected with two different siRNAs targeting the *Cbs* gene (siRNA Cbs #1 and #2) are shown. Gapdh mRNA was used as a reference. Transfections without siRNA (Control) or with scrambled siRNA (siRNAsc) were used as controls. *P*-values vs. ‘control -siRNA’ plus ‘siRNAsc’ were calculated by one-way ANOVA with Tukey’s multiple comparisons test. * $P < 0.05$, ** $P < 0.01$, *** $P < 0.001$, or **** $P < 0.0001$.

Gene	Primer sequence
APP	Forward: 5'-CTTCCCAAGATCCTGATAAACT-3'
App	Reverse: 5'-CCGGGTGTCTCCAGGTACT-3'
Atg5	Forward: 5'-AAGGCACACCCTGAAATGG-3'
	Reverse: 5'-TGATGTTCCAAGGAAGAGCTGAA-3'
Atg7	Forward: 5'-GCCAACTCCACACTGCTTTC-3'
	Reverse: 5'-TCTTCTGGGTCAGTTCGTGC-3'
β -actin	Forward: 5'-GCAGGAGTACGATGAGTCCG-3'
	Reverse: 5'-ACGCAGCTCAGTAACAGTCC-3'
Beclin-1	Forward: 5'-GAGGAAGCTCAGTACCAGCG-3'
	Reverse: 5'-CCAGATGTGGAAGGTGGCAT-3'
<i>Cbs</i>	Forward: 5'-GGTCTGGAATTCATATGTAGC-3'
	Wild type reverse: 5'CGGATGACCTGCATTCATCT-3' Mutant reverse: 5'-GAGGTGCGACGGTATCGATA-3'
	Forward: 5'-GGACTGGATAAGCAGGGCG-3'

<i>Gapdh</i>	Reverse: 5'-TTTTGTCTACGGGACGAGGC-3'
<i>mTOR</i>	Forward: 5'-GCCACTCTCTGACCCAGTTC 3'
	Reverse: 5'-ATGCCAAGACACAGTAGCGG-3'
<i>Phf8</i>	Forward: 5'-TGGGAGCATGCTTCAAGG-3'
	Reverse: 5'-GATTTCAAAGCAGGGTCATCA-3'
<i>p62</i>	Forward: 5'-GGGGAAGGGTTCAATGAGAG-3'
	Reverse: 5'-AATGGGCATATTTGGGGTCT-3'
<i>Nfl</i>	Forward: 5'-AGTTCGTTCCGGCTACGATCC-3'
	Reverse: 5'-TGGGCATCAAAGAGCCAGAG-3'
<i>Gfap</i>	Forward: 5'-AACCGCATCACCATTCTGT-3'
	Reverse: 5'-AAGGGAGAGCTGGCAGG-3'
<i>mTOR upstream TSS*</i>	Forward: 5'- TTGCCAACTGGTGCTCGTTT-3'
	Reverse: 5' AAG AAT TGG AGC TC GGG ACC 3'
<i>mTOR TSS*</i>	Forward: 5'-GGATGTTCCCTCCCAATCTTCG-3'
	Reverse: 5'-CAGACCCACCTAACTGACCGT-3'
<i>mTOR downstream TSS*</i>	Forward: 5'-TAGGGGGCAGATCCCGAAAC-3'
	Reverse: 5'-CACTGTAGCTGTA ACTCACAC-3'
* TSS, transcription start site	

Witucki Ł, Borowczyk K, Suszyńska-Zajczyk J, Warzych E, Pawlak P, Jakubowski H,

Deletion of the Homocysteine Thiolactone Detoxifying Enzyme Bleomycin Hydrolase, in Mice, Causes Memory- and Neurological Deficits and Worsens Alzheimer's Disease Related Behavioral and Biochemical Traits in the 5xFAD Model of Alzheimer's Disease,

Journal of Alzheimer's Disease, praca zaakceptowana w dniu 5.08.2023

Pięcioletni IF: 4,372, MEiN 100 punktów

Deletion of the Homocysteine Thiolactone Detoxifying Enzyme Bleomycin Hydrolase, in Mice, Causes Memory- and Neurological Deficits and Worsens Alzheimer's Disease-Related Behavioral and Biochemical Traits in the 5xFAD Model of Alzheimer's Disease

Łukasz Witucki^{a,c}, Kamila Borowczyk^{c, #}, Joanna Suszyńska-Zajczyk^a, Ewelina Warzych^b, Piotr Pawlak^b, and Hieronim Jakubowski^{a, c, *}

^a *Department of Biochemistry and Biotechnology, Poznań University of Life Sciences, Poznań, Poland*

^b *Department of Genetics and Animal Breeding, Poznań University of Life Sciences, Poznań, Poland*

^c *Department of Microbiology, Biochemistry and Molecular Genetics, Rutgers University, New Jersey Medical School, International Center for Public Health, Newark, NJ 07103, USA*

Present address: Department of Environmental Chemistry, Faculty of Chemistry, University of Łódź, Poland

* Correspondence: Hieronim Jakubowski, Department of Microbiology, Biochemistry and Molecular Genetics, Rutgers-New Jersey Medical School, International Center for Public Health, 225 Warren Street, Newark, New Jersey 07103, USA. E-mail: jakubows@rutgers.edu

Running Title: BLMH and Alzheimer's disease

Abstract

Background: Bleomycin hydrolase (BLMH), a homocysteine (Hcy)-thiolactone detoxifying enzyme, is attenuated in Alzheimer's disease (AD) brains. *Blmh* loss causes astrogliosis in mice while the loss of histone demethylase *Phf8*, which controls mTOR signaling, causes neuropathy in mice and humans.

Objective: To examine how *Blmh* gene deletion affects the *Phf8*/H4K20me1/mTOR/autophagy pathway, amyloid beta (A β) accumulation, and cognitive/neuromotor performance in mice.

Methods: We generated a new mouse model of AD, the *Blmh*^{-/-}5xFAD mouse. Behavioral assessments were conducted by cognitive/neuromotor testing. *Blmh* and *Phf8* genes were silenced in mouse neuroblastoma N2a-APP_{swe} cells by RNA interference. mTOR- and autophagy-related proteins, and APP were quantified by Western blotting and the corresponding mRNAs by RT-qPCR. A β was quantified by Western blotting (brains) and by confocal microscopy (cells).

Results: Behavioral testing showed cognitive/neuromotor deficits in *Blmh*^{-/-} and *Blmh*^{-/-}5xFAD mice. *Phf8* was transcriptionally downregulated in *Blmh*^{-/-} and *Blmh*^{-/-}5xFAD brains. H4K20me1, mTOR, phospho-mTOR, and APP were upregulated while autophagy markers *Becn1*, *Atg5*, and *Atg7* were downregulated in *Blmh*^{-/-} and *Blmh*^{-/-}5xFAD brains. A β was elevated in *Blmh*^{-/-}5xFAD brains. These biochemical changes were recapitulated in *Blmh*-silenced N2a-APP_{swe} cells, which also showed increased H4K20me1-*mTOR* promoter binding and impaired autophagy flux (Lc3-I, Lc3-II, p62). *Phf8*-silencing or treatments with Hcy-thiolactone or *N*-Hcy-protein, metabolites elevated in *Blmh*^{-/-} mice, induced biochemical changes in N2a-APP_{swe} cells like those induced by the *Blmh*-silencing. However, *Phf8*-silencing elevated A β without affecting APP.

Conclusion: Our findings show that *Blmh* interacts with APP and the *Phf8*/H4K20me1/mTOR/autophagy pathway, and that disruption of those interactions causes A β accumulation and cognitive/neuromotor deficits.

Keywords: Alzheimer's disease; APP; Bleomycin hydrolase; *Blmh*^{-/-}5xFAD mouse; N2a-APP_{swe} mouse neuroblastoma cells; homocysteine thiolactone; *Phf8*; H4K20me1; mTOR; autophagy

INTRODUCTION

Bleomycin hydrolase (*Blmh*), named for its ability to deaminate and inactivate the anticancer glycopeptide drug bleomycin, is a thiol-dependent cytoplasmic aminopeptidase expressed in human

and rodent organs, including the brain [1, 2]. In addition to the aminopeptidase activity, Blmh has a thiolactonase activity and takes part in homocysteine (Hcy) metabolism by detoxifying Hcy-thiolactone [3, 4].

Hcy-thiolactone is formed from Hcy in an error-editing reaction in protein biosynthesis catalyzed by methionyl-tRNA synthetase [5-7]. Accumulation of Hcy-thiolactone is harmful because of its ability to modify protein lysine residues [8], which generates structurally- and functionally-impaired *N*-homocysteinylation (*N*-Hcy)-proteins with proinflammatory, prothrombotic, and pro-amyloidogenic properties [6]. Hcy-thiolactone and *N*-Hcy-proteins accumulate in intellectually disabled cystathionine β -synthase (CBS)- and methylenetetrahydrofolate reductase (MTHFR)-deficient patients [6] and are mechanistically linked to neurological diseases such as Alzheimer's disease (AD) [9, 10], stroke [11], cognitive impairment [12], Parkinson's disease [13], and neural tube defects [14, 15], as well as cardiovascular disease [16], cancer [17-19], and rheumatoid arthritis [20].

BLMH has been linked to AD and Huntington disease (HD). Specifically, BLMH has the ability to process amyloid precursor protein (APP) to amyloid beta (A β) [21] and to further process A β [22]. BLMH has also the ability to generate *N*-terminal fragments of huntingtin, thought to be important mediators of HD pathogenesis [23]. In the human brain, BLMH is localized in neocortical neurons and in dystrophic neurites of senile plaques [24]. A single nucleotide polymorphism in human *BLMH* gene, resulting in I443V substitution in the BLMH protein, is associated with an increased risk of AD [25, 26]; however, no association was reported in other studies [27-29].

The Hcy-thiolactonase and aminopeptidase activities of BLMH are decreased in brains of AD patients, suggesting that the attenuated BLMH activity could contribute to the pathology of AD [30]. In mice, deletion of the *Blmh* gene causes astrogliosis and behavioral changes [31]. Furthermore, *Blmh*^{-/-} mice exhibit diminished ability to detoxify Hcy-thiolactone, which elevates brain Hcy-thiolactone levels, and increases neurotoxicity of Hcy-thiolactone injections [4]. Studies of *Blmh*^{-/-} mouse brain proteome demonstrated that Blmh interacts with diverse cellular processes, such as synaptic plasticity, cytoskeleton dynamics, cell cycle, energy metabolism, and antioxidant defenses that are essential for brain homeostasis [9]. Collectively, these findings suggest that Blmh plays a key role in the central nervous system (CNS).

Plant homeodomain finger protein 8 (PHF8) has been identified as one of the X chromosome genes linked to intellectual disability syndrome, autism spectrum disorder, attention deficit hyperactivity disorder [32], and severe mental retardation [33]. PHF8 is a histone demethylase that can demethylate H4K20me1, H3K9me2/me1, and H3K27me2. Demethylation of H4K20me1 by PHF8 is important for supporting homeostasis of mTOR signaling. The phenotype of human PHF8 deficiency

has been replicated in *Phf8*^{-/-} mice, which show impaired hippocampal long-term potentiation and behavioral deficits in learning and memory [34].

In the present work we examined the role of *Blmh* in the CNS by studying behavioral and biochemical consequences of *Blmh* gene deletion in mice. Since dysregulated mTOR signaling and autophagy have been implicated in A β accumulation in AD brains [35-38], and H4K20me1 demethylation by PHF8 is important for maintaining homeostasis of mTOR signaling, we examined how these processes are affected in brains of *Blmh*^{-/-} vs. *Blmh*^{+/+} mice as well as transgenic *Blmh*^{-/-} 5xFAD vs. *Blmh*^{+/+}5xFAD mice. We also examined how biochemical changes in these processes and in APP/A β expression relate to behavioral performance in *Blmh*^{-/-}5xFAD mice. We studied underlying molecular mechanisms by manipulating *Blmh* or *Phf8* expression or Hcy-thiolactone and *N*-Hcy-protein levels in mouse neuroblastoma N2a-APPswe cells.

MATERIALS AND METHODS

Mice and treatments

Blmh^{-/-} [39] and 5xFAD [40] mice on the C57BL/6J genetic background were housed and bred at the Rutgers-New Jersey Medical School Animal Facility. 5xFAD mice overexpress the K670N/M671L (Swedish), I716V (Florida), and V717I (London) mutations in human APP(695), and M146L and L286V mutations in human PS1 associated with familial early-onset Alzheimer's disease. 5xFAD mice accumulate elevated levels of A β 42 beginning around 2 months of age [40] (<https://www.alzforum.org/research-models/5xfad-b6sjl>). The *Blmh*^{-/-} mice were crossed with 5xFAD animals and the resulting heterozygotes were used to generate *Blmh*^{-/-}5xFAD mice and their *Blmh*^{+/+}5xFAD sibling controls, hemizygous for the 5xFAD transgene. Mouse *Blmh* genotype were established by PCR of tail clips using the following primers: *Blmh* intron 2 forward primer p1 (5'-CACTGTAGCTGTACTCACAC), *Blmh* exon 3 reverse primer p2 (5'-GCGACAGAGTACCATGTAGG-3') and neomycin cassette reverse primer p3 (5'-ATTTGTCACGTCCTGCACGACG-3') [39]. 5xFAD genotype was proven using human APP and PS1 primers (hAPP forward 5'-AGAGTACCAACTTGCATGACTACG-3' and reverse 5'-ATGCTGGATAACTGCCTTCTTATC-3'; hPS1 forward 5'-GCTTTTCCAGCTCTCATTACTC-3' and reverse 5'-AAAATTGATGGAATGCTAATT GGT-3'). The mice were fed with a standard rodent chow (LabDiet5010; Purina Mills International, St. Louis MO, USA) [4]. Two- and four-month-old *Blmh*^{-/-} mice and their *Blmh*^{+/+} siblings, as well as 5- and 12-month-old *Blmh*^{-/-}5xFAD mice and their *Blmh*^{+/+}5xFAD siblings were used in experiments. Hyperhomocysteinemia (HHcy) was induced pharmacologically, as needed, by providing drinking water supplemented with 1% methionine (a 'high Met diet') [41-43] to mice starting at 1 month of age. The high Met diet significantly increases plasma total Hcy levels ($P < 1.E-06$) (6-fold from 6.8 to 39 μ M in *Blmh*^{-/-} mice and 10-fold from 7.4 to

77 μM in *Blmh*^{+/+} mice) as well as N-Hcy-protein levels ($P < 0.001$) (3-fold from 2.8 to 8.4 μM in *Blmh*^{-/-} mice and 4.5-fold from 1.2 to 5.4 μM in *Blmh*^{+/+} mice) [4]. The groups were derived from multiple litters and equal number of males and females were used in each group. Animal procedures were approved by the Institutional Animal Care and Use Committee at Rutgers-New Jersey Medical School.

Behavioral testing

Novel Object Recognition test

NOR is a test of recognition memory [44]. The test was conducted in two sessions, divided by a 6-h intersession interval. During the first session (familiarization session), the animal was free to explore two similar objects, and during the second session (test session), one of the objects was replaced by a novel, unfamiliar object. No habituation phase was performed. A minimal exploration time for both objects during both the familiarization and test phase (~20 s) was used, with a maximal time of 10 min to reach the criterion. Mice were evaluated in a white plastic box (33 × 33 × 20 cm). We used objects that differ in shape and texture: towers of Lego bricks (8-cm high and 3.2-cm wide, built-in blue, yellow, red, and green bricks) and Falcon tissue culture flasks filled with sand (9.5 cm high, 2.5 cm deep and 5.5 cm wide, transparent plastic with a yellow bottle cap). We scored object exploration whenever the mouse sniffed the object or touched the object while looking at it (i.e., when the distance between the nose and the object was less than 2 cm). Climbing onto the object (unless the mouse sniffs the object it has climbed on) or chewing the object did not qualify as exploration.

Hindlimb test

The hindlimb clasping test is used to assess neurodegeneration in mouse models [45]. For this test, mice were suspended by the base of the tail and videotaped for 10 seconds. Three separate trials were taken over three consecutive days. Hindlimb clasping was scored from 0 to 3: 0 = hindlimbs splayed outward and away from the abdomen, 1 = one hindlimb retracted inwards towards the abdomen for at least 50% of the observation period, 2 = both hindlimbs partially retracted inwards towards the abdomen for at least 50% of the observation period, 3 = both hindlimbs completely retracted inwards towards the abdomen for at least 50% of the observation period. Hindlimb clasping scores were added together for the three separate trials.

Ledge test

The ledge test is used to assess motor deficits in rodent models of CNS disorders [46]. Typically, mice walk along the ledge of a cage and try to descend back into the cage. Three separate trials were taken for each mouse. Ledge test was scored from 0 to 3 points: 0 = a mouse walked along the ledge without slipping and lowered itself back into the cage using paws; 1 = the mouse lost its footing during walking along the ledge but otherwise appeared coordinated; 2 = the mouse did not

effectively use its hind legs and landed on its head rather than paws when descending into the cage; 3 = the mouse fell of the ledge or was shaking, barely moving.

Cylinder test

The cylinder test is used to assess sensorimotor function in rodent models of CNS disorders. A mouse was placed in the transparent 500 ml plastic cylinder. The number of times the mouse reared up and touched the cylinder wall during a period of 3 min was counted. A rear is defined as a vertical movement with both forelimbs off the floor so that the mouse is standing only on its hindlimbs. At the end of 3 min, the mouse was removed and placed back into its home cage. Because spontaneous activity in the cylinder is affected by repeated testing resulting in reduced activity over time, mice were only once in their lifetime.

Brain protein extraction

Mice were euthanized by CO₂ inhalation, the brains collected and frozen on dry ice. Frozen brains were pulverized with dry ice using a mortar and pestle and stored at -80°C. Proteins were extracted from the pulverized brains (50±5 mg; 30±3 mg brain was used for Aβ analyses) using RIPA buffer (4 v/w, containing protease and phosphatase inhibitors) with sonication (Bandelin SONOPLUS HD 2070) on wet ice (three sets of five 1-s strokes with 1 min cooling interval between strokes). Brain extracts were clarified by centrifugation (15,000 g, 30 min, 4°C) and clear supernatants having 8-12 mg protein/mL were collected (RIPA-soluble fraction). Protein concentrations were measured with BCA kit (Thermo Scientific).

For Aβ analyses, pellets after protein extraction with RIPA buffer were re-extracted by brief sonication in 2% SDS, centrifuged (15,000 g, 15 min, room temperature), and the supernatants again collected (SDS-soluble fraction). The SDS-extracted pellets were then extracted by sonication in 70% formic acid (FA), centrifuged, and the supernatants were collected (the FA-soluble fraction) [47].

Cell culture and treatments

Mouse neuroblastoma N2a-APP^{swE} cells, harboring a human APP transgene with the K670N and M671L Swedish mutations associated with familial early-onset Alzheimer's disease [48] were grown (37°C, 5% CO₂) in DMEM/F12 medium (Thermo Scientific) supplemented with 5% FBS, non-essential amino acids, and antibiotics (penicillin/streptomycin) (MilliporeSigma).

After cells reached 70-80% confluency, the monolayers were washed twice with PBS and overlaid with DMEM medium without methionine (Thermo Scientific), supplemented with 5% dialyzed fetal bovine serum (FBS) (MilliporeSigma) and non-essential amino acids. L-Hcy-thiolactone

(MilliporeSigma) or *N*-Hcy-protein, prepared as described in ref. [49], were added (at concentrations indicated in figure legends) and the cultures were incubated at 37°C in 5% CO₂ atmosphere for 24 h.

For gene silencing, *Blmh*-targeting siRNAs (Cat. # 100821 and s63474) or *Phf8* gene (Cat. # S115808, and S115809) (Thermo Scientific) were transfected into cells kept in Opti-MEM medium by 24-h treatments with Lipofectamine RNAiMax (Thermo Scientific). Cellular RNA for RT-qPCR analyses were isolated as described in section 2.5 below. For protein extraction, RIPA buffer (MilliporeSigma) was used according to manufacturer's protocol.

Western blots

Proteins were separated by SDS-PAGE on 10% gels (20 µg protein/lane) and transferred to PVDF membrane (0.2 µm; Bio-Rad, cat. # 1620177) for 20 min at 0.1 A, 25 V using Trans Blot Turbo Transfer System (Bio-Rad). After blocking with 5 % bovine serum albumin in 1X Tris-Buffered Saline, 0.1% Tween 20 Detergent buffer (TBST; 1 h, room temperature), the membranes were incubated overnight at 4°C with anti-*Blmh* (Abcam, AB188371), anti-*Phf8* (Abcam, ab36068), anti-H4K20me1 (Abcam ab177188), anti-mTOR (CS #2983), anti-pmTOR Ser2448 (CS, #5536), anti-Atg5 (CS, #12994), anti-Atg7 (CS, #8558), anti-Bcln1 (CS, #3495), anti-Lc3 (CS, #4599) anti-p62 (CS, #23214), anti-Gapdh (CS, #5174), or anti-App (Abcam, ab126732) for 1 hour. Membranes were washed three times with TBST, 10 min each, and incubated with goat anti-rabbit IgG secondary antibody conjugated with horseradish peroxidase. Positive signals were detected using Western Bright Quantum-Advansta K12042-D20 and GeneGnome XRQ NPC chemiluminescence detection system. Bands intensity was calculated using Gene Tools program from Syngene.

For Western blots analyses of Aβ, brain protein extracts (2 µL) were separated on 10 % Tricine gels, and then transferred (0.5 A, 25 V 10 min) onto 22 µm PVDF membranes (Bio-Rad). The membranes were washed 3 times with 1x TBST and then blocked with 5 % bovine serum albumin (BSA) for 1 h at RT. After blocking, membranes were washed 3 times with 1x TBST and then incubated with primary anti-Aβ antibody (D54D2, CS #8243). Membranes were washed 3 times with 1x TBS-T and incubated with anti-rabbit IgG HRP-linked antibodies (CS#7074) for 1 h at RT. Signals were collected using clarity Max Western ECL Substrate (Bio-Rad) and GeneGnome XRQ - Chemiluminescence imaging (Syngene).

RNA isolation, cDNA synthesis, RT-qPCR analysis

Total RNA was isolated using Trizol reagent (MilliporeSigma). cDNA synthesis was conducted using Revert Aid First cDNA Synthesis Kit (Thermo Fisher Scientific) according to manufacturer's protocol. Nucleic acid concentration was measured using NanoDrop (Thermo Fisher Scientific). RT-qPCR was performed with SYBR Green Mix and CFX96 thermocycler (Bio-Rad). The $2^{-\Delta\Delta Ct}$ method was

used to calculate the relative expression levels [50]. Data analysis was performed with the CFX Manager™ Software, Microsoft Excel, and GraphPad Prism7. RT-qPCR primer sequences are listed in Table S1.

Chromatin immunoprecipitation assay

For the CHIP assays, CUT&RUN Assay Kit #86652 (Cell Signaling Technology, Danvers, MA, USA) was used following the manufacturer's protocol. Each assay was done in triplicates. Cells (100 000/ assay) were trypsinized, harvested, washed 3x in ice-cold PBS, and bound to concanavalin A-coated magnetic beads for 5 min, RT. Cells were then incubated (4h, 4°C) with 2.5 µg of anti-PHF8 antibody (Abcam, ab36068) or anti-H4K20me1 antibody (Abcam, ab177188) in the antibody-binding buffer plus digitonin that permeabilizes cells. Next, cells are treated with pAG-MNase (1 h, 4°C), washed, and treated with CaCl₂ to activate DNA digestion (0.5 h, 4°C). Cells were then treated with the stop buffer and spike-in DNA was added for each reaction for signal normalization, and incubated (30 min, 37°C). Released DNA fragments were purified using DNA Purification Buffers and Spin Columns (CS #14209) and quantified by RT-qPCR using primers targeting the promoter, upstream, and downstream regions of the *mTOR* gene (Table S1).

Confocal microscopy, Aβ staining in N2a-APP_{swe} cells

Mouse neuroblastoma N2a-APP_{swe} cells were cultured in Millicell EZ SLIDE 8-well glass slides (Merck). After 24 h treatments, cells were washed with PBS (3 times, 10 minutes each) and fixed with 4% PFA (Sigma-Aldrich) (37°C, 15 min). After fixation, cells were again washed 3 times with PBS buffer and permeabilized in 0.1% Triton X-100 solution (RT, 20 min), blocked with 0.1% BSA (RT, 1h), and incubated with anti-Aβ antibody (CS #8243; 4°C, 16 h). Cells were then washed 3 times with PBS and stained with secondary antibody Goat Anti-Rabbit IgG H&L (Alexa Fluor® 488) (Abcam, ab150077; RT, 1 h) to detect Aβ. DAPI (Vector Laboratories) was used to visualize nuclei. Fluorescence signals were detected by using a Zeiss LSM 880 confocal microscope with a 488 nm filter for the Alexa Fluor® 488 (Aβ) and 420–480 nm filter for DAPI, taking a z stack of 20-30 sections with an interval of 0.66 µm and a range of 15 µm. Zeiss Plan-Apochromat X40/1.2 Oil differential interference contrast objective were used for imaging. Images were quantified with the ImageJ Fiji software (NIH). Negative controls without primary or secondary antibody, which yielded no fluorescent signals, and positive controls with an authentic Aβ₄₂ standard (1 µg/mL medium) (Abcam, ab120301), which showed fluorescent signals, were done to verify the specificity of the assay.

Statistical analysis

Data from in vivo and in vitro experiments are reported as mean ± standard deviation (SD). Values for each experimental/treatment group were normalized to controls. Data were analyzed using one-way

analysis of variance (ANOVA) with Tukey's multiple comparisons post-test using GraphPad Prism7 software (GraphPad Holdings LLC, San Diego CA, USA, <https://www.graphpad.com>). A two-sided unpaired Student *t* test was used for analysis of NOR data.

RESULTS

Blmh gene deletion impairs recognition memory, induces neurodegeneration, and sensorimotor deficits in *Blmh*^{-/-} and *Blmh*^{-/-}5xFAD mice

Blmh^{-/-} mice

To examine effects of *Blmh* depletion on cognition and sensorimotor activity, *Blmh*^{-/-} and *Blmh*^{+/+} mice fed with a control or high Met diet were assessed in the novel object recognition (NOR), hindlimb claspings, and ledge tests. We found that 4-month-old *Blmh*^{-/-} mice did not differentiate between novel and familiar objects in the NOR test, regardless of the diet (Fig. 1A, B), showing impaired recognition memory. As expected, 4-month-old control *Blmh*^{+/+} mice showed normal preference for novelty (Fig. 1A); however, the preference for novelty disappeared when the mice were fed with a high Met diet (Fig. 1B). In contrast, 2-month-old *Blmh*^{-/-} mice showed significant preference for a novel object, regardless of the diet, as did 2-month-old *Blmh*^{+/+} mice (Fig. 1A, B). These findings show that a longer exposure (>2-month) is needed for the manifestation of detrimental effects of *Blmh* depletion or high Met diet on cognition.

The hindlimb test showed more severe claspings (significantly higher scores) in *Blmh*^{-/-} mice vs. their *Blmh*^{+/+} siblings (Fig. 1C), showing neurological impairment in *Blmh*^{-/-} animals. High Met diet significantly increased the hindlimb scores, with greater increases in *Blmh*^{+/+} than in *Blmh*^{-/-} mice, resulting in attenuated *Blmh*^{-/-} vs. *Blmh*^{+/+} difference in high Met diet animals (Fig. 1C). Overall, high Met diet attenuated effects of the *Blmh*^{-/-} genotype on the hindlimb score.

The ledge test showed significantly higher scores for 4-month-old, but not in 2-month-old, *Blmh*^{-/-} vs. *Blmh*^{+/+} mice (Fig. 1D), indicating neuromotor deficiency in *Blmh*^{-/-} animals. High Met diet increased the ledge test scores, with greater increases in *Blmh*^{+/+} than in *Blmh*^{-/-} mice, resulting in attenuated *Blmh*^{-/-} vs. *Blmh*^{+/+} difference in high Met diet animals (Fig. 1D). Overall, high Met diet attenuated effects of the *Blmh*^{-/-} genotype on the ledge test score.

Blmh^{-/-}5xFAD mice

We also examined effects of *Blmh* depletion on cognition and neuromotor activity in 1-year-old *Blmh*^{-/-}5xFAD vs. *Blmh*^{+/+}5xFAD mice. We found that *Blmh*^{-/-}5xFAD mice fed with a standard chow or high Met diet did not differentiate between novel and familiar objects in the NOR test (Fig. 1E),

showing impaired recognition memory in *Blmh*^{-/-}5xFAD animals. In contrast, *Blmh*^{+/+}5xFAD mice fed with a standard chow diet or high Met diet showed normal preference for novelty (Fig. 1E).

The hindlimb clasping test showed significantly higher scores in *Blmh*^{-/-}5xFAD vs. *Blmh*^{+/+}5xFAD mice fed with a standard chow or high Met diet (Fig. 1F), showing that *Blmh*^{-/-} genotype promotes neuromotor deficits in *Blmh*^{-/-}5xFAD animals. High Met diet increased the hindlimb scores, with greater increase in *Blmh*^{+/+}5xFAD than in *Blmh*^{-/-}5xFAD mice and abrogated the *Blmh*^{-/-}5xFAD vs. *Blmh*^{+/+}5xFAD difference (Fig. 1F).

The cylinder test showed significantly reduced scores for *Blmh*^{-/-}5xFAD vs. *Blmh*^{+/+}5xFAD mice fed with a standard chow or high Met diet (Fig. 1G), showing that *Blmh*^{-/-} genotype promotes neuromotor deficits in *Blmh*^{-/-}5xFAD animals. High Met diet reduced the cylinder test scores, with greater relative reductions in *Blmh*^{-/-}5xFAD mice, resulting in increased *Blmh*^{-/-}5xFAD vs. *Blmh*^{+/+}5xFAD difference in high Met diet animals (Fig. 1G).

Blmh depletion downregulates histone demethylase Phf8 and upregulates H4K20me1 epigenetic mark in brains of *Blmh*^{-/-} and *Blmh*^{-/-}5xFAD mice

The present findings that *Blmh*-deleted mice showed behavioral deficits in memory that are like cognitive deficits in memory seen in *Phf8*-deleted mice [34] suggests that *Blmh* may interact with *Phf8*. To examine this possibility, we quantified *Phf8* protein in brains of young *Blmh*^{-/-} mice and their *Blmh*^{+/+} sibling controls by Western blotting. We also examined how HHcy, induced by supplying 1% methionine (Met) in drinking water, affects the *Blmh*-*Phf8* interaction. We found that *Phf8* protein was significantly downregulated in brains of *Blmh*^{-/-} mice vs. *Blmh*^{+/+} sibling controls in mice fed with a standard chow diet (Fig. 2A). The reduced *Phf8* expression in *Blmh*^{-/-} vs. *Blmh*^{+/+} brains was attenuated in mice fed with a high Met diet (Fig. 2A).

However, *Phf8* expression in *Blmh*^{-/-} mice was not affected by high Met diet (Fig. 2A). In contrast, in *Blmh*^{+/+} mice, high Met diet significantly downregulated *Phf8* levels (Fig. 2A), showing that the *Blmh*-*Phf8* interaction is affected by high Met diet.

The histone H4K20me1 epigenetic mark, which is controlled by *Phf8* [34], was significantly upregulated in brains of *Blmh*^{-/-} vs. *Blmh*^{+/+} mice fed with a standard chow diet (Fig. 2B). High Met diet significantly elevated H4K20me1 levels in *Blmh*^{+/+} mice but not in *Blmh*^{-/-} animals, thereby abrogating the effect of *Blmh*^{-/-} genotype on H4K20me1 (Fig. 2B).

To figure out how the *Blmh*-*Phf8* interaction is affected by A β accumulation, we quantified *Phf8* in brains of *Blmh*^{-/-} and *Blmh*^{+/+} mice on the 5xFAD background. We found significant downregulation of *Phf8* (Fig. S1A) and upregulation of H4K20me1 (Fig. S1B) in *Blmh*^{-/-}5xFAD vs. *Blmh*^{+/+}5xFAD mice, like those seen in *Blmh*^{-/-} vs. *Blmh*^{+/+} animals (Fig. 1A, B). High Met diet abrogated

effects of *Blmh* deletion on Phf8 and H4K20me1 levels in 12-month-old but not in 5-month-old *Blmh*^{-/-}5xFAD mice (Fig. S1A, B). These findings show that the *Blmh*-Phf8 interaction is independent of A β accumulation but is influenced by high-Met-diet.

Blmh deletion upregulates mTOR signaling and inhibits autophagy in brains of *Blmh*^{-/-} and *Blmh*^{-/-}5xFAD mice

Blmh^{-/-} mice

Because Phf8/H4K20me1 regulate mTOR signaling [34], we next examined effects of *Blmh* deletion on levels of mTOR and its active form, phosphorylated at Ser2448 (pmTOR). We found that mTOR protein was significantly upregulated in brains of *Blmh*^{-/-} vs. *Blmh*^{+/+} mice (Fig. 2C). The effect of *Blmh*^{-/-} genotype on mTOR expression was abrogated by high Met diet (Fig. 2C).

High Met diet significantly increased mTOR expression in *Blmh*^{+/+} mice (Fig. 2C). However, high Met diet did not affect mTOR levels in *Blmh*^{-/-} animals (Fig. 2C).

pmTOR was also significantly elevated in brains of *Blmh*^{-/-} vs. *Blmh*^{+/+} mice (Fig. 2D). The effect of *Blmh*^{-/-} genotype on pmTOR levels was abrogated by high Met diet in 2-months-old but not in 4-months-old mice.

High Met diet significantly elevated pmTOR levels in 2- and 4-month-old *Blmh*^{+/+} mice and in 2-month-old *Blmh*^{-/-} animals (Fig. 2D). These findings show that the elevation of pmTOR levels reflects the upregulation of mTOR in *Blmh*^{-/-} mice.

Because mTOR is a major regulator of autophagy, we quantified effects of *Blmh* depletion on autophagy-related proteins. We found that the regulators of autophagosome assembly *Becn1*, *Atg5*, and *Atg7* were significantly downregulated in brains of *Blmh*^{-/-} vs. *Blmh*^{+/+} mice (Fig. 2E, F, G). The effects of *Blmh*^{-/-} genotype on autophagy were attenuated (*Becn1*, *Atg7*) or abrogated (*Atg5*) by high Met diet.

Blmh^{-/-}5xFAD mice

We found that mTOR and pmTOR were significantly upregulated also in brains of *Blmh*^{-/-}5xFAD vs. *Blmh*^{+/+}5xFAD mice (Fig. S1C, D). High Met diet abrogated these effects on pmTOR in young (5-month) and old (12-month) mice (Fig. S1D), and on mTOR in old (12-month) *Blmh*^{-/-}5xFAD animals (Fig. S1C). High Met diet did not affect mTOR and pmTOR levels in *Blmh*^{-/-}5xFAD mice. However, high Met diet upregulated mTOR (Fig. S1C) and pmTOR (Fig. S1D) in 12-month-old, but not in 5-month-old, *Blmh*^{+/+}5xFAD mice.

Markers of autophagy such as *Beclin1*, *Atg5*, and *Atg7* were downregulated in 5- and 12-month-old *Blmh*^{-/-}5xFAD vs. *Blmh*^{+/+}5xFAD mice (Fig. S1E, F, G), like in young *Blmh*^{-/-} vs. *Blmh*^{+/+} animals

(Fig. 2E, F, G). Protein p62, a receptor for degradation of ubiquitinated substrates, was upregulated in 5-month-old, and to a lesser extent in 12-month-old *Blmh*^{-/-}5xFAD mice (Fig. S1H).

Becn1 and Atg5 (Fig. S1E, F) were also downregulated in *Blmh*^{-/-}5xFAD vs. *Blmh*^{+/+}5xFAD mice fed with high Met diet. However, high Met diet abrogated effects of the *Blmh*^{-/-} genotype on Atg7 (in 5- and 12-month-old mice, Fig. S1G) and p62 (in 12-month-old mice, Fig. S1H) in 5xFAD mice.

Blmh gene deletion upregulates App in *Blmh*^{-/-} and APP in *Blmh*^{-/-}5xFAD mouse brain

We found that App was significantly upregulated in brains of *Blmh*^{-/-} vs. *Blmh*^{+/+} mice fed with a standard chow diet (Fig. 2H). App was similarly upregulated in *Blmh*^{-/-} vs. *Blmh*^{+/+} mice fed with high Met diet (Fig. 2H).

We saw a similarly upregulated APP in 5- and 12-month-old *Blmh*^{-/-}5xFAD mice carrying a mutated human APP transgene (Fig. S1I). High Met diet had no effect on APP in brains of 5-month-old *Blmh*^{-/-}5xFAD and *Blmh*^{+/+}5xFAD mice. However, APP was upregulated in brains of 12-month-old *Blmh*^{+/+}5xFAD mice by high Met diet, which abrogated the difference in APP between *Blmh*^{-/-}5xFAD vs. *Blmh*^{+/+}5xFAD animals seen in animals fed with a control diet (Fig. S1I).

Blmh controls the expression of mTOR-, autophagy-related proteins, and APP in N2a-APPswe cells

To elucidate the mechanism by which *Blmh* depletion impacts Phf8 and its downstream effects on mTOR, autophagy, and APP we first examined whether our findings in *Blmh*^{-/-} mice can be recapitulated in cultured mouse neuroblastoma N2a-APPswe cells carrying a mutated human APP transgene. We silenced the *Blmh* gene in these cells by RNA interference using two different siRNA (siRNA *Blmh*#1 and siRNA *Blmh*#2) for transfections; controls were mock-transfected or transfected with scrambled siRNA (siRNAscr). The changes in gene expression at the protein and mRNA levels in *Blmh*-silenced vs. control cells were analyzed by Western blotting and RT-qPCR using *Gapdh* protein and mRNA, respectively, as a reference.

We found that the *Blmh* protein level was significantly reduced in *Blmh*-silenced cells (by 80%; Fig. S2A). We also found that the histone demethylase Phf8 protein level was also significantly reduced (Fig. S2B), while the histone H4K20me1 level was significantly elevated (Fig. S2C) in *Blmh*-silenced cells.

At the same time, mTOR protein was significantly upregulated in *Blmh*-silenced cells (Fig. S2D), as were pmTOR (Fig. S2E) and APP (Fig. S2F). Autophagy-related proteins Becn1, Atg5, and Atg7 were significantly downregulated in *Blmh*-silenced cells (Fig. S2G, H, I) .

To find whether *Blmh* depletion affects the autophagy flux, we quantified Lc3 and p62 in *Blmh*-silenced N2a-APPswe cells. We found significant reductions in soluble Lc3-I (Fig. S2J) and an

autophagosome-bound lipidated Lc3-II (Fig. S2K) in *Blmh*-silencing cells. The Lc3-II/Lc3-I ratio was also significantly reduced (Fig. S2L), while p62 was upregulated (Fig. S2M). These findings show that *Blmh* depletion impairs the autophagy flux.

To elucidate whether *Blmh* exerts a transcriptional control over the expression of APP, mTOR- and autophagy-related proteins, we quantified by RT-qPCR mRNAs for these proteins. We found that the changes in mRNA levels in *Blmh*-silenced N2a-APP_{swe} cells (Fig. S3) were like the changes in the corresponding protein levels (Fig. S2). Specifically, *Blmh* mRNA was significantly reduced (by 95%; Fig. S3A), as was *Phf8* mRNA (Fig. S3B). mTOR mRNA was significantly upregulated (Fig. S3C) as was APP mRNA (Fig. S3D) in *Blmh*-silenced cells, reflecting changes in the corresponding protein levels in these cells (Fig. S2A-F). mRNAs for autophagy-related proteins *Atg5*, *Atg7*, and *Becn1* (Fig. S3E, F, and G, respectively).

These findings show that *Blmh* transcriptionally controls the expression of these proteins and prove that the changes in *Phf8*, H4K20m1, mTOR signaling, autophagy, and APP induced by *Blmh* gene silencing in N2a-APP_{swe} cells (Fig. S2) recapitulate the *in vivo* findings in *Blmh*^{-/-} mouse brain (Fig. 2, Fig. S1).

Hcy-thiolactone and N-Hcy-protein modulate the expression of APP, mTOR- and autophagy-related proteins in N2a-APP_{swe} cells

The effects of *Blmh* deletion on *Phf8* and its downstream targets can be caused by the absence the *Blmh* protein or by Hcy-thiolactone and *N-Hcy-protein*, which are known to be elevated in *Blmh*^{-/-} mice [4]. To distinguish between these possibilities, we treated N2a-APP_{swe} cells with different concentrations of Hcy-thiolactone or *N-Hcy-protein*.

We found significantly reduced *Phf8* levels in N2a-APP_{swe} cells treated with Hcy-thiolactone or *N-Hcy-protein* compared to untreated control cells (Fig. 3A). Levels of methylated histone H4K20me1 were elevated in Hcy-thiolactone or *N-Hcy-protein* treated cells compared to untreated controls (Fig. 3B).

mTOR levels were significantly upregulated in N2a-APP_{swe} cells by treatments with Hcy-thiolactone or *N-Hcy-protein*, compared to untreated cells (Fig. 3C). Levels of pmTOR were also significantly upregulated by these treatments (Fig. 3D). Autophagy-related proteins *Becn1* (Fig. 3E) *Atg5* (Fig. 3F), and *Atg7* (Fig. 3G) were significantly downregulated in cells treated with Hcy-thiolactone or *N-Hcy-protein*.

APP levels were significantly upregulated in N2a-APPswe cells treated with Hcy-thiolactone or *N*-Hcy-protein compared to untreated controls (Fig. 2H). Representative images of western blots are shown in Fig. 2I.

To find whether Hcy-thiolactone or *N*-Hcy-protein can affect the autophagy flux, we quantified Lc3 and p62 in N2a-APPswe cells treated with these metabolites. We found that treatments with Hcy-thiolactone or *N*-Hcy-protein reduced levels of soluble Lc3-I (Fig. 3I) and an autophagosome membrane-bound lipidated Lc3-II (Fig. 2J). The Lc3-II/Lc3-I ratio, a measure of autophagy flux, was also reduced (Fig. 3K), while p62 was upregulated (Fig. 3L). Representative images of western blots are shown in Fig. 3M.

Taken together, these findings suggest that Hcy-thiolactone and *N*-Hcy-protein, metabolites that are elevated in *Blmh*^{-/-} mice [4], contribute to the detrimental effects of *Blmh* depletion on Phf8, mTOR signaling, autophagy flux, and APP in N2s-APPswe cells.

Blmh depletion by RNA interference increases H4K20me1 binding to the mTOR promoter in N2a-APPswe cells

To find whether increased levels of the histone H4K20me1 mark can promote mTOR gene expression by binding to its promoter in *Blmh*-depleted cells, we conducted ChIP experiments using anti-H4K20me1 monoclonal antibody in the CUT&RUN assay (Fig. 4). The *Blmh* gene was silenced by transfecting N2a-APPswe cells with two different *Blmh*-targeting siRNAs (siRNA *Blmh* #1 and #2). The cells were permeabilized, treated with the anti-H4K20me1 antibody and a recombinant protein A/G-tagged micrococcal nuclease. DNA fragments released from N2a-APPswe cells were quantified by RT-qPCR using primers targeting the transcription start site (TSS) of the *mTOR* gene as well as upstream (UP) and downstream (DOWN) regions from the TSS.

We found that the binding of H4K20me1 was significantly increased at the mTOR TSS, mTOR UP, and mTOR DOWN sites in the *Blmh*-silenced N2a-APPswe cells compared to controls (Fig. 4A). Importantly, we found significantly more DNA fragments from the mTOR TSS compared with the mTOR UP and mTOR DOWN sites (Fig. 4A). Control experiments showed that binding of H3K4me3 to RPL30 intron was not affected by *Blmh* gene silencing (Fig. 4B). These findings show that *Blmh* depletion promoted H4K20me1 binding at the mTOR TSS site more efficiently than at the UP and DOWN sites.

The CUT&RUN experiments using anti-Phf8 antibody showed that *Blmh* depletion did not affect the binding of Phf8 to the mTOR gene (not shown).

Hcy-thiolactone and N-Hcy-protein increase H4K20me1 binding to the mTOR promoter in N2a-APPswe cells

Because treatments with Hcy-thiolactone or *N*-Hcy-protein, metabolites that are elevated in *Blmh*-depleted mice [4], upregulated mTOR expression (Fig. 3C), it is likely that each of these metabolites can influence mTOR expression by promoting H4K20me1 binding at its promoter. To evaluate this contention, we conducted the CUT&RUN experiments in N2a-APPswe cells treated with Hcy-thiolactone or *N*-Hcy-protein using anti-H4K20me1 antibody and quantified the extent of H4K20me1 binding to the *mTOR* gene.

We found that Hcy-thiolactone significantly increased binding of H4K20me1 at the *mTOR* TSS site as well as at the UP, and DOWN sites [51] (Fig. 4C). *N*-Hcy-protein also significantly increased binding of H4K20me1 at the *mTOR* TSS and DOWN sites, but not at the UP site [51]. Control experiments show that the binding of H3K4me3 to RPL30 intron was not affected by treatments with Hcy-thiolactone or *N*-Hcy-protein [51] (Fig. 4D).

Binding of Phf8 at the *mTOR* TSS, UP and down sites was not affected by Hcy-thiolactone or *N*-Hcy-protein (not shown).

Blmh depletion by RNA interference or treatments with Hcy-thiolactone and *N*-Hcy-protein promotes A β accumulation in N2a-APPswe cells

To find whether *Blmh* depletion affects A β accumulation, we silenced the *Blmh* gene in N2a-APPswe cells by using RNA interference and quantified A β by fluorescence confocal microscopy. Towards this end, we transfected N2a-APPswe cells using two different *Blmh*-targeting siRNAs. The cells were permeabilized, treated with anti-A β antibody, A β was visualized with a fluorescent secondary antibody (Fig. 5A) and quantified (Fig. 5B). We found that the silencing of *Blmh* gene, which reduced *Blmh* protein levels by 80% (Fig. S2A), significantly increased the area and average size of fluorescent A β puncta in *Blmh* siRNA-treated cells compared to siRNAscr-treated cells or mock-treated cell without siRNA (Fig. 5B).

Because *Blmh* depletion elevates Hcy-thiolactone and *N*-Hcy-protein in mice [4] we next examined whether each of these metabolites can induce A β accumulation in N2a-APPswe cells. We found significantly increased area of fluorescent A β puncta in cells treated with Hcy-thiolactone or *N*-Hcy-protein, compared to untreated controls (Fig. 5C, D). However, while treatments with Hcy-thiolactone led to increased average size of the fluorescent A β puncta, treatments with *N*-Hcy-protein did not (Fig. 5C, D), suggesting different effects of these metabolites on the structure of A β aggregates. These findings suggest that Hcy-thiolactone and *N*-Hcy-protein promote accumulation of A β induced by *Blmh* depletion.

Blmh gene deletion increases A β accumulation in brains of 5xFAD mice

To examine if *Blmh* deletion can promote A β accumulation in the mouse brain, we generated *Blmh*^{-/-}5xFAD mice and their *Blmh*^{+/+}5xFAD siblings by crossing *Blmh*^{-/-} mice with A β -overproducing 5xFAD animals. We prepared SDS-soluble and formic acid (FA)-soluble A β fractions, which have most of the total A β [47], as well as an A β fraction extractable with a RIPA buffer, from brains of 5- and 12-month-old mice. A β was quantified in these brain extracts by Western blotting using monoclonal anti-A β antibody. Representative Western blots are shown in Fig. 6A, B, C, I, J.

We found that RIPA- and SDS-soluble A β were significantly elevated in brains of 5-month-old *Blmh*^{-/-}5xFAD mice compared to *Blmh*^{+/+}5xFAD sibling controls in mice fed with a standard diet (Fig. 6D). The high Met diet abrogated effects of *Blmh* depletion on RIPA-soluble and SDS-soluble A β , while FA-soluble A β remained unaffected by *Blmh* depletion (Fig. 6E). The high Met diet did not affect RIPA-, SDS-, and FA-soluble A β in *Blmh*^{+/+}5xFAD mice (Fig. 6F) and *Blmh*^{-/-}5xFAD animals (quantification not shown).

In brains of 12-month-old *Blmh*^{-/-}5xFAD mice fed with high Met diet, RIPA-, SDS-, and FA-soluble A β were significantly elevated compared with *Blmh*^{+/+}5xFAD sibling controls fed with high Met diet (Fig. 6I). High Met diet significantly elevated RIPA-, SDS-, and FA-soluble A β in *Blmh*^{+/+}5xFAD mice (Fig. 6J).

Phf8 depletion upregulates A β but not APP in N2a-APPsw cells

The findings that *Phf8* expression was significantly reduced in the brains of *Blmh*^{-/-} (Fig. 2A) and *Blmh*^{-/-}5xFAD mice (Fig. S1A) and in the *Blmh*-silenced (Fig. S2B, Fig. S3B) or Hcy metabolite-treated (Fig. 3A) mouse neuroblastoma N2a-APPsw cells, suggested that *Phf8* depletion by itself can affect biochemical pathways leading to A β accumulation. To examine this, we depleted *Phf8* in N2a-APPsw cells by RNA interference and quantified by Western blotting proteins that we found to be affected in the *Blmh*^{-/-} (Fig. 2) and *Blmh*^{-/-}5xFAD (Fig. S1A) mouse brains.

Transfections with *Phf8*-targeting siRNAs reduced *Phf8* protein levels in N2a-APPsw cells by 85% (Fig. S4A). Levels of H4K20me1 (Fig. S4B), mTOR (Fig. S4C), and pmTOR (Fig. S4D) were significantly upregulated in *Phf8*-silenced cells. Autophagy-related proteins Atg5 and Atg7 were significantly downregulated (Fig. S4E and F, respectively) while *Becn1* was not affected in the *Phf8*-silenced cells (Fig. S4G). Notably, APP levels were not affected in the *Phf8*-silenced cells (Fig. S4H).

We also quantified A β by fluorescence confocal microscopy and found that A β was upregulated in the *Phf8*-silenced cells, manifested by significantly increased average size and signal intensity of fluorescent A β puncta compared to controls without siRNA or with siRNAsc (Fig. S4J, K). These findings show that upregulation of A β in *Phf8*-silenced cells was associated with impaired autophagy and not with the APP levels.

DISCUSSION

Our present findings show that Blmh, a Hcy-thiolactone-hydrolyzing enzyme [3], has a protective role in the CNS. Specifically, we demonstrated that Blmh depletion, which causes accumulation of Hcy-thiolactone and *N*-Hcy-protein in mice [4], downregulated histone demethylase Phf8 and upregulated the H4K20me1 epigenetic mark. This increased H4K20me1 binding to the mTOR promoter and upregulated mTOR signaling, which in turn inhibited the autophagy flux. We also showed that Blmh depletion upregulated App and A β . These biochemical changes, also induced by Hcy-thiolactone and *N*-Hcy-protein in cultured neural cells, were associated with cognitive and neuromotor deficits in mice.

5xFAD mice accumulate high levels of A β beginning around 2 months of age [40] and develop cognitive impairments beginning at 4-5 months of age and sensorimotor impairments at about 9 months of age [52], performing worse than the wild type animals in the memory and sensorimotor tests (<https://www.alzforum.org/research-models/5xfad-b6sji>). In the present work we found that Blmh depletion aggravated those neurological impairments. Specifically, 1-year-old *Blmh*^{-/-}5xFAD mice performed worse than *Blmh*^{+/+}5xFAD animals in the NOR test (Fig. 1E), showing impaired memory, and in the hindlimb (Fig. 1F) and cylinder tests (Fig. 1G), showing sensorimotor impairments. We found similar memory and sensorimotor impairments also in 4-month-old *Blmh*^{-/-} vs. *Blmh*^{+/+} mice (Fig. 1A-D), which do not accumulate A β . Our findings suggest that the absence of the Blmh protein is a dominant determinant that causes memory and sensorimotor impairments regardless of the presence or absence of the A β -generating transgene.

Memory and sensorimotor impairments in *Blmh*^{-/-} and *Blmh*^{-/-}5xFAD mice can be caused, at least in part, by Phf8 depletion, which occurs in *Blmh*^{-/-} brains (Fig. 2A, Fig. S1A). Indeed, PHF8 depletion in humans is linked to intellectual disability, autism spectrum disorder, attention deficit hyperactivity disorder [32], and intellectual disability [33], while similar neurological deficits were found in *Phf8*^{-/-} mice [34]. However, Phf8 was not known to be associated with A β , a hallmark of AD. Our present findings that Phf8 depletion in mouse neuroblastoma cells, induced by *Phf8* gene silencing (Fig. S4A) or by supplementation with Hcy-thiolactone or *N*-Hcy-protein (Fig. 3A), significantly increased A β accumulation (Fig. S4J, K; Fig. 5C, D), suggest that Phf8 depletion can also underly the association of HHcy with AD [53].

In previous studies we found that Blmh is a Hcy-thiolactone-hydrolyzing enzyme [3] and that Hcy-thiolactone and *N*-Hcy-protein are elevated in *Blmh*^{-/-} mice [4]. In the present study, we showed that treatments with Hcy-thiolactone or *N*-Hcy-protein mimicked the effects of Blmh depletion by RNA interference in mouse neuroblastoma cells. Specifically, Hcy-thiolactone/*N*-Hcy-protein and Blmh

depletion downregulated Phf8 (Fig. S2B, Fig. 3A), elevated H4K20me1 (Fig. S2C, Fig. 3B), increased H4K20me1 binding at the mTOR promoter (Fig. 4A, C), and upregulated mTOR signaling (Fig. S2D, E; Fig. 3C, D), and affected autophagy-related proteins (Fig. S2G-M; Fig. 3E-G, 3I-L). These findings show that *Blmh* is a negative regulator of mTOR signaling by controlling levels of Hcy metabolites that affect the mTOR promoter occupancy by H4K20me1.

Our findings also show that Phf8 is a mediator of Hcy-thiolactone/*N*-Hcy-protein effects on mTOR signaling, autophagy, and A β accumulation (Fig. 7). These findings directly link Hcy-thiolactone and *N*-Hcy-protein with dysregulated mTOR signaling (Fig. 3C, D) and its downstream outcomes such as impaired autophagy flux (Fig. 3I, J, K, L) and increased A β accumulation (Fig. 5) thereby providing a likely mechanism explaining neuropathy resulting from *Blmh* deficiency (Fig. 7) and accounting for the association of HHcy with Alzheimer's disease [53]. This role of Phf8 is further supported by findings showing that *Phf8* gene silencing by RNA interference had the same effects on mTOR (Fig. S4C, D), autophagy (Fig. S4E, F, G), and A β (Fig. S4J, K) as did *Blmh* gene silencing (Fig. S2D, E, G-M, Fig. 5A, B) or the treatments with Hcy-thiolactone or *N*-Hcy-protein (Fig. 3, Fig. 5C, D).

In the present study we showed that *Blmh* gene deletion led to *App* upregulation in *Blmh*^{-/-} (Fig. 2H) and APP in *Blmh*^{-/-}5xFAD mice (Fig. S1I). These findings were recapitulated in mouse neuroblastoma cells by *Blmh* silencing, which upregulated *APP* gene expression at the protein (Fig. S2F) and mRNA levels Fig. S3D). In contrast, *Phf8* gene silencing did not affect APP expression (Fig. S4H). These findings suggest that *Blmh* and APP proteins interact with each other in the CNS while Phf8 does not interact with APP. The *Blmh*-APP interaction is most likely direct, as suggested by findings of other investigators. For example, one study has shown that human BLMH interacts with APP *in vitro* and that overexpressed BLMH has the ability to process human APP to A β in the 293-HEK and CHO cells [21]. Another study reported that rat *Blmh* can further hydrolyze A β *in vitro*, with fibrillar A β 40 and A β 42 being more resistant than nonfibrillar peptides [22]. Alternatively, BLMH can regulate mTOR expression via binding to the *mTOR* promoter. This possibility is supported by findings showing that BLMH binds to DNA [54, 55]. However, the mechanism underlying the regulation of APP by *Blmh* needs to be elucidated in future studies.

We found that *Blmh* depletion downregulated Phf8 in mouse brain (Fig. 2A, Fig. S1A) and mouse neuroblastoma cells (Fig. S2B, Fig. S3B), upregulated APP in mouse brain (Fig. 2H, Fig. S1I) and mouse neuroblastoma cells (Fig. S2F, Fig. S3D), and A β in mouse brain (Fig. 6D-E, I-J) and mouse neuroblastoma cells (Fig. 5A, B). In contrast, Phf8 depletion had no effect on APP (Fig. S4H, I) but still upregulated A β (Fig. S4J, K). These findings suggest that A β accumulation in *Blmh*-depleted mouse brains can occur via three pathways shown in Fig. 7.

In pathway (i) (Fig. 7A) Hcy metabolites upregulate APP in *Blmh*-depleted (Fig. S2F) or Hcy-thiolactone/*N*-Hcy-protein-treated mouse neural cells (Fig. 2H). In pathway (ii-a) (Fig. 7A), Hcy metabolites downregulate Phf8, which leads to reduced autophagy flux (Fig. 3I-K; Fig. S2J-L) resulting in A β accumulation due to impaired clearance. Direct depletion of Phf8 by RNA interference also starts a similar pathway (ii-b) (Fig. 7A) that leads to A β accumulation via impaired autophagy (Fig. S4). However, these pathways need to be confirmed in future experiments involving Phf8 overexpression or mTOR knockdown (by RNA interference or pharmacological inhibition with rapamycin) in *Blmh*-silenced cells.

Our findings that APP upregulation (Fig. 2H, Fig. S1I) was associated with *Becn1* downregulation in brains of *Blmh*^{-/-} (Fig. 2E) and *Blmh*^{-/-}5xFAD mice (Fig. S1E) as well as in N2a-APPsw mouse neuroblastoma cells (Fig. S2F, G; Fig. S3D, G) suggest another pathway ((iii) in Fig. 7B) leading to A β accumulation. Pathway (iii) involves the interaction between *Bcln1* and APP in which *Becn1* is a negative regulator of APP expression and processing (Fig. 7B). *Becn1*, a protein with a key role in the initiation of autophagy, is known to decrease in human AD brains while genetic reduction of *Becn1* in transgenic mice that overexpress APP (*APP*⁺*Becn*^{+/-} mice) increased A β accumulation in neuronal cells [38]. *Becn1* was also shown to regulate APP processing and turnover. Specifically, depletion of *Bcln1* by RNA interference in rat neuroblastoma cells expressing human APP transgene (B103/hAPPwt cells) increased APP, Lc3, and A β , while *Becn1* overexpression reduced APP levels [37]. The involvement of autophagy in *Blmh* depletion-induced APP and A β accumulation needs to be confirmed in future experiments by boosting autophagy (*e.g.*, by treatment with TAT-Beclin1), which should rescue APP and A β accumulation in *Blmh*-depleted cells.

Notably, we found that HHcy induced by a high Met diet *and Blmh* gene deletion caused similar changes in the Phf8->H4K20me1->mTOR->autophagy pathway (Fig. 2, Fig. S1) and A β accumulation (Fig. 6I, J). These findings can be explained by our earlier findings showing that a common primary biochemical outcome of the *Blmh* gene deletion and high Met diet was the same: accumulation of Hcy-thiolactone and *N*-Hcy-protein [4, 56]. Indeed, as we also found in the present study, treatments with Hcy-thiolactone or *N*-Hcy-protein induce changes in the Phf8->H4K20me1->mTOR->autophagy pathway and A β accumulation in mouse neuroblastoma cells (Fig. 3, Fig. 5C, D) like those seen in *Blmh*^{-/-} mice or mice fed with high Met diet (Fig. 2, Fig. S1, Fig. 6I, J). These findings also suggest that dysregulation of Hcy metabolism in general would affect the Phf8->H4K20me1->mTOR->autophagy pathway and the central nervous system. Indeed, homocysteine metabolites inhibit autophagy, elevate A β , and induce neuropathy by impairing Phf8/H4K20me1-dependent epigenetic regulation of mTOR in cystathionine β -synthase-deficient mice [57].

Notably, as shown in the present work, *Blmh* deficiency or HHcy induced by a high Met diet increased H4K20me1 methylation levels due to downregulation of the histone demethylase Phf8 (Fig. 2B, Fig. S1B). HHcy is also known to affect DNA and protein methylation via *S*-adenosylhomocysteine (AdoHcy, an inhibitor of cellular AdoMet-dependent methylation reactions), which underlies the pathology of HHcy-associated human disease (reviewed in ref. [58]). However, possible inhibition of H4K20 methylase by AdoHcy would have an opposing effect, *i.e.*, would reduce H4K20me1 levels. The present findings, linking *Blmh* with the status of the histone H4K20me1 methylation, are reminiscent of our recent findings showing that *Pon1* deletion in mice elevated the H4K20me1 methylation levels via downregulation of Phf8 [51]. Thus, these two Hcy-thiolactone-detoxifying enzymes exert similar effects on H4K20me1 levels. Although there is no evidence that *Blmh* or *Pon1* are linked to DNA methylation, our present and earlier findings supply the first evidence that *Blmh* and *Pon1* can affect histone methylation status.

In conclusion, our findings show that *Blmh* interacts with APP and the Phf8/H4K20me1/mTOR/autophagy pathway, and that disruption of these interactions leads to A β accumulation and cognitive and neuromotor deficits. By revealing the mechanism by which *Blmh* prevents A β generation and cognitive/neuromotor deficits, the hallmarks of AD, our findings significantly expand our understanding of how *Blmh* maintains brain homeostasis.

AUTHOR CONTRIBUTIONS

Ł. Witucki performed and analyzed the experiments; Ł. Witucki and K. Borowczyk, carried out behavioral assessments; J. Suszyńska-Zajczyk analyzed NOR data; P. Pawlak and E. Warzych provided advice on confocal microscopy experiments; H. Jakubowski conceived the idea for the project, designed the study, generated *Blmh*^{-/-}5xFAD mouse model, bred the mice, collected tissue samples, analyzed data, and wrote the paper. All authors have read and approved the final manuscript.

ACKNOWLEDGMENTS

We thank J. Lazo for kindly supplying the *Blmh*^{-/-} mouse and S. S. Sisodia for mouse neuroblastoma N2a-APP_{swe} cells.

FUNDING

Supported in part by grants 2018/29/B/NZ4/00771, 2019/33/B/NZ4/01760, and 2021/43/B/NZ4/00339 from the National Science Center, Poland, and Grant 17GRNT32910002 from the American Heart Association.

DATA AVAILABILITY STATEMENT

The data that support the findings of this study are available in the methods and/or supplementary material of this article.

CONFLICT OF INTEREST

HIERONIM JAJUBOWSKI is an Editorial Board Member of this journal but was not involved in the peer-review process nor had access to any information about its peer-review.

No conflicts of interest, financial or otherwise, are declared by the authors.

SUPPLEMENTARY MATERIAL

The supplementary material is available in the electronic version of this article.

REFERENCES

- [1] Bromme D, Rossi AB, Smeekens SP, Anderson DC, Payan DG (1996) Human bleomycin hydrolase: molecular cloning, sequencing, functional expression, and enzymatic characterization. *Biochemistry* **35**, 6706-6714.
- [2] Kamata Y, Itoh Y, Kajiya A, Karasawa S, Sakatani C, Takekoshi S, Osamura RY, Takeda A (2007) Quantification of neutral cysteine protease bleomycin hydrolase and its localization in rat tissues. *J Biochem* **141**, 69-76.
- [3] Zimny J, Sikora M, Guranowski A, Jakubowski H (2006) Protective mechanisms against homocysteine toxicity: the role of bleomycin hydrolase. *J Biol Chem* **281**, 22485-22492.
- [4] Borowczyk K, Tisonczyk J, Jakubowski H (2012) Metabolism and neurotoxicity of homocysteine thiolactone in mice: protective role of bleomycin hydrolase. *Amino Acids* **43**, 1339-1348.
- [5] Jakubowski H (2012) Quality control in tRNA charging. *Wiley Interdiscip Rev RNA* **3**, 295-310.
- [6] Jakubowski H (2019) Homocysteine Modification in Protein Structure/Function and Human Disease. *Physiol Rev* **99**, 555-604.
- [7] Jakubowski H (2011) Quality control in tRNA charging -- editing of homocysteine. *Acta biochimica Polonica* **58**, 149-163.
- [8] Jakubowski H (1997) Metabolism of homocysteine thiolactone in human cell cultures. Possible mechanism for pathological consequences of elevated homocysteine levels. *J Biol Chem* **272**, 1935-1942.
- [9] Suszynska-Zajczyk J, Luczak M, Marczak L, Jakubowski H (2014) Hyperhomocysteinemia and bleomycin hydrolase modulate the expression of mouse brain proteins involved in neurodegeneration. *J Alzheimers Dis* **40**, 713-726.
- [10] Bossenmeyer-Pourie C, Smith AD, Lehmann S, Deramecourt V, Sablonniere B, Camadro JM, Pourie G, Kerek R, Helle D, Umoret R, Gueant-Rodriguez RM, Rigau V, Gabelle A, Sequeira JM, Quadros EV, Daval JL, Gueant JL (2019) N-homocysteinylation of tau and MAP1 is increased in autopsy specimens of Alzheimer's disease and vascular dementia. *J Pathol* **248**, 291-303.
- [11] Undas A, Perla J, Lacinski M, Trzeciak W, Kazmierski R, Jakubowski H (2004) Autoantibodies against N-homocysteinylation proteins in humans: implications for atherosclerosis. *Stroke* **35**, 1299-1304.
- [12] Wloczkowska O, Perla-Kajan J, Smith AD, de Jager C, Refsum H, Jakubowski H (2021) Anti-N-homocysteine-protein autoantibodies are associated with impaired cognition. *Alzheimers Dement (N Y)* **7**, e12159.
- [13] Zhou L, Guo T, Meng L, Zhang X, Tian Y, Dai L, Niu X, Li Y, Liu C, Chen G, Liu C, Ke W, Zhang Z, Bao A, Zhang Z (2022) N-homocysteinylation of alpha-synuclein promotes its aggregation and neurotoxicity. *Aging Cell*, e13745.

- [14] Zhang Q, Bai B, Mei X, Wan C, Cao H, Dan L, Wang S, Zhang M, Wang Z, Wu J, Wang H, Huo J, Ding G, Zhao J, Xie Q, Wang L, Qiu Z, Zhao S, Zhang T (2018) Elevated H3K79 homocysteinylation causes abnormal gene expression during neural development and subsequent neural tube defects. *Nat Commun* **9**, 3436.
- [15] Mei X, Qi D, Zhang T, Zhao Y, Jin L, Hou J, Wang J, Lin Y, Xue Y, Zhu P, Liu Z, Huang L, Nie J, Si W, Ma J, Ye J, Finnell RH, Saiyin H, Wang H, Zhao J, Zhao S, Xu W (2020) Inhibiting MARSs reduces hyperhomocysteinemia-associated neural tube and congenital heart defects. *EMBO Mol Med* **12**, e9469.
- [16] Borowczyk K, Piechocka J, Glowacki R, Dhar I, Midtun O, Tell GS, Ueland PM, Nygard O, Jakubowski H (2019) Urinary excretion of homocysteine thiolactone and the risk of acute myocardial infarction in coronary artery disease patients: the WENBIT trial. *J Intern Med* **285**, 232-244.
- [17] Jakubowski H (1997) Synthesis of homocysteine thiolactone in normal and malignant cells In *Homocysteine Metabolism: From Basic Science to Clinical Medicine*, Rosenberg IH, Graham I, Ueland PM, Refsum H, eds. Kluwer Academic Publishers, Norwell, MA, pp. 157-165.
- [18] Wang D, Zhao R, Qu YY, Mei XY, Zhang X, Zhou Q, Li Y, Yang SB, Zuo ZG, Chen YM, Lin Y, Xu W, Chen C, Zhao SM, Zhao JY (2018) Colonic Lysine Homocysteinylation Induced by High-Fat Diet Suppresses DNA Damage Repair. *Cell Rep* **25**, 398-412 e396.
- [19] Jakubowski H (2019) Protein N-Homocysteinylation and Colorectal Cancer. *Trends Cancer* **5**, 7-10.
- [20] Colasanti T, Sabatinelli D, Mancone C, Giorgi A, Pecani A, Spinelli FR, Di Giamberardino A, Navarini L, Speziali M, Vomero M, Barbati C, Perricone C, Ceccarelli F, Finucci A, Celia AI, Currado D, Afeltra A, Schinina ME, Barnaba V, Conti F, Valesini G, Alessandri C (2020) Homocysteinylation of alpha 1 antitrypsin as an antigenic target of autoantibodies in seronegative rheumatoid arthritis patients. *J Autoimmun* **113**, 102470.
- [21] Lefterov IM, Koldamova RP, Lazo JS (2000) Human bleomycin hydrolase regulates the secretion of amyloid precursor protein. *Faseb J* **14**, 1837-1847.
- [22] Kajiya A, Kaji H, Isobe T, Takeda A (2006) Processing of amyloid beta-peptides by neutral cysteine protease bleomycin hydrolase. *Protein and Peptide Letters* **13**, 119-123.
- [23] Ratovitski T, Chighladze E, Waldron E, Hirschhorn RR, Ross CA (2011) Cysteine proteases bleomycin hydrolase and cathepsin Z mediate N-terminal proteolysis and toxicity of mutant huntingtin. *The Journal of biological chemistry* **286**, 12578-12589.
- [24] Namba Y, Ouchi Y, Takeda A, Ueki A, Ikeda K (1999) Bleomycin hydrolase immunoreactivity in senile plaque in the brains of patients with Alzheimer's disease. *Brain Res* **830**, 200-202.
- [25] Papassotiropoulos A, Bagli M, Jessen F, Frahnert C, Rao ML, Maier W, Heun R (2000) Confirmation of the association between bleomycin hydrolase genotype and Alzheimer's disease. *Mol Psychiatry* **5**, 213-215.
- [26] Montoya SE, Aston CE, DeKosky ST, Kamboh MI, Lazo JS, Ferrell RE (1998) Bleomycin hydrolase is associated with risk of sporadic Alzheimer's disease. *Nat Genet* **18**, 211-212.
- [27] Namba Y, Ouchi Y, Asada T, Hattori H, Ueki A, Ikeda K (1999) Lack of association between bleomycin hydrolase gene polymorphism and Alzheimer's disease in Japanese people. *Ann Neurol* **46**, 136-137.
- [28] Farrer LA, Abraham CR, Haines JL, Rogaeva EA, Song Y, McGraw WT, Brindle N, Premkumar S, Scott WK, Yamaoka LH, Saunders AM, Roses AD, Auerbach SA, Sorbi S, Duara R, Pericak-Vance MA, St George-Hyslop PH (1998) Association between bleomycin hydrolase and Alzheimer's disease in caucasians. *Ann Neurol* **44**, 808-811.
- [29] Thome J, Gewirtz JC, Sakai N, Zachariou V, Retz-Junginger P, Retz W, Duman RS, Rosler M (1999) Polymorphisms of the human apolipoprotein E promoter and bleomycin hydrolase gene: risk factors for Alzheimer's dementia? *Neurosci Lett* **274**, 37-40.
- [30] Suszynska J, Tisonczyk J, Lee HG, Smith MA, Jakubowski H (2010) Reduced homocysteine-thiolactonase activity in Alzheimer's disease. *J Alzheimers Dis* **19**, 1177-1183.

- [31] Montoya SE, Thiels E, Card JP, Lazo JS (2007) Astroglialosis and behavioral changes in mice lacking the neutral cysteine protease bleomycin hydrolase. *Neuroscience* **146**, 890-900.
- [32] Sobering AK, Bryant LM, Li D, McGaughan J, Maystadt I, Moortgat S, Graham JM, Jr., van Haeringen A, Ruivenkamp C, Cuperus R, Vogt J, Morton J, Brasch-Andersen C, Steenhof M, Hansen LK, Adler E, Lyonnet S, Pingault V, Sandrine M, Ziegler A, Donald T, Nelson B, Holt B, Petryna O, Firth H, McWalter K, Zyskind J, Telegrafi A, Juusola J, Person R, Bamshad MJ, Earl D, University of Washington Center for Mendelian G, Tsai AC, Yearwood KR, Marco E, Nowak C, Douglas J, Hakonarson H, Bhoj EJ (2022) Variants in PPH8 cause a spectrum of X-linked neurodevelopmental disorders and facial dysmorphology. *HGG Adv* **3**, 100102.
- [33] Laumonnier F, Holbert S, Ronce N, Faravelli F, Lenzner S, Schwartz CE, Lespinasse J, Van Esch H, Lacombe D, Goizet C, Phan-Dinh Tuy F, van Bokhoven H, Fryns JP, Chelly J, Ropers HH, Moraine C, Hamel BC, Briault S (2005) Mutations in PPH8 are associated with X linked mental retardation and cleft lip/cleft palate. *J Med Genet* **42**, 780-786.
- [34] Chen X, Wang S, Zhou Y, Han Y, Li S, Xu Q, Xu L, Zhu Z, Deng Y, Yu L, Song L, Chen AP, Song J, Takahashi E, He G, He L, Li W, Chen CD (2018) Pph8 histone demethylase deficiency causes cognitive impairments through the mTOR pathway. *Nat Commun* **9**, 114.
- [35] Khayati K, Antikainen H, Bonder EM, Weber GF, Kruger WD, Jakubowski H, Dobrowolski R (2017) The amino acid metabolite homocysteine activates mTORC1 to inhibit autophagy and form abnormal proteins in human neurons and mice. *FASEB J* **31**, 598-609.
- [36] Yates SC, Zafar A, Hubbard P, Nagy S, Durant S, Bicknell R, Wilcock G, Christie S, Esiri MM, Smith AD, Nagy Z (2013) Dysfunction of the mTOR pathway is a risk factor for Alzheimer's disease. *Acta Neuropathol Commun* **1**, 3.
- [37] Jaeger PA, Pickford F, Sun CH, Lucin KM, Masliah E, Wyss-Coray T (2010) Regulation of amyloid precursor protein processing by the Beclin 1 complex. *PLoS One* **5**, e11102.
- [38] Pickford F, Masliah E, Britschgi M, Lucin K, Narasimhan R, Jaeger PA, Small S, Spencer B, Rockenstein E, Levine B, Wyss-Coray T (2008) The autophagy-related protein beclin 1 shows reduced expression in early Alzheimer disease and regulates amyloid beta accumulation in mice. *J Clin Invest* **118**, 2190-2199.
- [39] Schwartz DR, Homanics GE, Hoyt DG, Klein E, Abernethy J, Lazo JS (1999) The neutral cysteine protease bleomycin hydrolase is essential for epidermal integrity and bleomycin resistance. *Proc Natl Acad Sci U S A* **96**, 4680-4685.
- [40] Oakley H, Cole SL, Logan S, Maus E, Shao P, Craft J, Guillozet-Bongaarts A, Ohno M, Disterhoft J, Van Eldik L, Berry R, Vassar R (2006) Intraneuronal beta-amyloid aggregates, neurodegeneration, and neuron loss in transgenic mice with five familial Alzheimer's disease mutations: potential factors in amyloid plaque formation. *J Neurosci* **26**, 10129-10140.
- [41] Chwatko G, Boers GH, Strauss KA, Shih DM, Jakubowski H (2007) Mutations in methylenetetrahydrofolate reductase or cystathionine beta-synthase gene, or a high-methionine diet, increase homocysteine thiolactone levels in humans and mice. *Faseb J* **21**, 1707-1713.
- [42] Pi T, Wei S, Jiang Y, Shi JS (2021) High Methionine Diet-Induced Alzheimer's Disease like Symptoms Are Accompanied by 5-Methylcytosine Elevated Levels in the Brain. *Behav Neurol* **2021**, 6683318.
- [43] Ishii I, Kamata S, Ito S, Shimonaga A, Koizumi M, Tsushima M, Miura A, Nagata T, Tosaka Y, Ohtani H, Kamichatani W, Akahoshi N (2022) A High-Methionine Diet for One-Week Induces a High Accumulation of Methionine in the Cerebrospinal Fluid and Confers Bipolar Disorder-like Behavior in Mice. *Int J Mol Sci* **23**.
- [44] Leger M, Quiedeville A, Bouet V, Haelewyn B, Boulouard M, Schumann-Bard P, Freret T (2013) Object recognition test in mice. *Nat Protoc* **8**, 2531-2537.
- [45] Lieu CA, Chinta SJ, Rane A, Andersen JK (2013) Age-related behavioral phenotype of an astrocytic monoamine oxidase-B transgenic mouse model of Parkinson's disease. *PLoS One* **8**, e54200.

- [46] Guyenet SJ, Furrer SA, Damian VM, Baughan TD, La Spada AR, Garden GA (2010) A simple composite phenotype scoring system for evaluating mouse models of cerebellar ataxia. *J Vis Exp*.
- [47] Murphy MP, Beckett TL, Ding Q, Patel E, Markesbery WR, St Clair DK, LeVine H, 3rd, Keller JN (2007) Abeta solubility and deposition during AD progression and in APPxPS-1 knock-in mice. *Neurobiol Dis* **27**, 301-311.
- [48] Thinakaran G, Teplow DB, Siman R, Greenberg B, Sisodia SS (1996) Metabolism of the "Swedish" amyloid precursor protein variant in neuro2a (N2a) cells. Evidence that cleavage at the "beta-secretase" site occurs in the golgi apparatus. *J Biol Chem* **271**, 9390-9397.
- [49] Gurda D, Handschuh L, Kotkowiak W, Jakubowski H (2015) Homocysteine thiolactone and N-homocysteinylated protein induce pro-atherogenic changes in gene expression in human vascular endothelial cells. *Amino Acids* **47**, 1319-1339.
- [50] Livak KJ, Schmittgen TD (2001) Analysis of relative gene expression data using real-time quantitative PCR and the 2(-Delta Delta C(T)) Method. *Methods* **25**, 402-408.
- [51] Witucki L, Jakubowski H (2023) Depletion of Paraoxonase 1 (Pon1) Dysregulates mTOR, Autophagy, and Accelerates Amyloid Beta Accumulation in Mice. *Cells* **12**.
- [52] O'Leary TP, Mantolino HM, Stover KR, Brown RE (2020) Age-related deterioration of motor function in male and female 5xFAD mice from 3 to 16 months of age. *Genes Brain Behav* **19**, e12538.
- [53] Smith AD, Refsum H (2021) Homocysteine - from disease biomarker to disease prevention. *J Intern Med* **290**, 826-854.
- [54] Joshua-Tor L, Xu HE, Johnston SA, Rees DC (1995) Crystal structure of a conserved protease that binds DNA: the bleomycin hydrolase, Gal6. *Science* **269**, 945-950.
- [55] Takeda A, Higuchi D, Yamamoto T, Nakamura Y, Masuda Y, Hirabayashi T, Nakaya K (1996) Purification and characterization of bleomycin hydrolase, which represents a new family of cysteine proteases, from rat skin. *J Biochem (Tokyo)* **119**, 29-36.
- [56] Jakubowski H, Perla-Kajan J, Finnell RH, Cabrera RM, Wang H, Gupta S, Kruger WD, Kraus JP, Shih DM (2009) Genetic or nutritional disorders in homocysteine or folate metabolism increase protein N-homocysteinylated in mice. *Faseb J* **23**, 1721-1727.
- [57] Witucki L, Jakubowski H (2023) Homocysteine metabolites inhibit autophagy, elevate amyloid beta, and induce neuropathy by impairing Phf8/H4K20me1-dependent epigenetic regulation of mTOR in cystathionine beta-synthase-deficient mice. *J Inherit Metab Dis*.
- [58] Perla-Kajan J, Jakubowski H (2019) Dysregulation of Epigenetic Mechanisms of Gene Expression in the Pathologies of Hyperhomocysteinemia. *Int J Mol Sci* **20**.

Figure legends

Fig. 1. Deletion of *Blmh* gene impairs recognition memory and sensorimotor activity. (A, B, C, D) *Blmh*^{-/-} vs. *Blmh*^{+/+} mice - (A, B) Novel object recognition (NOR) test: Time spent at novel and familiar objects. Std diet: N = 6, 7, 9, and 4 mice/group. Met diet: 7, 7, 8, and 10 mice/group. (C) Hindlimb clasping test scores. (D) Ledge test scores. Std diet: N = 8, 9, 30, and 14 mice/group. Met diet: 20, 11, 14, and 10 mice/group. (E, F, G) *Blmh*^{-/-}5xFAD vs. *Blmh*^{+/+}5xFAD mice - (E) NOR test: Time spent exploring novel and familiar objects. Std diet: N = 8 and 4 mice/group; Met diet: 8 and 5 mice/group. (F) Hindlimb clasping test scores. Std diet: N = 8 and 4; Met diet: 9 and 7 mice/group. (G) Cylinder test: number of rears. Std diet: N = 8 and 6; Met diet: 9 and 5 mice/group. *P*-values for the NOR test were calculated by the paired two-sided Student *t* test. *P*-values for the hindlimb, ledge, and cylinder tests were calculated by one-way ANOVA with Tukey's multiple comparisons test. * *P* < 0.05, ** *P* < 0.01, *** *P* < 0.001, or **** *P* < 0.0001

Fig. 2. *Blmh* depletion affects the expression of histone demethylase Phf8, histone H4K20me1 epigenetic mark, mTOR signaling, autophagy, and App in the *Blmh*^{-/-} mouse brain. One-month-old *Blmh*^{-/-} mice (n = 7 and 14) and *Blmh*^{+/+} sibling controls (n = 10 and 10) fed with a control or high Met diet (to induce HHcy) for one or three months were used in experiments. Each group included 7-14 mice of both sexes. Bar graphs illustrating quantification of the following brain proteins by Western blotting are shown: Phf8 (A), H4K20me1 (B), mTOR (C), pmTOR (D), Becn1 (E), Atg5 (F), Atg7 (G), and App (H). Gapdh protein was used as a reference for normalization. Representative pictures of Western blots used for protein quantification are shown in panel (I). Each mouse was assayed in three independent experiments and average values were used to calculate the mean ± standard deviation (SD) values for wrote down proteins in each experimental group. * *P* < 0.05, ** *P* < 0.01, *** *P* < 0.001, or **** *P* < 0.0001 were calculated by one-way ANOVA with Tukey's multiple comparisons test. The numbers above bars show *P* values 0.08 – 0.11. NS, not significant.

Fig. 3. Hcy-thiolactone and *N*-Hcy-protein downregulate Phf8, upregulate the H4K20me1 epigenetic mark, mTOR signaling, APP, and impair autophagy in mouse neuroblastoma N2a-APP^{swe} cells. N2a-APP^{swe} cells were treated with indicated concentrations of *N*-Hcy-protein (*N*-Hcy) or Hcy-thiolactone (HTL) for 24 h at 37°C. Bar graphs illustrating the quantification of Phf8 (A), H4K20me1 (B), mTOR (C), pmTOR (D), Becn1 (E), Atg5 (F), Atg7 (G), APP (H), Lc3-I (I), Lc3-II (J), Lc3-I/Lc3-II ratio (K), and p62 (L) based on Western blot analyses are shown. Gapdh was used as a reference protein. Each assay was repeated three times in three independent experiments. Mean ± SD values for each treatment group

are shown. *P*-values were calculated by one-way ANOVA with Tukey's multiple comparisons test. * *P* < 0.05, ** *P* < 0.01, *** *P* < 0.001, or **** *P* < 0.0001. The numbers above bars show *P* values 0.05 – 0.16. *NS*, not significant.

Fig. 4. *Blmh* gene silencing or treatment with Hcy-thiolactone or *N*-Hcy-protein increases H4K20me1 binding at the *mTOR* promoter in mouse neuroblastoma N2a-APP_{swe} cells. (A) CUT&RUN assays with anti-H4K20me1 antibody show specific binding of H4K20me1 at the transcription start site (TSS) of the *mTOR* gene as well as downstream and upstream sites in *Blmh* siRNA-silenced N2a-APP_{swe} cells. Bar graphs show the relative H4K20me1 binding at the indicated regions of the *mTOR* gene in N2a-APP_{swe} cells transfected with two different siRNAs targeting the *Blmh* gene (siRNA *Blmh* #1 and #2). Transfections without siRNA (Control -siRNA) or with scrambled siRNA (siRNA_{scr}) were used as controls. (B) Control CUT&RUN experiment with anti-H3K4me3 antibody shows that *Blmh* gene-silencing did not affect the binding of H3K4me3 at the Rpl30 intron. RT-qPCR was conducted on the input and precipitated DNA fragments. Data are averages of three independent experiments. (C) N2a-APP_{swe} cells were treated with the indicated concentrations of *N*-Hcy-protein or Hcy-thiolactone (HTL) for 24h at 37°C. Untreated cells were used as controls. The CUT&RUN assays with anti-H4K20me1 antibody show that H4K20me1 binds to the transcription start site (TSS) of the *mTOR* gene as well as downstream and upstream sites. Bar graphs show relative H4K20me1 binding at the indicated regions of the *mTOR* gene. (D) A control CUT&RUN experiment with anti-H3K4me3 antibody shows that Hcy-thiolactone and *N*-Hcy-protein did not affect the binding of H3K4me3 at the Rpl30 intron. Panels (C) and (D) were reproduced with permission from ref. [51]. RT-qPCR was conducted on the input and precipitated DNA fragments. Data are mean ± SD of three biologically independent experiments. *P*-values were calculated by one-way ANOVA with Tukey's multiple comparisons test. **P* < 0.05, ** *P* < 0.01, *** *P* < 0.001.

Fig. 5. *Blmh* gene silencing or treatment with Hcy-thiolactone or *N*-Hcy-protein promotes Aβ accumulation in mouse neuroblastoma cells. Analysis of Aβ in mouse neuroblastoma N2a-APP_{swe} cells was performed by confocal immunofluorescence microscopy using an anti-Aβ antibody. (A, B) The cells were transfected with siRNAs targeting the *Blmh* gene (siRNA *Blmh* #1 and #2). Transfections without siRNA (Control -siRNA) or with scrambled siRNA (siRNA_{scr}) were used as controls. Confocal microscopy images (A) are representative of at least N = 3 biologically independent experiments. Bar graphs (B) show the quantification of Aβ signals from *Blmh*-silenced and control cells. (C, D) N2a-APP_{swe} cells were treated with the indicated concentrations of *N*-Hcy-protein (*N*-Hcy) or Hcy-

thiolactone (HTL) for 24h at 37°C. Untreated cells were used as controls. Confocal microscopy images (C) are representative of at least N = 3 biologically independent experiments. Bar graphs (D) show the quantification of A β signals from cells treated with N-Hcy or HTL and untreated cells. Each data point is a mean \pm SD of three biologically independent experiments with triplicate measurements in each. Panels (C) and (D) were reproduced with permission from ref. [51]. *P*-values were calculated by one-way ANOVA with Tukey's multiple comparisons test. **P* < 0.05, ** *P* < 0.001, *** *P* < 0.0001.

Fig. 6. *Blmh* gene deletion promotes A β accumulation in 5xFAD mice. Analysis of A β in brains from 5-month-old (A-F) and 12-month-old (G-J) *Blmh*^{-/-}5xFAD and *Blmh*^{+/+}5xFAD mice fed with a standard or high Met diet (to induce HHcy) since weaning at the age of one month is shown. Brain extracts were analyzed on SDS-PAGE gels and A β was quantified by Western blotting. Representative pictures of Western blots of A β fractions extracted from brains with RIPA buffer (A, G), 2% SDS (B, H), and 70% formic acid (FA) (C) are shown. Numbers below each lane refer to the amount of brain (mg) from each mouse used in the experiment. A commercial A β ₄₂ standard is shown in the first lane from left in each blot. Total A β signals in each lane (standing for an individual mouse) were quantified by scanning all chemiluminescent bands. Bar graphs (D, E, F, I, L) show brain A β quantification for *Blmh*^{-/-}5xFAD and *Blmh*^{+/+}5xFAD mice (n = 8-10 mice/group). Data points for each mouse group represent mean \pm SD with four independent measurements for each mouse. *P*-values were calculated by one-way ANOVA with Tukey's multiple comparisons test. **P* < 0.05, ** *P* < 0.001, *** *P* < 0.0001.

Fig. 7. Hypothetical pathways leading to A β generation in *Blmh*^{-/-}5xFAD mice. Panel (A) illustrates the APP (*i*) and Phf8 (*ii-a*) pathways. Panel (B) highlights the interaction (*iii*) between autophagy (Becn1) and APP pathways. Up and down arrows show direction of changes in the indicated variables. *Blmh*, bleomycin hydrolase; Hcy, homocysteine; HTL, Hcy-thiolactone; APP, amyloid beta precursor protein; mTOR, mammalian target of rapamycin; pmTOR, phospho-mTOR; Phf8, Plant Homeodomain Finger

protein 8. See text for discussion.

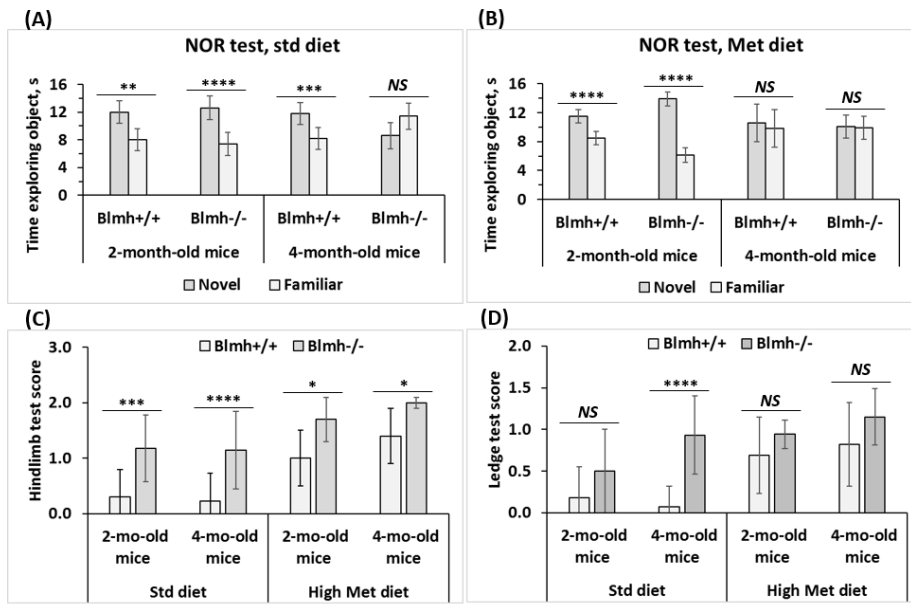


Figure 1A-D

* P < 0.05 ** P < 0.01 *** P < 0.001 **** P < 0.0001

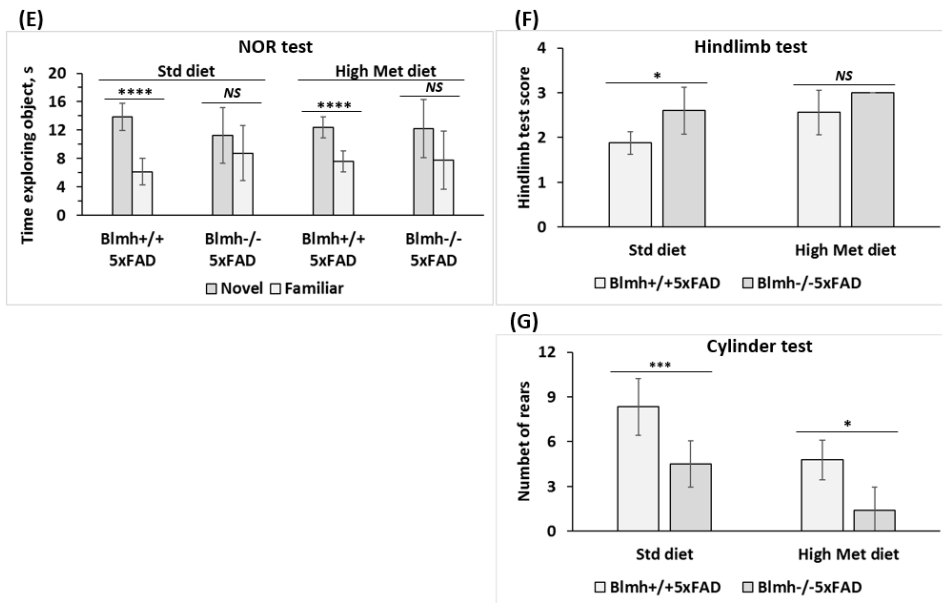


Figure 1E, F, G

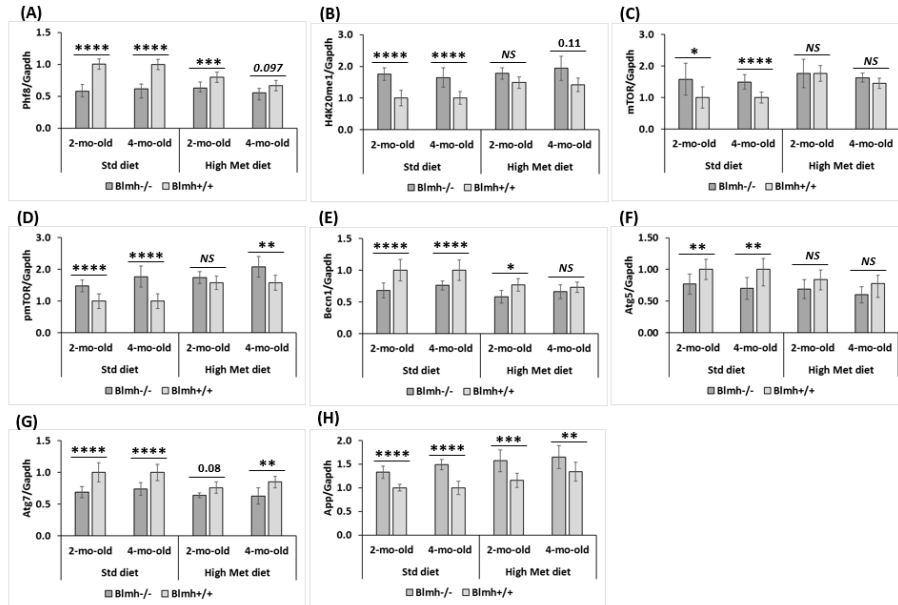


Figure 2A-H

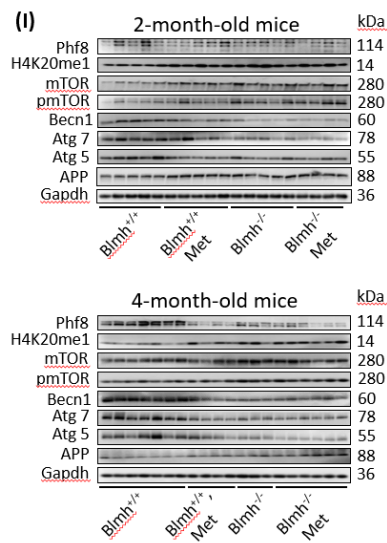


Figure 2I

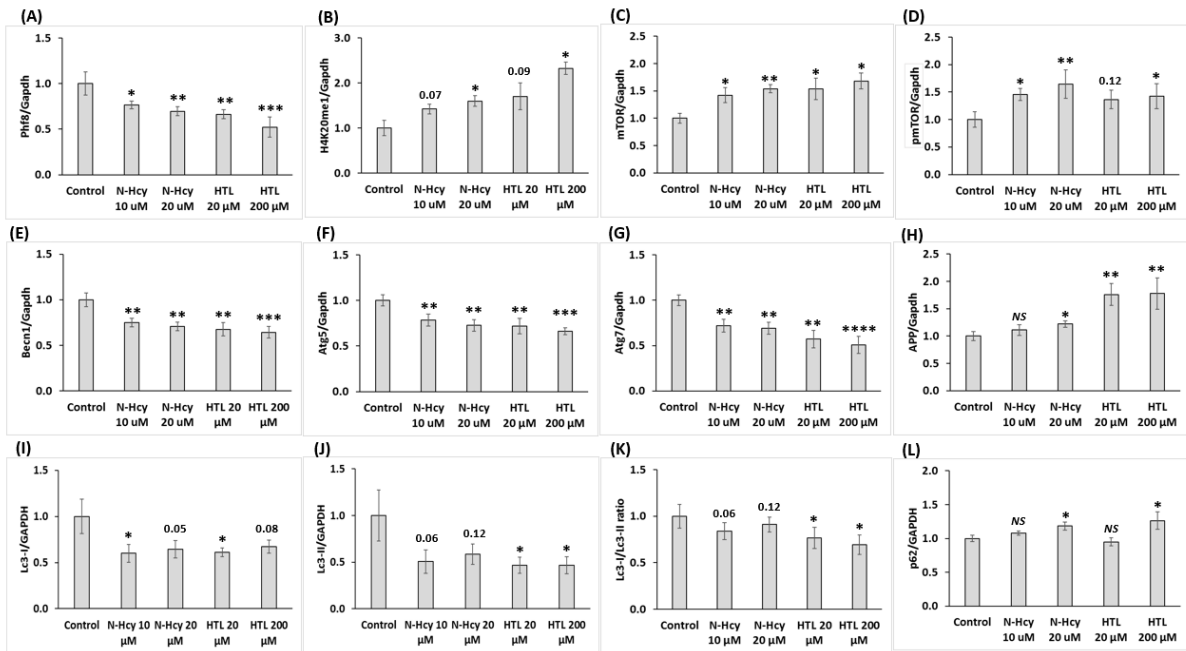


Figure 3A-L

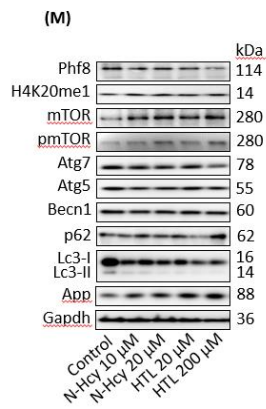


Figure 3M

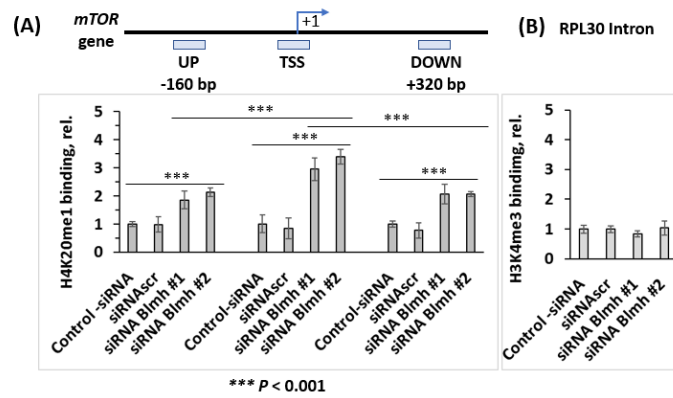


Figure 4A, B

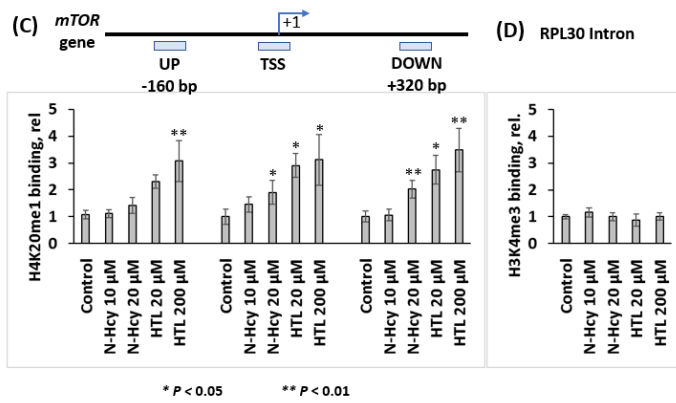


Figure 4C, D

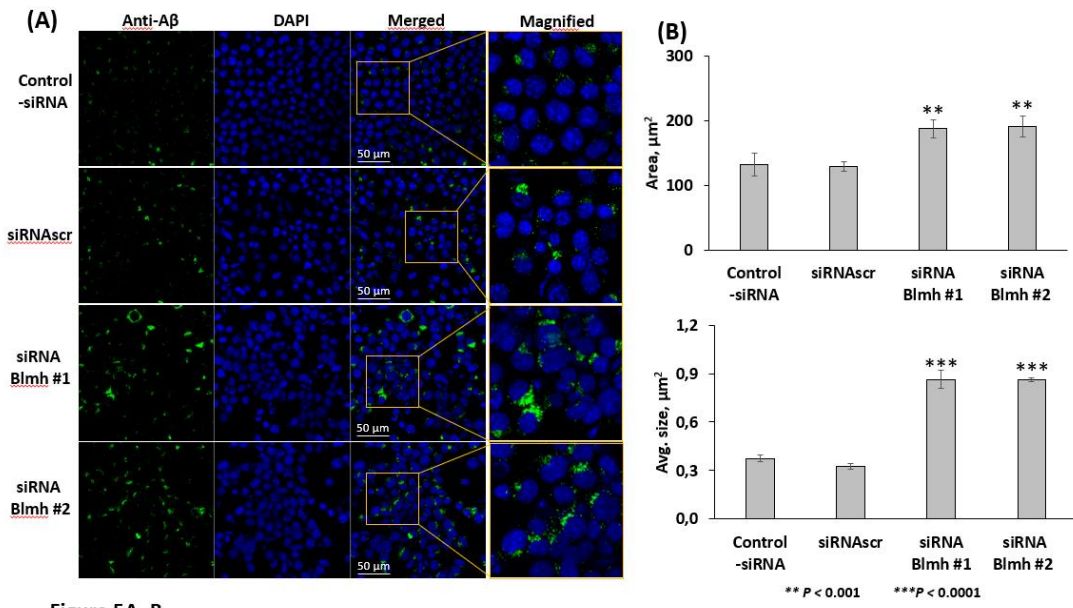


Figure 5A, B

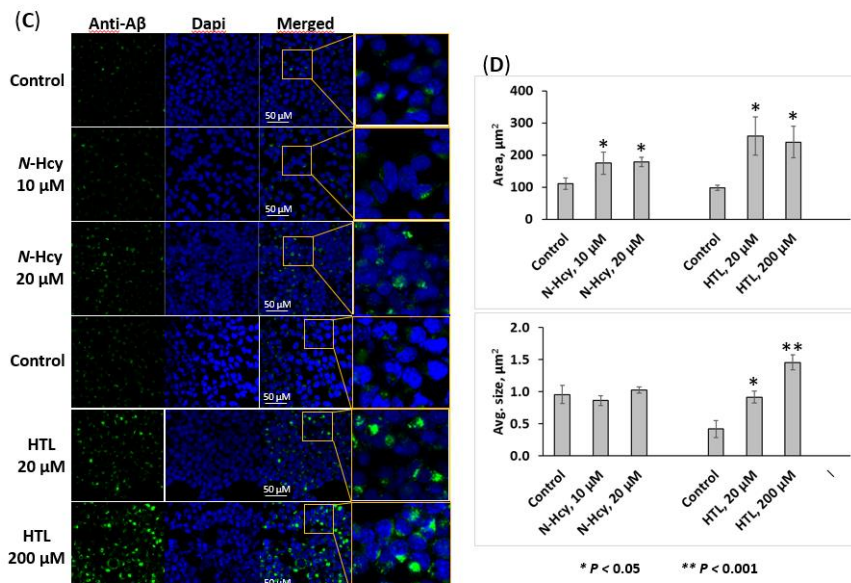


Figure 5C, D

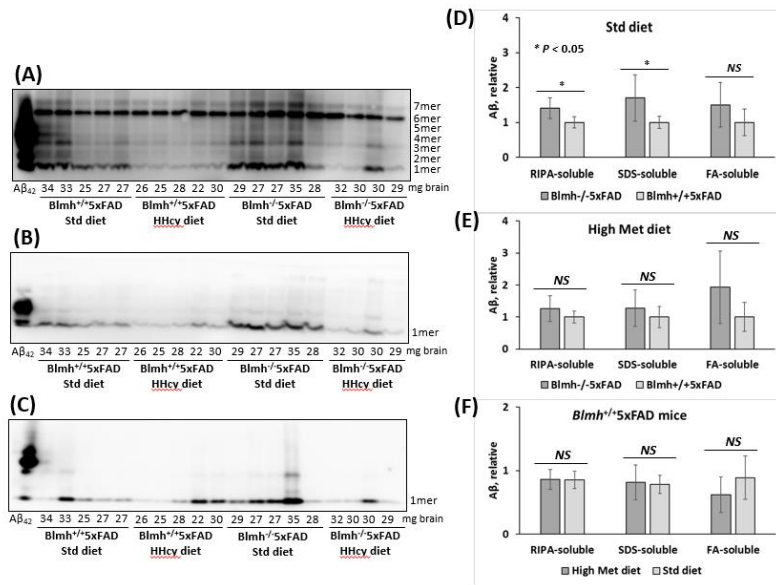


Figure 6A-F

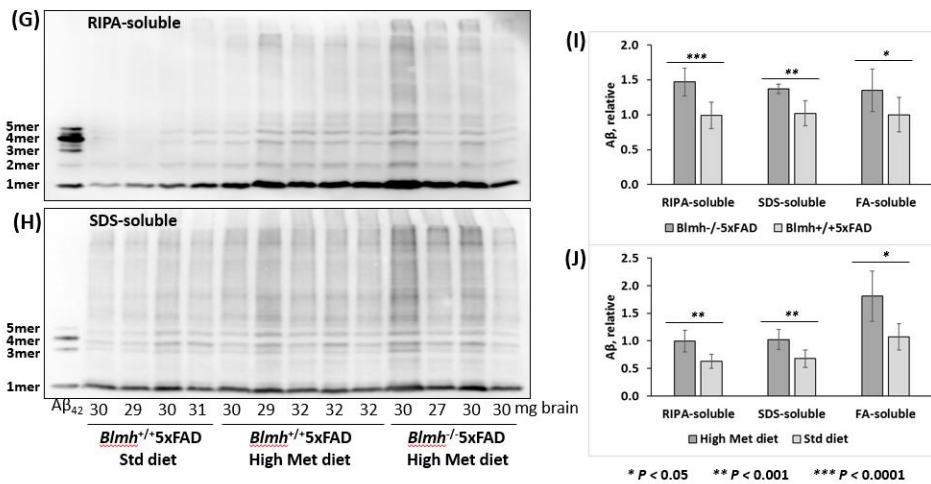


Figure 6G-J

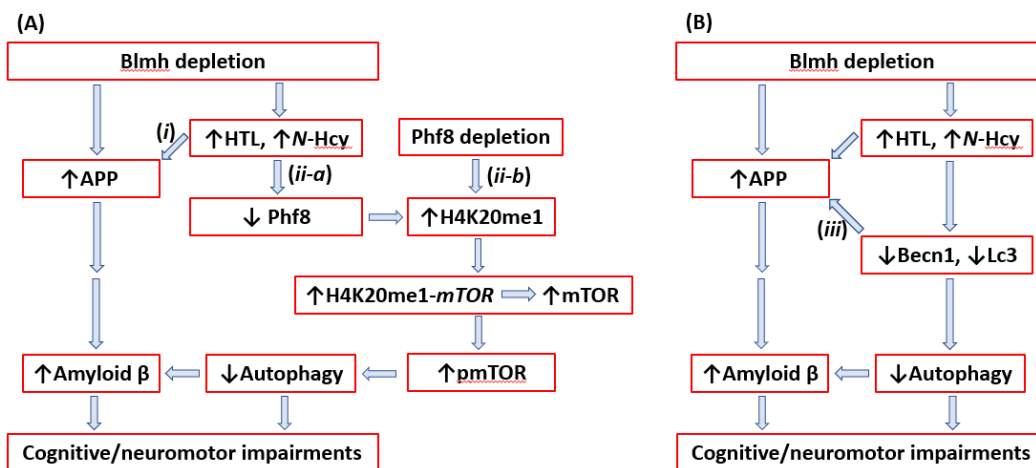


Figure 7

Deletion of the Homocysteine Thiolactone Detoxifying Enzyme Bleomycin Hydrolase, in Mice, Causes Memory- and Neurological Deficits and Worsens Alzheimer's Disease-Related Behavioral and Biochemical Traits in the 5xFAD Model of Alzheimer's Disease

Łukasz Witucki, Kamila Borowczyk, Joanna Suszyńska-Zajczyk, Ewelina Warzych, Piotr Pawlak, Hieronim Jakubowski*

Supplementary Material

Supplementary Figures S1, S2, S3, S4

Supplementary Table S1

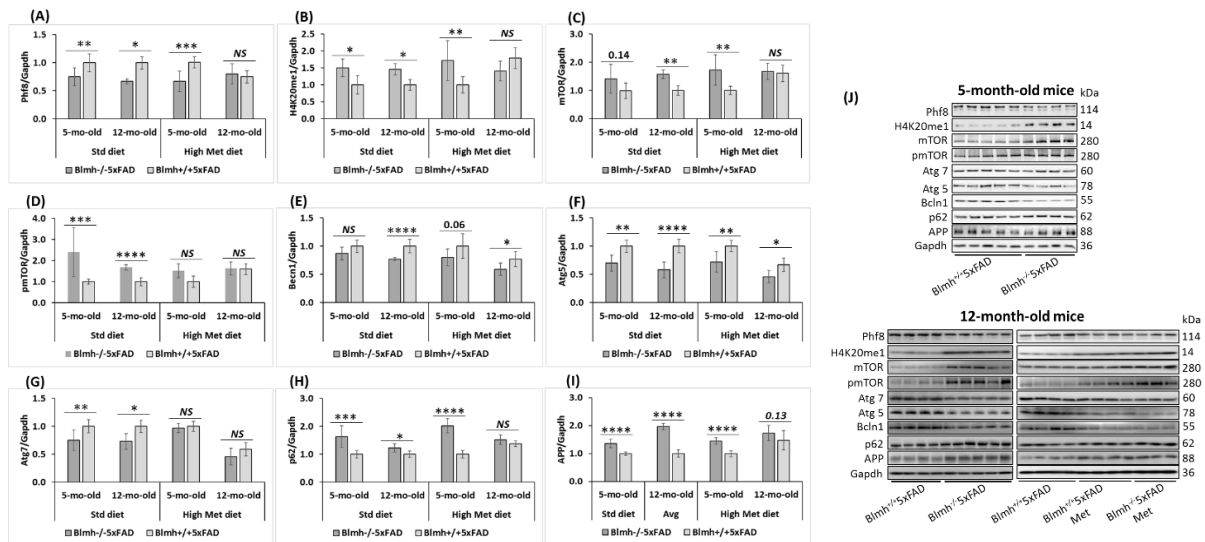


Fig. S1. *Blmh* depletion affects the expression of histone demethylase Phf8, histone H4K20me1 epigenetic mark, mTOR signaling, autophagy, and App in the *Blmh*^{-/-}5xFAD mouse brain. One-month-old *Blmh*^{-/-}5xFAD mice and *Blmh*^{+/+}5xFAD sibling controls fed with HHcy high Met diet (1% Met in drinking water) or control diet for 4 and 11 months were used in experiments. Each group included 7 - 10 mice of both sexes. Bar graphs illustrating quantification of the following brain proteins by Western blotting are shown: Phf8 (A), H4K20me1 (B), mTOR (C), pmTOR (D), Bcln1 (E), Atg5 (F), Atg7 (G), p62 (H), and APP (I). Gapdh protein was used as references for normalization. Panel (J) shows representative pictures of Western blots. Data are mean \pm SD values of three independent experiments. Numerical values in panels (E) and (I) show P values $> 0.05 < 0.015$. P values were calculated by one-way ANOVA with Tukey's multiple comparisons test. * $P < 0.05$, ** $P < 0.01$, *** $P < 0.001$, **** $P < 0.0001$ vs. control -siRNA plus siRNAsc.

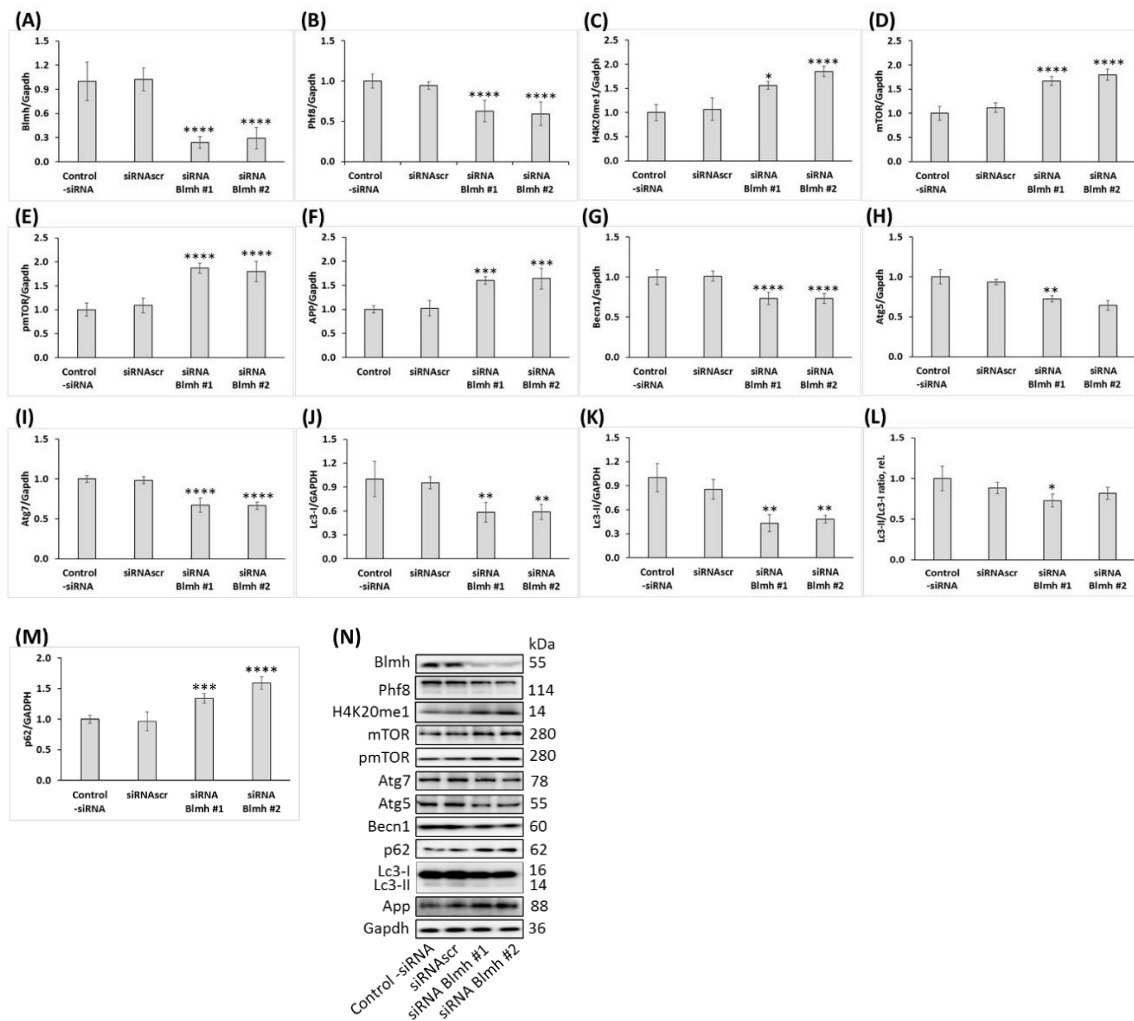


Fig. S2. *Blmh* gene silencing in mouse neuroblastoma N2a-APPsw cells recapitulates changes in histone demethylase Phf8, H4K20me1, mTOR signaling, APP, and autophagy-related protein levels seen in *Pon1*^{-/-} mouse brain. Bar graphs illustrating the quantification of Blmh (A), Phf8 (B), H4K20me1 (C), mTOR (D), pmTOR (E), App (F), Becn1 (G), Atg5 (H), Atg7 (I), Lc3-II/Lc3I ratio (J), Lc3-I (K), Lc3-II (L), and p62 (M) in N2a-APPsw cells transfected with two different siRNAs targeting the *Blmh* gene (siRNA *Blmh* #1 and #2) are shown. Transfections without siRNA (Control -siRNA) or with scrambled siRNA (siRNAAsc) were used as controls. Representative Western blots are shown in panel (N). Gapdh was used as a reference protein. Data are mean \pm standard deviation (SD) values of three biologically independent experiments. *P* values were calculated by one-way ANOVA with Tukey's multiple comparisons test. **P* < 0.05, ***P* < 0.01, ****P* < 0.001, *****P* < 0.0001 vs. 'control -siRNA' plus 'siRNAAsc.'

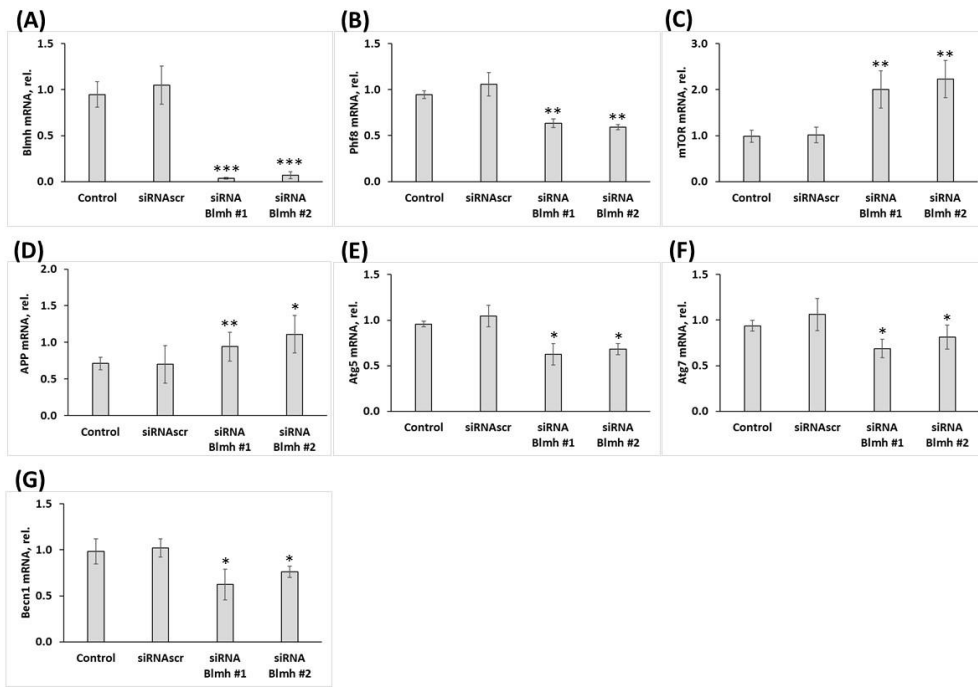
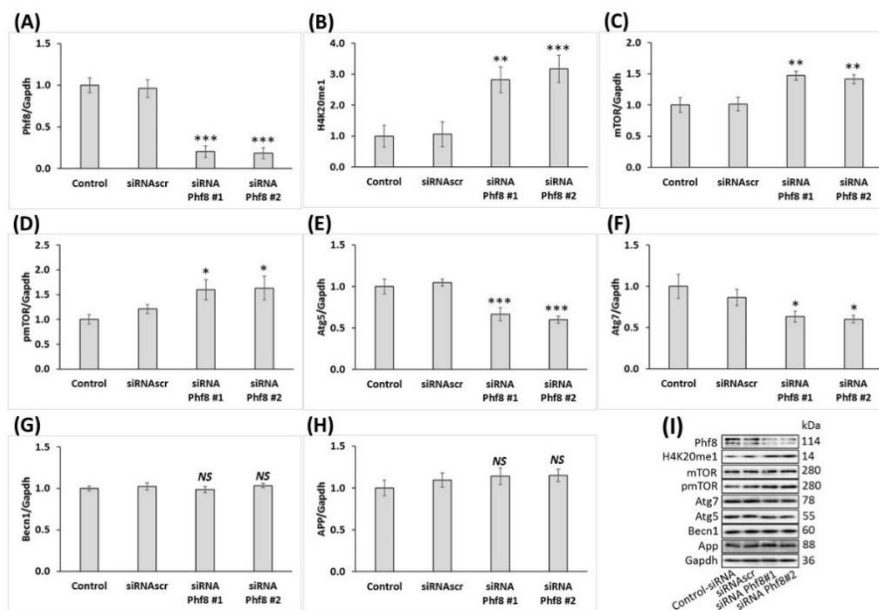


Fig. S3. *Blmh* gene silencing affects expression of mRNAs for Phf8, mTOR, APP, and autophagy-related proteins in mouse neuroblastoma N2a-APPsw cells. Bar graphs illustrating the quantification by RT-qPCR of mRNAs for *Blmh* (A), *Phf8* (B), *mTOR* (C), *App* (D), *Atg5* (E), *Atg7* (F), and *Bcln1* (G), in N2a-APPsw cells transfected with two different siRNAs targeting the *Blmh* gene (siRNA *Blmh* #1 and #2) are shown. *Gapdh* mRNA was used as a reference. Transfections without siRNA (Control) or with scrambled siRNA (siRNAAsc) were used as controls. Data are mean \pm standard deviation (SD) values from three biologically independent experiments. *P* values were calculated by one-way ANOVA with Tukey's multiple comparisons test. **P* < 0.01, ***P* < 0.001, or ****P* < 0.001 vs. 'control -siRNA' plus 'siRNAAsc.'



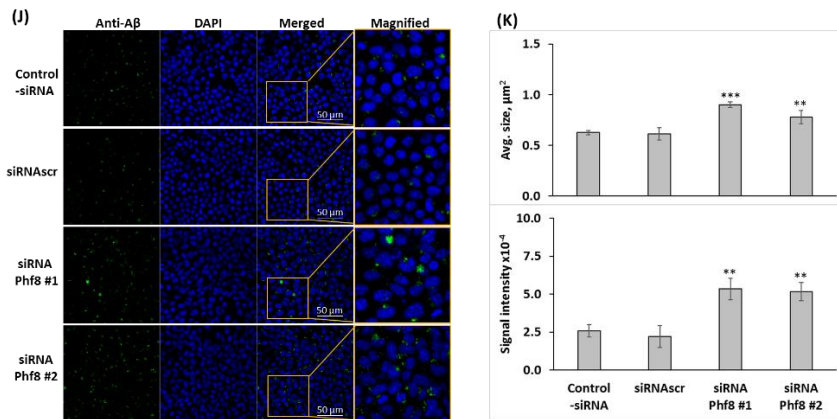


Fig. S4. Phf8 depletion promotes A β accumulation mediated by upregulation of mTOR signaling and inhibition of autophagy in the mouse neuroblastoma N2a-APPswe cells. The cells were transfected with siRNAs targeting the *Phf8* gene (Phf8 siRNA #1 and #2). Transfections without siRNA (Control -siRNA) or with scrambled siRNA (siRNAscr) were used as controls. Proteins were quantified by Western blotting. Bar graphs illustrate levels of (A) Phf8, (B) H4K20me1, (C) mTOR, (D) pmTOR, (E) Atg5, (F) Atg7, (G) Bcln1, and (H) App. A β was detected and quantified by confocal immunofluorescence microscopy using anti-A β antibody. (I) Confocal microscopy images of A β signals from *Phf8*-silenced and control N2a-APPswe cells. (J) Bar graphs show quantification of A β signals. Data are mean \pm standard deviation (SD) values from three biologically independent experiments. *P* values were calculated by one-way ANOVA with Tukey's multiple comparisons test. **P* < 0.01, ***P* < 0.001, or ****P* < 0.001 vs. 'control -siRNA' plus 'siRNAscr.' NS, not significant.

Table S1 Primers used for PCR or RT-qPCR	
Gene	Primer sequence
APP App	Forward: 5'-CTTCCCAAGATCCTGATAAACT-3'
	Reverse: 5'-CCGGGTGTCTCCAGGTA-3'
Atg5	Forward: 5'-AAGGCACACCCCTGAAATGG-3'
	Reverse: 5'-TGATGTTCCAAGGAAGAGCTGAA-3'
Atg7	Forward: 5'-GCCAACTCCACACTGCTTTC-3'
	Reverse: 5'-TCTTCTGGGTCAGTTCGTGC-3'
Actb	Forward: 5'-GCAGGAGTACGATGAGTCCG-3'
	Reverse: 5'-ACGCAGCTCAGTAACAGTCC-3'
Becn1	Forward: 5'-GAGGAAGCTCAGTACCAG CG-3'
	Reverse: 5'-CCAGATGTGGAAGGTGGCAT-3'
Blmh	Forward p1: 5'-CACTGTAGCTGTA-CTCACAC-3'
	Reverse p2: 5'-GCGACAGAGTACCATGTAGG-3' (exon 3); Reverse p3: 5'-ATTTGTCAGTCTGCACGACG-3' (neomycin cassette)
hAPP transgene in 5xFAD mice	Forward: 5'-AGAGTACCAACTTGCATGACTACG-3';
	Reverse: 5'-ATGCTGGATAACTGCCTTCTTATC-3'

<i>hPS1 transgene in 5xFAD mice</i>	<i>Forward: 5'-GCTTTTCCAGCTCTCATTACTC-3'</i>
	<i>Reverse: 5'-AAAATTGATGGAATGCTAATTGGT-3'</i>
<i>Gapdh</i>	<i>Forward: 5'-GGACTGGATAAGCAGGGCG-3'</i>
	<i>Reverse: 5'-TTTTGTCTACGGGACGAGGC-3'</i>
<i>mTOR</i>	<i>Forward: 5'-GCCACTCTTGACCCAGTTC-3'</i>
	<i>Reverse: 5'-ATGCCAAGACACAGTAGCGG-3'</i>
<i>Phf8</i>	<i>Forward: 5'-TGGGAGCATGCTTCAAGG-3'</i>
	<i>Reverse: 5'-GATTTCAAAGCAGGGTCATCA-3'</i>
<i>mTOR upstream TSS*</i>	<i>Forward: 5'-TTGCCAACTGGTGCTCGTTT-3'</i>
	<i>Reverse: 5'-AAGAATTGGAGCTCGGGACC-3'</i>
<i>mTOR TSS*</i>	<i>Forward: 5'-GGATGTTCTCCCAATCTTCG-3'</i>
	<i>Reverse: 5'-CAGACCCACCTAACTGACCGT-3'</i>
<i>mTOR downstream TSS*</i>	<i>Forward: 5'-TAGGGGGCAGATCCCGAAAC-3'</i>
	<i>Reverse: 5'-CACTGTAGCTGTAACCTCACAC-3'</i>
<i>* TSS, transcription start site</i>	

8. Życiorys naukowy

Edukacja

2016-2022 Studia III stopnia: profil biologiczny, Środowiskowe Studium Doktoranckie ICHB PAN

2013-2015 Studia II stopnia na kierunku biologia, Wydział Biologii Uniwersytetu im. Adama Mickiewicza w Poznaniu

2015 Tytuł magistra biologii. Wydział Biologii Uniwersytetu im. Adama Mickiewicza w Poznaniu. Praca magisterska pt. „Badanie efektów niespecyficzných wywołanych przez reagenty interferencji RNA” wykonana w Zakładzie Biomedycyny Molekularnej ICHB PAN, pod kierunkiem Prof. dr hab. Włodzimierza Krzyżosiaka

2010-2013 Studia I stopnia na kierunku: biologia molekularna; Wydział Biologii Uniwersytetu im. Adama Mickiewicza w Poznaniu

2013 Tytuł licencjata biologii molekularnej. Wydział Biologii Uniwersytetu im. Adama Mickiewicza w Poznaniu. Praca licencjacka pt. „Wykorzystanie metod sekwencjonowania nowej generacji w charakterystyce reagentów technologii interferencji RNA” wykonana w Zakładzie Biomedycyny Molekularnej ICHB PAN, pod kierunkiem Prof. dr hab. Włodzimierza Krzyżosiaka

Udział w projektach badawczych

1. Kierownik projektu Preludium, NCN 2016/23/N/NZ3/01216 „Zmiany w ekspresji mikroRNA wywołane przez homocysteinę oraz tiolakton homocysteiny”.

Opiekun naukowy: Prof. dr hab. Hieronim Jakubowski. W terminie od 08.2017 do 08.2022.

2. Wykonawca w projekcie NCN Opus 2019/33/B/NZ4/01760 „Mechanizmy epigenetycznych modyfikacji histonów w hiperhomocysteinemii”. Kierownik projektu: Prof. dr hab. Hieronim Jakubowski. W terminie od 12.2022 do 10.2023.

3. Wykonawca w projekcie NCN Opus 2018/29/B/NZ4/00771 „Rola Paraoksonazy 1 w Chorobie Alzheimer'a”. Kierownik projektu: Prof. dr hab. Hieronim Jakubowski. W terminie od 03.2019 do 11.2022.

4. Wykonawca w projekcie NCN Opus 2013/11/B/NZ1/00091 „Mechanizmy i konsekwencje inkorporacji homocysteiny do białek u ludzi”. Kierownik projektu: Prof. dr hab. Hieronim Jakubowski. W terminie od 02.2016 do 03.2019.

Publikacje

1. **Witucki Ł**, Jakubowski H, Depletion of Paraoxonase 1 (Pon1) Dysregulates mTOR, Autophagy, and Accelerates Amyloid Beta Accumulation in Mice. *Cells* 2023, 12(5), 746 DOI: 10.3390/cells12050746.

2. **Witucki Ł**, Jakubowski H, Homocysteine Metabolites Inhibit Autophagy and Elevate Amyloid Beta by Impairing Phf8/H4K20me1-dependent Epigenetic Regulation of mTOR in Cystathionine β -Synthase-Deficient Mice. *J Inherit Metab Dis.* 2023;1–17 DOI: 10.1002/jimd.12661.

3. **Witucki Ł**, Borowczyk K, Suszyńska-Zajczyk J, Warzych E, Pawlak P, Jakubowski H, Deletion of the Homocysteine Thiolactone Detoxifying Enzyme Bleomycin Hydrolase, in Mice, Causes Memory- and Neurological Deficits and Worsens Alzheimer’s Disease Related Behavioral and Biochemical Traits in the 5xFAD Model of Alzheimer’s Disease. *JAD* praca zaakceptowana 05.08.2023

4. **Witucki Ł**, Kurpiak M, Jakubowski H, Szulc M, Mikołajczak Ł, Jodynis-Liebert J, Kujawska M, Neuroprotective Effects of Cranberry Juice Treatment in a Rat Model of Parkinson’s Disease. *Nutrients* 2022, 14, 2014.

5. Kujawska M, Jourdes M, **Witucki Ł**, Karaźniewicz-Łada M, Szulc M, Górka A, Mikołajczak PŁ, Teissedre PL, Jodynis-Liebert J, Pomegranate Juice Ameliorates Dopamine Release and Behavioral Deficits in a Rat Model of Parkinson’s Disease. *Brain Sci.* 2021, 11, 1127.

6. Olejniczak M, Urbanek MO, Jaworska E, **Witucki Ł**, Szczesniak MW, Makołowska I, Krzyżosiak WJ, Sequence-non-specific effects generated by various types of RNA interference triggers. *Biochimica et Biophysica Acta (BBA) - Gene Regulatory Mechanisms*, 2016, 1859, 2, 306-314

Doniesienia konferencyjne

1. Poster i oral on demand: Amyloid beta accumulation in cystathionine B-synthase-deficiency is mediated by homocysteine metabolites-induced downregulation of Phf8 demethylase and increased mTOR promotor occupancy by histone mark H4K20me1. **Witucki Ł***, Jakubowski H. 17th International conference on Alzheimer`s and Parkinson`s diseases 28.03-01.04.2023, Goteborg, Szwecja, * autor prezentujący.

2. Poster: H4K20me1-mediated epigenetic dysregulation of mTOR/autophagy increases amyloid beta accumulation and cognitive/neuromotor deficits in hyperhomocysteinemic and bleomycin hydrolase- deficient mice. **Witucki Ł***, Suszyńska-Zajczyk J, Wróblewski J, Jakubowski H. AAT-AD/PDTM Advances in Alzheimer`s Therapies Focus Meeting, AD/PD, 15-20.03.2022, Barcelona, Hiszpania, * autor prezentujący.

3. Referat: Prenatal hyperhomocysteinemia upregulates mTOR signaling, downregulates autophagy, and increases accumulation of amyloid beta and tau in adult 3xTG-AD mice. Suszyńska-Zajczyk J*, **Witucki Ł**, Wróblewski J, Jakubowski H. 13th International Conference One-Carbon Metabolism, B Vitamins and Homocysteine 12-16.09.2021, Poznań, * autor prezentujący.

4. Referat: Phf8-mediated epigenetic dysregulation of mTOR/autophagy increases amyloid beta accumulation and cognitive deficits in hyperhomocysteinemic and bleomycin hydrolase-deficient mice. **Witucki Ł***, Suszyńska-Zajczyk J, Wróblewski J, Jakubowski H. 13th International Conference One-Carbon Metabolism, B Vitamins and Homocysteine 12-16.09.2021, Poznań, * autor prezentujący.

5. Referat: Silencing Cbs or Blmh gene promotes accumulation of amyloid beta via the Phf8/H4K20me1/mTOR/autophagy pathway in mouse neuroblastoma N2A-APP^{swE} cells. **Witucki Ł***, Suszyńska-Zajczyk J, Jakubowski H. Homocysteine Mini-Conference 25.09.2020, Poznań, * autor prezentujący.

6. Referat: Phf8-mediated epigenetic dysregulation of mTOR signaling/autophagy increases amyloid beta level and cognitive deficits in hyperhomocysteinemic and bleomycin hydrolase-deficient mice. **Witucki Ł***, Suszyńska-Zajczyk J, Jakubowski H. Advances in Alzheimer`s and Parkinson`s therapies an AAT-AD/PD Focus Meeting, 02-05.04.2020, Wiedeń, Austria, * autor prezentujący.

7. Referat: Epigenetic dysregulation of mTOR signaling and autophagy increases A β accumulation and cognitive deficits in hyperhomocysteinemia and bleomycin hydrolase

deficient mice. **Witucki Ł***, Suszyńska-Zajczyk J, Wróblewski J, Jakubowski H. Homocysteine Mini-Conference 26.09.2019 Poznań, * autor prezentujący.

8. Poster: Homocysteine and homocysteine thiolactone dysregulate autophagy in murine neuroblastoma cells N2a-APP^{Swe}. Kaptur R*, Suszyńska-Zajczyk J, **Witucki Ł**, Włoczkowska O, Jakubowski H. Homocysteine Mini-Conference 26.09.2019 Poznań, * autor prezentujący.

9. Poster: Dysregulation of mTOR signaling/autophagy via epigenetic mechanism accelerates neurodegeneration in hyperhomocysteinemia and bleomycin hydrolase-deficient mice. **Witucki Ł***, Suszyńska-Zajczyk J, Wróblewski J, Jakubowski H. The 44th FEBS Congress, July 6-11, 2019, Kraków, * autor prezentujący.

10. Poster: Hyperhomocysteinemia and bleomycin hydrolase deficiency accelerate neurodegeneration by epigenetic dysregulation of mTOR signaling and inhibition of autophagy in mice. Suszyńska-Zajczyk J*, **Witucki Ł**, Wróblewski J, Jakubowski H. EMBO Symposium: Probing neural dynamics with behavioral genetics. 09-13.04.2019, Heidelberg, Niemcy, * autor prezentujący.

11. Poster: Epigenetic deregulation of mTOR and autophagy pathways by hyperhomocysteinemia or bleomycin hydrolase deficiency causes neurodegeneration in mice. Suszyńska-Zajczyk J, **Witucki Ł***, Wróblewski J, Filipkowski R, Jakubowski H, AD/PD 14th International Conference on Alzheimer's & Parkinson's Diseases 26.03-3.04, 2019, Lizbona, Portugalia, * autor prezentujący.

12. Poster i referat: Hyperhomocysteinemia causes cognitive impairment by hyperactivating mTOR and impairing autophagy via the inhibition of Phf8 histone demethylase in mice, **Witucki Ł***, Suszyńska-Zajczyk J, Wróblewski J, Filipkowski R, Jakubowski H. Folic Acid, Vitamin B12, and One-Carbon Metabolism, Nowa Szkocja, Kanada 27.07. -03.08.2018. Poster wyróżniony nagrodą „Poster Award” dla 3 najlepszych posterów, * autor prezentujący.

Staż naukowe

27.07.2018 do 30.11.2018 staż naukowo-szkoleniowy w laboratorium Prof. Hieronima Jakubowskiego na Uniwersytecie Rutgers w Newark, NJ, USA.

9. Oświadczenia o wkładzie doktoranta w powstawanie prac naukowych wchodzących w skład rozprawy doktorskiej

**Oświadczenie doktoranta dotyczące jego udziału w powstawaniu pracy naukowej
wchodzącej w skład rozprawy doktorskiej**

Witucki L., Jakubowski H*

Depletion of Paraoxonase 1 (Pon1) Dysregulates mTOR, Autophagy, and Accelerates Amyloid
Beta Accumulation in Mice

Cells 2023, 12(5), 746 DOI: 10.3390/cells12050746

Oświadczam, że mój udział w tworzeniu niniejszej pracy polegał na:

1. Zaplanowaniu prac badawczych wspólnie z Prof. dr hab. Hieronimem Jakubowskim.
2. Wykonaniu wszystkich zamieszczonych w publikacji prac eksperymentalnych.
3. Przeprowadzeniu analizy statystycznej oraz interpretacji wyników pod kierunkiem Prof. dr hab. Hieronimem Jakubowskim.
4. Przygotowaniu materiałów do manuskryptu pod kierunkiem Prof. dr hab. Hieronimem Jakubowskim.

Witucki
.....

Mgr Lukasz Witucki

* - autor korespondencyjny

**Oświadczenie autora do korespondencji dotyczące udziału doktoranta w powstawaniu
pracy naukowej wchodzącej w skład rozprawy doktorskiej**

Witucki Ł, Jakubowski H*

Depletion of Paraoxonase 1 (Pon1) Dysregulates mTOR, Autophagy, and Accelerates Amyloid
Beta Accumulation in Mice

Cells 2023, 12(5), 746 DOI: 10.3390/cells12050746

Oświadczam, że wkład mgr Łukasza Wituckiego w powstawanie wyżej wymienione pracy
naukowej polegał na:

1. Współudziale w planowaniu prac badawczych.
2. Wykonaniu zamieszczonych w publikacji prac eksperymentalnych.
3. Przeprowadzeniu analizy statystycznej oraz współudziale w interpretacji wyników.
4. Przygotowaniu materiałów do manuskryptu.



Prof. dr hab Hieronim Jakubowski

*- autor korespondencyjny

**Oświadczenie doktoranta dotyczące jego udziału w powstawaniu pracy naukowej
wchodzącej w skład rozprawy doktorskiej**

Witucki Ł., Jakubowski H*

Homocysteine Metabolites Inhibit Autophagy and Elevate Amyloid Beta by Impairing
Phf8/H4K20me1-dependent Epigenetic Regulation of mTOR in cystathionine β -synthase-
deficient mice

J Inherit Metab Dis. 2023;1–17 DOI: 10.1002/jimd.12661

Oświadczam, że mój udział w tworzeniu niniejszej pracy polegał na:

1. Zaplanowaniu prac badawczych wspólnie z Prof. dr hab. Hieronimem Jakubowskim.
2. Wykonaniu wszystkich zamieszczonych w publikacji prac eksperymentalnych.
3. Przeprowadzeniu analizy statystycznej oraz interpretacji wyników pod kierunkiem Prof. dr hab. Hieronimem Jakubowskim.
4. Przygotowaniu materiałów do manuskryptu pod kierunkiem Prof. dr hab. Hieronimem Jakubowskim.



Mgr Łukasz Witucki

* - autor korespondencyjny

**Oświadczenie autora do korespondencji dotyczące udziału doktoranta w powstawaniu
pracy naukowej wchodzącej w skład rozprawy doktorskiej**

Witucki Ł, Jakubowski H*

Homocysteine Metabolites Inhibit Autophagy and Elevate Amyloid Beta by Impairing
Phf8/H4K20me1-dependent Epigenetic Regulation of mTOR in cystathionine β -synthase-
deficient mice

J Inherit Metab Dis. 2023;1–17 DOI: 10.1002/jimd.12661

Oświadczam, że wkład mgr Łukasza Wituckiego w powstawanie wyżej wymienione pracy
naukowej polegał na:

1. Współdziałanie w planowaniu prac badawczych.
2. Wykonaniu zamieszczonych w publikacji prac eksperymentalnych.
3. Przeprowadzeniu analizy statystycznej oraz współdziałanie w interpretacji wyników.
4. Przygotowaniu materiałów do manuskryptu.



Prof. dr hab Hieronim Jakubowski

* - autor korespondencyjny

**Oświadczenie doktoranta dotyczące jego udziału w powstawaniu pracy naukowej
wchodzącej w skład rozprawy doktorskiej**

Witucki Ł., Borowczyk K., Suszyńska-Zajczyk J., Warzych E., Pawlak P., Jakubowski H

Deletion of the homocysteine thiolactone detoxifying enzyme, bleomycin hydrolase, in mice, causes memory- and neurological deficits and exacerbates Alzheimer's disease-related behavioral and biochemical traits in the 5xFAD model of Alzheimer's disease.

Oświadczam, że mój udział w tworzeniu niniejszej pracy polegał na:

1. Współdziałanie w planowaniu prac badawczych.
2. Wykonaniu testów behawioralnych, współdziałanie w pobieraniu tkanek mysich, prowadzeniu hodowli komórkowych w tym pozyskanie i przygotowanie materiałów do wykonanych eksperymentów, wykonaniu analiz western blot oraz real-time PCR, współdziałanie w obrazowaniu amyloid beta, wykonaniu analiz immunoprecypitacji chromatyny.
3. Przeprowadzeniu analizy statystycznej oraz interpretacji uzyskanych wyników.
4. Przygotowaniu materiałów do manuskryptu.

.....*Witucki*.....

Mgr Łukasz Witucki

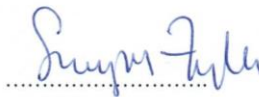
Oświadczenie współautora do korespondencji dotyczące udziału doktoranta w powstawaniu pracy naukowej wchodzącej w skład rozprawy doktorskiej

Witucki Ł, Borowczyk K, Suszyńska-Zajczyk J, Warzych E, Pawlak P, Jakubowski H

Deletion of the homocysteine thiolactone detoxifying enzyme, bleomycin hydrolase, in mice, causes memory- and neurological deficits and exacerbates Alzheimer's disease-related behavioral and biochemical traits in the 5xFAD model of Alzheimer's disease.

Oświadczam, że wkład mgr Łukasza Wituckiego w powstawanie wyżej wymienione pracy naukowej polegał na:

1. Współdziałanie w planowaniu prac badawczych.
2. Wykonaniu testów behawioralnych, współdziałanie w pobieraniu tkanek mysich, prowadzeniu hodowli komórkowych w tym pozyskanie i przygotowanie materiału do wykonanych eksperymentów, wykonaniu analiz western blot, immunoprecypitacji chromatyny oraz real-time PCR, współdziałanie w obrazowaniu amyloid beta.
3. Przeprowadzeniu analizy statystycznej oraz interpretacji uzyskanych wyników.
4. Przygotowaniu materiałów do manuskryptu.


.....

Oświadczenie współautora do korespondencji dotyczące udziału doktoranta w powstawaniu pracy naukowej wchodzącej w skład rozprawy doktorskiej

Witucki Ł, Borowczyk K, Suszyńska-Zajczyk J, Warzych E, Pawlak P, Jakubowski H

Deletion of the homocysteine thiolactone detoxifying enzyme, bleomycin hydrolase, in mice, causes memory- and neurological deficits and exacerbates Alzheimer's disease-related behavioral and biochemical traits in the 5xFAD model of Alzheimer's disease.

Oświadczam, że wkład mgr Łukasza Wituckiego w powstawanie wyżej wymienione pracy naukowej polegał na:

1. Współdziałanie w planowaniu prac badawczych.
2. Wykonaniu testów behawioralnych, współdziałanie w pobieraniu tkanek mysich, prowadzeniu hodowli komórkowych w tym pozyskanie i przygotowanie materiału do wykonanych eksperymentów, wykonaniu analiz western blot, immunoprecypitacji chromatyny oraz real-time PCR, współdziałanie w obrazowaniu amyloid beta.
3. Przeprowadzeniu analizy statystycznej oraz interpretacji uzyskanych wyników.
4. Przygotowaniu materiałów do manuskryptu.

Aveline Waupers-Plejer

Oświadczenie współautora do korespondencji dotyczące udziału doktoranta w powstawaniu pracy naukowej wchodzącej w skład rozprawy doktorskiej

Witucki L, Borowczyk K, Suszyńska-Zajczyk J, Warzych E, Pawlak P, Jakubowski H
Deletion of the homocysteine thiolactone detoxifying enzyme, bleomycin hydrolase, in mice, causes memory- and neurological deficits and exacerbates Alzheimer's disease-related behavioral and biochemical traits in the 5xFAD model of Alzheimer's disease.

Oświadczam, że wkład mgr Łukasza Wituckiego w powstawanie wyżej wymienionej pracy naukowej polegał na:

1. Współdziałanie w planowaniu prac badawczych.
2. Wykonaniu testów behawioralnych, współdziałanie w pobieraniu tkanek mysich, prowadzeniu hodowli komórkowych w tym pozyskanie i przygotowanie materiału do wykonanych eksperymentów, wykonaniu analiz western blot, immunoprecypitacji chromatyny oraz real-time PCR, współdziałanie w obrazowaniu amyloid beta.
3. Przeprowadzeniu analizy statystycznej oraz interpretacji uzyskanych wyników.
4. Przygotowaniu materiałów do manuskryptu.

Kamila Borowczyk

Oświadczenie współautora do korespondencji dotyczące udziału doktoranta w powstawaniu pracy naukowej wchodzącej w skład rozprawy doktorskiej

Witucki L., Borowczyk K, Suszyńska-Zajczyk J, Warzych E, Pawlak P, Jakubowski H

Deletion of the homocysteine thiolactone detoxifying enzyme, bleomycin hydrolase, in mice, causes memory- and neurological deficits and exacerbates Alzheimer's disease-related behavioral and biochemical traits in the 5xFAD model of Alzheimer's disease.

Oświadczam, że wkład mgr Łukasza Wituckiego w powstawanie wyżej wymienione pracy naukowej polegał na:

1. Współdziałanie w planowaniu prac badawczych.
2. Wykonaniu testów behawioralnych, współdziałanie w pobieraniu tkanek mysich, prowadzeniu hodowli komórkowych w tym pozyskanie i przygotowanie materiału do wykonanych eksperymentów, wykonaniu analiz western blot, immunoprecypitacji chromatyny oraz real-time PCR, współdziałanie w obrazowaniu amyloid beta.
3. Przeprowadzeniu analizy statystycznej oraz interpretacji uzyskanych wyników.
4. Przygotowaniu materiałów do manuskryptu.



dr hab. Piotr Pawlak

Oświadczenie autora do korespondencji dotyczące udziału doktoranta w powstawaniu pracy naukowej wchodzącej w skład rozprawy doktorskiej

Witucki Ł, Borowczyk K, Suszyńska-Zajczyk J, Warzych E, Pawlak P, Jakubowski H*

Deletion of the homocysteine thiolactone detoxifying enzyme, bleomycin hydrolase, in mice, causes memory- and neurological deficits and worsens Alzheimer's disease-related behavioral and biochemical traits in the 5xFAD model of Alzheimer's disease.

J Alzheimer's Dis 2023; accepted August 5.

Oświadczam, że wkład mgr Łukasza Wituckiego w powstawanie wyżej wymienione pracy naukowej polegał na:

1. Współdziałanie w planowaniu prac badawczych.
2. Wykonaniu testów behawioralnych, współdziałanie w pobieraniu tkanek mysich, prowadzeniu hodowli komórkowych w tym pozyskanie i przygotowanie materiału do wykonanych eksperymentów, wykonaniu analiz western blot, immunoprecypitacji chromatyny oraz real-time PCR, współdziałanie w obrazowaniu amyloid beta.
3. Przeprowadzeniu analizy statystycznej oraz współdziałanie w interpretacji uzyskanych wyników.
4. Przygotowaniu materiałów do manuskryptu.



Prof. dr hab Hieronim Jakubowski

* - autor korespondencyjny

